Johannes Gutenberg-Universität Mainz

Method development and application of quantitative analysis of lignin oxidation products as vegetation biomarkers in speleothems and cave drip water

Dissertation

zur Erlangung des akademischen Grades
„Doktor der Naturwissenschaften“
(Dr. rer. nat.)

Im Promotionsfach Chemie
am Fachbereich Chemie, Pharmazie und Geowissenschaften
der Johannes Gutenberg-Universität Mainz

vorgelegt von

Inken Heidke

geboren in Göttingen

Mainz im April 2021

"An expert is a person who has made all the mistakes that can be made in a very narrow field."

Niels Bohr

Zusammenfassung

Klimaarchive, wie z. B. Eisbohrkerne, Sedimente und Speläotheme, konservieren Informationen über das Klima und die Vegetation der Vergangenheit. Speläotheme haben gegenüber anderen Klimaarchiven bestimmte Vorteile: Sie kommen auf allen Kontinenten außer der Antarktis vor, können über mehrere tausend Jahre kontinuierlich und ohne Verlust der Zeitauflösung wachsen, und sie lassen sich mit der ^{230}Th-U-Methode präzise auf bis zu 640 000 Jahre vor unserer Zeit datieren. Die am häufigsten verwendeten Stellvertretersubstanzen (Proxies) in Speläothemen sind stabile Isotopenverhältnisse, wie z. B. δ^{13}C und δ^{18}O, sowie Spurenelemente. In den letzten Jahren haben jedoch organische Proxies und Multi-Proxy-Ansätze zunehmend an Aufmerksamkeit gewonnen. Lignin ist ein Biopolymer, das ausschließlich in Gefäßpflanzen produziert wird. Es besteht hauptsächlich aus drei phenolischen Monomeren, deren Verhältnis sich zwischen angiospermen und gymnospermen Pflanzen sowie zwischen verholzter und nicht verholzter Vegetation unterscheidet. Somit liefert die Analyse von Lignin nicht nur Informationen über die Vegetationsdichte, sondern auch über die Art der Vegetation, und eignet sich daher besonders gut als Vegetationsproxy in Klimaarchiven. Folglich ist die Verwendung von Ligninphenolen als Vegetationsproxies in Sedimenten, Torfbohrkernen und natürlichen Gewässern weit verbreitet. In Speläothemen dagegen wurden Ligninphenole zwar bereits nachgewiesen, aber es wurde noch keine quantitative Analyse von Ligninphenolen in Speläothemen durchgeführt. Da die Konzentration an organischem Material in Speläothemen sehr gering ist, ist eine sehr empfindliche und nachweisstarke Analysemethode erforderlich.

Im ersten Teil dieser Arbeit wurde eine selektive und empfindliche Methode für die quantitative Analyse von Ligninphenolen in Speläothemen, Höhlentropfwasser und Bodenproben entwickelt. Die Speläothemproben wurden in Säure aufgelöst und die saure Lösung durch Festphasenextraktion (SPE) extrahiert. Das in den Extrakten enthaltene polymere Lignin wurde mittels CuO-Oxidation oxidativ in monomere Ligninoxidationsprodukte (LOPs) aufgespalten. Die LOPs wurden anschließend durch SPE extrahiert und angereichert und schließlich mittels Ultra-Hochleistungs-Flüssigchromatographie gekoppelt an Elektrospray-Ionisation und hochauflösende Massenspektrometrie (UHPLC-ESI-HRMS) analysiert. Außerdem wurde eine elektrolytische Methode für den oxidativen Abbau von Lignin als Alternative zur CuO-Oxidation entwickelt, jedoch waren die LOP-Ausbeuten aus Speläothemproben nicht zufriedenstellend und es kam zu Problemen durch eine Überoxidation der freigesetzten LOPs. Alle Probenvorbereitungs- und Analyseschritte wurden optimiert und an die niedrigen Konzentrationen organischen Materials in Speläothemen und Höhlentropfwasser angepasst. Die Methode wurde erfolgreich getestet und validiert und zeigte eine ausreichende Empfindlichkeit um selbst Spurenkonzentrationen von Lignin nachzuweisen, wobei Nachweisgrenzen im niedrigen ng/g-Bereich erreicht wurden.

Im zweiten Teil dieser Arbeit wurde die entwickelte Analysemethode dann auf verschiedene Speläothem-, Boden- und Tropfwasserproben angewendet. Die Ergebnisse wurden mit Daten von stabilen Isotopen und Spurenelementen sowie mit bekannten Klima- und Vegetationsveränderungen verglichen und korreliert. Die erste Probe war ein 11 000 Jahre alter Stalagmit aus dem Holozän aus der Herbstlabyrinthhöhle in Deutschland. Zusätzlich wurde im Rahmen eines Höhlenmonitoring-Programms monatlich Tropfwasser aus der gleichen Höhle beprobt und auf LOPs analysiert, um jahreszeitliche Schwankungen des Lignineintrags zu untersuchen. Die Ergebnisse zeigten, dass die LOP-Signale im Stalagmiten eine signifikante zeitliche Variation auf der Zeitskala von Jahrhunderten bis Jahrtausenden aufwiesen. Die Gesamt-LOP-Konzentration, $\Sigma 8$, im Stalagmit war mit den Konzentrationen von Phosphor, Barium und Uran korreliert, welche in früheren Studien als Vegetationsproxies interpretiert wurden. Der klare Vorteil von $\Sigma 8$ im Vergleich zu diesen Spurenelementen besteht darin, dass das Lignin ausschließlich von höheren Pflanzen und nicht z. B. von Mikroorganismen oder dem Wirtsgestein stammt. Daher kann $\Sigma 8$ dazu beitragen, potenzielle Vegetationsproxies mit weniger eindeutigen Quellen besser zu interpretieren. Die Analyse des Höhlentropfwassers zeigte einen saisonalen Verlauf mit höheren LOP-Konzentrationen im Sommer und niedrigeren Konzentrationen im Winter. In zwei weiteren Anwendungsbeispiele wurde das Potenzial der LOPs als Vegetationsproxies anhand spezifischer Fragen der Paläovegetationsforschung untersucht. Das erste Beispiel war ein kleiner, nur 200 Jahre alter Stalagmit aus der Zoolithenhöhle in Deutschland. Aus historischen Quellen war in der Gegend um die Zoolithenhöhle eine schnelle Vegetationsänderung von Grasland zu Laubwald bekannt. Im Stalagmiten konnte jedoch bei den etablierten Vegetationsproxys, wie z. B. δ^{13}C, keine signifikante Veränderung der gemessenen Signale festgestellt werden. Die LOP-Signale hingegen konnten diese Vegetationsänderung sichtbar machen, und zwar sowohl in der Gesamt-LOP-Konzentration, $\Sigma 8$, als auch in den LOP-Verhältnissen C/V und S/V, welche Aufschluss über die Art der Vegetation geben. Im zweiten Beispiel wurden mehrere Proben eines Flowstones aus der Cueva Victoria im Südosten Spaniens analysiert. Die Proben stammten aus drei verschiedenen geologischen Epochen: dem Holozän, der letzten Eiszeit und dem Eem-Interglazial. Die δ^{13}C-Verhältnisse zeigten in diesen Flowstones mehrere ausgeprägte Schwankungen, welche als schnelle Verschiebungen zwischen feuchteren und trockeneren Klimaperioden interpretiert wurden, durch die sich auch die Art und Dichte der Vegetation veränderte. Die LOP-Analyse dieser Proben konnte die vermuteten Vegetationsveränderungen bestätigen und damit die Gesamtinterpretation zuverlässiger machen.

Ein weiteres wichtiges Ziel dieser Arbeit war es, besser zu verstehen, wie das Lignin aus dem Boden durch das Karstsystem in die Höhle transportiert wird und welche Rolle dabei z. B. der mikrobielle Abbau des Lignins oder die Wechselwirkung mit mineralischen Partikeln spielen. Diese Mechanismen scheinen einen größeren Einfluss auf die Ligninverhältnisse C/V und S/V zu haben. Insbesondere sollte die Frage beantwortet werden, ob die ursprüngliche Ligninzusammensetzung, welche direkt von der Art der über der Höhle befindlichen Vegetation abhängt, trotz der unterschiedlichen Einflüsse von Transport und Abbau bewahrt bleibt und aus der Analyse der Speläothemproben erhalten werden kann. Dazu wurde eine systematische Vergleichs-

studie mit Proben aus vier verschiedenen Höhlen aus verschiedenen Vegetationszonen in Neuseeland durchgeführt. Aus jeder Höhle wurden Boden-, Tropfwasser- und Speläothemproben analysiert und die Ligninzusammensetzung verglichen. Die Ergebnisse zeigten, dass trotz der diversen Einflüsse des Transports, des Abbaus und der Adsorption an Mineralien der "Fingerabdruck"der darüber liegenden Vegetation in der in den Speläothemen eingeschlossenen Ligninzusammensetzung erhalten bleibt. Die Ergebnisse zeigten aber auch, dass die C/V- und S/V-Verhältnisse des Lignins in den Speläothemen nicht als absolute Werte angesehen werden können, aus denen sich direkt ein bestimmter Pflanzentyp ableiten ließe, da die Prozesse während des Transports die C/V- und S/V-Verhältnisse signifikant verändern können. Die relativen Variationen, die durch die Veränderung der Vegetation über die Zeit an einem Höhlenstandort verursacht werden, werden jedoch wahrscheinlich im Lignin des Speläothems bewahrt, solange sich die Transportprozesse und -bedingungen oberhalb der Höhle nicht zu stark verändern.

Zusammenfassend lässt sich sagen, dass die Analyse von Ligninoxidationsprodukten einen neuen und hochspezifischen Vegetationsproxy zur Rekonstruktion der Paläovegetation und des Paläoklimas aus Speläothem-Archiven liefert. Damit steht ein weiteres, neues Werkzeug in der “Proxy-Toolbox” zur Verfügung, mit dem die Interpretation anderer Proxies insbesondere in Multi-Proxy-Ansätzen verbessert werden kann. Die Anwendung der in dieser Arbeit entwickelten Methode auf weitere Speläothem- und Tropfwasserproben aus verschiedenen Vegetationszonen und klimatischen Bedingungen kann zudem das Verständnis des Transports organischen Materials vom Boden in das Höhlensystem verbessern.

Abstract

Climate archives, such as ice cores, sediments and speleothems, preserve information on the climate and the vegetation of the past. Speleothems have certain advantages over other climate archives: they occur on all continents except Antarctica, can grow continuously for several thousand years without a loss in time resolution, and can be accurately dated up to 640 000 years before present using the ^{230}Th-U method. The most commonly used proxies in speleothems are stable isotope ratios, such as δ^{13}C and δ^{18}O, and trace elements. In recent years, however, organic proxies and multi-proxy approaches have gained increasing attention. Lignin is a biopolymer that is produced exclusively in vascular plants. It mainly consists of three phenolic monomers, whose proportion differs between angiosperm and gymnosperm plants and between woody and non-woody vegetation. This makes lignin particularly suitable as a vegetation proxy in climate archives, as its analysis provides not only information on the vegetation density, but also on the type of vegetation. Consequently, lignin phenols are widely used as vegetation proxies in sediments, peat cores and natural waters. Although they have already been detected in speleothems, a quantitative analysis of lignin phenols in speleothems has not yet been performed. Since the concentrations of organic matter enclosed in speleothems is very low, a sensitive analytical method is required.

In the first part of this work, a selective and sensitive method for the quantitative analysis of lignin phenols in speleothems, cave dripwater and soil samples was developed. The speleothem samples were dissolved in acid and the acidic solution extracted by solid phase extraction (SPE). The polymeric lignin contained in the extracts was oxidatively degraded into monomeric lignin oxidation products (LOPs) using CuO oxidation. The LOPs were then extracted and enriched by SPE and finally analyzed using ultrahigh-performance liquid chromatography coupled to electrospray ionization high-resolution mass spectrometry (UHPLC-ESI-HRMS). As an alternative to the CuO oxidation, an electrolytic method for the oxidative degradation of lignin was developed as well, but the LOP yields obtained from speleothem samples were not satisfactory and over-oxidation of the released LOPs was a problem. All sample preparation and analysis steps were optimized and adjusted to the low concentrations of organic matter in speleothems and cave dripwater. The method was successfully tested and validated and showed sufficient sensitivity to detect even trace concentrations of lignin, with detection limits in the low ng/g range reached.

In the second part of this work, the developed analytical method was then applied to different speleothem, soil and dripwater samples. The results were compared and correlated with data from stable isotopes and trace elements as well as with known climate and vegetation changes. The first sample was an 11 000 years old Holocene stalagmite from the Herbstlabyrinth Cave in Germany. In addition, dripwater from the same cave was sampled monthly in the framework of a cave monitoring program

and analyzed for LOPs in order to study seasonal variations in lignin input. The results showed that the LOP signals in the stalagmite had a significant variation over time on the centennial to millennial timescale. The total LOP concentration, $\Sigma 8$, in the stalagmite was correlated to phosphorous, barium and uranium concentrations, which have been interpreted as vegetation proxies in previous studies. The clear benefit of $\Sigma 8$ compared to these trace elements is that the sources of lignin are exclusively higher plants and not, for example, microorganisms or the host rock. Therefore, $\Sigma 8$ can help to better interpret potential vegetation proxies whose sources are less clear. The analysis of the cave dripwater showed a seasonal pattern with higher LOP concentrations in summer and lower concentrations in winter.

Two further application examples were carried out to test the potential of LOPs as a vegetation proxy by means of specific paleo-vegetation research questions. The first example was a small, only 200 years old stalagmite from the Zoolithen Cave in Germany. A rapid vegetation change from grassland to deciduous forest in the landscape around the Zoolithencave was known from historical sources, but the established vegetation proxies such as δ^{13}C did not show a significant change in their signals recorded in the stalagmite. The LOP signals, in contrast, were able to record this vegetation change both in the total LOP concentration, $\Sigma 8$, and in the LOP ratios C/V and S/V, which indicate the type of vegetation. In the second example, several samples from a flowstones from the Cueva Victoria in southeast Spain were analyzed. The samples date from three different geological eras: the Holocene, the Last Glacial Period and the Eemian interglacial. The δ^{13}C records of these flowstones showed several large excursions, which were interpreted as rapid shifts between more humid and more arid climate periods, resulting in a change in vegetation type and density. The LOP analysis of these samples was able to confirm the suspected vegetation changes, thus making the interpretation more robust.

Another important goal of this work was to better understand the mechanisms of lignin transport from the soil through the karst system into the cave, for example the influences of microbial degradation and the interaction of lignin with mineral particles. These effects seem to have a larger influence on the lignin ratios C/V and S/V. In particular, the question was to be answered whether the original source-dependent signal of the overlying vegetation is preserved despite the different influences of transport and degradation and can be recovered from the speleothem samples. Therefore, a systematic comparative study was carried out in four different caves from different vegetation zones in New Zealand. From each cave, soil, drip water and speleothem samples were analyzed and the lignin composition compared. The results showed that despite the various influences of transport, degradation and adsorption to minerals, the "fingerprint" of the overlying vegetation is preserved in the lignin composition enclosed in the speleothems. They also demonstrated, though, that the C/V and S/V ratios of lignin in speleothems cannot be considered absolute values indicative of specific plant types, since the processes during transport can significantly alter the C/V and S/V ratios. However, the relative changes caused by the temporal change of vegetation at the same cave site are likely to be preserved in the speleothem lignin as long as the transport processes and conditions above the cave do not change too much.

In conclusion, the analysis of lignin oxidation products provides a new and highly specific vegetation proxy for the reconstruction of paleo-vegetation and paleo-climate from speleothem archives, which can expand the proxy toolbox and improve the interpretation of other proxies, especially in multi-proxy approaches. In addition, the appliction of the method developed in this work to further speleothem and drip water samples from different vegetation zones and climatic conditions can improve the understanding of organic matter transport from the soil to the cave system.

Contents

Part I

Introduction and theoretical background

Introduction

The climate change on our planet is probably the greatest challenge for humanity in this century. In order to be able to make the right decisions to counteract global warming and to adapt to its impacts, it is essential to understand the underlying mechanisms. We need to examine how the climate has changed in the past and what the causes and consequences have been. To do this, we need data on the climate of the past, from a time long before people began to record temperature and precipitation, let alone to measure carbon dioxide concentrations. These data can be obtained from paleoclimate archives, for example from ice cores, sediment cores, tree rings or speleothems. They all preserve physical and chemical proxies for climate and environmental variables and can be dated by layer counting or analysis of radioactive isotopes. Each climate archive has its own advantages and disadvantages, and many different proxies and analysis methods are needed to extract the desired information to obtain a complete picture of past climate changes.

In the following three chapters, a short literature review and theoretical background of the analysis of lignin oxidation products as a proxy for vegetation and environmental changes in speleothem archives is provided. Chapter 1 presents the characteristics of speleothems as paleoclimate archives, explaining their formation and dating as well as the different proxies obtained from speleothems. Chapter 2 deals with the chemical, biochemical and geochemical properties of lignin and its application as a vegetation proxy. In chapter 3, the analytical techniques used in this work are presented.

1 Speleothems as paleoclimate archives

Speleothems, such as stalagmites and flowstones, are calcareous mineral deposits that form within caves in karstified carbonate rock. Speleothems preserve a variety of inorganic and organic *proxies*, that means measurable parameters which can yield information about climatic and hydrological conditions as well as the development of the vegetation and the soil above the cave (Fairchild and Baker, 2012, Blyth et al., 2016, McDermott, 2004). Therefore, they serve as paleoclimate archives. Compared to other paleoclimate archives, such as ice cores and marine or lacustrine sediments, speleothems have certain advantages: They can grow continuously for thousands of years and do not show a loss of time resolution with increasing age (Gałuszka et al., 2017, Fairchild et al., 2006), their age can be accurately determined up to 640 000 years back in time using the ^{230}Th/U-method (Cheng et al., 2016, Scholz and Hoffmann, 2008, Richards and Dorale, 2003), and the cave provides a preservative environment that protects the recorded chemical proxy signals against outer influences such as light, abrupt changes in temperature and, under ideal conditions, also mechanical disturbance. Moreover, speleothems occur on all continents except Antarctica and are thus not limited to certain climatic regions or vegetation zones.

1.1 Formation of speleothems

The formation of speleothems requires three things: *karst*, liquid water, and the availability of carbon dioxide, CO_2, which is produced by soil organisms and root respiration in the soil. *Karstic* host rock most often consists of carbonate rocks such as limestone, $CaCO_3$, or dolimite, $CaMg(CO_3)_2$. These rocks cannot hold surface water, but let it drain through pores and fissures into deeper zones of the host rock and are therefore called *aquifers*. When carbon dioxide dissolves in water, it forms carbonic acid, H_2CO_3, which is a weak acid and can deprotonate to hydrogencarbonate, HCO_3^- (equation (1.1)). This weakly acidic solution percolates through the soil to the *epikarst* zone (Fig. 1.1), which is the uppermost zone of the aquifer, where it dissolves the carbonate bedrock (equation (1.2)). This dissolution produces pores, holes and fissures in the bedrock, which can grow into caves and conduits holding underground streams. The part of the aquifer lying above the regional water table is called *vadose zone*, the part below the water table is called *phreatic zone*. However, the water table in a karstic system tends to lower over time, so that formerly water filled caves and conduits fall dry while new cavities are forming in deeper zones of the bedrock.

The acidic solution oversaturated in $CaCO_3$ finally reaches a cave. Due to ventilation, the partial pressure of carbon dioxide, pCO_2, in the cave air is similar to the atmospheric level and much lower than in the soil. Consequently, CO_2 degasses from the solution, shifting the equilibrium in equation (1.3) to the right side and leading to the precipitation of $CaCO_3$ and thus to the formation of speleothems.

In the soil: $$CO_{2(aq)} + 2\,H_2O \rightleftharpoons H_2CO_{3(aq)} + H_2O \rightleftharpoons HCO^-_{3(aq)} + H_3O^+ \tag{1.1}$$

In the bedrock: $$CaCO_{3(s)} + H_2CO_{3(aq)} \rightleftharpoons Ca^{2+}_{(aq)} + 2\,HCO^-_{3(aq)} \tag{1.2}$$

In the cave: $$Ca^{2+}_{(aq)} + 2\,HCO^-_{3(aq)} \rightleftharpoons CaCO_{3(s)} + H_2O + CO_{2(g)} \tag{1.3}$$

The most common types of speleothems are stalagmites, which are formed by water dripping on the ground of the cave, stalactites, which are their counterparts on the cave ceiling, and flowstones, which are formed by water films flowing on the cave walls and floor. Stalagmites usually have a flat upper surface and a simpler structure of the growth layers than stalactites, which makes it easier to determine the growth axis (Fig. 1.2). Therefore, stalagmites are more often used as paleoclimate archives than stalactites. However, the growth axis can shift its position when the drips change their landing position. A pause in growth, called *hiatus*, can sometimes, but not necessarily, be visible as a dust layer. It can either reflect changes in climate or just a local change in the flow path in the aquifer, causing the drops to land elsewhere than on the stalagmite surface. While stalagmites are typically fed by crack or seepage flow, flowstones build under thin sheets of water with higher discharge, such as conduit flows. Therefore, they build extended continuous layers, allowing to obtain duplicate records by coring in different places of the same flowstone.

The growth rate of stalagmites can reach up to a millimeter per year in warm, humid climate with a high soil activity and therefore high soil pCO_2, but is more commonly less than 100 µm per year in cool temperate regions (Fairchild and Baker, 2012). If the precipitation of $CaCO_3$ happens above the observed cave, in a higher cave or a cavity in the aquifer, this is called *prior calcite precipitation*, PCP. PCP can influence the saturation of the dripwater with respect to $CaCO_3$ and also other characteristics of the dripwater, such as stable isotope ratios and the concentrations of trace elements.

Speleothems posses a more or less pronounced lamination, visible for the eye or under UV-light. These layers can be caused by seasonal changes in temperature and precipitation, a change in the pCO_2 due to the growth season of the vegetation and the soil activity above the cave, or by different ventilation of the cave in summer and winter, leading to changes in relative humidity and pCO_2. If the speleothem grows fast enough, these seasonal changes can be conserved in the calcite as annual couplets, usually indicating warmer/cooler or wetter/drier alternations. In cool temperate climate, also a discrete, thin impulse lamina is common. This is caused by seasonal influx of soil-derived material, which is especially visible under UV-light. The lighter calcite in annual couplets can also be caused by fluid inclusions (Fairchild and Baker, 2012).

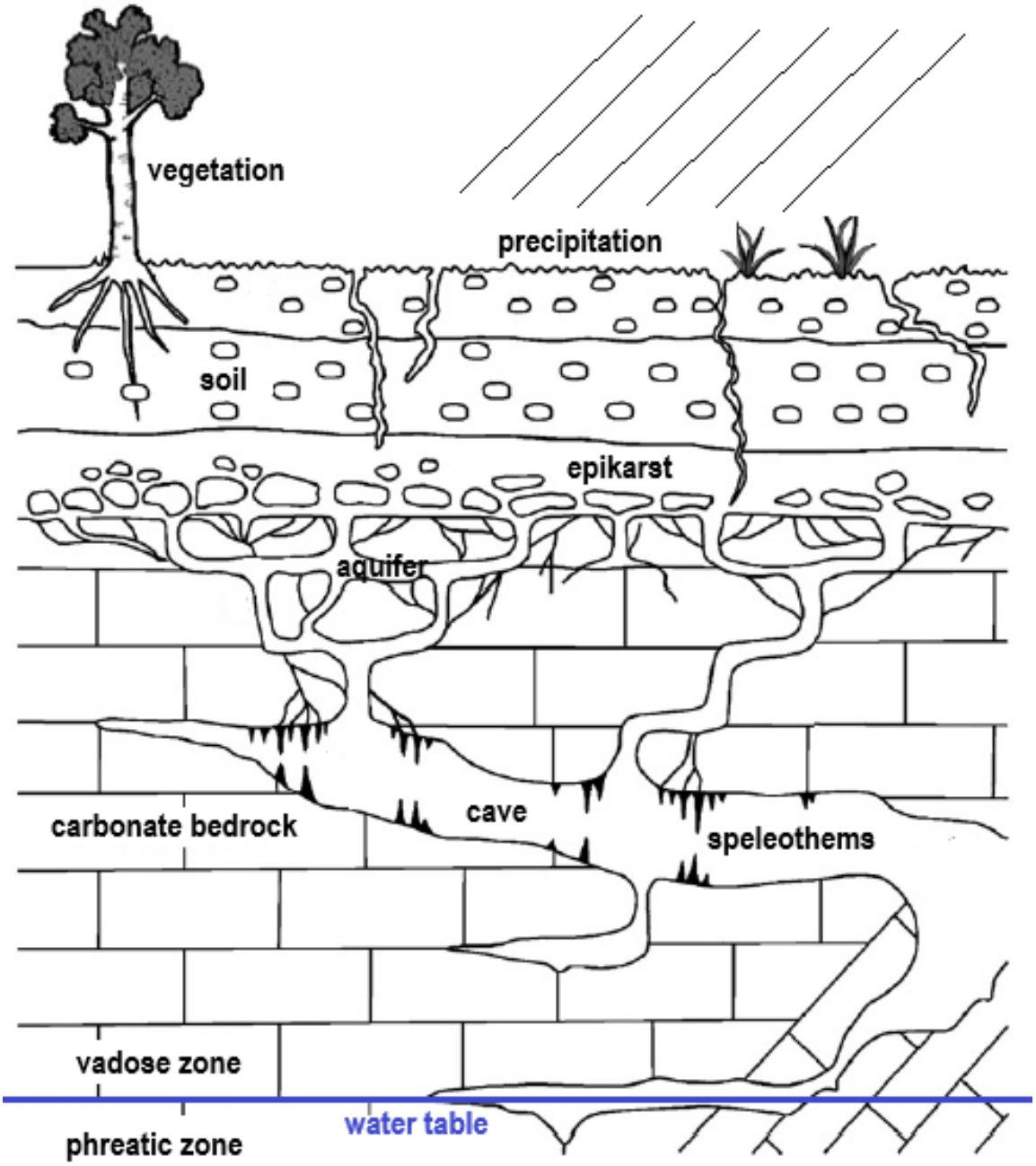

Figure 1.1: Schematic illustration of the cave system (modified after Tooth (2000)).

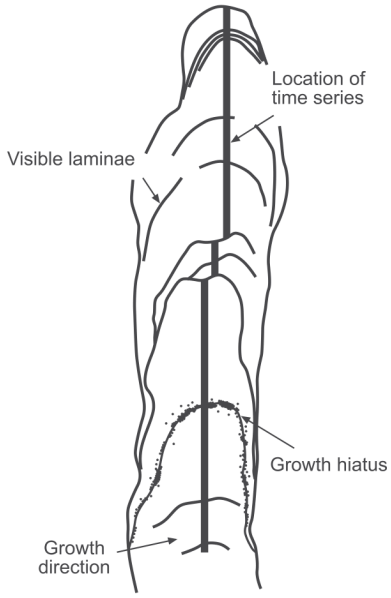

Figure 1.2: Schematic cross-section of a stalagmite with visible growth layers, a hiatus and a shift in position of the growth axis (reprinted by permission from Fairchild and Baker (2012)).

1.2 Dating of speleothems

To make use of the information that proxies can give about paleoclimate, it is indispensable to know the exact timing of events. This is especially important to understand the causes and effects of past climate changes. One method to determine the age of a speleothem is layer counting, similar to the counting of tree rings. However, this is only possible for speleothems that show visible annual layers and have been growing continuously without any hiatuses until the day of collection. If these conditions are not fulfilled, absolute dating methods are necessary. While wood and other organic materials that have been in exchange with atmospheric CO_2 during their formation can be dated using the radiocarbon (^{14}C) method, which reaches back up to 50,000 years (Fairbanks et al., 2005), this is not an option for old speleothems. The reason is that speleothems contain a mixture of dead carbon from the host rock and atmospheric carbon from plants and soil. However, the radiocarbon method provides accurate results for speleothems that are only a few decades old by using the ^{14}C peaks caused by nuclear bomb tests in the 1960s (Hua, 2009).

One of the greatest advantages of speleothems over other climate archives is that they can be absolutely dated using the ^{230}Th-U method, which allows dating to up to 640,000 years (Scholz and Hoffmann, 2008, Cheng et al., 2016). The method is based on the secular equilibrium that is reached between the activity of a daughter nuclide and the activity of its mother nuclide, provided that the half-life of the mother nuclide is much longer than the half-life of the daughter nuclide. For ^{234}U with a half-life of $T_{^{234}\mathrm{U}} = 2.453 \cdot 10^5$ a and its daughter nuclide ^{230}Th with a half-life of $T_{^{230}\mathrm{Th}} = 7.569 \cdot 10^4$ a, this condition is fulfilled (Fairchild and Baker, 2012). This means that after a sufficient time to reach the equilibrium, the quantity of ^{230}Th

atoms stays constant, because its rate of decay is the same as its rate of production by decay of ^{234}U.

The main principle of the ^{230}Th-U method is a natural disturbance of this equilibrium: U occurs mostly in the oxidation state U^{+6}, usually as water-soluble uranyl ion UO_2^{2+}, while Th occurs mostly in water-insoluble compounds with the oxidation state Th^{+4}. Consequently, U is transported with the dripwater and incorporated into the speleothem as uranium carbonate, while the insoluble Th cannot be transported by water and is therefore nearly absent in speleothem fabric (Ivanovich and Harmon, 1992). Once deposited, the speleothem constitutes a closed system, where no additional U or Th can get in or out. Over time, the decay of ^{234}U produces ^{230}Th and it is then possible to measure the degree to which the equilibrium has been restored since the formation of a specific layer of speleothem calcite by analyzing the ratio of ^{230}Th and ^{234}U.

Usually, several samples are dated along the growth axis of the speleothem. To determine the age of the layers in between the data points, an age-model is calculated, which describes the relationship between the age of a layer and its distance from top of the speleothem (Scholz and Hoffmann, 2011). In non-ideal samples, sometimes age reversals can occur, which means that stratigraphically younger samples are assigned an older age. This can be due to detrital Th that has been transported to the speleothem by adsorption onto particles. The analysis of ^{232}Th can indicate the presence of detrital Th. If the ratio of ^{232}Th to ^{230}Th is known, which is not always the case, the interference by detrital Th can be corrected. Other difficulties for the ^{230}Th−U method can be too low concentrations of U (Fairchild and Baker, 2012). To obtain best results, the ^{230}Th−U method can be combined with layer counting, and other radiometric methods can be used to validate the results. The state of the art for ^{230}Th−U dating is a precision (2 σ) of 100 years in samples that are up to 120,000 years old (Cheng et al., 2009).

As the decay of ^{234}U to ^{230}Th emits alpha radiation, one analytical technique to determine the ratio of ^{234}U and ^{230}Th is alpha spectrometry. However, this technique requires long measurement times of several days, a large sample size of more than 1 µg of total U, has an age limit of only 300,000 years and a precision of several % (Scholz and Hoffmann, 2008). Since the late 1980s, ^{230}Th−U dating is mostly done by mass spectrometry. Two techniques are possible here, thermal ionization mass spectrometry, TIMS, and multicollector inductively coupled plasma mass spectrometry, MC-ICP-MS. For TIMS, the sample solution is placed on a filament usually made of Rhenium, which is then heated and the chamber around evacuated, leading to evaporation and — to a small extent of approx. 1% — ionization of the analytes. The ions are then focused into the MS and separated by their mass-to-charge ratio by a magnetic analyzer. The measurement time for this technique is several hours, the sample size is in the range of tens to hundreds of ng of total U, and the precision is a few per mil. In MC-ICP-MS, the sample solution is nebulized in a spray chamber, mixed with Ar and injected into an inductively coupled plasma. In the approx. 8000 K hot plasma, more than 90% of the analytes are ionized. The ions are focused into the inlet of the MS, with 90% of the ions being lost. The double focusing analyzer in Nier-Johnson geometry consists of an electrostatic analyzer to

correct for different kinetic energies of the ions and a magnetic analyzer for the actual mass-to-charge separation. The transfer efficiency of the whole analyzing process is about 1%. The detection for both mass spectrometric techniques is similar and consists of a combination of faraday cups for the more abundant isotopes with ion beam intensities of more than 1 mV, and secondary electron multipliers for the minor isotopes. To avoid bias by unstable ion beam intensities, is is important to measure the isotopes simultaneously with several detectors, therefore the name multicollector. The measurement time of MC-ICP-MS is only 10-20 min per sample, only 5-10 ng of total U are needed, and the precision is comparable to TIMS with a few ‰ (Scholz and Hoffmann, 2008). Due to the smaller sample amounts and the faster analysis time, the MC-ICP-MS is the state-of-the-art technique for ^{230}Th−U dating and is used most frequently.

1.3 Proxies for the reconstruction of climate and paleo-vegetation in speleothems

In general, the signals preserved in speleothems can originate from the atmosphere (in the form of water, carbon dioxide or dust), the vegetation above the cave, the soil, the host rock or even the cave environment. Most elements and molecules are transported by water, though the transport can occur in different forms: in solution, as particles or bound to colloidal organic material. The incorporation into the speleothem can happen in various ways, too. The following sections 1.3.1 about stable isotopes, 1.3.2 about trace elements, and 1.3.3 about organic molecules will give a short overview over the most important proxies analyzed in speleothems.

1.3.1 Stable isotopes

The same analytical techniques as for the analysis of U and Th, MC-ICP-MS and TIMS (see section 1.2), can also be used to analyze stable isotopes of oxygen and carbon. Reviews about the analysis and interpretation of stable isotopes in speleothems are given for example in Fairchild et al. (2006), Fairchild and Baker (2012) and McDermott (2004). In the beginning of geochemical speleothem research in the 1970s, the hope was to be able to use oxygen isotopes (δ^{18}O) as a proxy for paleotemperature, since isotopic fractionation is temperature dependent and the cave temperature usually is a very close approximation of the mean annual air temperature. However, the processes in the karst and cave system as well as the influences on the isotopic composition of meteoric water turned out to be much more complicated than anticipated (Fairchild et al., 2006). The δ^{18}O values measured in the speleothem calcite are representative for the δ^{18}O values of the precipitation only if the deposition of the calcite happened in isotopic equilibrium with the dripwater. This means that no isotopic fractionation, for example by evaporation of water on the speleothem surface, must have occurred before the calcite precipitated. This is often the case in humid, temperate caves, but usually not in caves in arid or semi-arid climates (McDermott, 2004). The δ^{18}O values of meteoric water can be influenced by many

factors besides temperature, such as the $\delta^{18}O$ values of the oceans or surface water reservoirs where the cloud water comes from or the relative proportion of these different water sources. The latter varies depending on wind direction and large-scale weather patterns. The $\delta^{18}O$ values of oceans can be influenced over long time spans by the melting and freezing of the polar ice caps and by global circulation patterns such as the thermohaline circulation. Therefore, $\delta^{18}O$ values are used as proxies for changes in global circulation patterns, for example the North Atlantic Oscillation (NAO) (Mischel et al., 2017, Fairchild et al., 2006) or the El Niño-Southern Oscillation (ENSO) (Fairchild et al., 2006). However, the signal of these global effects can be disturbed by local effects on the $\delta^{18}O$ values of meteoric water, such as the so-called "amount effect", which describes the fact that the water from heavy rainfall events contains more light ^{16}O (lower $\delta^{18}O$) than average precipitation.

Stable carbon isotopes ($\delta^{13}C$) in speleothems can be influenced by the isotopic compositions of the soil CO_2 and of the host rock carbonate. In an open system, where the water in the epikarst is always in contact with the soil air, the cave dripwater $\delta^{13}C$ is only influenced by the soil CO_2. In regions with a vegetation consisting solely of C3-plants, $\delta^{13}C$ values of dissolved inorganic carbon in cave dripwater are around -14‰– -18‰. In a closed system, on the other hand, were there is no exchange with the soil air anymore after the beginning of the dissolution of $CaCO_3$ in the epikarst, the $\delta^{13}C$ values of the dripwater will be a mix of the soil gas $\delta^{13}C$ (around -23‰), and the host rock (arount +1‰), resulting in values around -11‰. In arid or semi-arid regions, often large shifts of $\delta^{13}C$ can be observed because of the shift from C3-plants ($\delta^{13}C$ of -26‰– -20‰) to C4-plants ($\delta^{13}C$ of -16‰– -10‰) (McDermott, 2004). This allows a straightforward interpretation, especially, if the vegetation change can be verified by pollen records from the same region. In temperate regions, where there is no natural occurring C4-vegetation, the interpretation of $\delta^{13}C$ values is more difficult. Higher $\delta^{13}C$ values can occur in very wet conditions, when the water runs through the soil too quickly to equilibrate completely with the soil air, resulting in more isotopically heavier atmospheric CO_2 and less lighter soil CO_2 being dissolved in the cave dripwater. On the other hand, higher $\delta^{13}C$ values in speleothems can also be caused by evaporation of cave dripwater and degassing of lighter CO_2 in the cave or, in connection with prior calcite precipitation, in the vadose zone above. These processes occur during drier conditions. Over longer time spans, the building up of soil thickness and increase in soil activity and therefore in soil pCO_2, for example at the transition from a glacial period to a period with warmer climate, can lead to decreasing $\delta^{13}C$ values in speleothems (McDermott, 2004). Because of the many different influencing factors, $\delta^{13}C$ analysis should ideally be accompanied by a multi-proxy analysis, for example of trace elements or molecular vegetation markers such as lignin oxidation products, to narrow down the choice of probable influencing factors.

1.3.2 Trace elements

An extensive overview over trace elements in speleothems as recorders of environmental change is given in Fairchild and Treble (2009). Most trace elements detected in speleothems originate from the bedrock, when it is dissolved by carbonic acid from the soil. For example, Mg and Sr mostly originate from carbonate bedrock, although

Sr can also come from clay minerals, and P usually stems from the mineral apatite. Many elements sourcing from the bedrock are first recycled by vegetation and soil organisms before they are transported to the cave. The atmosphere plays a minor role as source, though Mg and Sr can also come from sea-salt aerosols and Sr and Si can stem from aeolian dust. sulfur, mostly as sulphate ion, SO_4^{2-}, can indicate anthropogenic air pollution or volcanic activity (Fairchild and Treble, 2009).

Trace elements can be incorporated into the speleothem in different ways. Divalent ions of a suitable size, such as Mg^{2+} or SO_4^{2-}, substitute for Ca^{2+} or CO_3^{2-} ions in the crystal lattice. Other ions adsorb to defect sites in the crystal, especially Sr^{2+}, PO_4^{3-}, Na^+, Br^- and rare earth elements such as Y^{3+}. Singly and triply charged ions compensate in pairs to maintain the charge balance. Another possibility is the incorporation of elements associated to organic colloids or fine detrital particles, which often occurs in visible or fluorescent annual layers. This is often the case for PO_4^{3-}, Y^{3+} and other rare earth elements, and transition metal ions, e.g. Mn^{2+}, Cu^{2+}, Ni^{2+}, Zn^{2+} or Pb^{2+}, which can be complexed by organic matter. Soluble salts such as NaCl are often incorporated into the calcite matrix in aqueous fluid inclusions (Fairchild and Treble, 2009).

The most reliable trace element proxy so far is the covariance of Sr/Ca and Mg/Ca ratios, often accompanied by a covariance of $\delta^{13}C$. A simultaneous increase in these ratios indicates a drier climate with higher prior calcite precipitation. The reason is that the Mg-containing mineral dolomite dissolves more slowly than the Mg-free calcite, therefore the Mg/Ca ratio in the dripwater is usually low. When it is dry and the remaining water in the aquifer is stored long enough in one place, the slowly dissolving dolomite can lead to increased ratios of Mg/Ca in the dripwater. In addition, when PCP occurs, the Ca concentration in the dripwater decreases more than the concentration of trace elements such as Mg or Sr. Therefore, increased Mg/Ca and Sr/Ca ratios are good indicators for aridity and prior calcite precipitation. However, PCP can also be induced by falling pCO_2 in the cave atmosphere, e.g. by more efficient ventilation of the cave, instead of dryness. Therefore, a monitoring of the actual conditions in the cave is important (see 1.4).

Other possible influences on Mg concentrations can be dilution through heavy dripwater flow, and the routing of the dripwater, i.e. whether the drip point is fed by slow seepage flow or by faster crack flow. Strontium can also originate from aeolian dust and can therefore, under certain circumstances, be used as a proxy for a change in the prevailing wind direction. Moreover, Sr is an indirect proxy for growth rate and hydrology. It binds to defect sites on the crystal surface. When the speleothem grows faster, there are more defect sites to which the Sr can bind. When there are high concentrations of phosphate in the dripwater, which often happens because of flushing of organic colloids into the cave during autumnal storms, phosphate outcompetes Sr for the defect sites and Sr concentrations in the speleothem calcite decrease (Fairchild and Treble, 2009).

Autumnal storms and high infiltration events in general can flush organic material into the cave, which can be recorded as visible or fluorescent layers in speleothems. These layers are often associated with higher concentrations of many trace elements, especially P, Y, rare earth elements and transition metals such as Mn, Cu or Ni, which

are complexed and transported by organic colloids. It is not known whether these elements are incorporated into the calcite as free ions or still bound to the colloids. They can serve as proxies for high rainfall and infiltration, although they cannot yield a quantitative rainfall record. Sometimes, the increase in organic colloid transported trace elements can also happen as a consequence of deforestation, because the soil is not protected by a tree canopy anymore and can be flushed into the cave more easily. In general, however, trace elements can help to disentangle temperature and rainfall signals in stable isotopes, and the annual laminae of trace elements can help to determine exact annual growth rates of the speleothem, which is a proxy in itself.

Phosphorous is extensively recycled by the vegetation during the growing season. In summer, when there is a soil water deficit, P uptake of plants is limited. In autumn, when high infiltration events come together with the die-back of the vegetation, a peak concentration of P can be recorded in the speleothem. Over longer time periods, P concentrations in speleothems can be lower during drier and cooler climate periods because of reduced vegetation and soil activity. Uranium often shows similar trends as P because the uranyl ion, UO_2^{2+}, can be transported as uranyl-phosphate complex (Fairchild and Treble, 2009).

The most frequently used method for analysis of trace elements in speleothems today is laser ablation inductively coupled plasma mass spectrometry (LA-ICP-MS). The advantages of this technique are that it can be used for most elements, is fast, and can be automated, enabling long records with annual resolution on moderate to fast growing speleothems. If a smaller spot size down to 1µm and hence higher temporal resolution is needed, electron microprobe, secondary ionization mass spectrometry (SIMS) or micro X-ray fluorescence spectrometry can be used. However, these techniques are either slower, not sensitive enough for all trace elements, or, in the case of the latter, require synchrotron radiation, which is not always available. A problem for SIMS and LA-ICP-MS is the need for matrix-matched standards, which are difficult to obtain in sufficient homogeneity. The best accuracy and lowest detection limits, though with larger samples size, can be obtained by drilling, dissolving the sample powder in dilute acid and analyzing by ICP-MS. For higher concentrated elements, also atomic absorption spectrometry (AAS) or inductively coupled plasma optical emission spectrometry (ICP-OES) are possible techniques (Fairchild and Treble, 2009).

1.3.3 Organic molecules

The amount of organic carbon in speleothems is very low, it is estimated to be around 0.01–0.3% of total carbon (Blyth et al., 2016). However, the analysis of organic matter (OM) in speleothems can yield valuable information about paleovegetation and climate conditions. Organic molecules preserved in speleothems can originate from the overlying vegetation, the soil or the vadose and be transported into the cave by water, or they can be generated directly in the cave by microbial communities. The transport by water can occur as dissolved organic matter (DOM), as suspended organic colloidal particles, or the organic molecules can be adsorbed to fine mineral particles.

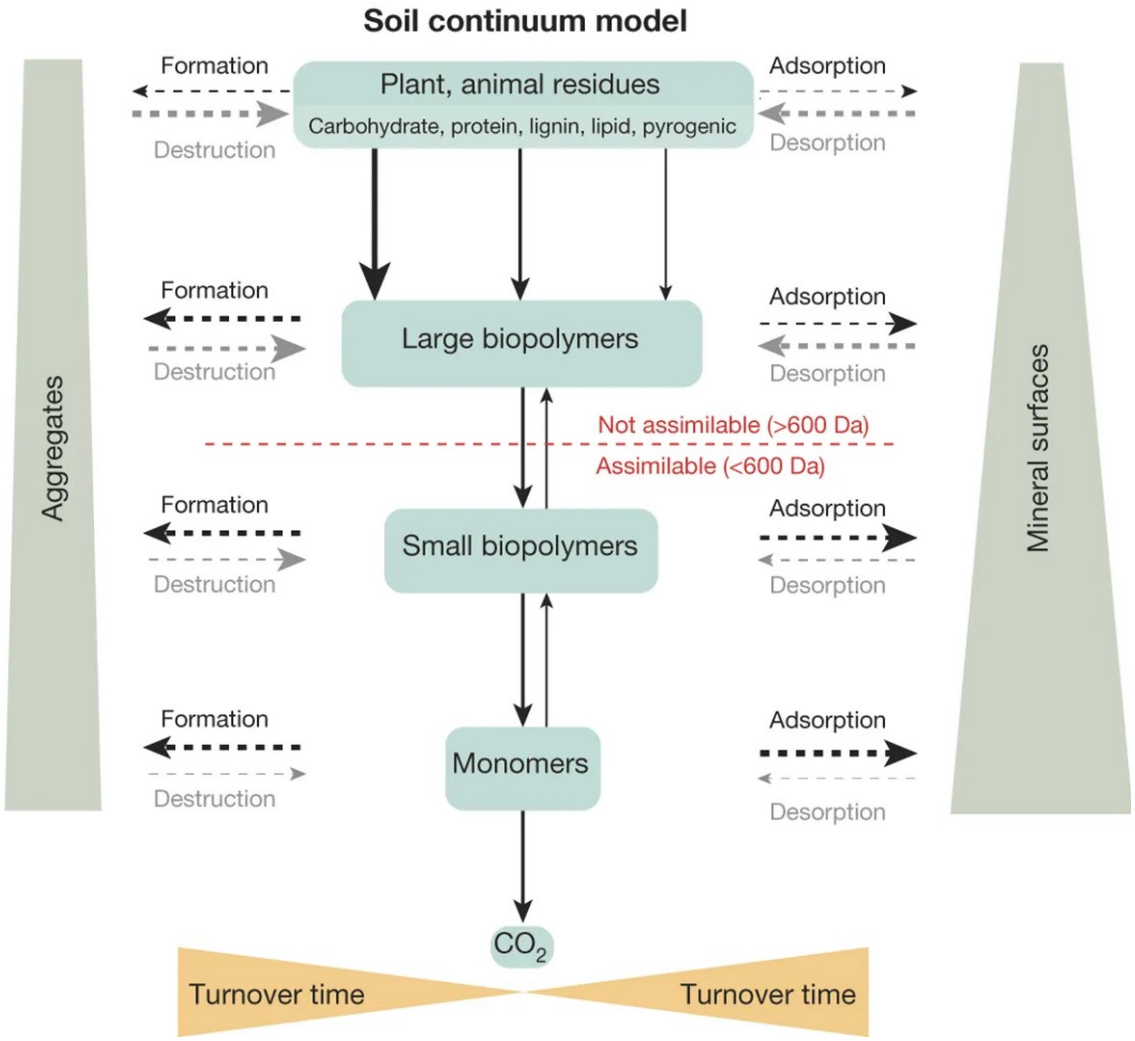

Figure 1.3: Soil continuum model according to Lehmann and Kleber (2015) (reprinted by permission from Lehmann and Kleber (2015)).

In general, the decomposition of soil organic matter can be described by the soil continuum model (SCM, Fig. 1.3), which was established by Lehmann and Kleber (2015). The model states that organic residues of plants and animals, e.g. carbohydrates, proteins, lignin, lipids and pyrogenic material, are continuously degraded by microbial communities in the soil, from large biopolymers to smaller biopolymers to monomers and finally to CO_2. In any state of decomposition, larger self-assembled aggregates of organic molecules can form or be destroyed again, and molecules can adsorb or desorb on mineral surfaces. With increasing decomposition, the oxidation state of the molecules increases, resulting in better water solubility. At the same time, a higher oxidation state also leads to an increased affinity of adsorption on mineral surfaces. The rate of microbial decomposition depends on temperature, humidity and additional energy sources for the decomposer organisms, but also on the accessibility of the organic matter, whereby mineral adsorption and formation of aggregates hamper the accessibility. Shen et al. (2015) compare the transport of

OM through the soil column with a chromatography, with the most hydrophilic and least bioavailable substances having the shortest retention time, more hydrophobic substances being preferentially adsorbed to mineral surfaces and more bioavailable substances being decomposed by microorganisms.

For the analysis of organic molecules as environmental proxies in speleothems, this means that the amount and composition of OM preserved in speleothems depends on the way of transport through the vadose zone: fracture flows transport more particulate and colloidal OM, whereas water from porous seepage flows contains mostly dissolved organic matter. Therefore, flowstones fed by fracture flow will contain more OM and also a different composition of OM than stalagmites or soda straws formed by seepage water.

The analysis of organic proxies in speleothems is a small but growing research area. Most often, OM in speleothems is analyzed as total organic carbon (TOC) or by fluorescence spectroscopy (Blyth et al., 2008). Fluorescence spectroscopy of speleothems is mostly used to determine annual layers and changes in growth rate (Baker et al., 2015, Driese et al., 2016) or flow regime (Orland et al., 2012). A combination of fluorescence spectroscopy and TOC analysis allows high resolution two-dimensional mapping of OM content in speleothems (Quiers et al., 2015), but only limited information on the composition of OM, although the fluorescence wavelength can yield information on hydrophobicity and aromaticity of OM. Newer non-destructive or minimally destructive approaches are the use of electron paramagnetic resonance spectroscopy (Perrette et al., 2015), which can yield "fingerprints" of OM sources, and laser micropyrolysis coupled to gas chromatography coupled to mass spectrometry (La-Py-GC-MS)(Blyth et al., 2015), which allows the molecular analysis of organic inclusions in speleothems. However, both approaches need further research on their applicability as proxies for OM in speleothems.

The analysis of molecular organic proxies in speleothems usually requires larger samples sizes of 0.2–20 g calcite (Blyth et al., 2016). The calcite matrix is dissolved by acid digestion and the organic matter is extracted from the solution by liquid-liquid extraction, soxhlet extraction or solid phase extraction (Blyth et al., 2006, 2016). Special care must be taken to avoid contamination during laboratory handling, especially for ubiquitous substance classes such as lipids. A thorough cleaning procedure and regular blank control samples are necessary (Wynn and Brocks, 2014).

Bacterial membrane lipids, glycerol dialkyl glycerol tetraethers (GDGTs), have been analyzed in speleothems and are shown to originate from microbial communities inside the cave or even on the speleothem surface (Blyth et al., 2014, Baker et al., 2016, 2019). The speleothem GDGT TEX86 index can be used as a relatively robust paleothermometer (Blyth, Shutova and Smith, 2013, Baker et al., 2019). Also of microbial origin are low molecular weight fatty acids with a chain length of C_{12}–C_{20}, which have been used as proxies for microbial activity in the soil and the cave system (Blyth et al., 2011, Bosle et al., 2014). Longer chain *n*-alkanes with a marked odd-over-even preference in chain length have been analyzed as proxies for plant leaf waxes, using the ratio of n-alkanes with a chain length of C_{31} to n-alkanes with a chain length of C_{29} or C_{27} to differentiate between grassy and woody vegetation (Xie, 2003, Blyth et al., 2007, 2011). However, this interpretation was later challenged by

a meta-analysis by Bush and McInerney (2013), which found that the use of chain length distributions to derive vegetation types was not robust.

According to Blyth et al. (2016), the most promising avenue for the reconstruction of paleovegetation from speleothems is the analysis of lignin phenols. Lignin phenols originate from higher plants only, that means they have a defined source, they are less prone to laboratory contamination than lipds, and they can give information not only about the abundance, but also about the type of vegetation. Qualitative analysis of liginin phenols using thermochemolysis in the presence of tetramethylammonium hydroxide (TMAH) coupled to gas chromatograph–mass spectrometry (GC-MS) has revealed the presence of lignin derived compounds in speleothems (Blyth and Watson, 2009, Blyth et al., 2010), but no quantitative records have been produced yet. The characteristics, analysis and interpretation of lignin as a vegetation proxy is discussed in more detail in chapter 2.

Further new approaches are the analysis of OM in speleothems or cave dripwater via high resolution mass spectrometry (fourier transform ion cyclotron resonance mass spectrometry, FT-ICR-MS), enabling a "fingerprinting" of organic matter (Lechleitner et al., 2017), or the analysis of stable carbon isotopes (δ^{13}C) of the OM enclosed in speleothems. The latter can be done either of bulk organic matter (Blyth and Schouten, 2013, Li et al., 2014, Lechleitner et al., 2019) or compound specific, e.g. for plant-derived *n*-alkanes (Blyth, Smith and Drysdale, 2013) or fatty acids (Wang et al., 2019). This method promises new insights into the fate of organic carbon in the soil, the influence of OM on the δ^{13}C signals preserved in speleothems, and, when combined with ^{14}C analysis (Lechleitner et al., 2019), about the provenance and age of OM in speleothems.

1.4 Cave monitoring and analysis of cave dripwater

For a better understanding of the processes involved in the formation of speleothems, the transport of environmental proxies and the various influences on signal variability, it is helpful to systematically monitor a cave system for a longer period, ideally several years. These cave monitoring programs often involve the measurement of air and water temperature, air pressure and humidity, carbon dioxide concentrations, radon activity, air movements, and the discharge of drips and cave streams (Fairchild and Baker, 2012). As most proxies in speleothems are transported by water, their concentrations should be measured in the dripwater as well. Regular, e.g. monthly measurements over a longer period of time make it possible to observe seasonal changes in dripwater discharge and composition (Mischel et al., 2015, Mischel, 2016). Especially for organic proxies, it is also useful to trace their path from the soil through the aquifer to the cave by analyzing soil water, dripwater from sites with different discharge rates, and water from cave pools. Artificial irrigation of the site above a cave can be used to study various cave processes Rutlidge et al. (2014, 2015). In this context, size exclusion chromatography coupled to organic carbon detection (LC-OCD) was applied to divide organic matter in cave dripwater in different fractions, such as biopolymers and humic substances (Rutlidge et al., 2015), and the sources of speleothem GDGT composition were elucidated (Baker et al., 2016). Other cave

dripwater studies investigated how trace metals are transported by natural organic matter from the soil to the cave by using TOC, fluorescence spectroscopy and ICP-MS analysis (Hartland et al., 2012) or followed the molecular transformations of dissolved organic matter on its journey from the surface to the cave by using FT-ICR high resolution mass spectrometry.

2 Lignin as a vegetation proxy

Lignin is an aromatic biopolymer and one of the main constitutents of wood and woody parts of plants. Accounting for about 30% of the organic carbon in the biosphere, lignin is the second most abundant biopolymer after cellulose. Forming parts of the secondary cell walls, lignin gives the plant stability and mechanical strenght. Due to its hydrophobicity, it also plays an important role in water transport, and it protects the cells from pathogens and the polysaccharides in the cell walls from microbial degradation (Vanholme et al., 2010). The lignin polymer consists mainly of three monomers: p-coumaryl alcohol, guaiacyl alcohol and syringyl alcohol. These so-called monolignols are polymerized in a radical coupling mechanism under combinatorial control (Boerjan et al., 2003), which is described in section 2.1.

The resulting polymer is highly recalcitrant towards chemical and biological degradation. In nature, only white-rot fungi are able to completely degrade and mineralize lignin to CO_2, whereas brown-rot fungi and possibly some other microorganisms are only able to induce structural changes to lignin (Kögel-Knabner, 2002). As lignin is a waste product in the paper industry with millions of tonnes produced every year, there is a strong interest in using this renewable raw material to produce value-added low-molecular weight substances. Therefore, different ways to depolymerize lignin are currently explored, and depolymerization is also necessary to analyze the composition of lignin (section 2.2).

The relative resistance to microbial degradation makes it possible to use lignin as a vegetation proxy, which will be discussed in section 2.3. In natural surface waters such as rivers and oceans, lignin is used as a marker for terrestrial plant material – as opposed to material from algae and aquatic plants (Opsahl and Benner, 1997). In climate archives, such as marine and lacustrian sediment cores as well as peat cores and speleothems, lignin can be used as a vegetation proxy to reconstruct the vegetation of the past (Jex et al., 2014). The particular advantage of lignin compared to other vegetation proxies is that it not only preserves information about the abundance of vegetation, but also about the type of vegetation: The ratio of the three aforementioned monolignols forming the lignin polymer varies between different types of plants. By analyzing these ratios, it is possible to distinguish between angiosperms and gymnosperms and between woody and non-woody plants. However, there are still many open questions concerning the transport and alteration of lignin in the soil, as well as the influence of analytical sample pretreatment steps.

2.1 Lignin structure and biosynthesis

Lignin is a complex aromatic polymer resulting from the oxidative radical coupling of p-hydroxyphenylpropanoid monomers (Boerjan et al., 2003, Ralph et al., 2004,

Vanholme et al., 2010). It consists mainly of three monomers differing in their degree of methoxylation: p-coumaryl alcohol $\mathbf{M_H}$, coniferyl alcohol $\mathbf{M_G}$ and sinapyl alcohol $\mathbf{M_S}$ (Fig. 2.1 **a)**), which are synthesized from the amino acid phenylalanine. In the polymer, the generic lignin units formed from these monolignols are called p-hydroxyphenyl $\mathbf{P_H}$, guaiacyl $\mathbf{P_G}$ and syringyl $\mathbf{P_S}$ units, (Fig. 2.1 **b)**). Lignin from gymnosperm (softwood) plants consists mainly of $\mathbf{P_G}$ units and low levels of $\mathbf{P_H}$ units, whereas lignin from dicotyledonous angiosperm (hardwood) plants consists of $\mathbf{P_G}$ and $\mathbf{P_S}$ units with only traces of $\mathbf{P_H}$ units. Lignin from grasses (monocots) incorporates $\mathbf{P_G}$ and $\mathbf{P_S}$ units and higher levels of $\mathbf{P_H}$ units than dicots (Boerjan et al., 2003).

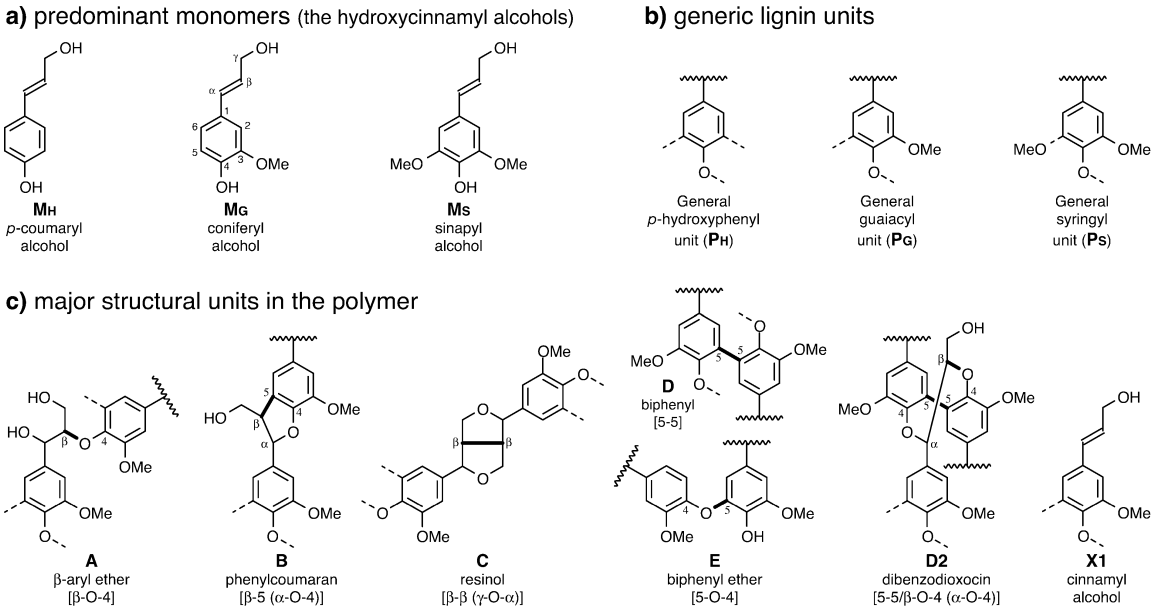

Figure 2.1: **a)** Predominant monomers (or monolignols) **M**. **b)** Generic lignin polymer units **P**. **c)** Major structural units in the polymer; the bolded bonds are the ones formed in the radical coupling reactions (reprinted by permission from Ralph et al. (2004)).

Besides the three main monolignols, various other monomers can be incorporated into the lignin polymer during the lignification process (Fig. 2.2). For example, up to 10% of the lignin units in grass and 17% in maize were found to be γ-*p*-coumarate monomers **M11**, and kenaf bast fibers contain up to 50% of γ-acetylated monomers **M9**. In addition, the ferulates $\mathbf{M4_G}$ (**M4** with one methoxy group) are involved in cross-linking lignins and polysaccharides in grasses, accounting for up to 1% of the cell wall mass (Ralph et al., 2004).

After their synthesis, the monolignols (4-hydroxycinnamyl alcohols) are transported to the cell wall, were they are dehydrogenated at the 4-hydroxy-position by peroxidase and possibly also laccase enzymes (Vanholme et al., 2010). The resulting monolignol radicals are stabilized by electron delocalisation, with single-electron density situated at the O-4 position, the positions 1, 3 and 5 of the benzene ring, and the β-position of the side chain (see Fig. 2.1 **a)** for atom numbering). The radicals can now couple with other monolignol radicals to build dimers or with a preformed

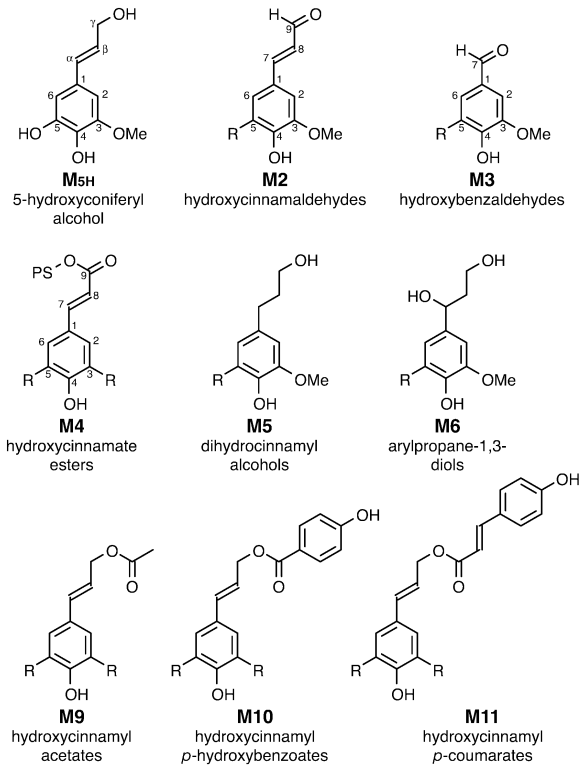

Figure 2.2: Other monomers that can be incorporated into the lignin polymer (reprinted by permission from Ralph et al. (2004)).

lignin oligomer radical. Although the coupling with other monolignol radicals is the preferred reaction, this option is hindered by the rate of monolignol supply and radical formation. The growth of the lignin polymer is not a radical chain reaction, but consists of repeated recombinations of two radicals. Since the growing lignin polymer is too bulky to be dehydrogenated in the substrate channel of the peroxidase enzyme, the monolignol radicals also function as radical shuttles transferring their radical character to other mono- or oligomers, coupling only if they encounter another radical (Vanholme et al., 2010). The preferred coupling position of the monolignol radicals is the β position, and of the lignin oligomers, where the β position is already occupied, the O-4 position. Therefore, the most frequent inter-unit linkage is the [β-O-4] β-aryl ether linkage (Fig. 2.1 **c) A**). This is also the only linkage that can be cleaved easily by chemical methods such as thioacidolysis and the chemical pulping processes applied in the paper industry (Boerjan et al., 2003, Ralph et al., 2004). Other common linkages, which are all more resistant to chemical degradation, are the [β-5 (α-O-4)] linkage producing the phenylcoumaran **B**, the [β-β (γ-O-4)] linkage giving the resinol **C**, the [5-5] biphenyl linkage **D** and the [5-O-4] biphenyl ether linkage **E** (Boerjan et al., 2003). Since the position 5 is occupied in $\mathbf{P_S}$ units, the [β-5 (α-O-4] and [5-O-4] linkages can only occur when at least one of the coupling partners is a $\mathbf{P_G}$ or $\mathbf{P_H}$ unit, or both partners for the [5-5] linkage. As a result, lignin with a high contribution of $\mathbf{P_S}$ units (e.g. hardwood) is less branched, because the [5-O-4] and [5-5] linkages represent branching points in the polymer. However, the degree of branching is generally low even in gymnosperm lignin (Ralph et al., 2004),

and the chain length has been found to be between 13 and 20 monomers in poplar lignin (Vanholme et al., 2010). An example of a lignin polymer structure is shown in Fig. 2.3.

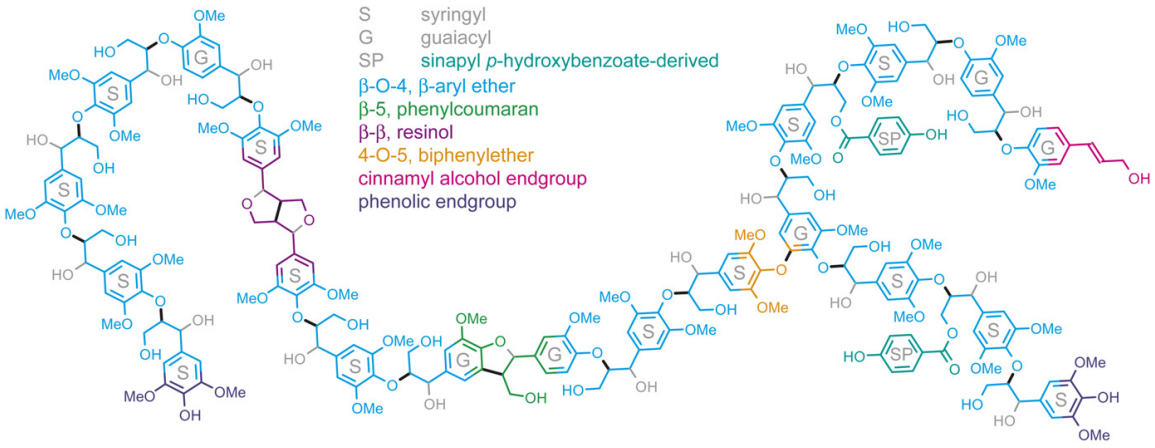

Figure 2.3: Example of a lignin polymer structure from poplar wood as predicted from NMR-based analysis (reprinted by permission from Vanholme et al. (2010)).

2.2 Depolymerization of lignin

Lignin is very resistant to chemical and biological degradation because it is held together by strong C-C and ether bonds and because it forms a complex three-dimensional network that makes it difficult for degrading enzymes to access it. White-rot fungi are the only organisms that are able to completely mineralize lignin, while brown-rot and soft-rot fungi are only able to induce structural changes to the lignin polymer (Kögel-Knabner, 2002, Ruiz-Dueñas and Martínez, 2009). Ligninolytic fungi secrete high-redox-potential peroxidase enzymes, which are able to abstract one electron from the benzene ring of the lignin units. The resulting unstable radical cations undergo various consecutive reactions, including the breaking of C_α–C_β bonds and C_β–O–4 ether bonds. These bond breakdown reactions release the corresponding aromatic aldehydes, e.g. vanillin in the case of a guaiacyl unit, which are then intracellulary mineralized by the fungi (Ruiz-Dueñas and Martínez, 2009). The rate of lignin biodegradation in the soil depends, among other things, on the availability of other, more easily accessible organic substances, which serve as an energy source for the degrading organisms (Klotzbücher et al., 2011).

Lignin not only accounts for approximately 30% of organic carbon in the biosphere, but it is also a waste product in the pulp and paper industry with millions of tons produced every year, which are mainly burned for energy production. In times of progressive depletion of oil reserves and increasing environmental consciousness, numerous approaches to transform lignin into renewable fuel or valuable chemical building blocks are currently explored. These approaches include, among others, thermal degradation/pyrolysis, acid or base catalyzed hydrolysis, homogeneous or

heterogeneous catalytic oxidation or hydrogenation, electrochemical or photochemical conversion, and enzymatic degradation (Brebu and Vasile, 2010, Pandey and Kim, 2011, Xu et al., 2014, Zakzeski et al., 2010, Zirbes and Waldvogel, 2018, Li et al., 2016). Depending on whether the goal is quantity – usually obtained as an unspecific mixture of high and low molecular weight products – or selectivity, all methods require a more or less complex clean-up procedure. For example, Schmitt et al. (2015) applied electrochemical conversion using nickel anodes followed by adsorption on anion exchange resins to obtain approx. 1 wt% of vanillin out of an aqueous alkaline Kraft lignin solution. The mechanism of the electrochemical depolymerization of lignin using nickel electrodes was desribed by Pardini et al. (1991) and Miao et al. (2014) and involves single electron transfer from a nickel oxyhydroxide (NiOOH) species (Fig. 2.4). Electrolytic methods are also explored for the analytical degradation of lignin in this work and will be further discussed in chapter 2.

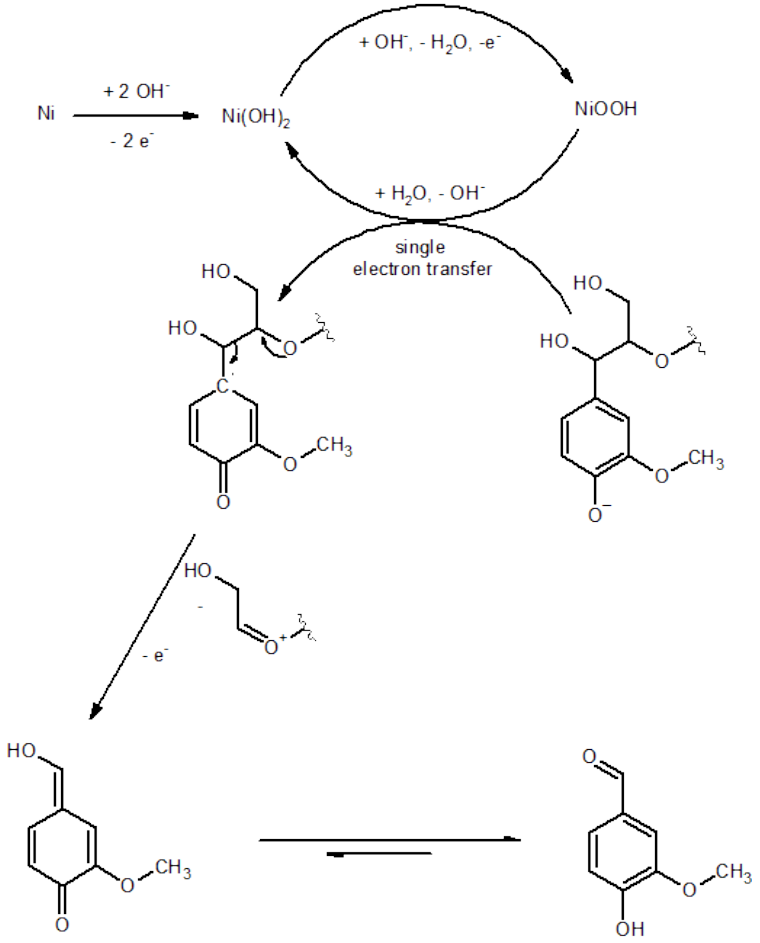

Figure 2.4: Mechanism of the electrolytic depolymerization of lignin using Ni electrodes according to Pardini et al. (1991) and Miao et al. (2014).

The aim of analytical lignin degradation methods is to obtain information about the composition and structure of the lignin polymer. Therefore, the original structure should be altered as little as possible by the degradation method, but the polymer should be converted into monomeric lignin units, which can be analyzed by chro-

matographic and mass spectrometric methods. The most commonly used analytical lignin degradation method is alkaline oxidation with copper(II)-oxide, developed by Hedges and Ertel (1982) based on previous work by Pearl (1967) and Sarkanen and Ludwig (1971). In this method, a lignin containing sample (plant material, soil, sediment or aqueous solution) is mixed in an oxygen-free atmosphere with 2 M sodium hydroxide solution, CuO as oxidizing agent and $Fe(NH_4)_2(SO_4)_2 \cdot 6\,H_2O$ as oxygen scavenger, and the mixture is heated to 150–170 °C for 1.5–3 h in a pressure-tight vessel. The method produces so-called lignin oxidation products (LOPs): specific aldehyde, methyl ketone and acid derivatives of the lignin phenols (Fig. 2.5). The

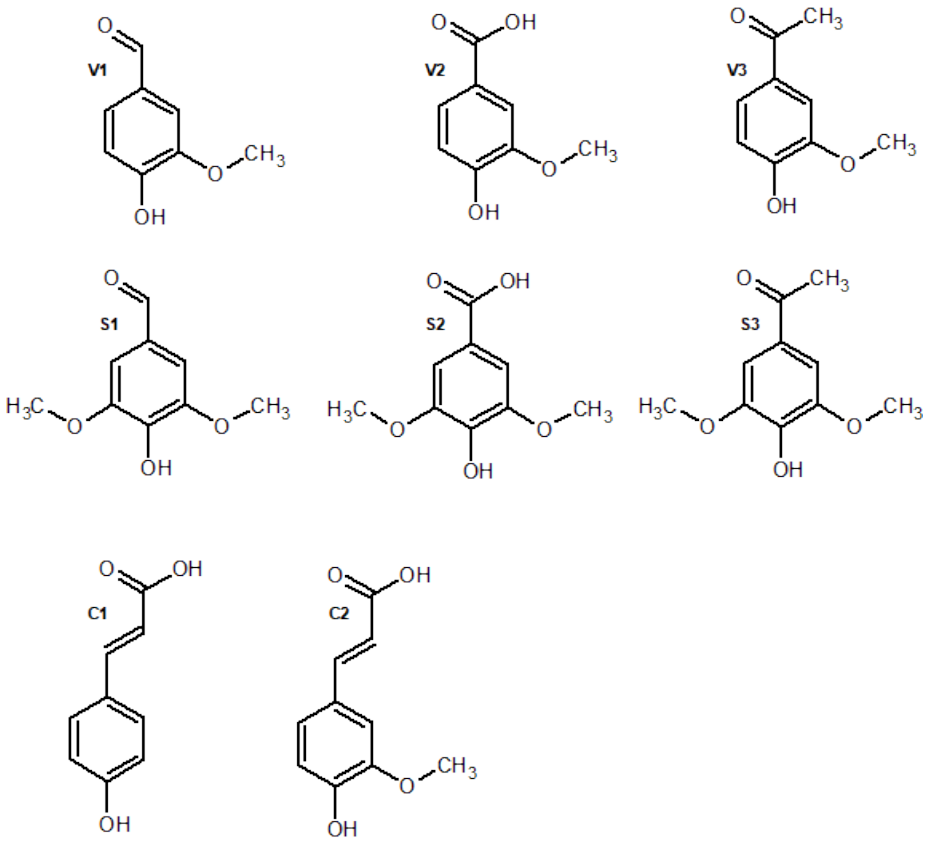

Figure 2.5: Products of lignin depolymerization via CuO oxidation according to Hedges and Ertel (1982). Products of the vanillyl group: **V1** vanillin, **V2** vanillic acid, **V3** acetovanillone. Products of the syringyl group: **S1** syringaldehyde, **S2** syringic acid, **S3** acetosyringone. Products of the cinnamyl group: **C1** *p*-hydroxycoumaric acid, **C2** *trans*-ferulic acid.

mechanism of alkaline oxidation of lignin is not yet fully elucidated; both ionic and radical pathways have been proposed in literature (Schutyser et al., 2018). However, the most conclusive mechanism so far consists of sequential single-electron oxidations of phenolat ions followed by a retroaldol reaction forming aldehyde molecules (Fig. 2.6, Tarabanko et al. (2004), Tarabanko and Tarabanko (2017), Schutyser et al. (2018)). The formation of aceto derivatives (e.g., acetovanillone) can be explained by the same retroaldol mechanism passing via a γ-hydroxy-α-carbonyl aldol instead

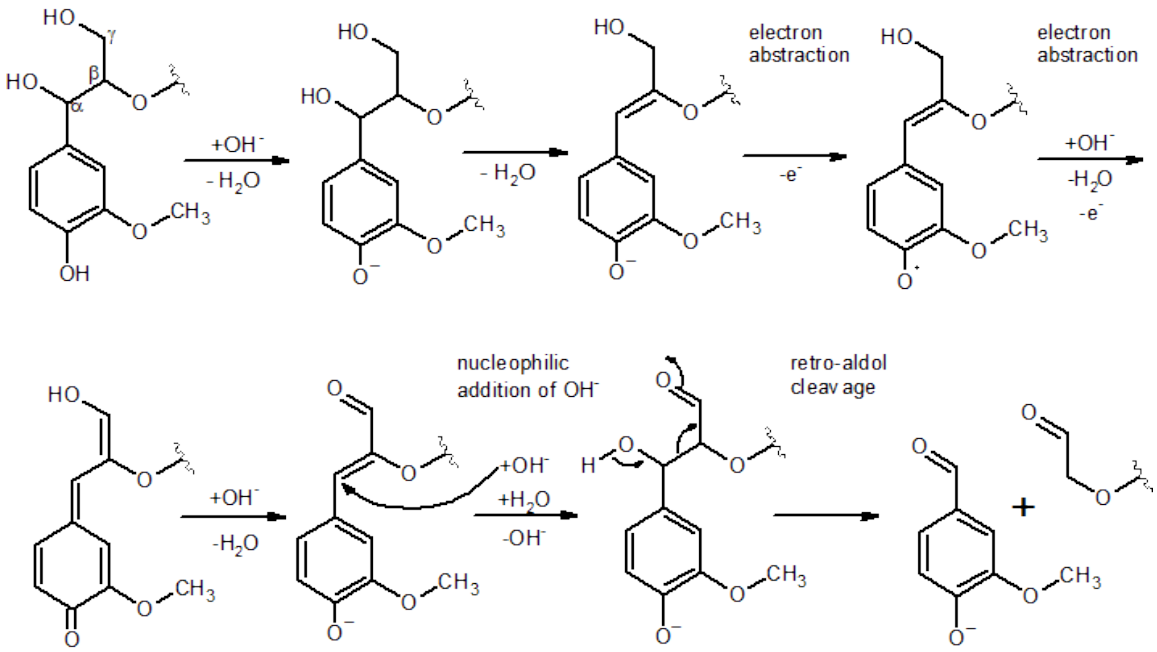

Figure 2.6: Mechanism of the depolymerization of lignin by CuO oxidation according to Tarabanko et al. (2004) and Schutyser et al. (2018).

of an α-hydroxy-γ-carbonyl aldol in the last step and occurs as a side reaction. Acid derivatives (e.g., vanillic acid) can be produced from microbially or geochemically altered lignin units that already have an α-carbonyl group before analytical depolymerization (Tarabanko et al., 2004). The redox potential of the redox pair CuO/Cu_2O with -0.16 V at pH 14 is sufficient for the oxidation of lignin to aldehydes, but low enough not to cause excessive oxidation of the product aldehydes (Schutyser et al., 2018). The presence of oxygen, however, can lead to over-oxidation of the formed aldehydes, therefore an inert atmosphere is necessary.

Other common methods for analytical lignin degradation include the oxidation with nitrobenzene (Freudenberg et al., 1940), which is similar to the CuO oxidation method, but has the disadvantage of producing a number of organic byproducts that can interfere with the analysis of lignin phenols (Hedges and Ertel, 1982), and thermochemolysis with tetramethylammonium hydroxyde (TMAH) (Hatcher et al., 1995). The latter method consists of heating the dry sample together with an excess of TMAH to 250–400 °C for 30 min. The mechanism for lignin degradation by TMAH thermochemolysis has been described by Filley et al. (1999). In strongly alkaline conditions, the α- or γ-hydroxyl groups of a lignin unit can form an intramolecular epoxide, eliminating a phenolate ion from the β-position (Fig. 2.7). The epoxide is then opened by a nucleophilic attack of a methoxide ion in α-, β- or γ-position. All remaining hydroxyl and phenolate groups are subsequently methylated by TMAH. As the epoxides are highly unstable, they can undergo a number of rearrangements that can lead to the formation of aldehyde, ketone and ester products (Fig. 2.8). TMAH thermochemolysis can only cleave β-O-4 bonds that have a hydroxyl group on an adjacent carbon atom. Microbial or geochemical alterations of lignin can reduce the number of such β-O-4 bonds with adjacent hydroxyl group, therefore the yield

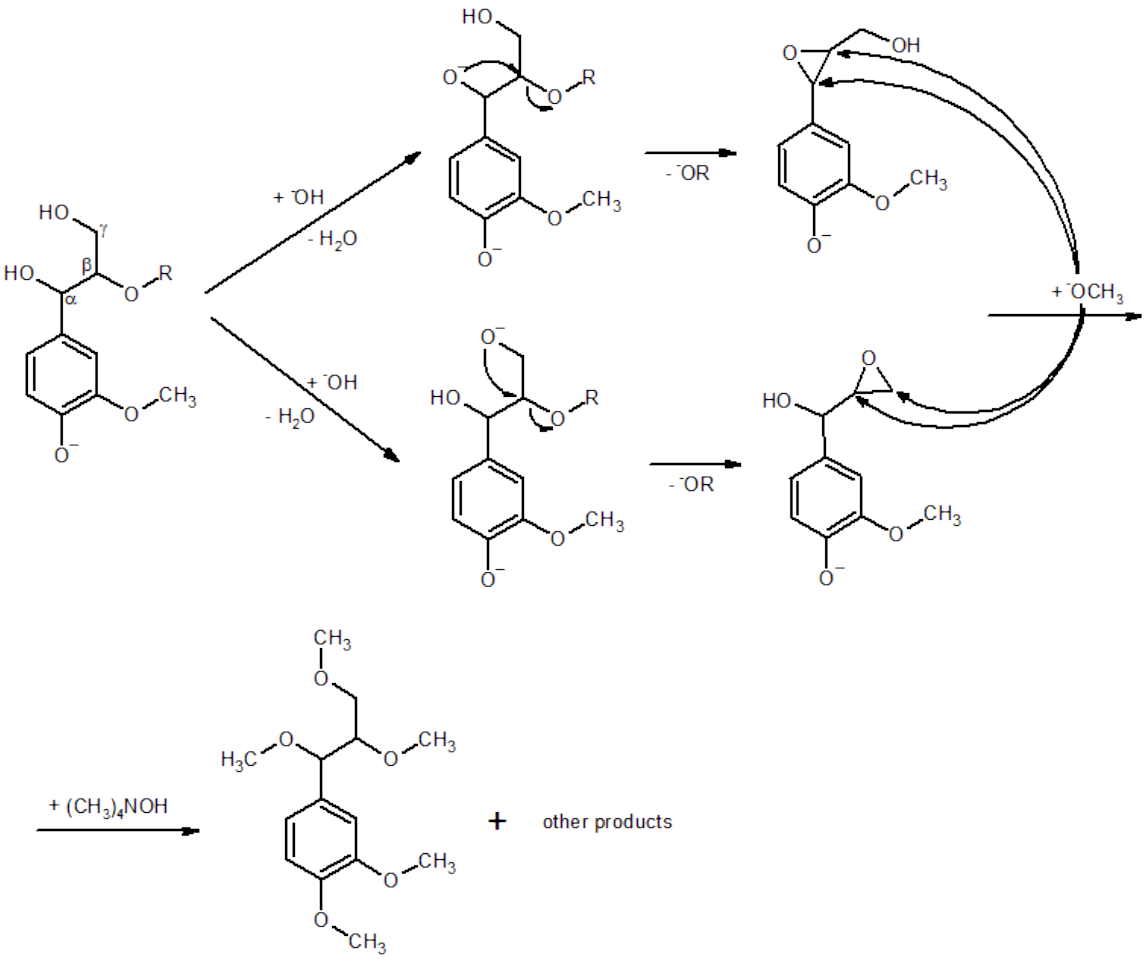

Figure 2.7: Mechanism of lignin degradation by TMAH thermochemolysis according to Filley et al. (1999).

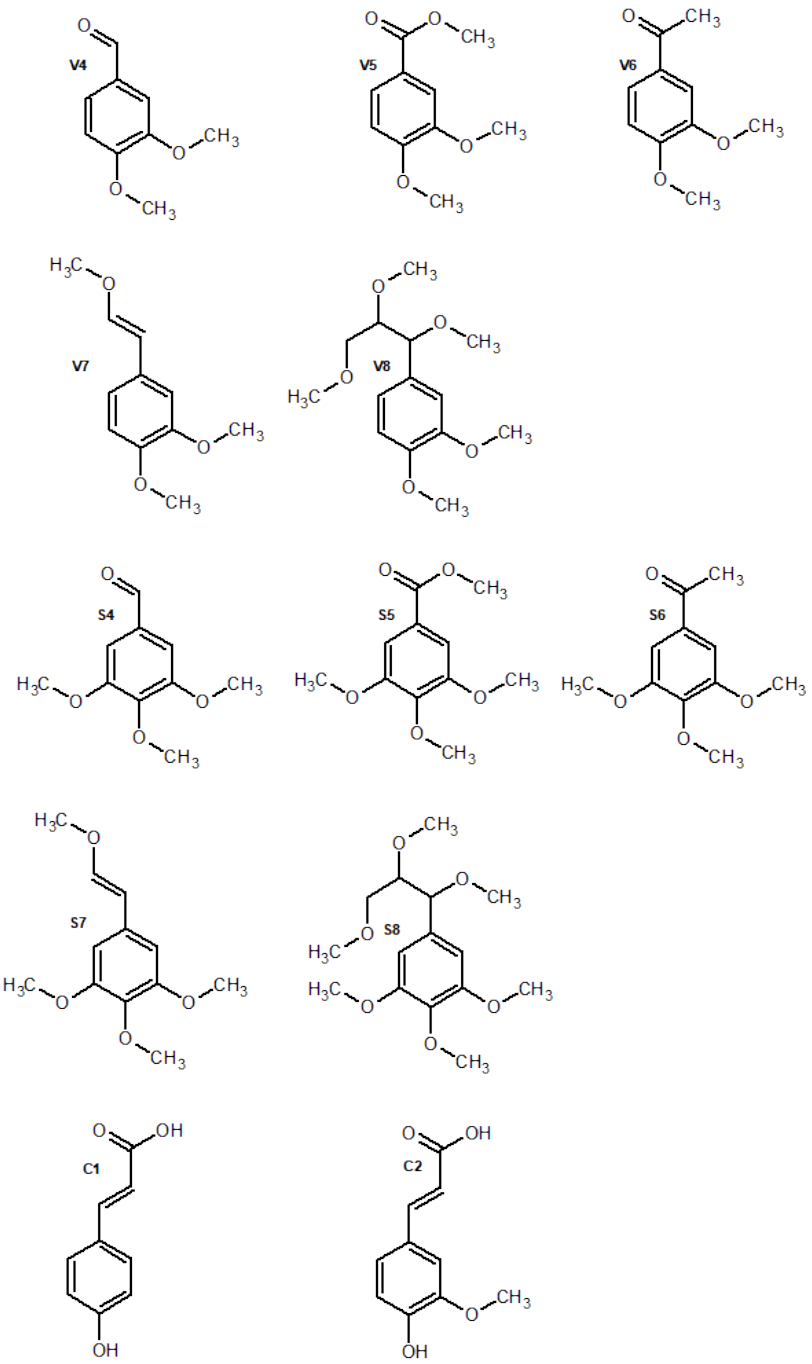

Figure 2.8: Products of lignin depolymerization via TMAH thermochemolysis according to Wysocki et al. (2008).

of TMAH thermochemolysis is higher for fresh lignin and lower for more degraded lignin.

Several studies have compared TMAH thermochemolysis and CuO oxidation for the analytical degradation of lignin and stated significant differences in the results due to the different depolymerization mechanisms (Hatcher et al., 1995, Wysocki et al., 2008, Klotzbücher et al., 2011, Younes and Grasset, 2018). CuO oxidation usually gives higher overall yields of lignin phenols, especially for microbially or geochemically altered lignin, because it can cleave ether and C–C bonds, while TMAH thermochemolysis is only able to cleave labile β-O-4 ether and hydrolyzable ester bonds. In addition, the resulting compound mixture of CuO oxidation is simpler and more specific for lignin, while TMAH yields a more complex product mixture that also includes products from tannins and other non-lignin sources, which cannot be distinguished from lignin-derived products. However, the latter problem can be solved by using isotopically labeled TMAH, which allows to distinguish between methyl groups that were already present in the source material and those that were introduced during thermochemolysis (Wysocki et al., 2008, Klotzbücher et al., 2011). Nevertheless, the source indicators used to differentiate between different types of plants, which are discussed in detail in section 2.3, differ significantly between CuO oxidation and TMAH thermochemolysis and should not be compared directly without taking into account the different mechanisms (Wysocki et al., 2008).

2.3 Analysis of lignin phenols as a vegetation proxy

The analytical method for the analysis of lignin oxidation products has been optimized many times. Hedges and Ertel (1982) used an oven with Parr bombs for the CuO oxidation at a temperature of 170 °C and a duration of 3 h, liquid-liquid extraction (LLE) with ethyl ether to extract the LOPs from the aqueous digestion solution, derivatization with trimethylchlorosilane, and finally gas chromatography (GC) with flame ionization detection (FID) for quantification and GC coupled to mass spectrometry (MS) for identification of the LOPs. Goñi and Montgomery (2000) developed a microwave digestion method applying 150 °C for 90 min for the CuO oxidation step. In addition, they used ethyl acetate instead of ethyl ether as a solvent for the LLE. Other groups replaced the LLE by the faster solid phase extraction (SPE)(Kögel and Bochter, 1985, Kaiser and Benner, 2012), or used high-performance liquid chromatography (HPLC) coupled to UV-detection instead of GC-FID or GC-MS, which does not require a derivatization step (Lobo et al., 2000, Sun et al., 2015). Yan and Kaiser (2018a) developed an analysis method using ultrahigh-performance liquid chromatography (UHPLC) coupled to electrospray ionization (ESI) triple quadrupole mass spectrometry (QqQ-MS). This UHPLC-ESI-QqQ-MS method is similar to the UHPLC-ESI-HRMS method developed in this work, but both methods were developed independently. For the analysis of LOPs in natural water samples, usually an extraction and enrichment step with SPE cartridges is required before the CuO oxidation, but direct CuO oxidation of water samples is also possible (Reuter et al., 2017). In addition, Yan and Kaiser (2018b) developed a new lignin depolymeriza-

tion method for ultralow sample volumes (200 µL) using soluble $CuSO_4$ instead of insoluble CuO.

The CuO (or $CuSO_4$) oxidation of lignin releases a number of phenolic acids, aldehydes and ketones, which can be divided into four groups: The vanillyl group (V) consisting of vanillic acid, vanillin and acetovanillone, the syringyl group (S) consisting of syringic acid, syringaldehyde and acetosyringone, the cinnamyl group (C) consisting of trans-ferulic acid and p-coumaric acid, and the p-hydroxyl group (P) consisting of p-hydroxybenzoic acid, p-hydroxybenzaldehyde and p-hydroxyacetophenone (Fig. 2.5). Hedges and Mann (1979) and Hedges and Parker (1976) analysed fresh plant tissues of 23 different plant species and showed that the composition of the obtained lignin oxidation products (LOPs) varies between plant types. Gymnosperm plants (i.e. non-flowering plants, e.g. conifers) yield only phenols of the vanillyl group, whereas angiosperm plants (i.e. flowering plants, e.g. hard wood trees, herbs and grasses) yield phenols of the vanillyl and the syringyl group. The C-group phenols, p-coumaric acid and trans-ferulic acid, are only obtained from non-woody plant tissues. Consequently, Hedges and Mann (1979) introduced the LOP parameters S/V, to distinguish between gymnosperm (S/V = 0) and angiosperm (S/V > 0) plants, and C/V, to distinguish between woody (C/V = 0) and non-woody (C/V > 0) plant tissues. When the S/V ratio is plotted versus the C/V ratio, the different plant types plot in specific regions of the diagram (Fig. 2.9). Tareq et al. (2004) combined the information from S/V and C/V ratios in the one-dimensional *lignin phenol vegetation index*, LPVI, which is defined in equation (2.1).

$$LPVI = \left(\frac{S(S+1)}{V+1} + 1\right) \cdot \left(\frac{C(C+1)}{V+1} + 1\right) \tag{2.1}$$

The phenols of the p-hydroxyl group (P) can originate from gymnosperm and non-woody angiosperm plant tissues, but are also oxidation products of the amino acid tyrosin and can be obtained from non-vascular plants (Hedges and Parker, 1976) and protein rich organisms, such as bacteria and plankton (Jex et al., 2014). Therefore, the P-group phenols are not used in the parameters to determine lignin sources. The parameter Σ_8 is the sum of the eight phenols of the C-, S- and V-group related to the sample size and is used to represent the total lignin concentration in a sample. Similar parameters are Λ_8, which is the sum of the same 8 phenols related to 100 mg of organic carbon in the sample, and Λ_6, which is the sum of the 6 phenols of the S- and V-group related to 100 mg of organic carbon in the sample.

Controlled biodegradation studies of lignin with white rot and brown rot fungi showed that syringyl phenols were degraded faster than vanillyl phenols, and that the concentration of aldehyde LOPs decreased faster than the concentration of ketone LOPs, while the concentration of vanillic acid even increased with the duration of degradation (Hedges et al., 1988). Therefore, Hedges et al. (1988) introduced the ratios of vanillic acid to vanillin, $(Ac/Al)_V$, and syringic acid to syringaldehyde, $(Ac/Al)_S$, as indicators for the degradation state of lignin, with ratios of $(Ac/Al)_V > 0.6$ and $(Ac/Al)_S > 0.16$ indicating highly degraded lignin. However, Hernes et al. (2007) later showed that similar and even higher acid-to-aldehyde ratios can be reached by fractionation of lignin through leaching and sorption to mineral surfaces, thus questioning the applicability of these ratios to determine degradation state.

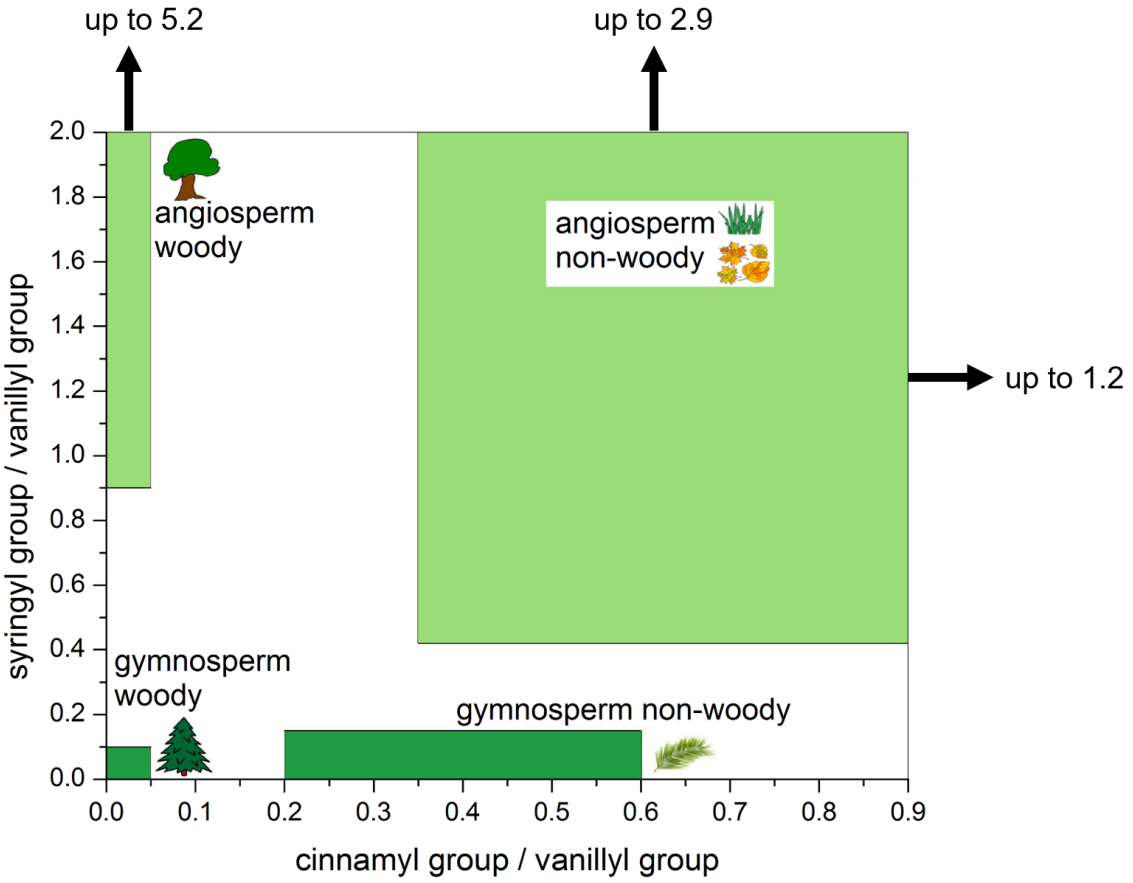

Figure 2.9: Scatter plot of the syringyl group-to-vanillyl group (S/V) ratio versus the cinnamyl group-to-vanillyl group (C/V) ratio for the determination of lignin sources. The boundaries are according to Hedges and Mann (1979) and Jex et al. (2014) and references therein.

Lignin oxidation products have first been used as marker compounds to trace the origin and transport of land derived organic matter in natural surface waters and have been analyzed in marine sediments (e.g., Hedges and Parker, 1976, Loh et al., 2008, Zhang et al., 2013) and dissolved and particulate organic matter in rivers and oceans (e.g., Standley and Kaplan, 1998, Hernes and Benner, 2002). Since the early 1990s, LOPs have also been analyzed as proxies for vegetation change in Quarternary archives such as peat cores, lake sediments, salt marsh and marine sediment cores (see review by Jex et al., 2014). In speleothems, lignin has been highlighted as a promising vegetation proxy in several reviews (Blyth et al., 2008, Jex et al., 2014, Blyth et al., 2016), and Blyth and Watson (2009) have successfully detected lignin derived phenols in speleothems using TMAH thermochemolysis. However, no quantitative analysis of LOPs has been conducted in speleothems so far.

The advantage of peat and sediment cores over speleothems is that they contain much higher amounts of organic carbon and thus of lignin. However, speleothems have unique advantages as described in chapter 1, for example, they can be absolutely dated up to 640 000 years back in time without loss in time resolution. It is therefore useful to develop an analytical method for the analysis of trace concentrations of lignin preserved in the calcite matrix of speleothems. Moreover, since lignin is only produced by vascular plants and not, for example, by microorganisms, it is much more specific than the vegetation proxies previously used in speleothems, e.g. n-alkanes or fatty acids (Jex et al., 2014). Therefore, LOPs can help to interpret other vegetation markers, trace elements and stable isotopes in speleothems.

Although the sources of lignin are well defined, there are still many open questions concerning the fate of lignin in the soil, its interaction with minerals and, in the case of speleothem archives, its transport from the soil through the karst system into the cave. According to Thevenot et al. (2010), the composition of measurable LOPs in the soil depends not only on the type of vegetation, climate and land-use, but also on the soil depth and particle size. Hernes et al. (2007) observed a fractionation of lignin phenols caused by the processes of leaching of plant litter and sorption of the leachate to mineral surfaces, resulting in an up to ten-fold increase of C/V, S/V and acid-to-aldehyde ratios compared to the unprocessed plant litter. Moreover, a fraction of the lignin apparently can be bound irreversibly to mineral surfaces, and this fraction depends both on the type of mineral and on the type of lignin (Hernes et al., 2013). According to Hernes et al. (2013), this could mean that the biochemical signature conserved in the soil or sediment of a given landscape could be less representative of the original vegetation, but more indicative of the mineral preferences for certain compounds. In any case, these effects could alter the original source-dependent LOP signals, especially the C/V and S/V ratios, and thus complicate their interpretation with regard to vegetation changes in Quarternary archives such as speleothems . Therefore, it is important to study the transport of lignin from the surface through the soil and the aquifer to the cave. A better understanding of the various influences on the LOP signals can be achieved for example by analyzing and comparing LOPs in soil, cave dripwater and speleothem samples of different sites and different seasons.

3 Analytical methods and instruments

The analytical method developed and applied in this work is shown schematically in Fig. 3.1. The speleothem sample is dissolved in hydrochloric acid and the resulting acidic solution is extracted with solid phase extraction (SPE). The eluent is then subjected to alkaline CuO oxidation in a microwave assisted digestion method. The oxidized sample solutions are again extracted and enriched by SPE, and the LOPs are then separated and detected by ultrahigh-performance liquid chromatography coupled to electrospray ionization high-resolution mass spectrometry (UHPLC-ESI-HRMS).

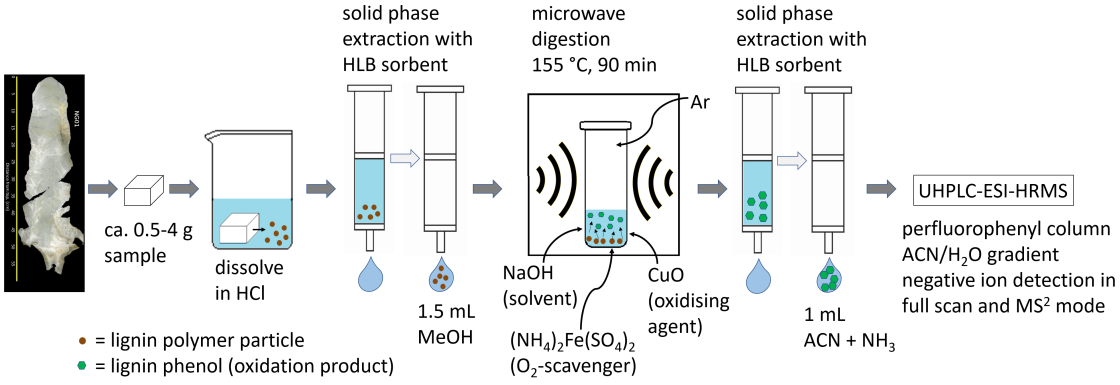

Figure 3.1: The analytical method developed and applied in this work.

The analytical techniques and instruments applied in this method, i.e. solid phase extraction (section 3.1), liquid chromatography (section 3.2) and mass spectrometry (section 3.3), are briefly described in the following sections.

3.1 Solid phase extraction

Solid phase extraction (SPE) is a quick and easy extraction technique for enriching samples with very low concentrations and removing matrix components. It was invented in the 1970s as an alternative to conventional liquid-liquid extraction, which consumes a lot of solvent, uses cumbersome glassware and often has the problem that emulsions are formed (Thurman and Mills, 1998). Detailed descriptions of SPE can be found in various reviews and monographies, e.g. Thurman and Mills (1998), Hennion (1999), or Poole (2003a). The sample solution to be extracted passes through an SPE cartridge, which contains a stationary phase (sorbent). Similar to the stationary

phase in liquid chromatography (section 3.2), this sorbent can be silica-based or polymeric and have a reversed phase, normal phase or ion exchange functionality. In case of a reversed phase sorbent, unpolar analytes are retained on the stationary phase while the aqueous solution with dissolved ionic or strongly polar matrix components passes through the cartridge. The analytes are then eluted from the cartridge with a small volume of an organic solvent and thereby concentrated, while more strongly adsorbed unpolar matric components remain retained on the sorbent.

A typical SPE method is shown in Fig. 3.2. Before adding the sample solution, the stationary phase must be conditioned with an organic solvent (**a** in Fig. 3.2). This serves as a cleaning step and also to open up the alkyl chains of the stationary phase so that they can be wetted by water (McDowell et al., 1986). The aqueous sample is then applied by positive pressure, gravity or a vacuum manifold and runs through the cartridge (**b**). Care must be taken to ensure a slow and uniform drip rate so that the analytes have time to adsorb on the stationary phase. Subsequently, in one or more washing steps, the less strongly bound, polar matrix components are washed out of the cartridge (**c** and **d**), before the analytes are eluted with a suitable solvent (**e**). Matrix components which are more strongly bound than the analytes are retained in the cartridge and thus also separated. If the eluent for the analytes is not miscible with water, or if water in the eluate interferes with further analysis, a drying step must be inserted between the washing step and the elution. Compared to

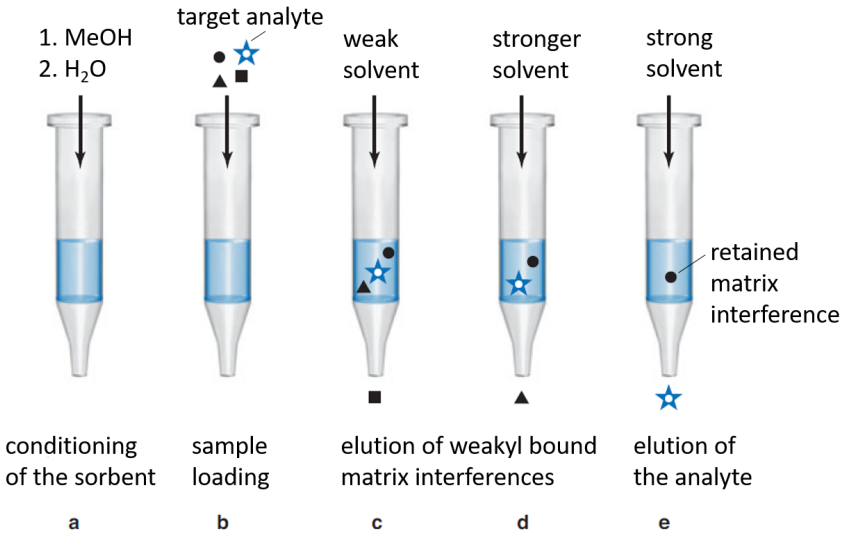

Figure 3.2: Procedure of a solid phase extraction (adapted from Harris (2014)).

conventional liquid-liquid extraction, SPE has the advantages that less solvent is used and that the method is faster and easier to automate, making it suitable for large numbers of samples. For many years, porous silica gels, which have a surface area of 500-600 $g \cdot cm^{-2}$, with chemically bonded alkyl chains, especially dodecyl (C18) and decyl (C8), were mainly used as reversed-phase SPE sorbents (Hennion, 1999). Due to steric hindrance between the alkyl chains, some free silanol groups always remain on the silica surface, which can provide an additional retention mechanism

for more polar analytes, but also strongly bind analytes with basic functional groups. Depending on the target analytes, these remaining silanol groups can be endcapped with trimethylsilanes or remain non-endcapped. However, the retention of very polar analytes with silica-based sorbents remains challenging. In addition, silica-based sorbents are stable only in a pH range of 2–8 (Poole, 2003a). Today, many different polymeric phases based on a poly(styrene-divinylbenzene) copolymer with high surface areas of 700–1200 $g \cdot cm^{-2}$ are available. They are stable in the full pH range, and the high surface area provides higher retention (Poole, 2003a). One limitation of both reversed-phase silica sorbents and many polymeric sorbents is that they need to be conditioned with a wetting solvent before loading the aqueous sample and must not run dry at any time (Hennion, 1999). Polymeric sorbents that are functionalized with polar groups, such as the poly(divinylbenzene-N-vinylpyrrolidone) copolymer (Oasis HLB, Fig. 3.3), do not show these limitations and provide better retention for polar analytes (Poole, 2003a, Hennion, 1999).

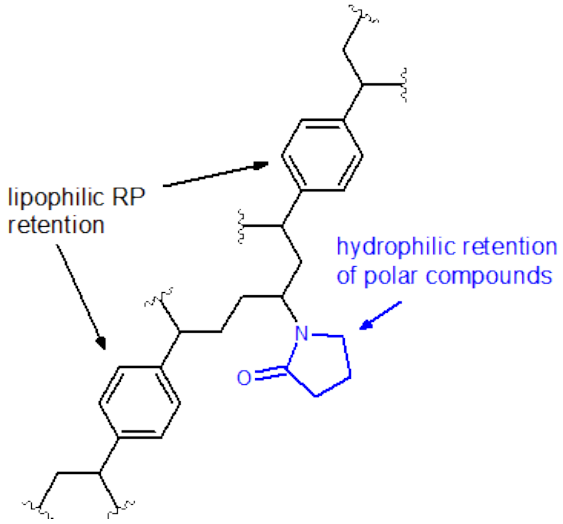

Figure 3.3: Structure of the poly(divinylbenzene-N-vinylpyrrolidone) copolymer of the Oasis HLB sorbent.

3.2 High performance liquid chromatography

Chromatography is an analytical separation method based on the different distribution coefficients of analytes between a mobile phase and a stationary phase. The movement of the mobile phase relative to the stationary phase leads to a repeated adjustment of the distribution equilibrium between the two phases. The mobile phase can be gaseous (gas chromatography, GC) or liquid (liquid chromatography, LC). GC is often preferred because it is cheaper, has a greater separation efficiency and consumes less solvent. However, it is only suitable for analytes that are sufficiently volatile and thermally stable, and it often requires derivatization. Therefore, for many rather polar analyte classes in environmental and life science, LC and especially reversed-phase LC is the method of choice (Harris, 2014). The principles and

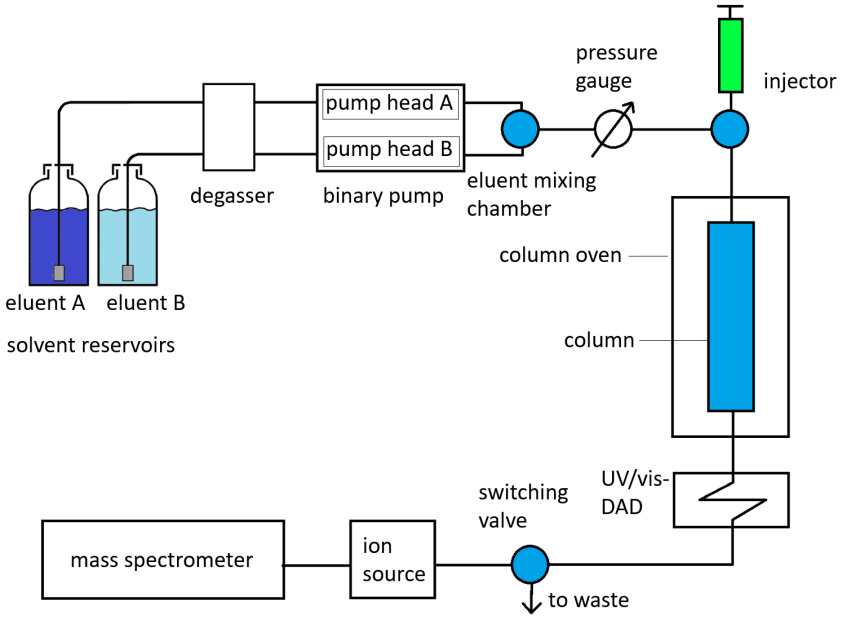

Figure 3.4: Schematic setup of a HPLC system with UV/vis diode aray detection (UV/vis-DAD) coupled to a mass spectrometer.

developments of high-performance liquid chromatography (HPLC) are described in many textbooks and monographies, e.g. Poole (2003b), Harris (2014) or Skoog et al. (2018).

The schematic setup of an HPLC system is shown in Fig. 3.4. The two eluents A and B are pumped from the solvent reservoirs and first pass through a degasser. Here, dissolved gases, especially nitrogen and oxygen, are removed from the solvents, since these could otherwise outgas from the compressed solvents in the column and thus impair the reproducibility of the separation. Reversed phase chromatography mainly uses water and either acetonitrile or methanol as eluents, which can be mixed in the mixing chamber. The separation method can be performed isocratically with a constant eluent composition or as a gradient program with changing eluent composition over time. The choice of the eluent composition and the gradient is decisive for a successful separation of the analytes. The injector injects the sample solution via a six-way valve and a sample loop into the eluent stream, which transports it to the separation column.

In reversed phase HPLC, chemically modified silica gel is mainly used as column material. These are porous, spherical microparticles whose hydroxyl groups on the surface are modified with alkyl chains, e.g. n-octyl (C8), n-octadecyl (C18), phenyl or pentafluorophenyl (PFP) chains. While the alkyl chains of C8 and C18 phases provide only hydrophobic interactions with the analyte, polar interactions can be introduced by leaving some of the silica hydroxyl groups uncapped. Phenyl and PFP phases provide additional selective retention of aromatic analytes by pi stacking. The separation column can be heated by a column oven, which is particularly advantageous for strongly retained or poorly soluble analytes.

After the separation column, the eluate passes through the detector chamber of, for example, a UV/vis, fluorescence or electrochemical detector. In Fig. 3.4, a UV/vis diode array detector (UV/vis-DAD) is shown, which is a detector with a continuous radiation source in the ultraviolet and visible range allowing the detection of the entire spectrum via a diode array. Provided that the analytes have double bonds or free electron pairs and are thus UV/vis active, they can be identified by their spectrum or each analyte can be quantified at the wavelength of its strongest absorption band using Lambert-Beer's law. This detection is non-destructive and can be combined with additional mass spectrometric detection.

To separate many compounds in a short analysis time, a high resolution is necessary. The chromatographic resolution R of two analytes A and B is defined in equation (3.1),

$$R = \frac{t_R(\mathrm{B}) - t_R(\mathrm{A})}{\frac{1}{2}\left(w_{base}(\mathrm{A}) + w_{base}(\mathrm{B})\right)} \tag{3.1}$$

with the respective retention times t_R(A) and t_R(B) and the baseline widths w_{base}(A) and w_{base}(B). To obtain a high resolution, a narrow baseline width of the signals must be achieved. The broadening of the signals depends mainly on diffusion. Since diffusion in liquids is slow, the diffusion paths in a LC column must be short to allow a fast adjustment of the distribution equilibrium between the two phases. Therefore, only packed columns are used in LC, compared to capillary columns used in GC. The distance the mobile phase travels in the separation column until the distribution equilibrium is reached is called the height equivalent to a theoretical plate (HETP). The smaller the HETP and the longer the separation column, i.e. the greater the number of separation stages N_{th}, the better the separation.

The van Deemter equation (3.2) relates the HETP, which is proportional to signal broadening, to the eluent velocity u and the different parameters responsible for signal broadening.

$$HETP = A + \frac{B}{u} + C \cdot u \tag{3.2}$$

A describes the influence of eddy diffusion on signal broadening. This means that two similar analyte molecules must randomly travel different distances in the column and therefore arrive at the detector at different times. The smaller the particles in the column, the smaller these random path differences become and the narrower the signals are. In Fig. 3.5, the van Deemter equation is plotted for different particle sizes of the stationary phase. The B term describes the influence of the longitudinal diffusion of the molecules in the column. This term is almost irrelevant in LC, since the diffusion coefficients in liquids are very small, but for GC it must be taken into account. The C term describes the influence of mass transfer, i.e. the finite rate at which the distribution equilibrium between stationary and mobile phase is reached. This is mainly determined by the diffusion coefficients of the molecules in the liquid and by the path length between the particles that the molecules have to overcome by diffusion. Here, too, smaller particles contribute to a better separation performance, as they allow a faster equilibrium adjustment due to shorter diffusion paths. In addition, smaller particles allow a considerably higher flow velocity of the mobile phase without increasing the HETP, as can be seen from the graph in Fig. 3.5, thus

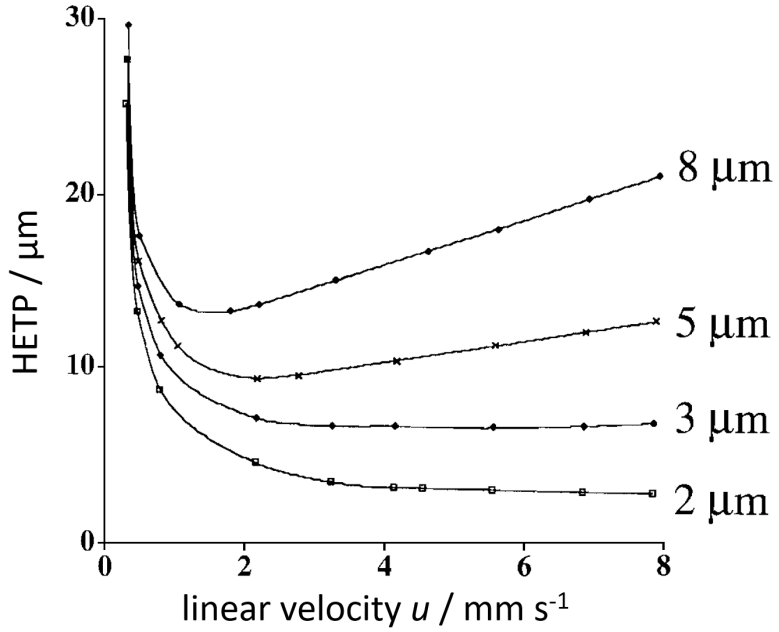

Figure 3.5: Van Deemter equation relating the height equivalent to a theoretical plate, *HETP*, to the linear velocity u of the mobile phase, plotted for different particle sizes (adapted by permission from Poole (2003b)).

enabling shorter analysis times. For these reasons, the trend in HPLC is towards ever smaller particle diameters. However, as the particle diameter d_p decreases, not only the number of separation stages N_{th} increases, but also the back pressure p in the column, as shown in equations (3.3) and (3.4) (Harris, 2015),

$$N_{th} \approx \frac{3000 \cdot L\,[\mathrm{cm}]}{d_p\,[\mu\mathrm{m}]} \tag{3.3}$$

$$p = f\frac{u\eta L}{\pi r^2 d_p^2} \tag{3.4}$$

where L is the length and r the radius of the column, η is the viscosity of the mobile phase and f is a factor depending on particle shape and packing. While for HPLC with particle diameters of 3–5 µm a pressure of 70–400 bar was sufficient, the newer ultrahigh-performance liquid chromatography (UHPLC) with particle diameters of $1.5 - 2.0$ µm requires pressures of up to 1000 bar. In addition, the UHPLC columns must be very thin in order to sufficiently dissipate the frictional heat generated by the dense packing. With a particle diameter of 1.7 µm, the column diameter should not be thicker than 2.1 mm (Harris, 2014). Due to the high flow rate and high separation power, the analysis time with UHPLC is reduced to about one tenth compared to conventional HPLC, so that even complex analyte mixtures can be separated within a few minutes.

3.3 Mass spectrometry

Mass spectrometry is probably the most widely applicable analytical technique and the most powerful detector for chromatography. It can be used to clarify the structure and elemental composition of inorganic, organic and biological molecules as well as for the qualitative and quantitative analysis of complex mixtures. There are many textbooks and monographs on mass spectrometry, for example Gross (2017), Skoog et al. (2018) or Harris (2015). At this point only a short overview of the instruments used in this work shall be given.

The main principle of mass spectrometry (MS) is the separation of ions in an electromagnetic field according to their mass-to-charge ratio. To achieve this, the mass spectrometer consists of the following parts (Fig. 3.6): An inlet and an ionization source to form gaseous ions out of uncharged molecules or atoms, a mass analyzer to perform the actual separation of the mass-to-charge ratios (m/z), and a detector. Since a certain mean free path length of the ions is necessary to perform their sepa-

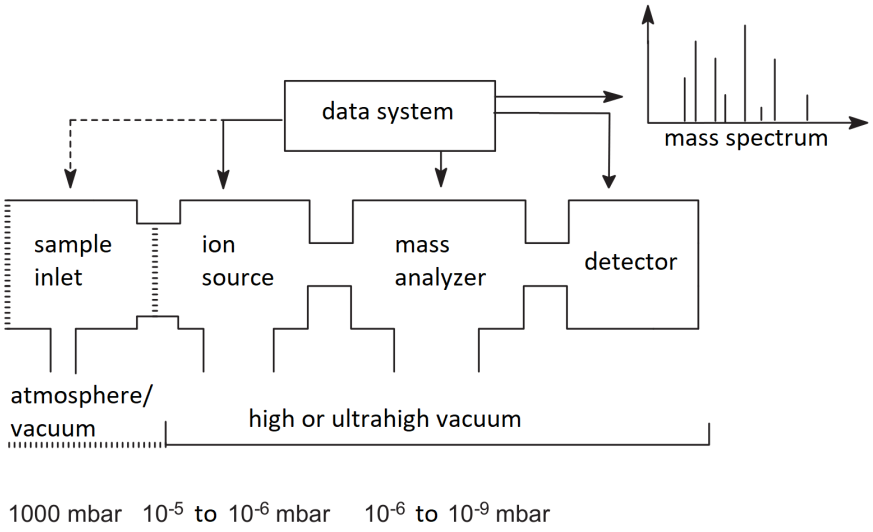

Figure 3.6: Schematic setup of a mass spectrometer (adapted by permission from Gross (2017)).

ration and detection, a high-performance vacuum system is required. A data system is used to control all components of the mass spectrometer and to save and analyze the resulting data.

In this thesis, a Q Exactive™ Hybrid Quadrupole-Orbitrap Mass Spectrometer from Thermo Scientific was used, whose schematic setup is shown in Fig. 3.7. As ion source, an electrospray ionization (ESI) source is used, which will be described in section 3.3.1. Alternatively, an atmospheric pressure chemical ionization (APCI) source can be applied. The ions are guided via an S-lens and a curved ion guide into a linear quadrupole analyzer (described in section 3.3.2), where precursor ions for tandem MS can be selected. From there, the ions are transferred via a transfer octapole to a C-trap, which can store ions and inject an ion packet very rapidly into the Orbitrap. Alternatively, the ions can be transferred from the C-trap into a

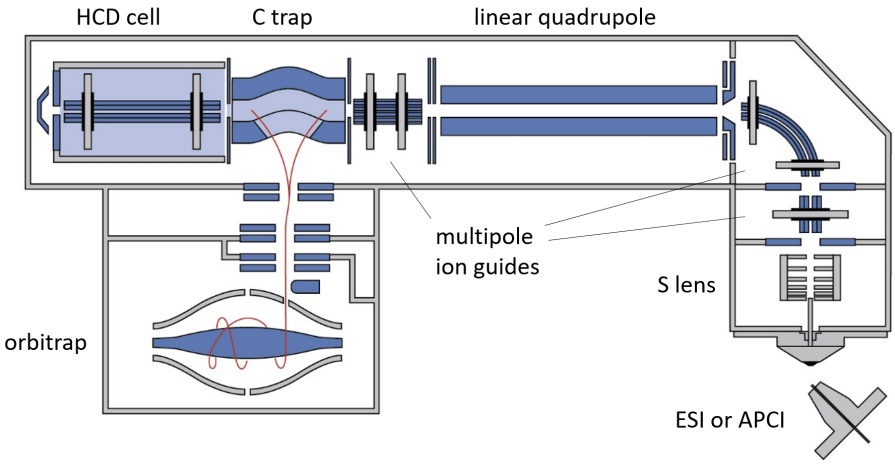

Figure 3.7: Schematic setup of a Q Exactive^{TM} Hybrid Quadrupole-Orbitrap Mass Spectrometer from Thermo Fisher Scientific (adapted from Thermo Fisher Scientific (2020)).

higher-energy collision dissociation (HCD) cell, where they are fragmented by radio frequency excitation and collisions with buffer gas. Ion guides, C-trap and HCD cell will be described in section 3.3.3. The fragments are then transferred back to the C-Trap and from there into the Orbitrap, which is a high resolution mass analyzer (section 3.3.4).

3.3.1 Electrospray ionization

In LC-MS, the inlet of the mass spectrometer is coupled to the outlet of the LC, which is under atmospheric pressure. The LC flow contains a large volume of solvent, which forms an even larger gas volume after evaporation. Ideally, however, only the analyte ions should enter the mass spectrometer, which is under high vacuum. To manage this transition, various techniques for atmospheric pressure ionization (API) have been developed. The two most commonly used API sources are electrospray ionization (ESI) and atmospheric pressure chemical ionization (APCI). For particularly photoactive analytes, atmospheric pressure photoionisation (APPI) may also be an option. In the following, the ESI source is described, as it is used in this thesis. The liquid emerging from the LC capillary is nebulized by means of a concentric nitrogen stream. A voltage of $\pm 2 - -6$ kV is applied between the end of the capillary and a counter electrode. This causes a charge separation in the solution and the formation of charge-carrying droplets. The remaining solvent in the droplets is evaporated by a heated transfer capillary or a heated nitrogen countercurrent and removed by the vacuum pumps. The pressure is reduced by stepwise differential pumping from atmospheric pressure via a fore-vacuum to high vacuum. Via a stacked-ring ion guide (S-lens) and an octapole, the now desolvated ions finally reach the mass analyzer (Fig. 3.7).

The mechanism of the formation of desolvated ions from the charge-carrying droplets is shown in Fig. 3.8 and can be divided into three stages: the formation of charge-

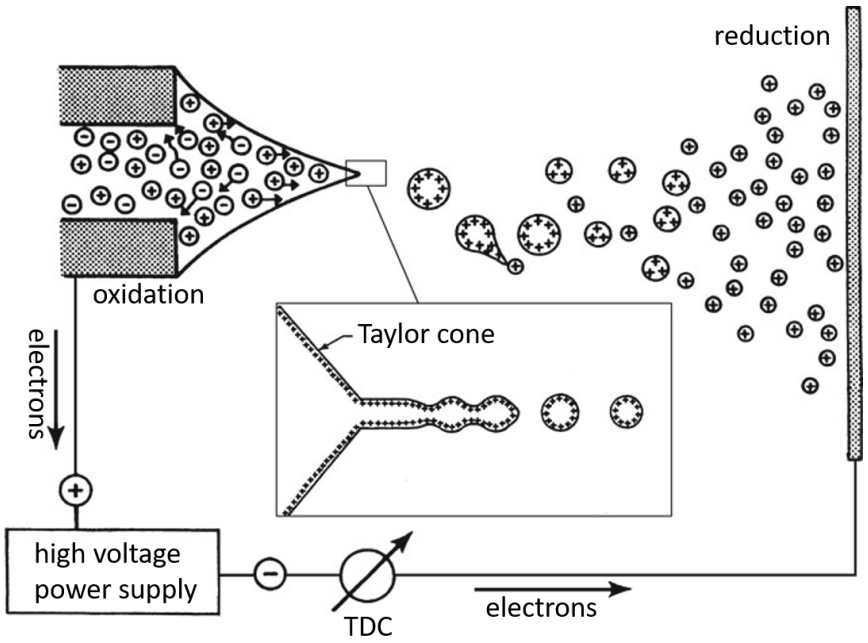

Figure 3.8: Schematic representation of the electrospray ionization process with Taylor cone formation, ejection of a jet, its disintegration into fine droplets and the formation of desolvated ions (reprinted by permission from Gross (2017)).

carrying droplets, the reduction of these droplets and finally the formation of gaseous ions. In the positive mode shown, a negative voltage is applied between the LC capillary and the counter electrode. The anions contained in the solution are drawn to the wall of the capillary and discharged or oxidized there. The cations, on the other hand, are attracted by the distant counterelectrode and concentrate on the surface of the liquid at the outlet of the capillary. Due to the equilibrium between the surface tension of the solvent and the electrostatic repulsion of the positive charges accumulated on the surface, a so-called Taylor cone is formed, which becomes unstable at its tip and first changes into a fine jet, which finally breaks up into small droplets. These droplets, which are only a few µm in size, contain a high charge surplus of several 10^4 charges and therefore repel each other, resulting in a fine spray (Gross, 2017). As the solvent evaporates from the droplets, the excess charge on the surface increases even further until the repulsion of the charges is finally greater than the surface tension of the droplet. The droplets then decay via surface vibrations and structures similar to the Taylor cone into several smaller droplets that carry the majority of the charges. The limit at which the repulsion of the charges is greater than the surface tension is called the Rayleigh limit. This process of evaporation and disintegration of the droplets repeats until highly charged microdroplets are left.

For the formation of gaseous ions from these highly charged microdroplets, there are two different models. The older *charged residue model* (CRM) assumes that in the end, the remaining solvent evaporates from a droplet of only a few nanometers in size, leaving behind a single desolvated ion. The newer *ion emission model* (IEM)

states that, as a competitive reaction to further Rayleigh decay, gaseous ions are emitted from a highly charged microdroplet with a radius of about 8 nm and 70 elementary charges . Presumably, both models apply to reality depending on the size of the molecules (Gross, 2017).

A more recent development of the ESI is the HESI (heated ESI), in which the LC capillary, which supplies the sample solution, is heated. This allows eluents with a high water content, as often used in reversed phase HPLC, to be evaporated more easily and the spray becomes more stable. However, caution should be taken with analytes that are easily thermally decomposed.

3.3.2 Linear quadrupole mass analyzer

A mass analyzer separates the ions according to their m/z ratio. Depending on the application and required resolution, different analyzers are used. The resolving power R_{MS} in mass spectrometry, which is necessary to resolve the signal of a m/z ratio m from an adjacent m/z at a distance of δm, is defined in equation (3.5).

$$R_{MS} = \frac{m}{\Delta m} \tag{3.5}$$

A linear quadrupole analyzer, also known as transmission quadrupole mass analyzer, is an inexpensive, compact mass analyzer. It has a relatively small mass range of max. m/z 3000–4000 (Skoog et al., 2018) and is usually operated at unit resolution, which means that the resolving power at m/z 2000 is approximately 2000 and at m/z 200 approx. 200 (Gross, 2017). It is often used in conjunction with GC or HPLC and consists of four parallel metal rods, which ideally have a hyperbolic cross section (Fig. 3.9). A direct current (DC) voltage is applied to these metal rods, which is

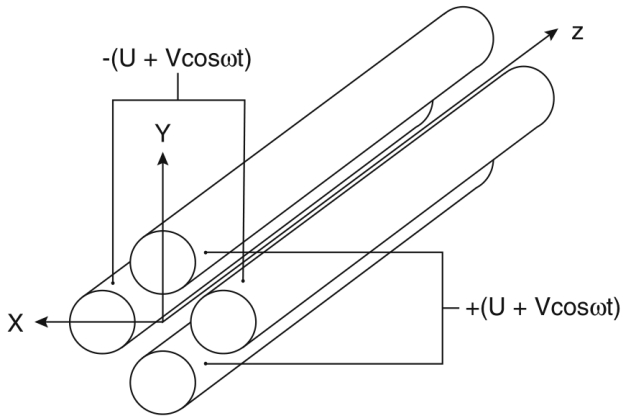

Figure 3.9: Schematic of a linear quadrupole mass analyzer with direct potential U and radio frequency potential V with the frequency ω. The ions travel in z-direction. (Reprinted by permission from Gross (2017).)

superimposed by a high-frequency alternating current (AC) voltage in the MHz range (radio frequency, RF). This creates a hyperbolic alternating electric field between the rods. When the ions are injected axially into the analyzer, they are deflected from

their path by this alternating field. Only ions with a certain m/z ratio have stable orbits and can pass the analyzer and reach the detector. Ions heavier than the desired mass cannot follow the rapid field changes, collide with the rods and are discharged. Lighter ions, on the other hand, are excited by the alternating field to increasingly larger orbit radii and finally leave the analyzer between the rods. By varying the voltage, ions of different m/z ratios can pass through the analyzer one after the other. The quadrupole analyzer is thus a continuously operating, scanning mass analyzer. Equipped with a detector, usually a conversion dynode with a continuous-dynode electron multiplier, also called channeltron (Harris, 2015), it can be used as a standalone mass spectrometer. However, linear quadrupole analyzers are often part of hybrid mass spectrometers, such as triple quadrupole (QqQ), quadrupole time-of-flight (Q-TOF) or quadrupole Orbitrap mass spectrometers. In this case, the quadrupole analyzer serves to select precursor ions, which are then fragmented in a collision cell and the fragments analyzed in a subsequent mass analyzer.

3.3.3 Multipole ion guides, C-trap and higher-energy collision dissociation cell

A quadrupole operated only with RF potential without a DC potential applied functions as a wide band pass filter and can be used to guide ions from one unit of a mass spectrometer to another, for example from the inlet to the actual mass analyzer. Analogously, RF-only hexapoles and RF-only octapoles are used as ion guides. A curved ion guide improves the removal of neutral particles, which cannot follow the bend and fly straight ahead between the rods. If a multipole is filled with a collision gas, e.g. helium, nitrogen or argon, it can be used as a collision cell, for example in triple quadrupole mass spectrometers (QqQ, or actually rather QhQ or QoQ with hexapol or octapol collision cells). This collision induced dissociation (CID) generates fragment ions, which can be analyzed by a second mass analyzer to generate tandem mass spectra.

If electrodes with a sufficiently high DC potential are attached to both ends of a linear multipole, the ions within the multipole are trapped in a potential well and a linear ion trap is obtained. By collisions with a light buffer gas, e.g. helium or nitrogen at a pressure of $10^{-3} - 10^{-2}$ mbar, the kinetic energy of the trapped ions can be reduced, which is called collisional cooling and leads to the ions focusing towards the central axis of the trap. Exciting the ions with an RF potential leads to higher-energy collisions with the buffer gas and thus to fragmentation of the ions. Linear quadrupole ion traps (LIT) and also the related three-dimensional quadrupole ion traps (QIT) can be used as standalone tandem mass spectrometers, because they are able to eject the trapped ions (or their fragment ions) sequentially according to their m/z ratio directly on a detector. Hexapole or octapole ion traps, on the other hand, are only able to eject all ions at once, and therefore only serve as collision cells (Gross, 2017). Such an octapole collision cell is for example used in the Orbitrap Q Exactive mass spectrometer, where it is called higher-energy collisional dissociation (HCD) cell.

A linear ion trap can also be used to store ions produced by a continuously operating ion source and later inject them as a concentrated ion bunch into a pulsed mass analyser. A special form of the ion trap designed for exactly this purpose is the C-trap, which is bent into a C-shape. It is used in Orbitrap mass spectrometers to very rapidly inject a bunch of ions into the Orbitrap analyzer. The ions are trapped between the rods by an RF field, collisional cooling with nitrogen gas is applied to focus the ion bunch in the center of the C-trap, and finally the ions are ejected through a slit in the inside wall of the C-trap by rapidly ramping down the RF field and applying a DC potential. Thus, injection times of as low as 0.1 ms can be reached.

3.3.4 Orbitrap mass analyzer

The Orbitrap is a new type of high-resolution mass analyzer, which is commercially available since 2005 and is based on earlier concepts of the Knight-style Kingdon Trap. It can offer a resolving power of more than 200 000 (140 000 for the model Q-Exactive Orbitrap used in this work) and mass accuracies of 0.5–5 ppm (Gross, 2017). The high resolution and high mass accuracy allow to calculate the sum formula of detected molecules directly from the measured m/z ratios. This is especially important for the identification of unknown molecules, but it is also helpful for target anlysis of complex mixtures.

The Orbitrap analyzer consists of a spindle-shaped inner electrode situated in a barrel-shaped outer electrode, which is split in two halves (Fig. 3.10). A voltage of

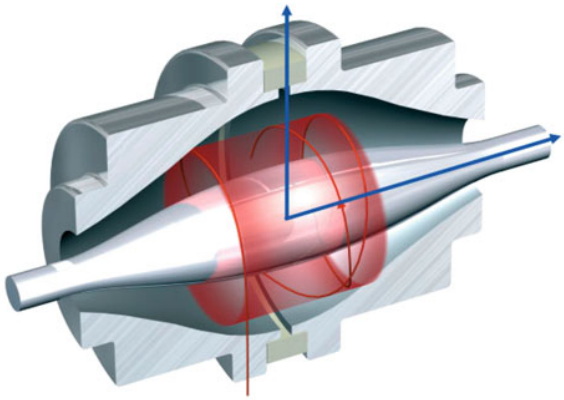

Figure 3.10: Schematic of the Orbitrap mass analyzer (reprinted by permission from Gross (2017)).

approximately 5 kV is applied between the inner and outer electrodes, the two halves of the outer electrode being electrically insulated from each other and at ground potential. An ion packet is injected radially into the Orbitrap through an off-center opening (red line in Fig. 3.10). The ions are attracted to the inner electrode and, due to their initial kinetic energy, swing into a circular orbit around the inner electrode. The spindle shape of the inner electrode creates a field gradient that causes the ions to oscillate in the axial direction, i.e. along the inner electrode, in addition to their rotation around the inner electrode. The frequency of this axial oscillation depends

on the m/z ratio of the ions and is independent of their kinetic energy. An amplifier is connected between the two halves of the outer electrode, which measures the mirror current of the ion movements in the trap. From this mirror current, the m/z ratios of all ions in the trap are calculated by Fourier transformation. Since the accuracy of this calculation and thus the resolving power of the Orbitrap increases with the recording time of the mirror current, the ions must perform an undisturbed oscillation for about 0.1–1.5 s and must not collide with other particles. This requires a vacuum of 10^{-10} mbar and therefore places high demands on the vacuum system.

Orbitrap analyzers are often used in proteomics, but they also have a great potential for the analysis of small molecules in complex mixtures as they often occur in environmental samples.

Thesis objectives and outline

In order to better understand and predict climate changes in the future, it is necessary to study the climate of the past. Natural climate archives, such as ice cores, sediments and speleothems, preserve valuable information about climate and vegetation changes in the past. Speleothems are useful climate archives because they can be absolutely dated up to 640 000 years back in time using the ^{230}Th-U method and can grow continuously over thousands of years. Moreover, they occur on all continents and preserve a variety of inorganic and organic proxies, which are enclosed in the calcite matrix of the speleothem and thus protected from external influences.

Until recently, mostly stable isotopes and trace elements have been analyzed in speleothems. However, the interpretation of these proxies sometimes can be difficult, as they can be influenced by many different processes and sources. Therefore, multi-proxy studies combining, for example, stable isotopes, trace elements, fluorescent organic matter and also molecular organic biomarkers are employed today to unravel climatic and ecological signals. Vegetation proxies can not only complement other climate proxies, but also provide information about the effects of temperature and precipitation changes on vegetation development. Hence, they play an important role in the proxy toolbox of paleo-climate and especially paleo-vegetation reconstruction. So far, only very few studies on organic biomarkers in speleothems are available, probably due to the fact that speleothems contain very low concentrations of organic matter compared to other climate archives. Consequently, sensitive analytical methods need to be developed to access the information contained in organic biomarkers in speleothems.

Lignin is a biopolymer that is produced exclusively in vascular plants. It mainly consists of three phenolic monomers, whose proportion differs between angiosperm and gymnsperm plants and between woody and non-woody vegetation. In contrast to other biomolecules such as fatty acids or n-alkanes, lignin therefore has a precisely defined source, and it is also less prone to laboratory contamination. In addition, its analysis provides information not only on the density but also on the type of vegetation. These advantages make it particularly suitable as a vegetation proxy. Lignin phenols have already been detected in speleothem samples (Blyth and Watson, 2009), but no quantitative analysis of lignin or its oxidation products in speleothems has been performed yet.

The first part of this doctoral work (part II of this thesis) was to develop and validate a sensitive and selective method to quantitatively analyze the amount and composition of lignin traces preserved in speleothems. Before the actual analysis, several sample preparation steps are necessary. First, the speleothem calcite must be dissolved and the polymeric lignin extracted from the solution. Second, the polymeric lignin needs to be oxidatively degraded into the monomeric lignin oxidation products (LOPs), which then must be extracted and enriched. Third, the LOPs are analyzed

using liquid chromatography coupled to electrospray ionization high resolution mass spectrometry. The method had to be suitable for dripwater and soil samples as well, since these sample types were to be analyzed to better understand the processes of lignin transport in the cave system. The development and optimization of the analytical method is the subject of chapter 4, which is also published as a first-author publication in the journal *Biogeosciences*.

The sample preparation step that contributed the most to analytical uncertainty was the lignin degradation via CuO oxidation. Therefore, an attempt was made to find an alternative lignin degradation method based on electrolysis, which was hoped to have lower blank values and a higher reproducibility. This attempt is described in chapter 5.

In the second part (part III of this thesis), the developed analytical method was then applied to different speleothem, soil and dripwater samples. The results were compared and correlated with data from stable isotopes and trace elements as well as with known climate and vegetation changes. These experiments served to explore the potential of LOPs as a vegetation proxy in speleothem archives and to improve our knowledge on the transport and alteration of lignin in the soil, karst and cave system.

The first sample was an 11 000 years old Holocene stalagmite from the Herbstlabyrinth Cave in Germany. This sample was chosen for a proof of principle analysis because it was already well characterized by stable isotope and trace element analysis, the general vegetation and climate changes in the Holocene in central Germany are relatively well known, and because it had a fast growth rate, which offered sufficient sample material to test and apply the method. In addition, dripwater from the Herbstlabyrinth was sampled monthly in the framework of a cave monitoring program and analyzed for LOPs in order to study seasonal variations in lignin input. The results from the Herbstlabyrinth are presented in chapter 6 and published as a first-author publication in the journal *Climate of the Past*.

In chapter 7, a small, only 200 years old stalagmite from the Zoolithen Cave in Germany was analyzed. The purpose of this study was to test the potential of LOPs as a vegetation proxy by means of a specific paleo-vegetation research question. In this case, a rapid vegetation change from grassland to deciduous forest in the landscape around the Zoolithencave was known from historical sources, but the established vegetation proxies such as $\delta^{13}C$ did not show a significant change in their signals recorded in the stalagmite. The question was to evaluate whether LOP analysis can be used to detect such a rapid vegetation change. A particular challenge was the very small sample size of only 0.5 g per sample.

Chapter 8 presents the analysis of samples from two flowstones from Cueva Victoria in southeast Spain. The samples date from three different geological eras: the Holocene, the Last Glacial Period and the Eemian interglacial. The carbon isotope records of these flowstones showed several large excursions, which were interpreted as rapid shifts between more humid and more arid climate periods, resulting in a change in vegetation type and density. The aim of this study was to prove that LOPs can support the interpretation of stable isotope records by providing information about the input of vegetation derived material.

Another important goal of this work was to better understand the mechanisms of lignin transport from the soil through the karst system into the cave, for example the interaction of lignin with mineral particles. From the gained knowledge, conclusions for the suitability and interpretation as a vegetation proxy should be drawn. In particular, the question was to be answered whether the original source-dependent signal of the overlying vegetation is preserved despite the different influences of transport and degradation and can be recoverd from the speleothem samples. Therefore, a systematic comparative study was carried out in four different caves from different vegetation zones in New Zealand. From each cave, soil, dripwater and speleothem samples were analyzed and the lignin composition compared. The results are presented in chapter 9.

Part II

Method development

4 Method development for the quantification of lignin oxidation products as vegetation biomarkers in speleothems and cave dripwater

This chapter is a reprint of the manuscript published in *Biogeosciences*:

Biogeosciences, 15, 5831–5845, 2018
https://doi.org/10.5194/bg-15-5831-2018

Biogeosciences Open Access EGU

Quantification of lignin oxidation products as vegetation biomarkers in speleothems and cave drip water

Inken Heidke[1], Denis Scholz[2], and Thorsten Hoffmann[1]

[1]Institute of Inorganic Chemistry and Analytical Chemistry, Johannes Gutenberg University of Mainz, Duesbergweg 10–14, 55128 Mainz, Germany
[2]Institute of Geosciences, Johannes Gutenberg University of Mainz, J.-J.-Becher-Weg 21, 55128 Mainz, Germany

Correspondence: Thorsten Hoffmann (t.hoffmann@uni-mainz.de)

Received: 28 May 2018 – Discussion started: 25 June 2018
Revised: 6 September 2018 – Accepted: 18 September 2018 – Published: 4 October 2018

Abstract

Here we present a sensitive method to analyze lignin oxidation products (LOPs) in speleothems and cave dripwater to provide a new tool for paleo-vegetation reconstruction. Speleothems are valuable climate archives. However, compared to other terrestrial climate archives, such as lake sediments, speleothems contain very little organic matter. Therefore, very few studies on organic biomarkers in speleothems are available. Our new sensitive method allows to use LOPs as vegetation biomarkers in speleothems.

Our method consists of acid digestion of the speleothem sample followed by solid phase extraction (SPE) of the organic matter. The extracted polymeric lignin is degraded in a microwave assisted alkaline CuO oxidation step to yield monomeric LOPs. The LOPs are extracted via SPE and finally analyzed via ultrahigh-performance liq-

uid chromatography (UHPLC) coupled to electrospray ionization (ESI) and high-resolution orbitrap mass spectrometry (HRMS). The method was applied to stalagmite samples with a sample size of 3–5 g and cave dripwater water samples with a sample size of 100–200 mL from the Herbstlabyrinth-Advent-Cave in Germany. In addition, fresh plant samples, soil water and powdered lignin samples were analysed for comparison. The concentration of the sum of eight LOPs (Σ8) was in the range of 20–84 ng $\cdot$ g^{-1} for the stalagmite samples and 230–440 ng $\cdot$ L^{-1} for the cave dripwater samples. The limits of quantification for the individual LOPs ranged from 0.3–8.2 ng per sample or 1.5–41.0 ng $\cdot$ mL^{-1} of the final sample solution.

Our method represents a new and powerful analytical tool for paleo-vegetation studies and has great potential to identify the pathways of lignin incorporation into speleothems.

4.1 Introduction

Speleothems are calcareous mineral deposits that form within caves in karstified carbonate rock. The most common types of speleothems are stalagmites, which are formed by water dripping on the ground of the cave, stalactites, which are their counterparts on the cave ceiling, and flowstones, which are formed by water films flowing on the cave walls and floor. Speleothems preserve information about climatic and hydrological conditions and the vegetation development above the cave and therefore serve as paleoclimate archives (Fairchild and Baker, 2012, McDermott, 2004). Compared to other paleo-climate archives, such as ice cores and marine or lacustrine sediments, speleothems have certain advantages. They can grow continuously for 10^3–10^5 years, their growth layers are mechanically undisturbed and they do not show a loss of time resolution with increasing age (Gałuszka et al., 2017, Fairchild et al., 2006). They can be accurately dated up to 500 000 years back in time using the ^{230}Th/U-method (Scholz and Hoffmann, 2008, Richards and Dorale, 2003). Moreover, they occur on all continents except Antarctica and are thus not limited to certain climatic regions.

Most studies of speleothems focus on the analysis of stable isotope ratios (δ^{13}C, δ^{18}O (McDermott, 2004) and inorganic trace elements (Fairchild and Treble, 2009). The organic content of speleothems has so far mostly been analyzed as total organic carbon content or fluorescent organic matter (Quiers et al., 2015). However, in recent years, the interest in molecular organic proxies in climate archives has increased (Giorio et al., 2018, Blyth et al., 2008, Blyth and Watson, 2009, Blyth et al., 2010, 2016). In speleothems, in particular lipid biomarkers, such as fatty acids reflecting changes in vegetational and microbial activities (Xie, 2003, Blyth et al., 2006, Bosle et al., 2014) and membrane lipids (glycerol dialkyl glycerol tetraethers, GDGTs) serving as paleo temperature proxies (Blyth, Smith and Drysdale, 2013, Baker et al., 2016), have been studied.

Lignin occurs almost exclusively in terrestrial vascular plants and is one of the main constituents of wood and woody plants (Jex et al., 2014). It is a biopolymer that mainly consists of three monomers: sinapyl alcohol, coniferyl alcohol and p-coumaryl alcohol. The proportion of these three monomers varies with the type of

plant, such as gymnosperm or angiosperm and woody or non-woody material. Thus, by analyzing the composition of lignin, it is possible to determine the source and type of plant material.

Lignin has been widely used as paleo-vegetation proxy in lake sediment (Tareq et al., 2011) and peat cores (Tareq et al., 2004). In marine sediments (e.g., Zhang et al., 2013) and natural waters (Standley and Kaplan, 1998, Hernes and Benner, 2002), lignin analysis has been used to determine the source of dissolved organic matter. Blyth and Watson (2009) have successfully detected lignin pyrolysis products in speleothems by applying a tetramethylammonium hydroxide (TMAH) thermochemolysis method, but there have been no quantitative studies of lignin in speleothems yet.

Lignin has to be degraded before the molecular composition of its phenolic components can be analyzed. The most common method for degradation of lignin is the alkaline oxidation with cupric oxide (CuO), developed by Hedges and Parker in 1976. This method releases a number of phenolic acids, aldehydes and ketones, which can be divided into four groups: The vanillyl group (V) consisting of vanillic acid, vanillin and acetovanillone, the syringyl group (S) consisting of syringic acid, syringaldehyde and acetosyringone, the cinnamyl group (C) consisting of trans-ferulic acid and p-coumaric acid, and the p-hydroxyl group (P) consisting of p-hydroxybenzoic acid, p-hydroxybenzaldehyde and p-hydroxyacetophenone. Hedges and Mann (1979) analysed fresh plant tissues and showed that the phenols of the syringyl group are only obtained from angiosperm, but not from gymnosperm plant tissues. Likewise, the phenols of the cinnamyl group are only obtained from non-woody and not from woody plant tissues, whereas the phenols of the vanillyl group are found in all kind of vascular plant tissues (angiosperm and gymnosperm, woody and non-woody). These results led to the introduction of the lignin oxidation product (LOP) parameters C/V and S/V, where C, for example, is defined as the sum of all lignin oxidation products of the C-group (Hedges and Mann, 1979). The phenols of the p-hydroxyl group can originate from gymnosperm and non-woody angiosperm plant tissues, but are also oxidation products of protein rich organisms such as bacteria and plankton. Therefore, the P group is not used in the parameters to determine the source of lignin (Jex et al., 2014). The parameter $\Sigma 8$ gives the sum of the eight analytes of the C, S and V-group and is used to estimate the total amount of LOPs in a sample.

The oxidation with CuO has been optimized many times in the past. For example, Goñi and Montgomery (2000) developed a microwave digestion method. Other groups improved the sample clean-up by replacing the formerly used liquid-liquid extraction (LLE) with solid phase extraction (SPE) (Kögel and Bochter, 1985, Kaiser and Benner, 2012). As the CuO oxidation method is broadly used, there are many data sets to compare with. This is certainly an advantage compared to the above mentioned TMAH thermochemolysis method, which is less often used and produces more complex methylated reaction product mixtures (Wysocki et al., 2008). For the detection of the LOPs, gas chromatography coupled to mass spectrometry (GC-MS) is often used, which requires a derivatization step. Liquid chromatography is also used, either in combination with UV detection or coupled to mass spectrometry.

The purpose of this study was to develop and validate a sensitive and selective method for the quantification of LOPs in both speleothem and cave dripwater samples using liquid chromatography electrospray ionization mass spectrometry (LC-ESI-MS). This method offers new possibilities for paleo-vegetation reconstruction since it combines the advantages of lignin analysis as a highly specific vegetation biomarker with the above mentioned benefits of speleothems as unique terrestrial climate archives. Lignin as a vegetation biomarker is much more specific for higher plants than for example n-alkanes or fatty acids (Jex et al., 2014), and thus can help to interpret other vegetation markers and stable isotope records. Up to now, lignin analysis for paleo-vegetation reconstruction has only been applied to lake sediments and peat cores, which contain much larger amounts of organic matter than speleothems. Our method allows to analyse the lignin composition of trace amounts of organic matter preserved in speleothems. The stalagmite samples are first acid digested, and the acidic solution is then extracted by SPE. The eluent is then subjected to CuO oxidation in a microwave assisted digestion method. The oxidised sample solutions are again extracted and enriched by SPE, and the LOPs are then separated and detected by ultrahigh-performance liquid chromatography coupled to electrospray ionization high-resolution mass spectrometry (UHPLC-ESI-HRMS).

4.2 Experimental section

4.2.1 Chemicals and materials

Analytical standards of acetosyringone (97%), acetovanillone ($\geq$ 98%), para-coumaric acid ($\geq$ 98%), ethylvanillin (99%), ferulic acid (99%), para-hydroxyacetophenone ($\geq$ 98%), para-hydroxybenzaldehyde ($\geq$ 97.5%), syringaldehyde (98%), syringic acid ($>$ 95%) and cinnamic acid (97%) as well as copper(II) oxide ($>$ 99%) and ammonium iron(II) sulfate (99%) were purchased from Sigma Aldrich. Analytical standards of para-hydroxybenzoic acid (99%) and vanillin (99%) were obtained from Acros Organics, an analytical standard of vanillic acid (98%) was obtained from Alfa Aesar. Sodium hydroxide (pellets, $\geq$ 99%) was purchased from Carl Roth, hydrochloric acid (HCl, suprapure, 30%) from Merck KGaA. Lignin from mainly coniferous wood was obtained from BASF SE. Mixed lignin from wheat straw and various kinds of wood was purchased from Bonding Chemical. Solid phase extraction columns (Oasis HLB, 3 mL tubes, 60 mg packing material) were purchased from Waters. Ultrapure solvents (Optima LC/MS grade) acetonitrile (ACN), water (H_2O) and methanol (MeOH) were obtained from Fisher Scientific. Dichloromethane (DCM) ($\geq$ 99.9% (GC)) was obtained from Honeywell Riedel-de Haën. Ultrapure water with 18.2 MΩ resistance was produced using a Milli-Q water system from Merck Millipore (Darmstadt, Germany).

4.2.2 Methods

The overall sample preparation procedure is shown as process chart in Figure 4.1. The different steps of the sample preparation will be described in detail in the following paragraphs.

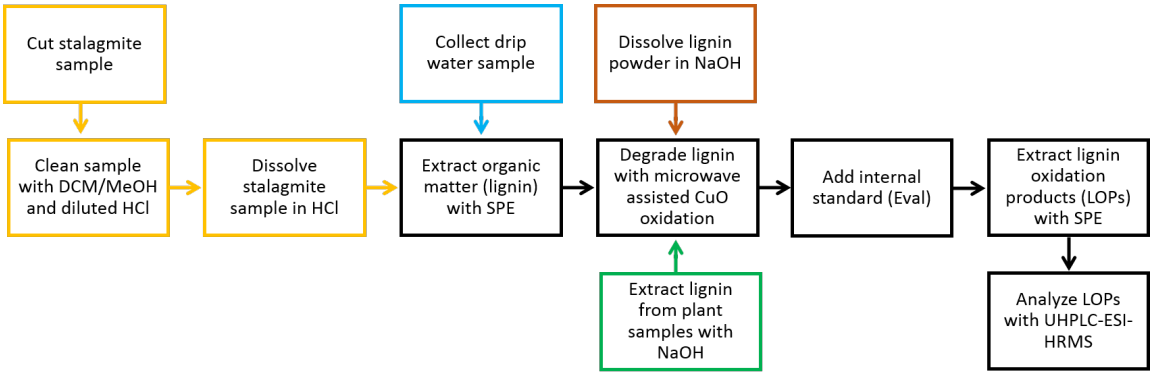

Figure 4.1: Process chart of the overall sample preparation procedure. A detailed description of the individual steps is given in section 4.2.2.

Preparation of standards

Stock solutions of all analytical standards were prepared at a concentration of 1 mg · mL^{-1} in ACN. A mixed stock solution of all analytical standards was prepared by dilution of the individual stock solutions to a concentration of 10 µg · mL^{-1} in ACN. The stock solutions were stored at -18 °C. For the external calibration standards, the mixed stock solution was freshly diluted to the appropriate concentrations ranging from 20 ng · mL^{-1} to 2000 ng · mL^{-1} in H_2O/ACN 9:1 (v/v). To optimize the SPE procedure for the LOPs, 100 µL of a 1 µg · mL^{-1} mixed standard solution in H_2O/ACN 9:1 (v/v) was added to 20 mL of a 2 mol · L^{-1} sodium chloride solution that was acidified to pH 2 with HCl (30%) to simulate the sample solution after the microwave digestion step.

Sampling and preparation of stalagmite samples

Stalagmite *NG01* from the Herbstlabyrinth-Advent-Cave, central Germany, was 50 cm long and had a diameter of approximately 15 cm. It was cut along the growth axis using a diamond blade saw. From one of the two halves, a 1 cm thick slab was cut, which was then dated using the ^{230}Th/U-method (Mischel et al., 2017). This showed that the oldest part of the stalagmite grew at ca. 11 000 years BP, whereas the youngest part stems from recent time. Thus, the stalagmite covers the Holocene. The inner part of the stalagmite slab, close to the growth axis, was already used for stable isotope and trace element (Mischel et al., 2017) as well as fatty acid analysis (Bosle et al., 2014). Thus, the samples for this study had to be taken from the outer part of one half of the stalagmite slab. Pieces of calcite with approximately 0.5–1.2 cm in width, 2.5–3.7 cm in length and a weight of 3.0–5.4 g were cut from the slab using a diamond wire saw following the growth lines of the stalagmite. Care was taken to always leave 2 cm space to the outer surface of the stalagmite to avoid contamination and dating problems.

To clean the stalagmite samples, each sample was covered with DCM/MeOH 9:1 (v/v) and cleaned for 10 min at 35 °C in an ultrasonic bath. The solvent was discarded, and the cleaning was repeated a second time. Afterwards, the samples

were rinsed with ultrapure water, then each sample was covered with ultrapure water, and 250 µL of HCl (30%) were added to etch away the outermost layer of calcite, which might be contaminated. After 5 min, the samples were rinsed with ultrapure water, dried and weighed. The samples were then placed in clean glass vials and 2.1 mL of HCl (30%) per gram stalagmite were added to dissolve the calcite over night at room temperature. Before extracting the solutions using SPE, they were diluted 1:1 with ultrapure water to prevent clogging of the cartridges.

Sampling and preparation of dripwater samples

The dripwater samples were collected in the framework of a monthly cave monitoring program (Mischel et al., 2017, 2015). All samples presented here were sampled in October 2014 at different drip sites (two fast drip sites, *D1* and *D5*, with a drip rate of 0.3–0.5 drops·s^{-1}, one slow drip site, *D2*, with a drip rate of approx. 60 mL·month^{-1}, and one sample from a cave pool, *PW*). In addition, soil water (*SW*) was sampled in a meadow above the cave, and rain water (*RW*) was sampled at a weather station above the cave. More information on the sampling techniques can be found in (Mischel et al., 2017, 2015). The samples were collected in pre-cleaned glass vessels. To prevent the growth of microorganisms, 5% (w/w) of acetonitrile were added shortly after sampling. The samples were then stored at 4 °C in the dark for several months. Before extracting the samples using SPE, they were acidified to pH 1–2 with HCl.

Preparation of lignin and fresh plant tissue samples

The lignin powder was dissolved in NaOH (2 mol·L^{-1}) at a concentration of 1 mg·mL^{-1}. 100 µL of this solution were added into the microwave reaction vessel. The plant samples (leaves and branches of Amur maple, and needles and branches of European yew, all collected in Mainz, Germany) were cut in small pieces and dried in an oven at 50 °C for two days. 10 mg·mL^{-1} were soaked in NaOH (2 mol·L^{-1}) for several days. 1 mL of this solution was filtered over 1 μm filters and added into the microwave reaction vessels.

Solid phase extraction of organic matter in dissolved stalagmite solution and dripwater samples

The SPE cartridges were preconditioned with 3 mL of MeOH followed by 3 mL of ultrapure water, which was acidified to pH 1–2 with HCl. The diluted stalagmite solution or the acidified dripwater sample were loaded onto the cartridges using sample reservoirs. The drip rate was always below 1 drop·s^{-1}. The cartridges were washed twice with 3 mL of acidified ultrapure water and dried for 20 min by sucking ambient air through the cartridges using a vacuum manifold. The lignin was eluted with 6 portions of 250 µL of MeOH. The solvent was evaporated to almost dryness under a gentle stream of nitrogen at 30 °C. The residue was re-dissolved in 1.5 mL of NaOH (2 mol·L^{-1}), the solution was sonicated for 10 min at 45 °C and added into the microwave reaction vessel. The sample vial was sonicated again with 1.5 mL of NaOH (2 mol·L^{-1}) and this solution was added into the microwave reaction vessel, too.

Microwave assisted CuO oxidation

The microwave assisted CuO oxidation procedure was performed according to the method described by Goñi and Montgomery (2000) with slight modifications. An Ethos Plus Microwave Labstation (MLS GmbH, Germany) was used with an HPR-1000/10S high pressure segment rotor, which can hold up to 10 reaction vessels, and an ATC-CE temperature sensor to measure the temperature inside one reaction vessel. 100 mL Teflon vessels were used as reaction vessels. Each vessel was loaded with 250 mg of CuO, 50 mg of $(NH_4)_2Fe(SO_4)_2{\cdot}6\ H_2O$ and 8 mL of NaOH (2 mol·L^{-1}) in total, including the sample solution. The NaOH solution was purged with nitrogen for 30 min before use to remove dissolved oxygen, which could lead to over-oxidation of the lignin oxidation products. For the same reason, the vessels were purged with an argon flow of 1 mL·min^{-1} for 1 min and then quickly capped to ensure an inert gas atmosphere in the vessels. The vessels were shaken well and then placed in the high-pressure segment rotor of the microwave oven. The temperature was increased to 155 °C in 5 min and then hold at 155 °C for 90 min. Afterwards, the vessels were allowed to cool down to room temperature overnight. Directly after opening the vessels, 50 µL of a 1 $\mu g \cdot mL^{-1}$ standard solution of ethyl vanillin in H_2O/ACN (9:1, v/v) were added as an internal standard into each vessel except the blank sample. The reaction solutions were transferred to 15 mL centrifuge tubes and the reaction vessels were rinsed twice with 3 mL of NaOH (2 mol·L^{-1}). The combined solutions were centrifuged for 10 min at 3000 rpm and the supernatant was decanted into glass vessels. The residue was suspended in 5 mL of NaOH (2 mol·L^{-1}) using a vortex mixer, centrifuged again for 10 min at 3000 rpm and the supernatant was combined with the sample solution.

Solid phase extraction of LOPs in the oxidized sample solution

The oxidized sample solution was acidified to pH 1–2 with HCl. The conditioning, loading, washing and drying steps of the SPE cartridges were the same as described in section 4.2.2. The LOPs were eluted with four portions of 250 µL of ACN with 2% of ammonia added to reach a basic pH of 8–9. The eluate was evaporated to dryness in a gentle stream of nitrogen at 30 °C and the residue was re-dissolved in 200 µL H_2O/ACN (9:1).

UHPLC-ESI-HRMS analysis

The analysis of the lignin oxidation products was carried out on a Dionex Ultimate 3000 ultrahigh-performance liquid chromatography system (UHPLC) that was coupled to a heated electrospray ionization source (ESI) and a Q-Exactive Orbitrap high-resolution mass spectrometer (HRMS) (all by Thermo Fisher Scientific). To separate the LOPs, a Hypersil Gold pentafluorophenyl (PFP) column, 50 mm x 2.1 mm with 1.9 µm particle size (also by Thermo Fisher Scientific) was used. The injection volume was 15 µL. A H_2O/ACN-gradient program was applied. The gradient started with 10% eluent B (consisting of 98% ACN and 2% H_2O) and 90% eluent A (consisting of 98% H_2O, 2% ACN and 400 $\mu L \cdot L^{-1}$ formic acid), which was held for 0.5 min. Eluent B was increased to 12% within 2 min, held for 1 min, was further

increased to 50% within 1.25 min, held for 0.75 min and increased to 99%. This composition was held for 2 min, then eluent B was decreased to the initial value of 10%. The ESI source was operated in negative mode, so that deprotonated molecular ions $[M\text{-}H]^-$ were formed. The spray voltage was -4.0 kV, the ESI probe was heated to 150 °C to improve the evaporation of the aqueous solvent, the capillary temperature was 350 °C, the sheath gas pressure was 60 psi and the auxiliary gas pressure was 20 psi. The mass spectrometer was operated in full scan mode with a resolution of 35 000 and a scan range of *m/z* 80–500. At the respective retention time windows, the full scan mode was alternated with a targeted MS^2-mode with a resolution of 17 500 to identify the LOPs by their specific daughter ions, see Table 4.1. For the MS^2-mode (i.e., *parallel reaction monitoring mode* in the software *XCalibur*, provided by Thermo Fisher Scientific), higher-energy collisional dissociation (HCD) was used with 35% normalized collision energy (NCE) for all analytes. The actual collision energy was calculated by the software on basis of mass and charge of the selected precursor ions and was in the range of 10–14 eV.

Table 4.1: Names and abbreviations of the analytes with the respective *m/z* values of their deprotonated molecular ions $[M\text{-}H]^-$ and their specific daughter ions.

Name of analyte	Abbreviation	*m/z* of $[M\text{-}H]^-$	*m/z* of specific daughter ion (lost neutral fragment)
p-hydroxybenzoic acid	p-Hac	137.02441	93.03455 (-CO_2)
p-hydroxybenzaldehyde	p-Hal	121.02943	121.02943 (no loss)
p-hydroxyacetophenone	p-Hon	135.04517	135.04517 (no loss)
vanillic acid	Vac	167.03498	152.01151 (-CH_3)
vanillin	Val	151.04007	136.01657 (-CH_3)
acetovanillone	Von	165.05572	150.03220 (-CH_3)
ethylvanillin (internal standard)	Eval	165.04518	136.01659 (-CH_2CH_3)
syringic acid	Sac	197.04555	182.02234 (-CH_3)
syringaldehyde	Sal	181.05063	166.02708 (-CH_3)
acetosyringone	Son	195.06628	180.04292 (-CH_3)
trans-ferulic acid	t-Fac	193.05063	134.03734 (-CH_3, -CO_2)
p-coumaric acid	p-Cac	163.04007	119.05024 (-CO_2)
trans-cinnamic acid (internal standard)	t-Ciac	147.04520	147.04520 (no loss)

4.3 Results and Discussion

4.3.1 Method development

Separation of LOPs with LC gradient elution and identification of LOPs with MS/MS-experiments

A sufficient separation of the eleven LOPs and two internal standards was achieved within 4.5 min on a PFP column with H_2O/ACN-gradient elution, as can be seen in Figure 4.2, which shows the normalized chromatogram of 14 LOP standards. The analytes were identified via the exact mass of their molecular ion, their retention time compared to standards and their fragmentation pattern in the MS^2 spectrum. As the chromatograms of the real samples were very complex, all three methods were indeed required to identify and quantify the analytes. Whenever possible, the quantification was done by integrating the chromatographic peak of the molecular ion. However, when the target analyte peak could not be baseline separated from another signal, the chromatographic peak of a specific daughter ion was used to quantify the analyte.

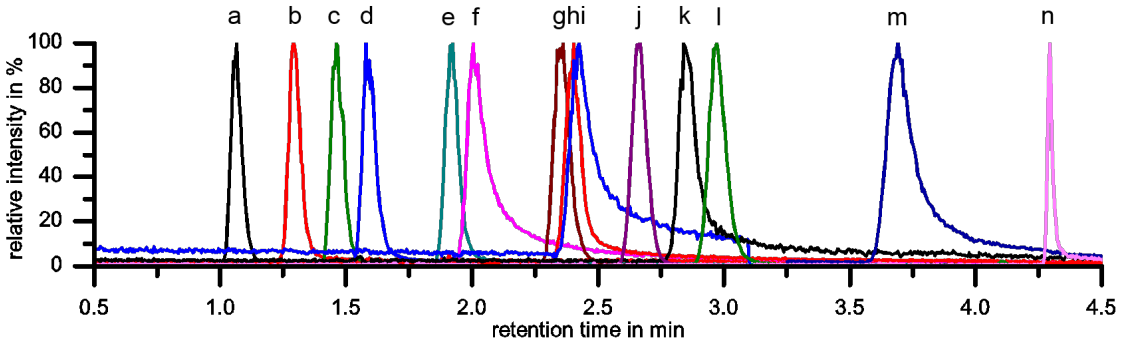

Figure 4.2: Normalized chromatogram of 14 LOP standards on a PFP column. Explanation of the peak numbers (for abbreviations see Table 4.1): (a) p-Hac, (b) Vac, (c) Sac, (d) p-Hal, (e) p-Hon, (f) Val, (g) p-Cac, (h) Sal, (i) Von, (j) c-Fac, (k) Son, (l) t-Fac, (m) EVal, (n) t-Ciac.

Optimisation of the solid phase extraction procedure for LOPs

Two different types of SPE-cartridges were tested. The polymer-based Oasis HLB cartridges (hydrophilic lipophilic balanced polymer, Waters) showed better reproducibility and equal recovery values compared to the silica-based Supelco C18 cartridges (Sigma Aldrich). The recovery rates could be improved by adding ammonia to the elution solvent, ACN or MeOH, as can be seen in Figure 4.32. The basic pH value of the eluent leads to deprotonation of the phenolic hydroxyl group. In this ionic state, the analytes are better soluble in the polar mobile phase and their adsorption to the stationary phase is weakened. Since we observed an oxidation of aldehydes and an isomerization of p-coumaric acid and ferulic acid when MeOH was used as elution solvent – an observation that has been made before (Lima et al.,

2007) – ACN with ammonia was used as elution solvent. The recovery rates ranged from 69% to 101% and are shown in Fig. 4.3 and Table 4.2.

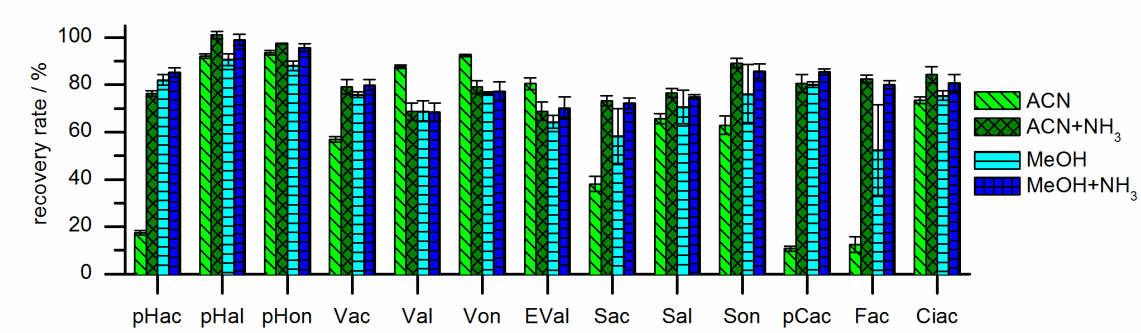

Figure 4.3: Recovery rates of the 13 LOPs on oasis HLB SPE cartridges, eluted with acetonitrile (ACN), acetonitrile with ammonia (ACN+NH_3), methanol (MeOH) and methanol with Ammonia (MeOH+NH_3). The recovery rates improved significantly if ammonia was added to the elution solvent.

Ethyl acetate was tested as elution solvent, too, as used by Kögel and Bochter; however, the recovery rates were lower than with methanol or acetonitrile. In addition, it was observed that with ethyl acetate, aldehydes were lost in the evaporation step (Fig. A.1 in the supplement in section A.1 in appendix A). The SPE method was tested with spikes of LOP standards of different concentrations reaching from 25 ng to 1000 ng in 20 mL of surrogate sample solution (i.e. 1.25–50 ng $\cdot$ mL^{-1} in the surrogate sample solution or 125–5000 ng $\cdot$ mL^{-1} in the final sample solution injected into the LC-MS system). The recovery rate was constant at all concentration levels and the linearity was very good ($R^2 > 0.9990$) for all analytes (Fig. A.2 and A.3 in the supplement in section A.2 in appendix A).

Comparison of different durations and temperatures of the CuO oxidation method

In former studies, the duration of the CuO oxidation method varied between 90 min and 180 min and temperatures of 150 °C or 170 °C have been applied. Therefore, we compared temperatures of 155 °C and 175 °C (the temperature of the microwave program was chosen 5 °C higher than the desired temperature in the Teflon vessels) and durations of 90 min and 180 min, using 100 µg of mixed lignin as standard sample and three subsamples for each constellation. The results are shown in Figure 4.4. At a temperature of 175 °C and a duration of 180 min, the concentrations of almost all LOPs were dramatically diminished, probably due to over-oxidation. For Val, Von, Sal, pCac and Fac, the highest concentrations were reached with 155 °C and 90 min, every increase in temperature or duration of the oxidation step resulted in a loss of analyte. In consequence, the C/V ratio decreased from 0.037 for 155 °C, 90 min to 0.018 for increased temperature, to 0.014 for increased duration and to 0.009 if both were increased. Similarly, the Vac/Val ratio increased from 0.44 for 155 °C, 90 min to 0.83 for increased temperature and to 0.54 for increased duration. For the Sac/Sal ratio, the increase was from 0.16 for 155 °C, 90 min to 0.37 and 0.28, respectively.

These results show, that especially the C-group LOPs, pCac and Fac, as well as the aldehydes Val and Sal and the ketone Von are prone to over-oxidation. Therefore, care should be taken to adjust temperature and duration of the CuO oxidation step to avoid over-oxidation of the LOPs, otherwise the lignin oxidation parameters C/V, S/V and acid/aldehyde ratios will be distorted. The prevention of over-oxidation by the addition of glucose was also tested; however, this did not improve the analysis (see Figs. A.4 and A.5 in the supplement in section A.3 in appendix A).

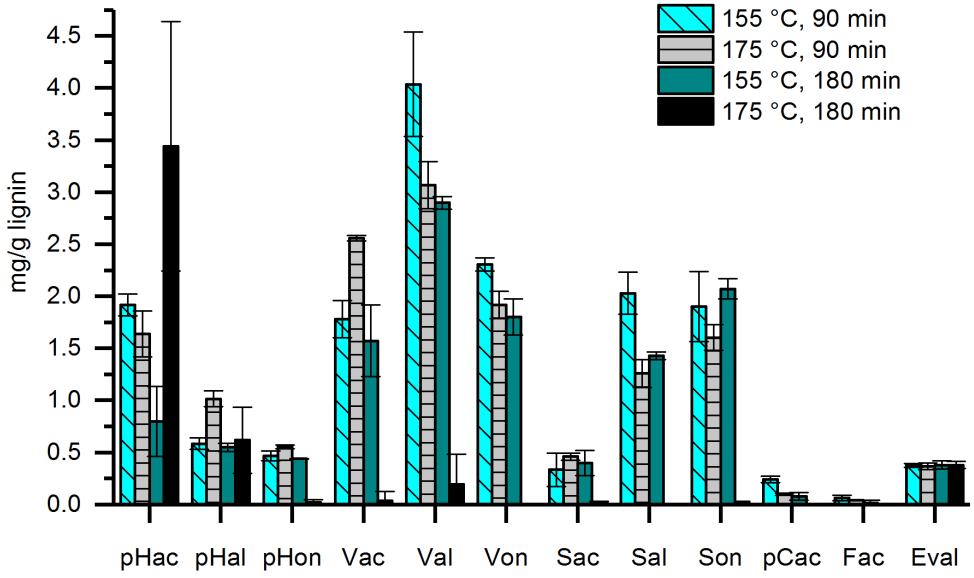

Figure 4.4: Results of a CuO oxidation step at 155 °C and 90 min (light blue bars with diagonal stripes), 175 °C and 90 min (grey bars with horizontal stripes), 155 °C and 180 min (dark cyan bars) and 175 °C and 180 min (black bars). Eval was added after the CuO oxidation step as internal standard.

Comparison of two sample preparation methods – acid digestion of the stalagmite samples and direct CuO oxidation of stalagmite powder

Obviously, each individual step in the analytical sample preparation method includes the risk of positive or negative artifacts, especially if large amounts of chemicals are added. Therefore, experiments were performed to test whether the HCl dissolving step can be skipped by grinding the stalagmite sample and directly adding the powder into the microwave reaction vessels. 24 g of cleaned stalagmite sample were coarsely crushed and mixed. 12 g of this sample mixture were dissolved in HCl and extracted via SPE as described above. The solution was then divided into three subsamples. The other 12 g were finely ground in a mortar, divided into three subsamples and added directly into the microwave reaction vessels. Figure 4.5 shows that the LOP concentrations found in the acid digested samples were higher for most analytes than in the ground samples. An explanation for this finding might be that at least a part

of the lignin particles is bound in the calcite crystals and is only fully released in the acid digestion method. Blyth et al. (2006) already stated similar findings for lipid biomarkers. Consequently, the acid digestion step is essential for the analysis of the target analytes in speleothems.

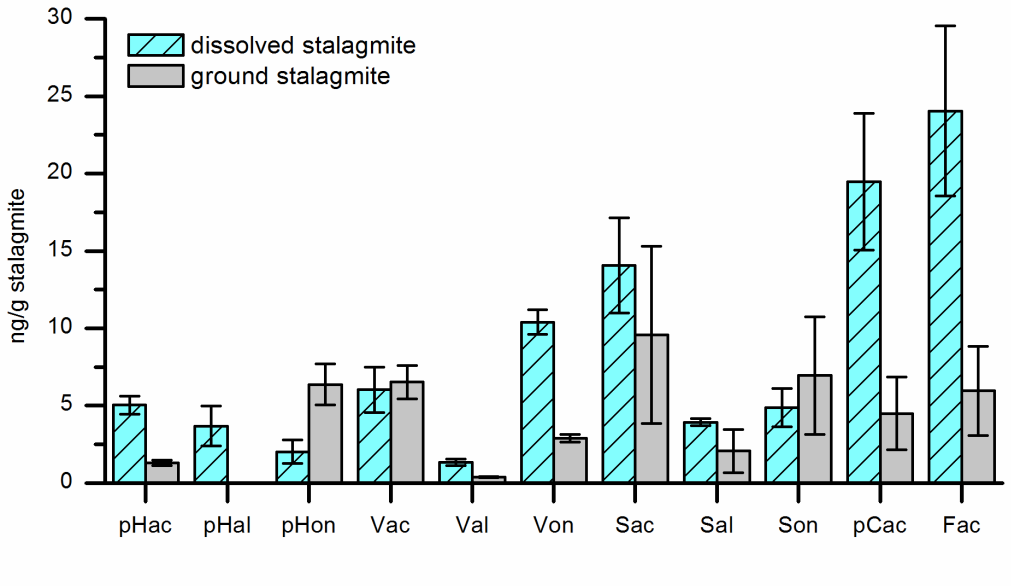

Figure 4.5: Results of dissolved stalagmite samples (light blue bars with diagonal stripes) compared to ground stalagmite samples (grey bars). Dissolving of the samples lead to higher amounts of LOPs.

4.3.2 Method validation and quality assurance

Selectivity

The selectivity of the method was assured by using three parameters for peak identification: the retention time, the exact m/z ratio of the analyte, and the MS^2-spectra, as described in section 4.3.1. The variation in the retention time was ± 0.01 min. To assure that the measured peak area was caused only by the analyte, the corrensponding peak area of the reagent blank measurement was subtracted.

Calibration and linearity

External calibration with a standard mixture containing all analytes was performed. The calibration function was obtained using the linear regression method. The parameters of the individual calibration functions are shown in Table A.1 in the supplement in section A.4 in appendix A. The concentrations of the standards ranged from 20–500 ng $\cdot$ mL^{-1} for stalagmite and dripwater samples and up to 2000 ng $\cdot$ mL^{-1} for plant and lignin samples. The calibration was linear in this range.

Limits of detection and quantification and reagent blanks

The instrumental limits of detection (LOD) and quantification (LOQ) were calculated by using equations (4.1) and (4.2), with σ_0 = standard deviation of the peak area of the solvent blank, or, if no signal was detectable for the solvent blank, of the lowest calibration standard, and the slope of the calibration function, m. The results are shown in Table A.1 in the supplement in section A.4 in appendix A.

$$\text{instrumental limit of detection} \qquad \text{LOD} = \frac{3.3 \cdot \sigma_0}{m} \tag{4.1}$$

$$\text{instrumental limit of quantification} \qquad \text{LOQ} = \frac{10 \cdot \sigma_0}{m} \tag{4.2}$$

To eliminate the influence of possible contamination sources on the results, a reagent blank, which had undergone all sample preparations steps, was analyzed with every batch of samples. The concentrations of LOPs measured in this reagent blank were subtracted from the concentrations measured in the samples. The mean values of six reagent blanks measured on different days are shown in Table 4.2 (the concentrations refer to the final sample solution injected into the LC-MS system). The values ranged from 1.0 ng $\cdot$ mL^{-1} to 680 ng $\cdot$ mL^{-1}, depending on the analyte (see also 4.3.2). The blank value varied from batch to batch, which is reflected in the standard deviations of the blank values given in Table 4.2. Therefore, the method detection limit (MDL) and the method quantification limit (MQL) were calculated using only the standard deviation of the peak area of the reagent blank, as shown in equations (4.3) and (4.4), with σ_B = standard deviation of the peak area of the reagent blank and m = slope of the calibration function. The MDL was below 13.7 ng $\cdot$ mL^{-1} for all relevant analytes and the MQL was below 41.5ng $\cdot$ mL^{-1} for all relevant analytes.

$$\text{method detection limit} \qquad \text{MDL} = \frac{3.3 \cdot \sigma_B}{m} \tag{4.3}$$

$$\text{method quantification limit} \qquad \text{MQL} = \frac{10 \cdot \sigma_B}{m} \tag{4.4}$$

Origin of blank values

The blank values shown in Table 4.2 reflect the natural occurrence of the different analytes. The highest blank values have been found for the p-hydroxy group, p-coumaric acid, cinnamic acid, vanillin and vanillic acid. The p-hydroxy group is known to originate not only from lignin, but also from protein rich material such as bacteria (Jex et al., 2014). For p-hydroxy acetophenone, which has a lower blank value than p-hydroxy benzoic acid and p-hydroxy benzaldehyde, it is in discussion whether it originates from lignin or from other sources (Dittmar and Lara, 2001). P-coumaric acid occurs in sporopollenin (Fraser et al., 2012, Montgomery et al., 2016), which is a major component of pollen and fungal spores and also occurs in some form of algae (Delwiche et al., 1989). Therefore, para-coumaric acid might be introduced into the sample via the laboratory air or via insufficiently purified water. Vanillin and its oxidised form vanillic acid are frequently used as perfumes and flavourings in

Table 4.2: Method detection limit after subtraction of the reagent blank (MDL) in $ng \cdot mL^{-1}$, method quantification limit after subtraction of the reagent blank (MQL) in $ng \cdot mL^{-1}$, mean value of three subsamples of 3.4 g stalagmite after blank subtraction in $ng \cdot mL^{-1}$ and in $ng \cdot g^{-1}$ of the initial stalagmite sample, mean blank value of six reagent blanks measured on different days in $ng \cdot mL^{-1}$, and recovery values of the SPE procedure to extract LOPs (Recov. SPE) in %. All concentrations in $ng \cdot mL^{-1}$ refer to the final sample solution injected into the LC-MS system. The errors stated in this table are standard deviations of n samples. For the methods of calculation used please refer to the text. The abbreviations for the analytes are shown in Table 4.1.

Analyte	MDL /$ng \cdot mL^{-1}$	MQL /$ng \cdot mL^{-1}$	Mean stalagmite /$ng \cdot mL^{-1}$ (n=3)	Mean stalagmite /$ng \cdot g^{-1}$ (n=3)	Mean blank /$ng \cdot mL^{-1}$ (n=6)	Recov. SPE /% (n=3)
p-Hac	13.8	41.9	5 ± 30	2.9 ± 1.8	155 ± 130	76 ± 1
p-Hal	25.9	78.4	2 ± 85	1.5 ± 5.0	680 ± 330	101 ± 2
p-Hon	2.3	7.0	55 ± 5	3.2 ± 0.3	8 ± 20	97 ± 0
Vac	13.7	41.5	330 ± 80	19.4 ± 4.7	60 ± 30	79 ± 3
Val	8.2	24.8	0 ± 20	0.0 ± 1.2	65 ± 30	69 ± 4
Von	3.7	11.3	1405 ± 140	82.6 ± 8.2	20 ± 10	79 ± 3
Sac	0.3	0.8	140 ± 10	8.2 ± 0.6	6 ± 3	73 ± 2
Sal	2.3	7.1	13 ± 6.5	0.8 ± 0.4	5 ± 4	77 ± 2
Son	2.5	7.7	110 ± 30	6.5 ± 1.8	4 ± 4	89 ± 2
t-Fac	2.0	6.2	100 ± 0.5	5.9 ± 0.0	5 ± 2	83 ± 2
p-Cac	0.2	0.7	195 ± 60	11.5 ± 3.5	445 ± 505	81 ± 4
Eval (IS)	0.6	1.8	147 ± 4	8.6 ± 0.2	1 ± 1	69 ± 4
Ciac	3.8	11.6	105 ± 35	6.2 ± 2.1	100 ± 20	84 ± 3

food, cosmetics and household cleaning products. Therefore, these compounds might also be introduced into the sample via the laboratory air or via detergents used to clean the lab ware. Cinnamic acid is used as a perfume and flavouring, too, and it also occurs naturally in bacteria, fungi and algae, as it is part of the shikimate pathway (Dewick, 2009). In this study, cinnamic acid was found in the blank and in all samples. Therefore, cinnamic acid is not suitable as internal standard in the analysis of LOPs in natural samples, although it has been used as internal standard in many studies before (Goñi and Montgomery, 2000, Kaiser and Benner, 2012). Ethyl vanillin is much more suitable as internal standard because, as an artificial compound, it has very low blank values and does not occur in natural samples.

Repeatability

To determine the repeatability of the sample preparation and analysis method, 10.2 g stalagmite were dissolved, and the solution divided into three subsamples containing

3.4 g stalagmite. The mean values and standard deviations for all analytes are shown in Table 4.2. The relative standard deviations ranged from 0.7% to 32% for analytes with more than 2.6 ng (50% for Sal with 2.6 ± 1.3 ng). For the p-hydroxy group, the relative standard deviations were higher, but these analytes were not used for the determination of LOP parameters. The LOP parameters calculated from these three subsamples were a C/V ratio of 0.17 ± 0.04 and an S/V ratio of 0.15 ± 0.02. The variability was mainly caused by the CuO oxidation step, which is known to cause relatively high variability even in samples with higher lignin content (for example Hedges and Mann (1979) with standard deviations ranging between 3% and more than 80%). The SPE method used for the extraction of LOPs had standard deviations between 1–6% (Table 4.2) and therefore did not contribute much to the overall variability of the method.

Estimation of uncertainty

According to Konieczka and Namieśnik (2010), the main factors contributing to the uncertainty budget are the uncertainty of the measurement of the weight or volume of the sample, u_r(sample), the repeatability of the sample preparation procedure, u_r(rep.), the recovery determination of the internal standard, u_r(recov.), the calibration step, u_r(cal.), and the uncertainty associated with analyte concentrations close to the limit of detection, u_r(LOD). The combined relative uncertainty U_r is expressed in equation 4.5.

$$U_r = \sqrt{(u_r(\text{sample}))^2 + (u_r(\text{rep.}))^2 + (u_r(\text{recov.}))^2 + (u_r(\text{cal.}))^2 + (u_r(\text{LOD}))^2} \tag{4.5}$$

In our method, u_r(sample) is relatively small with 1 mg or 1 mL, which is usually $< 1\%$. The uncertainty associated with the repeatability of the sample preparation, calculated as the standard deviation of three individually prepared subsamples as explained in section 4.3.2, has the largest influence and can equal 1–30%. The uncertainty of the recovery determination of the internal standard, calculated as the standard deviation of the internal standard, contributes with 1–6%. u_r(cal.), calculated as the standard deviation of the concentration determination of three injections of the same sample into the LC-MS-system, can equal 1–15%, but is usually around 3–5%. u_r(LOD), calculated according to equation (4.6), depends strongly on the concentration c of the analyte.

$$u_r(\text{LOD}) = \frac{\text{LOD}}{c} \tag{4.6}$$

In the data for stalagmite samples presented in Table 4.2, u_r(LOD) equals 0.1–5% for most analytes, 17% for Sal and 27–100% for the p-hydroxy group.

The errors for all results presented in this work were calculated using the law of propagation of uncertainty. All equations used for calculating concentrations, lignin oxidation parameters and errors are shown in section A.5 in the supplement in appendix A.

4.3.3 Application to real samples

Analysis of plant and lignin samples

The method was applied to different natural samples from known sources to verify that the C/V and S/V ratios are in accordance with published values. The results are shown in Table 4.3, and their S/V and C/V ratios are visualized in Figure 4.6. As expected, the highest concentrations of LOPs are found in the lignin from conifer wood with a Σ8 value of 75.76 $mg \cdot g^{-1}$ as well as in the lignin from wheat straw and mixed wood with a Σ8 value of 14.16 $mg \cdot g^{-1}$. This means that the CuO oxidation method has a conversion factor of 1.4–7.6% (w/w) if applied to pure lignin, and that the conversion factor also depends on the type of lignin. The plant tissue samples gave LOP concentrations (Σ8) of 2.3–6.8 $mg \cdot g^{-1}$ for the wood and bark samples and 1.24–1.30 $mg \cdot g^{-1}$ for the leave and needle samples. These concentrations can be explained by the respective lignin content of the different samples. Figure 4.6 shows the C/V versus S/V diagram for all samples. The regions for different plant types have been defined by Hedges and Mann in 1979 and are based on the analysis of different plant species. Gymnosperm woody samples contain mainly V-group LOPs. Therefore, they plot close to the origin of the diagram. Angiosperm woody samples contain V- and S-group LOPs, but almost no C-group LOPs. Consequently, they plot close to the S/V-axis. Gymnosperm non-woody samples contain V- and C-group LOPs, but almost no S-group LOPs. Accordingly, they plot close to the C/V-axis. Angiosperm non-woody samples contain all three groups of LOPs and thus show a wide range of C/V and S/V ratios. The analyzed plant samples in our study plot all in or close to the expected regions according to their plant type. Only the maple wood and bark sample and the maple leaves sample plot slightly outside of the regions for angiosperm woody and angiosperm non-woody material, respectively. For the maple wood and bark sample, this could be due to a higher contribution of C-group LOPs in the bark compared to pure woody samples. However, it is important to keep in mind that these regions are just broadly defined and are based on a limited number of analyses and a limited number of different plant species.

Analysis of stalagmite samples

With a Σ8 value of ca. 40–110 $ng \cdot (g\,\text{stalagmite})^{-1}$ (Table 4.4), the LOP concentration of the stalagmite samples is five orders of magnitude lower than for the vegetation samples and three to four orders of magnitude lower than the typical concentration of sediment samples (e.g., Σ8 is 0.15–0.75 $mg \cdot (g\,\text{sediment})^{-1}$ in Tareq et al. (2011)). Because of these low concentrations, 3–5 g stalagmite were required for an analysis to be above the limit of quantification. The C/V ratios of the stalagmite samples were all above 0.5, and the S/V ratios were all above 1.0, which suggests a significant contribution of angiosperm woody and angiosperm non-woody vegetation. However, gymnosperm woody and gymnosperm non-woody material might also have contributed to the lignin pool. This suggests a mixed deciduous forest above the cave, and would be in accordance with the results of Litt et al., who analyzed pollen from Holocene lake sediments from the Westeifel Volcanic Field (Litt et al., 2009), which is relatively close to the Herbstlabyrinth.

Table 4.3: Concentrations of the V, S and C-group LOPs, the sum of all 8 LOPs (Σ8) and the ratios C/V and S/V in fresh plant and lignin samples.

Sample	V-group /mg · g^{-1}	S-group /mg · g^{-1}	C-group /mg · g^{-1}	Σ8 /mg · g^{-1}	C/V	S/V
lignin from	75.12	0.293	0.345	75.76	0.00	0.00
conifer wood	± 0.77	± 0.015	± 0.012	± 0.77	± 0.00	± 0.00
lignin from	7.42	6.483	0.255	14.16	0.03	0.87
wheat straw and	± 0.10	± 0.078	± 0.009	± 0.13	± 0.00	± 0.02
mixed wood						
yew wood and	2.25	0.024	0.083	2.35	0.04	0.01
bark	± 0.04	± 0.001	± 0.001	± 0.04	± 0.00	± 0.00
maple wood and	2.87	3.626	0.303	6.80	0.11	1.27
bark	± 0.04	± 0.089	± 0.002	± 0.10	± 0.00	± 0.04
yew needles	0.74	0.059	0.494	1.30	0.66	0.08
	± 0.02	± 0.001	± 0.010	± 0.02	± 0.02	± 0.00
maple leaves	0.75	0.314	0.184	1.24	0.25	0.42
	± 0.02	± 0.005	± 0.003	± 0.02	± 0.01	± 0.01

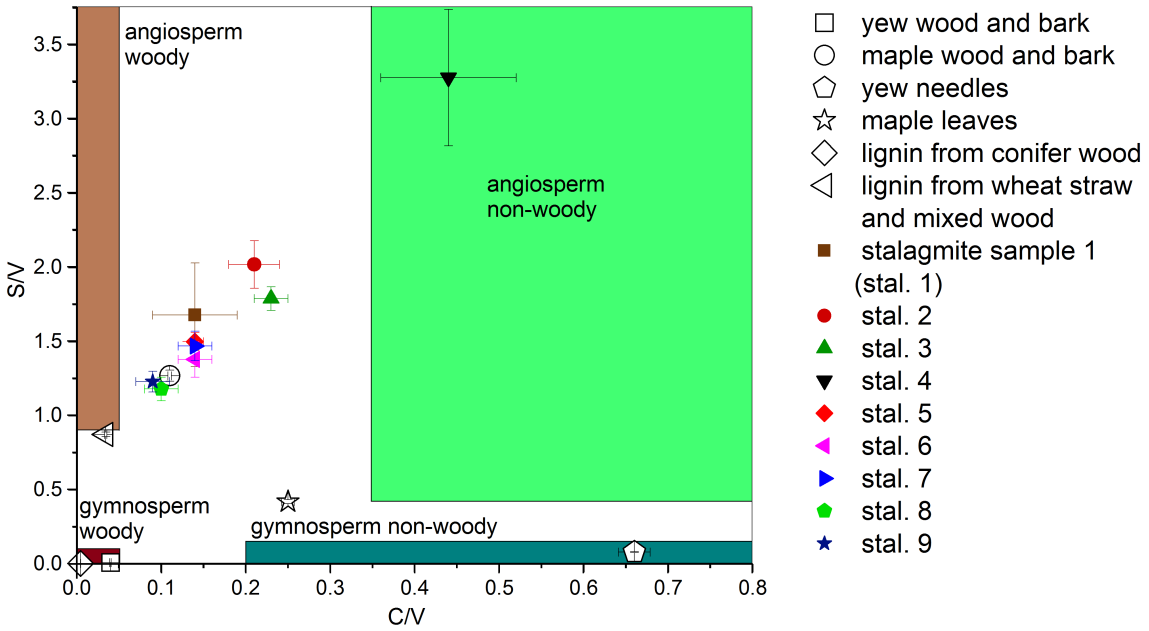

Figure 4.6: Lignin oxidation parameters S/V vs. C/V of different real samples and regions for different sample types defined by Hedges and Mann in 1979.

Table 4.4: Concentrations of the V-, S- and C-group LOPs and the sum of all 8 LOPs (Σ8) in $ng \cdot g^{-1}$ of the initial stalagmite samples (stal.)and the ratios C/V and S/V. All samples are from stalagmite *NG01* from the Herbstlabyrinth-Advent Cave.

Sample	V-group $/ng \cdot g^{-1}$	S-group $/ng \cdot g^{-1}$	C-group $/ng \cdot g^{-1}$	Σ8 $/ng \cdot g^{-1}$	C/V	S/V
stal. 1	20.9 ± 3.6	41.0 ± 3.8	3.4 ± 0.7	65.3 ± 5.3	0.16 ± 0.05	1.96 ± 0.39
stal. 2	19.5 ± 1.4	45.5 ± 3.2	4.7 ± 0.5	69.7 ± 3.5	0.24 ± 0.03	2.33 ± 0.23
stal. 3	17.4 ± 0.8	37.1 ± 1.4	4.8 ± 0.3	59.3 ± 1.6	0.27 ± 0.02	2.14 ± 0.13
stal. 4	7.6 ± 0.9	29.1 ± 2.0	3.8 ± 0.3	40.6 ± 2.2	0.51 ± 0.07	3.84 ± 0.51
stal. 5	38.2 ± 2.6	67.3 ± 3.4	6.4 ± 0.6	111.9 ± 4.3	0.17 ± 0.02	1.76 ± 0.15
stal. 6	24.5 ± 1.5	40.0 ± 1.7	4.1 ± 0.3	68.6 ± 2.3	0.17 ± 0.01	1.63 ± 0.12
stal. 7	24.4 ± 1.4	42.1 ± 2.2	3.9 ± 0.2	70.4 ± 2.6	0.16 ± 0.01	1.72 ± 0.14
stal. 8	25.7 ± 1.3	35.5 ± 1.7	2.9 ± 0.2	64.1 ± 2.2	0.11 ± 0.01	1.38 ± 0.10
stal. 9	39.1 ± 2.8	56.2 ± 2.8	4.1 ± 0.3	99.4 ± 3.9	0.10 ± 0.01	1.44 ± 0.13

The nine stalagmite samples were taken at different distances from the top of the stalagmite. This analysis shall serve as a proof of principle for a higher-resolution analysis of the whole stalagmite. In Figure 4.7, the C/V and S/V ratios are plotted against distance from top (dft). Both ratios show a pronounced peak at 20 cm dft.

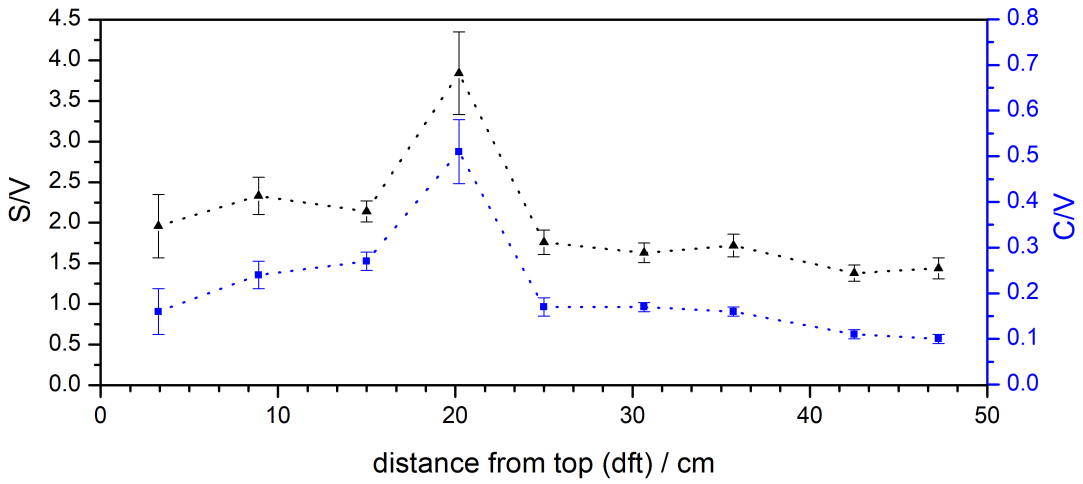

Figure 4.7: S/V (black triangles, left axis) and C/V (blue squares, right axis) ratios of stalagmite *NG01* plotted against the distance from the top of the stalagmite.

Furthermore, both ratios show higher values in the top 15 cm and lower values with a decreasing trend between 30 and 50 cm dft. A higher S/V ratio indicates a higher contribution of angiosperm vegetation to the lignin source, and a higher C/V ratio suggests a higher contribution of non-woody vegetation. Therefore, the peak at 20 cm dft could be interpreted as increased input of non-woody, angiosperm

vegetation, such as grasses, and less input of wood. The decreasing trend in the lower part of the stalagmite indicates a trend towards more woody, gymnosperm vegetation, such as pine forest. Of course, these presumptions have to be proven by a complete analysis of the stalagmite and a comparison with the other proxy data (Mischel et al., 2017). In addition, a comparison with Holocene pollen records from the area may confirm these preliminary results. Overall, these first results show significant variability of the C/V and S/V ratios and, therefore, the lignin sources. This promising result encourages us to use the analysis of LOPs in stalagmites for paleo-vegetation reconstruction.

Analysis of cave dripwater samples

Very little is known about how lignin is transported from the soil into the cave and how it is incorporated into a stalagmite. To gain further understanding about these processes, it is useful to also analyze lignin in cave dripwater. The lignin concentration in cave dripwater is even lower than in stalagmite samples, because crystallization of calcite also serves as an enrichment step for the organic components contained in the water. Therefore, a sample volume of 100–200 mL water was used. Here we show the results of the analysis of six different water samples from the Herbstlabyrinth-Advent-Cave, all sampled in October 2014 (Table 4.5). As expected,

Table 4.5: Concentrations of the V-, S- and C-group LOPs, the sum of all 8 LOPs (Σ8) and the ratios C/V and S/V in different water samples (rain water *RW*, soil water *SW*, two fast dripping sites *D1* and *D5*, a slow dripping site *D2* and cave pool water *PW*) collected at the Herbstlabyrinth-Advent-Cave in October 2014.

Sample	Volume /L	V-group /ng · L^{-1}	S-group /ng · L^{-1}	C-group /ng · L^{-1}	Σ8 /ng · L^{-1}	C/V	S/V
RW	0.185	918	345	76	1339	0.08	0.38
		± 69	± 31	± 17	± 77	± 0.02	± 0.04
SW	0.076	1370	363	42	1775	0.03	0.26
		± 101	± 54	± 38	± 121	± 0.03	± 0.04
D1	0.265	271	87	7	365	0.03	0.32
		± 21	± 16	± 11	± 29	± 0.04	± 0.07
D5	0.258	175	95	6	275	0.03	0.54
		± 20	± 19	± 12	± 30	± 0.07	± 0.13
D2	0.205	157	107	4	269	0.03	0.68
		± 15	± 29	± 14	± 35	± 0.09	± 0.19
PW	0.253	114	88	8	210	0.07	0.77
		± 23	± 29	± 21	± 42	± 0.18	± 0.29

the soil water (*SW*) has the largest lignin content with 1.8 µg · L^{-1}. The rain water (*RW*) also has a relatively large lignin content of 1.3 µg · L^{-1}, which is surprising since this water has not been in contact with soil or vegetation. The lignin content of the cave dripwater samples is much lower, ranging from 0.21 µg · L^{-1} for the pool water to

0.36 µg · L^{-1} for the fast drip site *D1*. The concentrations of all LOPs decrease from the soil water to the cave dripwater, but to a different extent. Whereas V-group LOPs and C-group LOPs decrease by 80–92% and 82–90%, respectively, the concentration of S-group LOPs decreases only by 70–76% (Fig. 4.8). This is also reflected in higher S/V ratios in the cave dripwater than in the soil water, with an increasing trend from the soil water over the two fast drip sites *D1* and *D5* and the slow drip site *D2* to the cave pool water. This could be due to different residence times in the cave and the overlaying karst of the water from the different drip sites. These hypotheses should be proven by a further systematic analysis of cave dripwater. This would also enable the study of seasonal variations in the lignin input. The monthly cave monitoring program of Mischel et al. (Mischel et al., 2017, 2015) combined with our new method for the analysis of LOPs even in low-concentration cave dripwater could be a valuable tool to further investigate these topics.

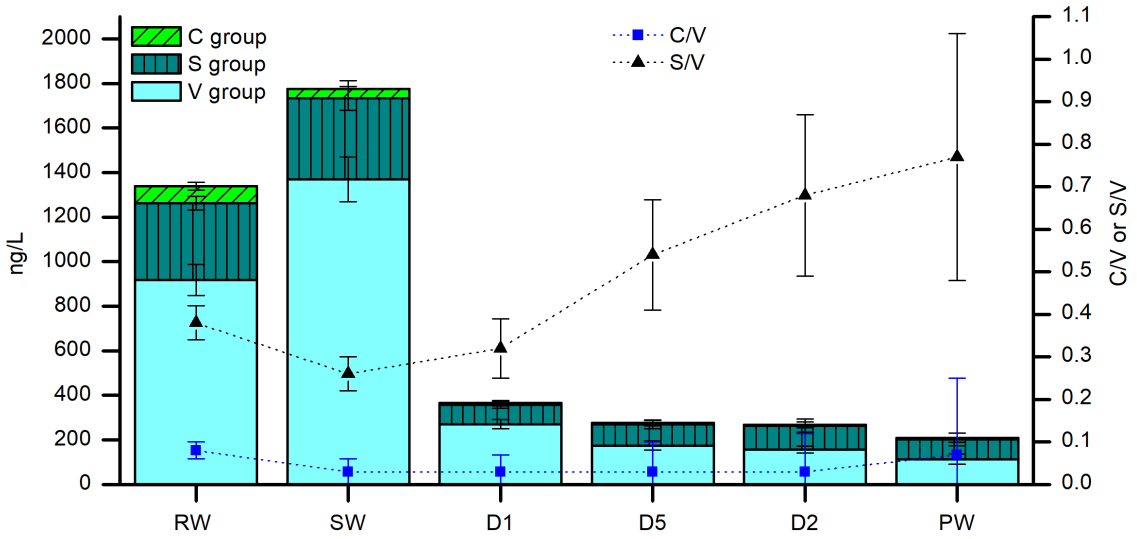

Figure 4.8: LOP concentrations (stacked columns with left axis) and LOP ratios (symbols with right axis) of rain water (*RW*), soil water (*SW*), cave dripwater from fast drip sites (*D1* and *D5*), a slow drip site (*D2*) and cave pool water (*PW*). The stacked columns contain the V-group LOPs (light cyan bars), S-group LOPs (dark cyan bars with vertical stripes) and C-group LOPs (green bars with diagonal stripes). Black triangles show the S/V ratio and blue squares show the C/V ratio.

4.4 Aspects of green analytical chemistry

When developing a new analytical method, it is advantageous to consider how environment-friendly (*green*) the different approaches are. The principles of green analytical chemistry include, among others, to generate as little waste as possible, to eliminate or replace toxic reagents, to miniaturize analytical instruments or to avoid derivatization (Gałuszka et al., 2013, Armenta et al., 2008). In our method, we tried

to favour greener approaches over less green approaches whenever possible without sacrificing other qualities like sensitivity. We used solid phase extraction, which consumes considerably less solvent than liquid-liquid extraction, and UHPLC, which is less solvent and time consuming than HPLC. In addition, liquid chromatography does not require a derivatization step, as opposed to gas chromatography. However, the least green step in our method is the CuO oxidation step, as it generates toxic waste and consumes energy. We still chose the CuO oxidation method for our proof of principle analysis because it is the most widely used lignin degradation method for the analysis of LOPs and therefore allows us to compare our results with existing LOP records. In future, however, a greener approach to the degradation of lignin to LOPs should be chosen, which could, for example, be based on electrolysis, preferably in a miniaturized flow cell (Leppla, 2016).

4.5 Conclusions and outlook

We developed a sensitive method for the quantification of LOPs in speleothems and cave dripwater and tested it successfully on samples from the Herbstlabyrinth-Advent-Cave. This is, to our knowledge, the first quantitative analysis of LOPs in speleothems and cave dripwater. Our method provides a new and highly specific vegetation proxy for the reconstruction of paleo-vegetation and paleo-climate from speleothem archives. The method was adjusted to the low concentrations of organic matter in speleothems and cave dripwater and showed sufficient sensitivity to detect even trace concentrations of lignin. The use of the established CuO oxidation method allows to compare the results to LOP records in other archives. However, as the CuO oxidation step is the main source of variability in our method, an alternative degradation method for lignin with higher reproducibility should be developed. This method could, for example, be based on electrolysis. In addition, LOPs in speleothem samples from other caves in different vegetation and climate zones should be analyzed and compared with stable isotope and trace element records in order to gain more insight into the relation of vegetation, climate and the LOP signal in speleothems. The analysis of cave dripwater, sampled monthly within the framework of a cave monitoring program, could elucidate seasonal variations of lignin input as well as possible fractionation processes during its pathway from the soil to the cave.

Acknowledgements

We thank Simon Mischel for providing stalagmite and cave drip water samples from the Herbstlabyrinth-Advent Cave.

Author contributions

Conception and design of the work were done by IH, DS and TH. Data collection, performing of the experiments and drafting of the article were done by IH. Data

analysis and interpretation, critical revision of the article, and final approval of the version to be published were done by IH, DS and TH.

5 Comparison of electrochemical oxidation and CuO oxidation for the degradation of lignin

5.1 Introduction

As described in section 4.3.2, the main source of uncertainty in the sample preparation and analysis method is the CuO oxidation step. This is probably due to the relatively large amounts of reagents (NaOH, CuO, $(NH_4)_2Fe(SO_4)_2$) compared to the low lignin concentrations, which can lead to high blank values impeding the integration and quantification of LOPs. In addition, the composition of the product mixture of CuO oxidation depends on many factors, for example the organic carbon content, the temperature and duration of the degradation step, and the presence of oxygen. Therefore, an alternative, cleaner and more reproducible degradation method would be beneficial for the analysis of trace concentrations of lignin.

As described in section 2.2, the degradation of lignin into useful monomeric building blocks is also interesting for the chemical industry. Therefore, different approaches have been tested during the last decades, including thermal, microbial or enzymatic degradation, catalytic oxidation or hydrogenation, and electrolysis (Brebu and Vasile, 2010, Pandey and Kim, 2011, Xu et al., 2014, Zakzeski et al., 2010, Zirbes and Waldvogel, 2018, Li et al., 2016). Electrolysis is environmentally friendly as no toxic reagents such as transition metal catalysts or organic solvents are needed, and it uses less energy than, for example, thermal degradation due to the lower temperature and pressure. Although yields of up to 10% of monomeric lignin phenols can be achieved by electrolysis processes, these are usually obtained as a complex product mixture, which requires a difficult purification process (Zirbes and Waldvogel, 2018). The Waldvogel laboratory developed a selective method for the production of vanillin in a yield of up to 1.8% from Kraft lignin using electrodes made of different transition metal alloys. Nickel electrodes proved to be particularly well suited because they are resistant to corrosion and even show increased yields of vanillin upon repeated use of the electrodes due to a modification of the surface (Schmitt et al., 2015, Zirbes et al., 2019). The mechanism of the electrolytic degradation of lignin using nickel electrodes was desribed by Pardini et al. (1991) and Miao et al. (2014) and involves nickel oxyhydroxide (NiOOH) as the electrocatalytically active species at the anodic surface, which is regenerated during lignin oxidation (Fig. 2.4 in section 2.2).

For the application in trace analysis of lignin, electrolysis has the particular advantages that it leads to low blank values because no additional reagents are needed, and that it is miniaturizable, which allows the use of smaller sample volumes and thus

less dilution. Furthermore, the electrolysis method is less time-consuming than the CuO oxidation method. It is therefore worth exploring electrolysis as an alternative to the conventional CuO oxidation method for the analysis of trace concentrations of lignin in environmental samples. Two methods, one using undivided electrolytic cells with a capacity of 5 mL and one using flow cells with a capacity of 1.2 mL, were developed during a master thesis, and their potential for trace analysis of lignin in speleothems was evaluated (Leppla, 2016). In addition, the influence of various parameters such as current density, temperature, charge quantity and the flow rate in flow cell experiments was investigated.

In this chapter, a direct comparison between the electrolytic degradation method developed by Leppla (2016) and the CuO oxidation method described in chapter 4 for the analysis of speleothem and plant samples is presented. In addition, the oxidation sensitivity of the individual LOPs is investigated.

5.2 Materials and methods

The preparation of the speleothem, plant and lignin samples up to the degradation step was the same as described in section 4.2.2. Three subsamples of the stalagmite were used and single samples for all other sample materials.

The reaction conditions for the batch electrolysis experiments have been optimized during a master thesis (Leppla, 2016). 1 mL of the sample solution in 2 $mol \cdot L^{-1}$ NaOH was transferred into undivided electrochemical cells made from PTFE with a capacity of 5 mL, see Fig. 5.1. The volume was filled up to 5 mL with 2 $mol \cdot L^{-1}$ NaOH. Nickel electrodes with a surface of 1.6 cm^2 were used. A magnetic stirrer ensured homogenous mixing. The electrolysis was carried out at room temperature (unless stated otherwise) in galvanostatic mode with a current of 20 mA, a current density of 12.5 $mA \cdot cm^{-2}$ and a terminal voltage of 1.5 V. A blank sample consisting of 5 mL 2 $mol \cdot L^{-1}$ NaOH was processed in the same way as the samples. For all screening experiments, a sample solution containing 0.2 $mg \cdot mL^{-1}$ of lignin from wheat straw and mixed wood was used. For the screening of the charge quantity, the electrolysis duration was varied between 15 s (0.3 C) and 45 min (54 C). For all other experiments, the charge quantity was set to 3.0 C (150 s) (Leppla, 2016).

For the flow experiments, a flow cell with a capacity of 1.2 mL was used, see Fig. 5.2, equipped with a steel cathode and a nickel anode with a surface of 12 cm^2. The terminal voltage was 3.3 V. For the screening of the flow rate, the current was set to 150 mA (12.5 $mA \cdot cm^{-2}$) and the flow rate was varied from 0.1 to 3.3 $mL \cdot min^{-1}$. For the screening of the current, the flow rate was set to 1.0 $mL \cdot min$ and the current was varied from 6 mA (0,5 $mA \cdot cm^{-2}$) to 240 mA (20 $mA \cdot cm^{-2}$).

After the electrolysis, 1 mL of every screening sample was transferred into a new vial, spiked with 50 µL 1 $\mu g \cdot mL^{-1}$ Eval, and acidified with HCl. For the batch samples, the whole sample solution was transferred and the vessels and electrodes were rinsed with NaOH, which was added to the sample solution. The solution was spiked with 100 µL 1 $\mu g \cdot mL^{-1}$ Eval for plant and lignin samples and with 50 µL 1 $\mu g \cdot mL^{-1}$ Eval for stalagmite samples, and acidified with HCl. The further processing and analysis of the samples was carried out as described in section 4.2.2.

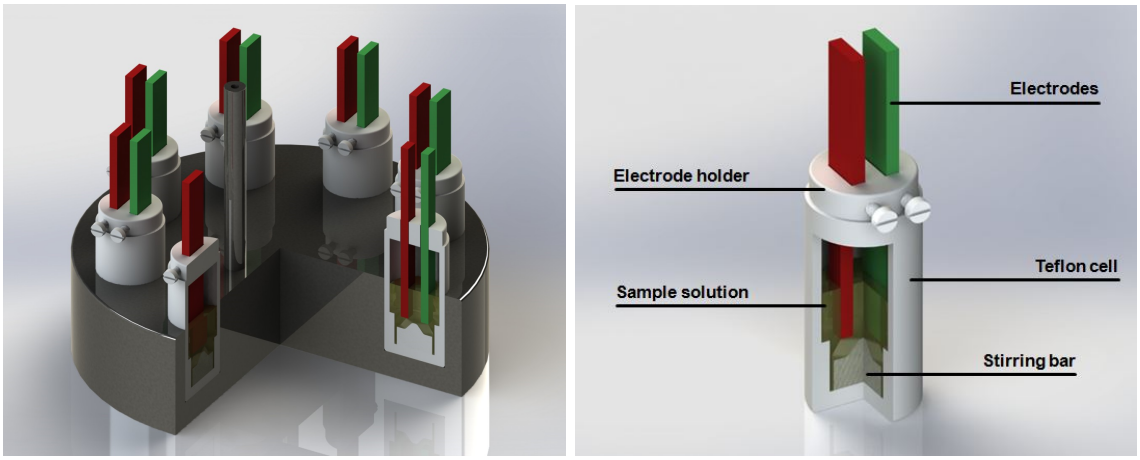

(a) Screening block with eight electrochemical cells.

(b) Electrochemical cell with description of the parts.

Figure 5.1: Schematic view of the electrochemical cell (images courtesy of Waldvogel Lab).

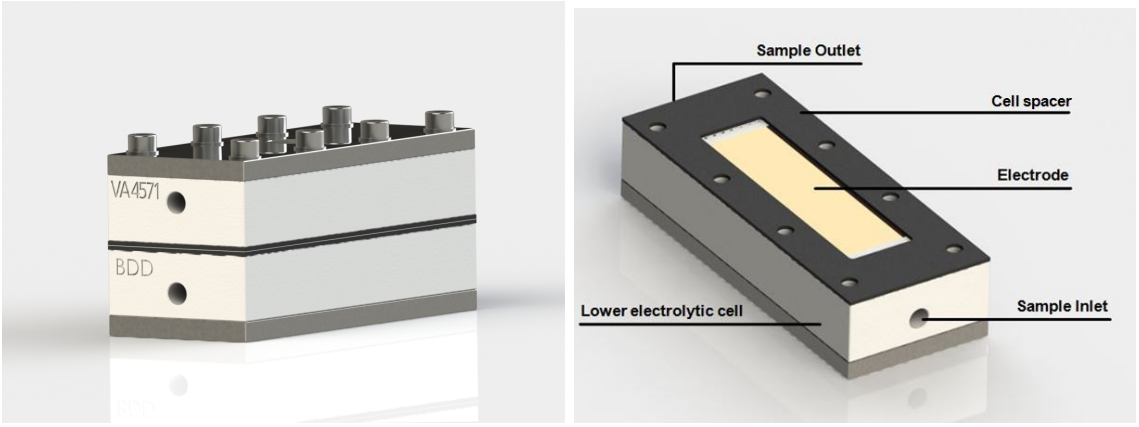

(a) Assembled flowcell.

(b) Lower part of the flowcell with description of the parts.

Figure 5.2: Schematic view of the flowcell (images courtesy of Waldvogel Lab).

.

For comparison, the samples were also analyzed without any degradation method. 1 mL of the initial sample solution were filtered over 1 µm filters, acidified with HCl and directly extracted via SPE.

5.3 Results and discussion

Figure 5.3 shows the comparison of the Σ8 concentrations of plant and lignin samples treated with CuO oxidation, electrolysis or without a degradation method. The CuO oxidation methods yields much higher concentrations of LOPs than the electrolysis method. In fact, the LOP concentrations reached with electrolysis are barely higher than the LOP concentrations that are already available without any degradation, just by base hydrolysis. In the stalagmite samples, the difference between the LOP concentrations reached by CuO oxidation and by electrolysis is even more pronounced, see Fig. 5.4. This is probably due to the fact that in the stalagmite samples, there are almost no freely available LOPs contained. The electrolysis results in the stalagmite samples are almost at the same level as the results without degradation. Therefore, we conclude that electrolysis is not a suitable alternative for the CuO oxidation method for the analysis of LOPs in stalagmite samples yet.

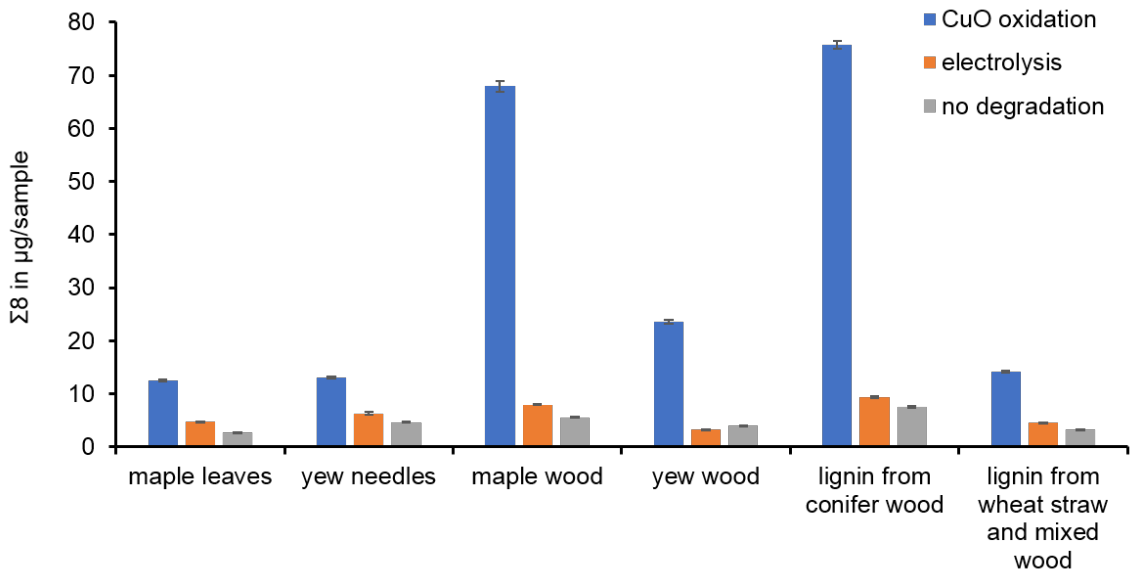

Figure 5.3: Comparison of the Σ8 concentrations of plant and lignin samples treated with CuO oxidation (blue bars), electrolysis (orange bars) or without degradation method (grey bars).

Figure 5.5 shows the C/V and S/V ratios obtained by CuO oxidation, electrolysis and without degradation. For lignin from conifer woods, the results are similar for all degradation methods and plot close to the origin. For lignin from wheat straw and mixed woods, yew wood and yew needles, the results of all three methods plot relatively close to each other and also in or close to the respective region in the diagram (angiosperm woody, gymnosperm woody, gymnosperm non-woody). For

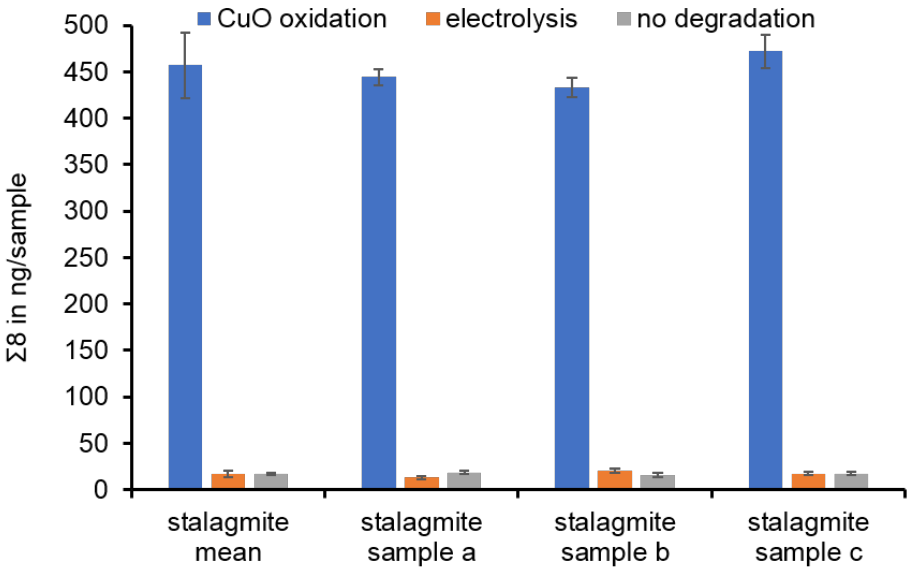

Figure 5.4: Comparison of the Σ8 concentrations of stalagmite samples treated with CuO oxidation (blue bars), electrolysis (orange bars) or without degradation method (grey bars).

maple leaves, maple wood and the stalagmite samples, there are larger differences between the results of the three methods. There is no clear trend that one method always yields higher or lower C/V or S/V ratios than the other methods. Because of the low LOP yields reached in the stalagmite samples with electrolysis and without degradation, these samples show much higher standard deviations then with CuO oxidation, both for the analysis of single subsamples (stalagmite a, b and c) and for the mean value of the three subsamples (stalagmite mean).

However, the electrolysis degradation method has got one clear advantage over the CuO oxidation method, namely a much lower blank value. This can be seen in the comparison of the total ion chromatograms of both methods in Fig. 5.6. The higher blank value in the CuO oxidation is probably caused by the various reagents, which are not needed in the electrolysis method. Admittedly, a low blank value is not an advantage in itself if the price is a very low analyte yield.

Another goal of the electrolysis experiments was to investigate the oxidation sensitivity of the individual LOPs. Therefore, screening experiments for different parameters were conducted. Figure 5.7 shows the results of a screening of the charge quantity using the batch cells. Only the concentrations of the P-group LOPs, especially pHal and pHon, show an increase with increasing charge quantity, whereas the concentrations of all other LOPs diminish with higher charge quantities (i. e. longer electrolysis time). For the C-group and S-group LOPs, the decline in the concentrations is faster and more pronounced than for the V-group LOPs. After the application of 54 $C \cdot mg(lignin)^{-1}$, the concentrations of all S- and C-group LOPs are below 20% of their initial values or even not detectable anymore, whereas the concentrations of Vac and Von have declined only by 50% and even show a rise from

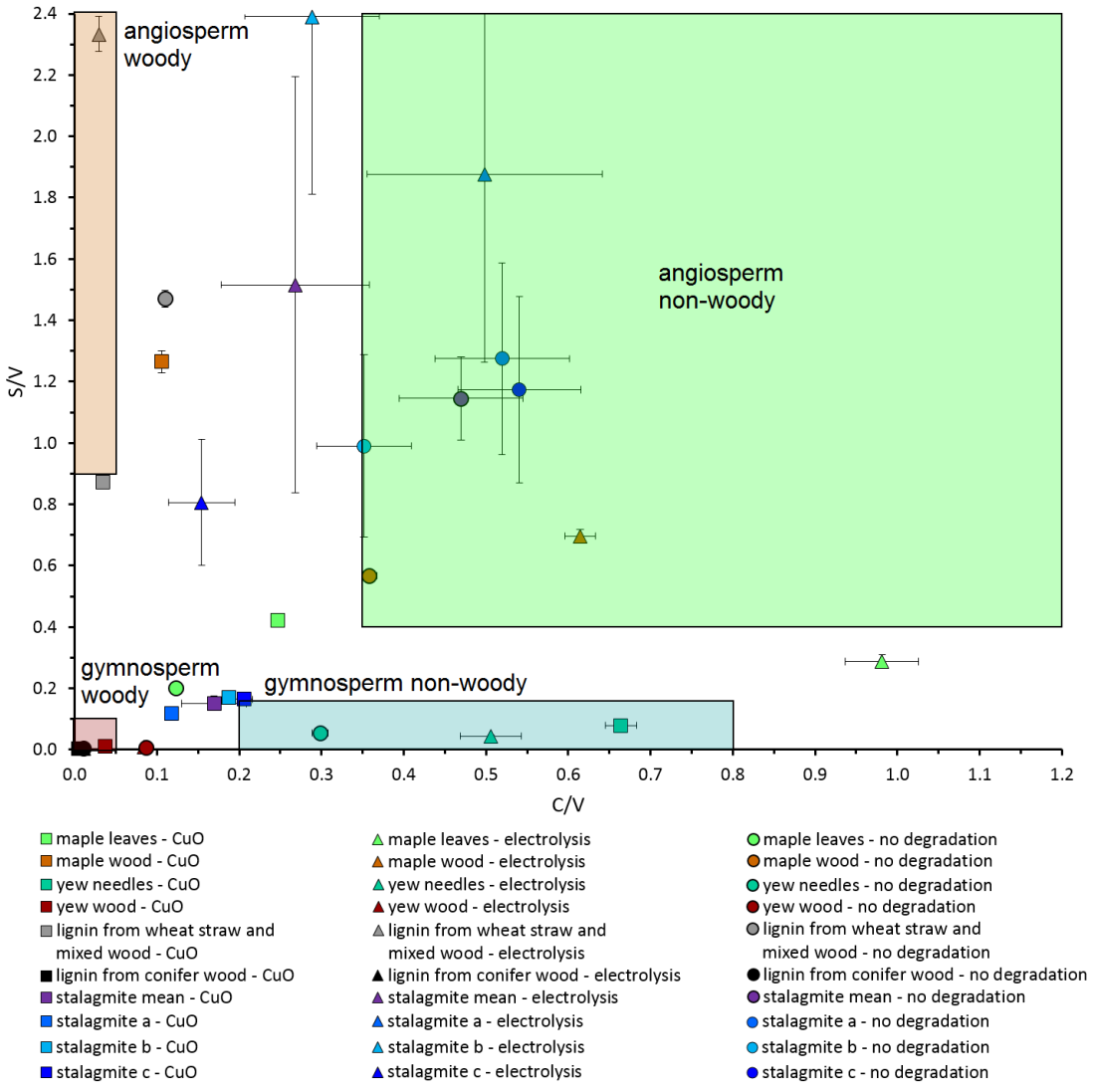

Figure 5.5: S/V versus C/V ratios of plant, lignin and stalagmite samples treated with CuO oxidation, electrolysis and without degradation.

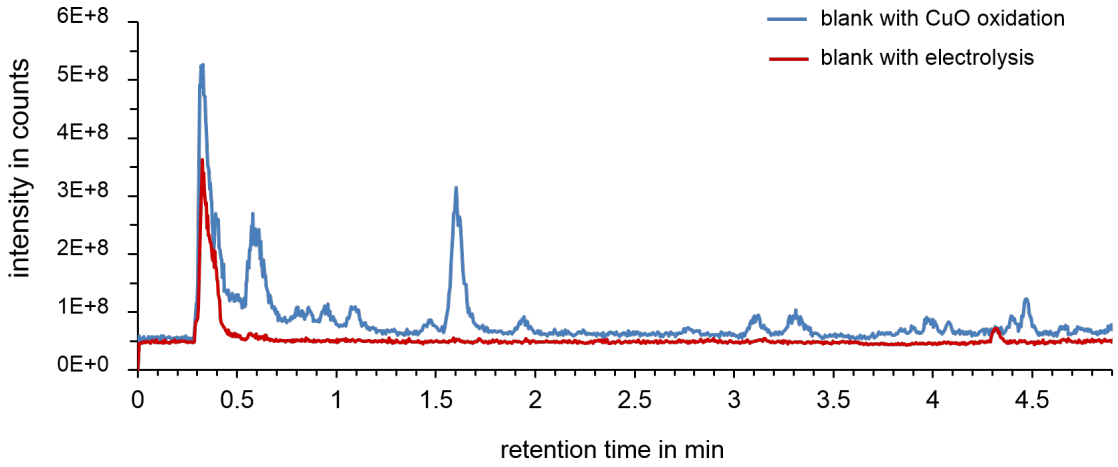

Figure 5.6: Comparison of the total ion chromatogram of a blank sample treated with CuO oxidation (blue line) and electrolysis (red line).

36 to 54 $C \cdot mg(lignin)^{-1}$. The general decrease in most LOP concentrations with increasing charge quantity could mean either, that no polymeric lignin is degraded into LOPs and only the free LOPs get over-oxidized, or it could mean that even if polymeric lignin is degraded into LOPs, these LOPs get over-oxidized immediately. If the latter is the case, it would be beneficial to use flow cells instead of batch cells, because in a flow cell, the released monomeric LOPs are removed from the electrodes immediately after their formation. Therefore, several screening experiments with a flow cell were performed.

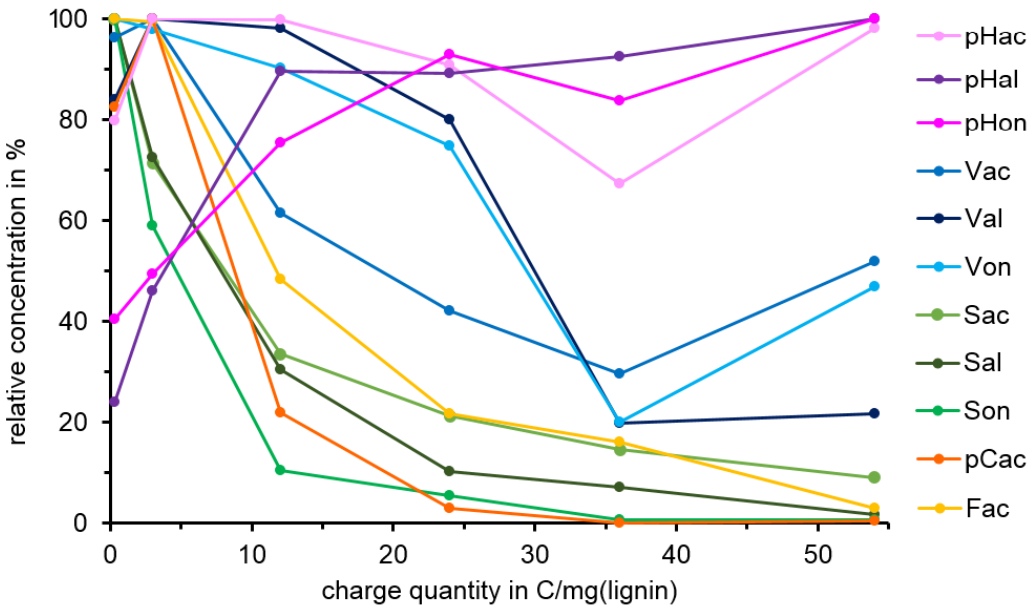

Figure 5.7: Screening of the carge quantity. Electrolysis conditions: batch cell, current 20 mA, current density 12.5 $mA \cdot cm^{-2}$, temperature 80 °C.

Figure 5.8 shows the screening results of the flow rate using a flow cell. A lower flow rate means that the contact time with the electrodes is longer and therefore a higher charge quantity acts on the analytes. Only the concentrations of pHon, pHal and Ciac show an increase with increased conctact time (i. e. lower flow rate). All other analytes show a drastic decline with decreasing flow rate. The strongest decrease was observed for pCac and Son with less than 20% of their initial concentrations at a flow rate of 0.1 mL $\cdot$ min^{-1}. For higher flow rates, the concentrations of all analytes approach a limit.

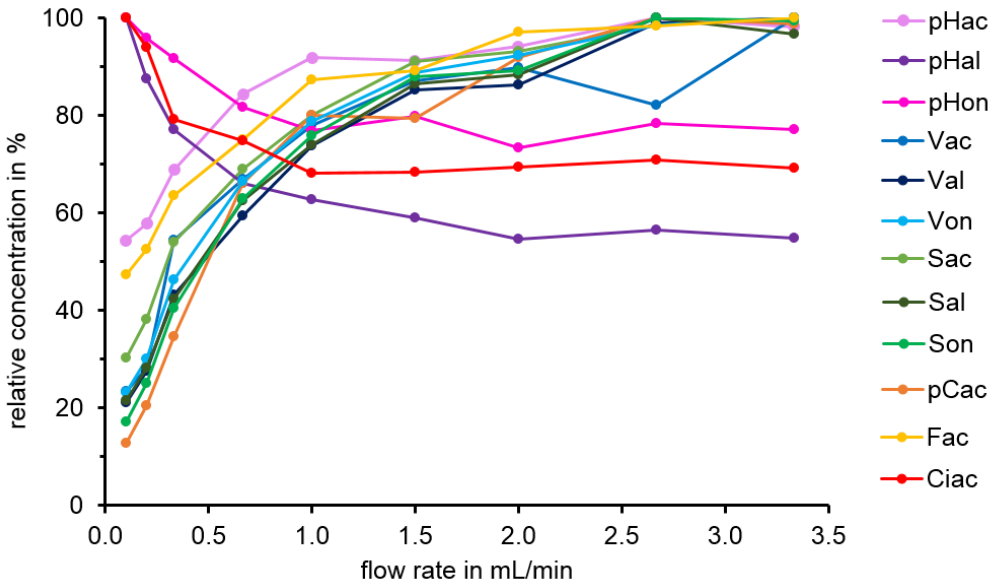

Figure 5.8: Screening of the flow rate. Electrolysis conditions: flow cell, current 150 mA, current density 12.5 mA $\cdot$ cm^{-2}, temperature 25 °C.

Figure 5.9 shows the screening results of the current intensity using a flow cell. Most analytes show a decreasing concentration with increasing current, but the decrease is strongest for the analytes of the S-group, followed by V- and C-group LOPs. The concentration of the P-group LOPs stays relatively constant or even increases slightly.

To sum up, the analytes of the S-group are the most sensitive to over-oxidation in all screening experiments. This can be explained by the higher electron density in the aromatic ring caused by the mesomeric effect of the two methoxy groups in the S-group analytes. The sensitivity order of the C- and V-group LOPs to over-oxidation was not clear in the three screening experiments, but both groups are sensitive to over-oxidation. The opposite behaviour of the P-group analytes and Ciac in all screenings can be explained by the fact that these analytes are not or not only part of the lignin polymer, but come from other biological sources present in plant samples. These analytes seem to be faster released from their sources during the electrolysis than they get over-oxidized.

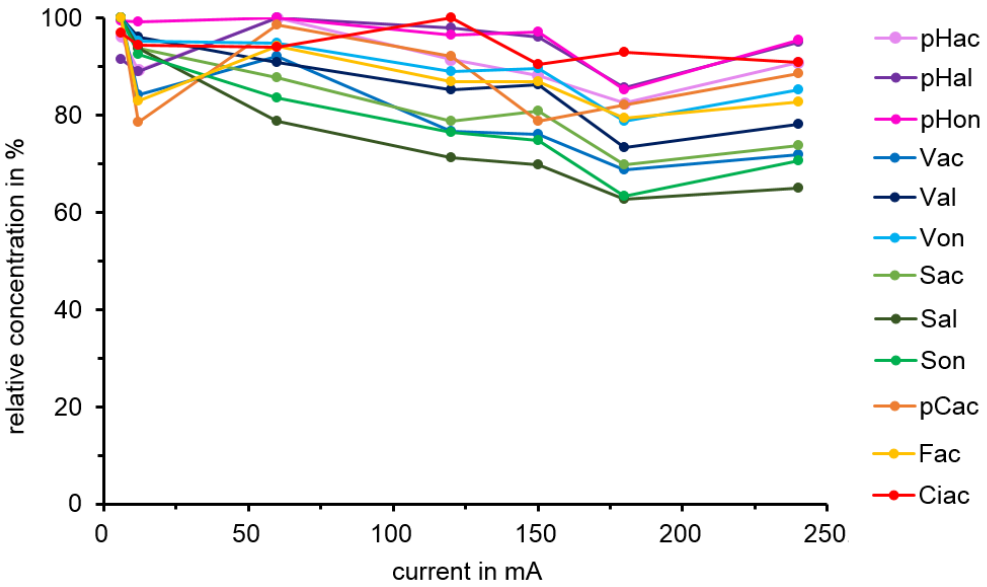

Figure 5.9: Screening of the current intensity. Electrolysis conditions: flow cell, flow rate 1 mL · min^{-1}, current density 12.5 mA · cm^{-2}, temperature 25 °C.

5.4 Conclusion

At this point, the electrolysis is not yet suitable as alternative lignin degradation method to replace the CuO oxidation step in the analysis of speleothem samples. Although the lower blank values and shorter reaction times are promising, the LOP yields are not yet satisfactory and over-oxidation of the released LOPs is a problem. In addition, the existence of freely available LOPs in the plant and lignin samples complicated the method development of the electrolysis method, because most of the observations made were caused by the degradation and over-oxidation of these free LOPs and not by the release of LOPs through the degradation of the lignin polymer (Leppla, 2016). In future, a lignin-containing sample (speleothem or other) that does not contain any free LOPs should be used for the method development. This will make it easier to investigate the electrolytic degradation of the lignin polymer. The findings of the screening experiments, which show that the different LOPs differ in their sensitivity towards over-oxidation, emphasize once more the need to consider the history of lignin particles, both in the soil and during the sample pretreatment in the lab, when calculating source parameters like C/V and S/V ratios.

Part III

Application

6 Lignin analysis in speleothems and cave dripwater – A first record from the Herbstlabyrinth Cave, central Germany

This chapter is a reprint of the manuscript published in *Climate of the Past*:

Clim. Past, 15, 1025–1037, 2019
https://doi.org/10.5194/cp-15-1025-2019

Climate of the Past Open Access EGU

Lignin oxidation products as a potential proxy for vegetation and environmental changes in speleothems and cave drip water – a first record from the Herbstlabyrinth, central Germany

Inken Heidke[1], Denis Scholz[2], and Thorsten Hoffmann[1]

[1]Institute of Inorganic Chemistry and Analytical Chemistry, Johannes Gutenberg University of Mainz, Duesbergweg 10–14, 55128 Mainz, Germany
[2]Institute of Geosciences, Johannes Gutenberg University of Mainz, J.-J.-Becher-Weg 21, 55128 Mainz, Germany

Correspondence: Thorsten Hoffmann (t.hoffmann@uni-mainz.de)

Received: 10 January 2019 – Discussion started: 15 January 2019
Revised: 17 April 2019 – Accepted: 1 May 2019 – Published: 14 June 2019

Abstract

Here we present the first quantitative speleothem record of lignin oxidation products (LOPs), which has been determined in a Holocene stalagmite from the Herbstlabyrinth Cave in central Germany. In addition, we present LOP results from 16 months of dripwater monitoring. Lignin is only produced by vascular plants and therefore has the potential to be an unambiguous vegetation proxy and to complement other vegetation and climate proxies in speleothems. We compare our results with stable isotope and trace element data from the same sample. In the stalagmite, LOP concentrations show a similar behaviour as P, Ba and U concentrations, which have previously been interpreted as vegetation proxies. The LOP ratios S/V and C/V, which are usually used to differentiate between angiosperm and gymnosperm

and woody and non-woody vegetation, show complex patterns suggesting additional influencing factors, such as transport and microbiological effects. The dripwater from a fast drip site shows a seasonal pattern of LOPs with low LOP concentrations in winter and higher LOP concentrations in summer. These results indicate the potential of LOPs as a new proxy for vegetational and environmental changes in speleothems, but also demonstrate the complexity and the current limitations of our understanding of the transport of lignin from the soil into the cave and the speleothems.

6.1 Introduction

Speleothems are valuable climate archives because they can grow continuously for thousands of years and can be dated accurately 640,000 years back in time using the ^{230}Th-U method (Cheng et al., 2016, Richards and Dorale, 2003, Scholz and Hoffmann, 2008). Furthermore, the cave provides a preservative environment that protects the recorded chemical proxy signals against outer influences such as light, abrupt changes in temperature and, under ideal conditions, also mechanical disturbance. Until recently, mostly stable isotope ratios and trace elements have been used as climate proxies in speleothems (McDermott, 2004, Fairchild and Treble, 2009). The methodology is well-established, but the records sometimes cannot be interpreted without doubt, unless other proxies are available for comparison (Lachniet, 2009, Fairchild and Treble, 2009, Mischel et al., 2017, Scholz et al., 2012). Therefore, it is important to expand the proxy toolbox of paleoclimate and especially paleo-vegetation reconstruction. The calcite crystal is able to incorporate and thus preserve not only trace elements and stable isotope ratios, but also organic molecules.

Organic matter in speleothems and cave dripwater has most often been analyzed as total organic carbon (TOC) or by fluorescence spectroscopy (Quiers et al., 2015). Size exclusion chromatography coupled to organic carbon detection (LC-OCD) was applied to divide organic matter in cave dripwater in different fractions, such as biopolymers and humic substances (Rutlidge et al., 2015). Only very few molecular organic analytes have been analyzed in speleothems so far. Glycerol dialkyl glycerol tetraethers (GDGTs), which are produced by microorganisms in situ in the cave or the overlaying vadose zone, have been implemented as organic temperature proxies (Blyth, Smith and Drysdale, 2013, Blyth et al., 2014). Lipid biomarkers, such as fatty acids (Bosle et al., 2014) and especially long chain *n*-alkanes from plant leave waxes, have been used as vegetation proxies, and there have been approaches to use the chain length distribution of *n*-alkanes to distinguish between the input of grasses and woody plants (Xie, 2003, Blyth et al., 2007, 2011). However, there are uncertainties about the validity of chain length distributions to distinguish between different plant groups (Bush and McInerney, 2013, Blyth et al., 2016). In addition, lipid biomarkers are especially prone to laboratory contamination, which poses a general problem for biomarker analysis (Wynn and Brocks, 2014). Therefore, a more specific plant biomarker is needed that is less prone to contamination.

Lignin is one of the main constituents of wood and woody plants. In the soil, lignin contributes to soil organic matter and can be found in the alkaline extracts traditionally referred to as humic substances, mainly in the humic acids fraction

(Kögel-Knabner, 2002, Lehmann and Kleber, 2015). The microbial degradation of lignin is comparably slow, as only white-rot fungi are able to completely mineralize it to CO_2 in co-metabolism with other energy sources, whereas some other microorganisms are only able to induce structural changes to lignin (Kögel-Knabner, 2002). Although the exact fate of lignin in soils is still a matter of debate (Thevenot et al., 2010), its relative recalcitrance has led to lignin oxidation products being widely used as paleo-vegetation proxy in archives, such as peat, lake sediments and marine sediment cores (see, for instance, the review by Jex et al., 2014) and as a proxy for terrestrial input of plant biomass in natural waters, like rivers and oceans (e.g., Zhang et al., 2013, Standley and Kaplan, 1998, Hernes and Benner, 2002). Blyth and Watson (2009) first detected lignin phenols in speleothems, and Blyth et al. (2008) and Blyth et al. (2016) have highlighted lignin oxidation products as promising vegetation proxies in speleothems. Recently, Heidke et al. (2018) developed a method to quantitatively analyze lignin as a paleo-vegetation proxy in speleothems and cave dripwater. The advantage of lignin as a vegetation proxy is that it is only produced by vascular plants and not by microorganisms. Thus, it is very specific, and the risk of laboratory contamination is also much lower than for ubiquitous substances, such as lipids. In addition, lignin analysis does not only give information about the abundance, but also about the type of vegetation. The biopolymer lignin consists of three different monomers, coniferyl alcohol, sinapyl alcohol and p-coumaryl alcohol. The proportion of these three monomers varies with the type of vegetation. Lignin from gymnosperm wood mainly consists of coniferyl alcohol, whereas lignin from angiosperm wood contains coniferyl and sinapyl alcohol. Non-woody vegetation, like grasses, leaves and needles, is characterized by a higher proportion of p-coumaryl alcohol and ester-bound p-coumaric acid and ferulic acid (Boerjan et al., 2003). To analyze the lignin composition, the lignin polymer has to be oxidatively degraded into monomeric lignin oxidation products (LOPs). The guaiacyl phenylpropanoid (from coniferyl alcohol) is oxidized to vanillic acid, vanillin and acetovanillone (V-group LOPs), the syringyl phenylpropanoid (from sinapyl alcohol) to syringic acid, syringaldehyde and acetosyringone (S-group LOPs), and the p-hydroxyphenyl phenylpropanoid (from p-coumaryl alcohol) to p-hydroxybenzoic acid, p-hydroxybenzaldehyde and p-hydroxyacetophenone (H-group LOPs). Since the H-group LOPs can also originate from other sources than lignin, such as soil microorganisms or the degradation of protein-rich material, they are usually not used as vegetation proxies. The C-group LOPs consist of ferulic acid and p-coumaric acid. Usually, the sum parameter $\Sigma 8$, which is the sum of all eight individual LOPs from the C-, S- and V-group, is used to present the total lignin concentration. In addition, the ratios of the different LOP groups, C/V and S/V, are used to present the type of lignin, where a higher C/V ratio indicates a higher contribution of non-woody vs. woody plant material and a higher S/V ratio indicates a higher contribution of angiosperm vs. gymnosperm plant material (Hedges and Mann, 1979).

It is still a subject of research to what extent and how these ratios are affected by factors such as transport, microbial transformation, soil characteristics and land use as well as the interaction with mineral surfaces (Hernes et al., 2007, Thevenot et al., 2010, Hernes et al., 2013, Jex et al., 2014). A clarification of all these aspects

is beyond the scope of this study. The aim of this study is to present first results on the application of the lignin analysis method developed by Heidke et al. (2018) to speleothem and cave dripwater samples to generally evaluate the potential of LOPs as a proxy for vegetational and environmental changes in speleothem archives. We present the first quantitative record of lignin oxidation products from a Holocene speleothem from the Herbstlabyrinth in central Germany. Our objectives were (i) to investigate, if the sensitivity of our method is high enough to detect and quantify LOPs with a sufficient temporal resolution to reveal centennial to millennial climate changes, and (ii), if and how the LOP signal in speleothems varies with climatic and vegetational changes and how it compares with other, established proxy signals, such as trace elements and stable isotopes. Therefore, we compared our LOP results with trace element and stable isotope records from the same sample (Mischel et al., 2017). In addition, we aimed to improve our knowledge on how lignin is transported into the cave, which is a key question in understanding LOPs as an environmental proxy in speleothem archives. Therefore, we investigated seasonal variations of LOP concentrations in dripwater from the same cave, sampled monthly over a period of 16 months in the framework of a cave monitoring program.

We chose the Herbstlabyrinth Cave for our first quantitative LOP analysis because of an ongoing cave monitoring program, and the specific Holocene stalagmite was chosen because it was already well characterized by stable isotope and trace element analysis, the general vegetation and climate changes in the Holocene in central Germany are relatively well known (e. g. Litt et al., 2009), and last but not least, the fast growth rate of the stalagmite offered sufficient sample material to test and apply our method.

6.2 Materials and methods

6.2.1 The cave monitoring program in the Herbstlabyrinth

From 2010 to 2015, a monthly cave monitoring program, including dripwater sampling and the measurement of cave air temperature and pCO_2 as well as meteorological data, was conducted at the Herbstlabyrinth. A detailed description of the monitoring program, the cave and its environment can be found in Mischel et al. (2015) and Mischel et al. (2017). In brief, the Herbstlabyrinth is situated in the Rhenish Slate Mountains in central Germany. The cave system is about 11 km long and well decorated with different kinds of speleothems. The vegetation above the cave consists of deciduous forest and grassland, and the soil above the cave is a 60 cm-thick Cambisol (Terra fusca). The mean annual temperature at the cave site is 9.0 °C, and the mean annual precipitation is around 800 $mm \cdot a^{-1}$, with evenly distributed rainfall throughout the year. Due to higher evapotranspiration during summer, the recharge of the aquifer and thus the dripwater mainly consists of winter precipitation, but heavy rainfall events in summer can also have a substantial contribution (Mischel et al., 2015). The dripwater samples used for lignin analysis were sampled monthly from May 2014 until August 2015. They were collected in precleaned glass vessels from one fast drip site (*D1*, average drip rate approx. 0.3–0.5 drops per second),

one slow drip site (*D2*, average drip rate approx. 60 mL per month) and one cave pool (*PW*). To prevent the growth of microorganisms, 5% (w/w) of acetonitrile was added to the samples, which were then stored in the dark at 4 °C for several months.

6.2.2 The stalagmite sample

Stalagmite NG01 has a light whitish to yellowish colour, is 50 cm long, has a diameter of 15 cm, and grew during the Holocene (Mischel et al., 2017). It was dated via the ^{230}Th–U method using multicollector-ICP-MS (Mischel et al., 2017). To calculate the age-depth model, the algorithm StalAge was used (Scholz and Hoffmann, 2011). The stalagmite samples used for lignin analysis were cut from a 1 cm thick slab following visible growth lines and had a width along the growth axis of 0.5–2.0 cm, a length of 1.2–4.8 cm and a weight of 2.4–6.2 g. To determine the age and the corresponding error of these samples, the calculated ages for the mid depth and the depth of the upper and lower edges of the sample were used.

6.2.3 Analytical methods

The analytical method for the analysis of LOPs is described in detail in Heidke et al. (2018). In brief, the stalagmite samples for LOP analysis were cleaned with organic solvents, edged on the outside with diluted HCl to prevent the influence of potential laboratory contamination (Wynn and Brocks, 2014), and finally dissolved in ultrapure 30% HCl. These sample solutions as well as the dripwater samples were extracted via solid phase extraction (SPE), and the extracted lignin was degraded via microwave-assisted CuO oxidation. The resulting lignin oxidation products (LOPs) were again extracted via SPE and then analyzed via ultrahigh-performance liquid chromatography (UHPLC) coupled to heated electrospray ionization (HESI) high resolution mass spectrometry (HRMS) using a Dionex Ultimate 3000 UHPLC system and a Q-Exactive Orbitrap mass spectrometer (Thermo Fisher Scientific). A detailed discussion of possible blank contaminations and measures to prevent these is given in Heidke et al. (2018).

The methods used for dating of the stalagmite samples, the analysis of trace elements and stable isotopes as well as the calculation of the drip rate for the cave dripwater samples and the growth rate of the stalagmite are described in detail in Mischel et al. (2017) and references therein. To compare the LOP results with stalagmite data of stable isotopes and trace elements, which have a much higher resolution of 2 mm per sample, a mean value of the higher-resolution data according to the sample size of the LOP samples was calculated, and the standard deviation of these mean values was used as error-bars. In the discussion, only these lower-resolution data will be shown and discussed. The original data can be found in Mischel et al. (2017). For the dripwater stable isotope and trace element data, the uncertainty is very small and therefore not shown here, but it is provided in Mischel et al. (2017). For the dripwater LOP data, the uncertainty was calculated as described in Heidke et al. (2018), and for the stalagmite LOP data, the calculation of the uncertainty is described in section 6.3.1.

6.3 Results

6.3.1 LOPs in stalagmite samples

One complication of studies with a large number of samples that have to be analyzed over an extended period of time are so-called batch effects, which occur because measurements are affected by laboratory conditions, such as reagent lots, instrumental drift, stability of the reference standards or a varying efficiency of the sample preparation steps (e.g., CuO oxidation step). Since such effects are almost unavoidable, adjustment strategies are generally required (Wehrens et al., 2016, Kirwan et al., 2013, Surowiec et al., 2017), which is especially true when temporal records of the target analytes are the aim of the study. To do so, the stalagmite samples for LOP analysis were analyzed in six batches with nine samples and one blank sample per batch. To recognize systematic errors leading to batch effects, the samples within each batch were not located side by side in the stalagmite, but evenly distributed over the whole length of the stalagmite. In fact, in the results of the LOP concentrations and the C/V and S/V ratios, we observed a regular pattern, which corresponded to the different batches. To determine the original signal and overcome the differences in instrumental response between the batches, the results of the individual measurements were revised based on the following correction procedure. In the oldest part of the stalagmite (11.2–8.6 ka BP), the pattern was most visible and least superimposed by original signals. Therefore, we used only this part to calculate a correction factor using equation (6.1),

$$x_{\text{smoothed}} = x - \bar{X}_{\text{batch k}} + \bar{X}, \tag{6.1}$$

with x_{smoothed} representing the corrected (smoothed) value of Σ8, C/V or S/V, x representing the original value of Σ8, C/V or S/V, $\bar{X}_{\text{batch } k}$, k = 1,2,...,6, the mean value of all x_i in batch k, and $\bar{X}$ the mean value of all x_i of all batches in the oldest part of the stalagmite. The error bars $\Delta x_{\text{smoothed}}$ for the smoothed values were calculated by equation (6.2),

$$\Delta x_{\text{smoothed}} = \sqrt{(\Delta x)^2 + (\Delta \bar{X}_{\text{batch k}})^2 + (\Delta \bar{X})^2}, \tag{6.2}$$

with $\Delta \bar{X}_{\text{batch k}}$ and $\Delta \bar{X}$ representing the standard deviations of the respective mean values and Δx representing the uncertainty of a single sample analysis as described in Heidke et al. (2018). The smoothed and original data for Σ8 are shown in Fig. 6.1, and for C/V and S/V in Fig. 6.2.

Figure 6.1 shows the concentrations of the C-, S- and V-group LOPs as well as the Σ8 concentrations plotted against the age of the stalagmite. Figure 6.2 shows the C/V and S/V ratios. The ratios of vanillic acid to vanillin (Vac/Val) and syringic acid to syringaldehyde (Sac/Sal) can be seen in Fig. B.1 in appendix B. The mean Σ8 concentration in the whole stalagmite was 51±15 ng · g^{-1}. The highest concentrations of up to 92 ng · g^{-1} occurred shortly after the hiatus at the beginning of the middle part at 7.6 ka BP, followed by the lowest concentrations with 19 ng · g^{-1} at 7.0 ka BP. The mean C/V ratio was 0.32 ± 0.15, with the lowest ratio of 0.12 at 10.9 ka BP and the highest ratios of up to 0.68 at 0.3, 6.5 and 7.2 ka BP. The mean S/V ratio

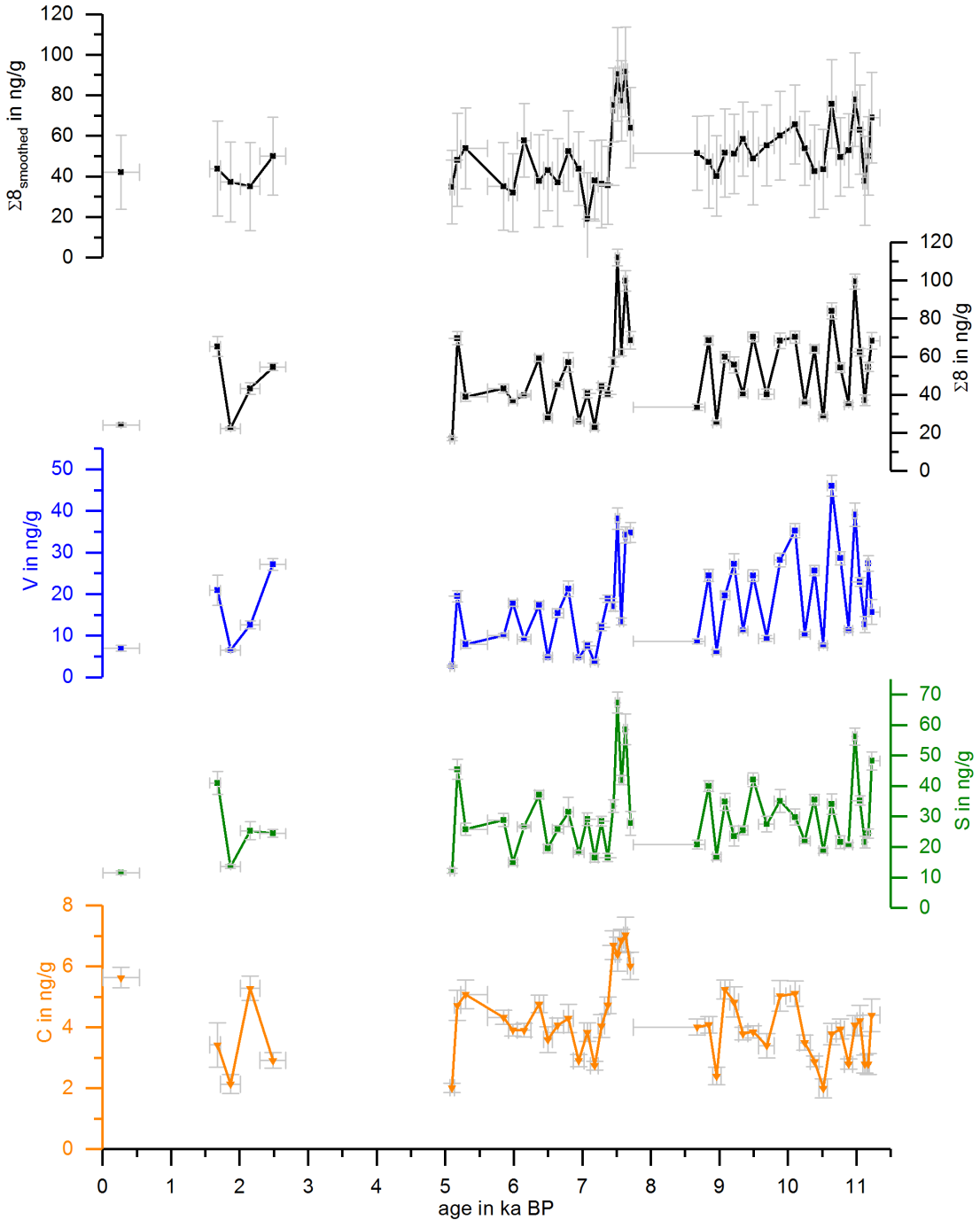

Figure 6.1: Concentrations of the C-, S- and V-group LOPs and Σ8 concentrations plotted against the age of the stalagmite. The uppermost plot shows the smoothed results of Σ8 concentrations.

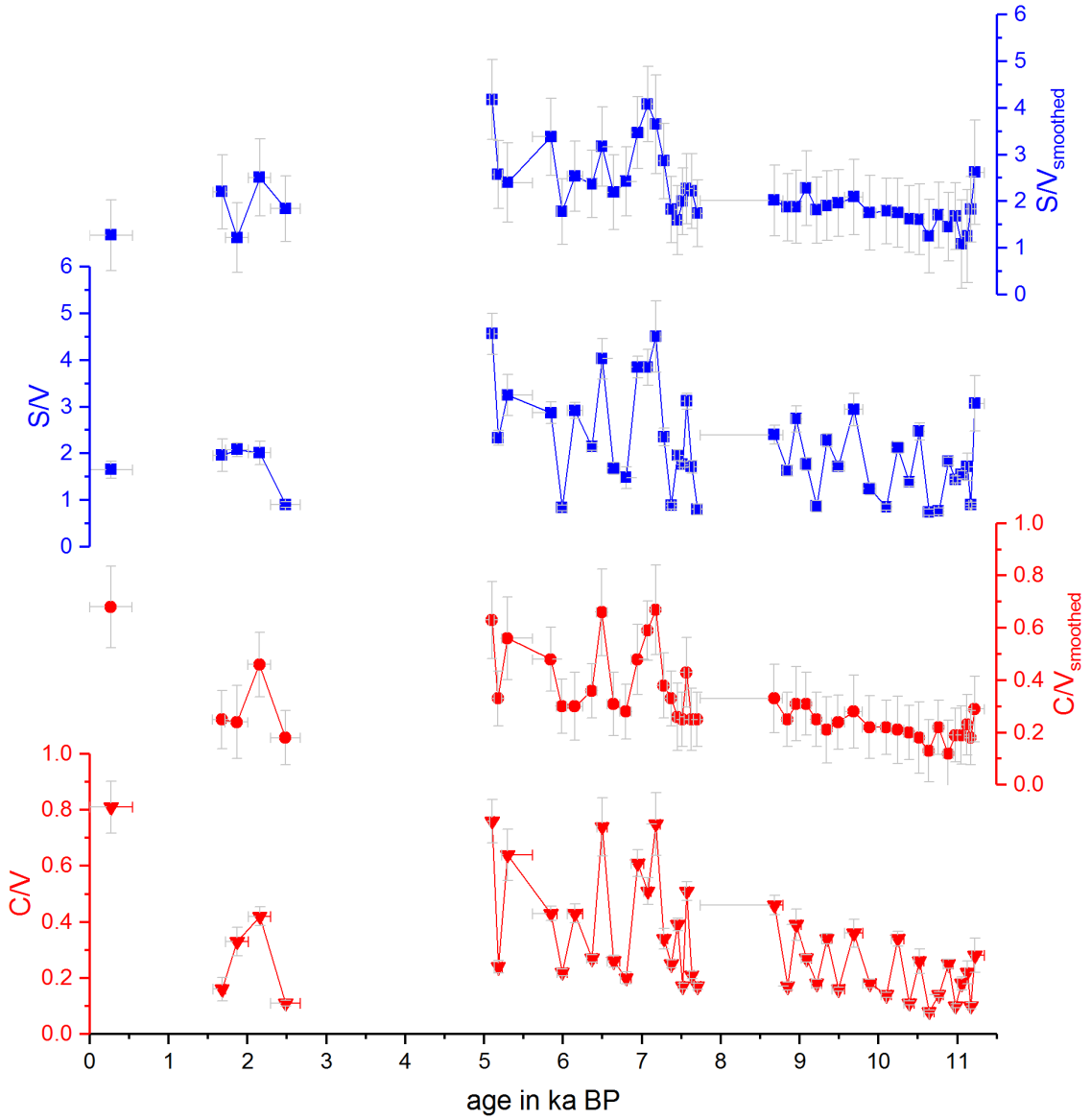

Figure 6.2: Ratios of C/V (red) and S/V (blue), original data and smoothed data, plotted against the age of the stalagmite.

was 2.15 ± 0.71, with the lowest ratio of 1.08 at 11.1 ka BP and the highest ratios of up to 4.18 at 5.1 and 7.1 ka BP.

6.3.2 LOPs in dripwater samples

In Fig. 6.3, the LOP results of the fast drip site, *D1*, the slow drip site, *D2*, and the cave pool water, *PW*, are shown. The height of the columns represents the sum of the LOP concentrations, Σ8, and the different colors show the contribution of the C-, S- and V-group LOPs. In general, the V-group LOPs contribute the largest part to the total LOP concentration, followed by the S-group and the C-group LOPs. *D1* shows a strong seasonal pattern with high LOP concentrations between 500 and 1800 $ng \cdot L^{-1}$ from May to August 2014 and from April to August 2015, and low LOP concentrations between 30 and 400 from September 2014 to February 2015. For July 2014 and March 2015, no data are available. For the slow drip site, *D2*, the concentrations do not show a seasonal pattern, but are highly variable between 80 and 3000 $ng \cdot L^{-1}$. In May, July and August 2014 and June, July and August 2015, there are no data available, mainly because the drip rate was too low to collect a sufficient sample volume. In the pool water, *PW*, the LOP concentrations show a similar seasonal pattern as in the fast drip site, but less pronounced with concentrations between 140 and 650 $ng \cdot L^{-1}$ from September 2014 to February 2015 and between 440 and 1100 $ng \cdot L^{-1}$ in the other months, with one exception in April 2015 with more than 2500 $ng \cdot L^{-1}$.

In Fig. 6.4, the C/V and S/V ratios are shown for *D1*, *D2* and *PW*. Because concentrations of individual analytes were below the limit of detection, the ratios could not be calculated for every sample. For the different drip sites, the ratios are in a similar range. The ranges of the ratios in *D1* are 0.02–0.33 for C/V and 0.14–1.21 for S/V. In D2, the ranges are 0.00–0.20 for C/V and 0.08–0.68 for S/V. In *PW*, the ranges are 0.00–0.43 for C/V and 0.18–0.77 for S/V. The ratios of vanillic acid to vanillin (Vac/Val) and syringic acid to syringaldehyde (Sac/Sal) are shown in Fig. B.2 in appendix B.

6.4 Discussion

6.4.1 Stalagmite samples

First of all, we can state that LOPs were detectable in all stalagmite samples and above the quantification limit. Moreover, the signals show a variation over time on the centennial to millennial scale. In Fig. 6.5, the lignin parameters Σ8, C/V and S/V of the stalagmite samples are compared with several trace elements, stable isotopes and the growth rate of the stalagmite. To get an overview of the correlations between the LOPs and the trace element and stable isotope data, we performed a principal component analysis (PCA).[1] As the three growth phases of the stalagmite show a different behaviour in several proxies and the growth rate (Mischel et al.,

[1]The PCA is based on Pearson's linear correlation. In contrast to Mischel et al. (2017), we did not detrend the records before calculating the correlations.

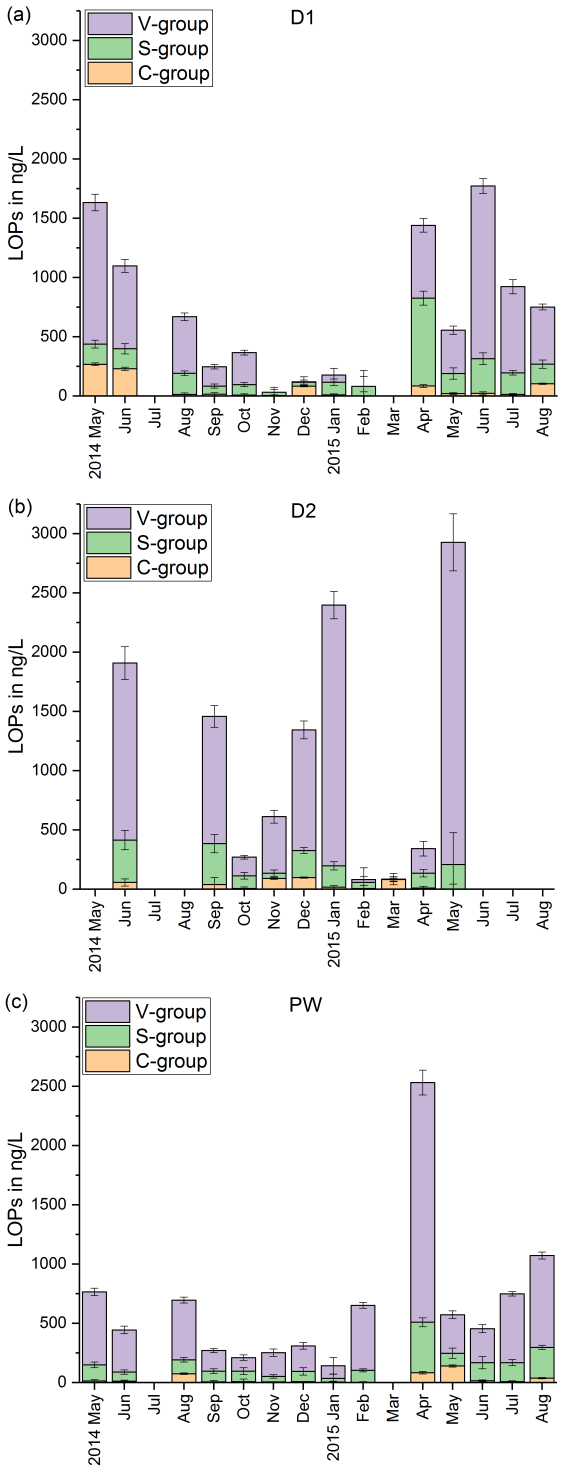

Figure 6.3: LOP results in dripwater. (a) fast drip site *D1*, (b) slow drip site *D2*, (c) cave pool water. The height of the columns represents the sum of the LOP concentrations, Σ8, and the different colors show the contribution of the C-, S- and V-group LOPs.

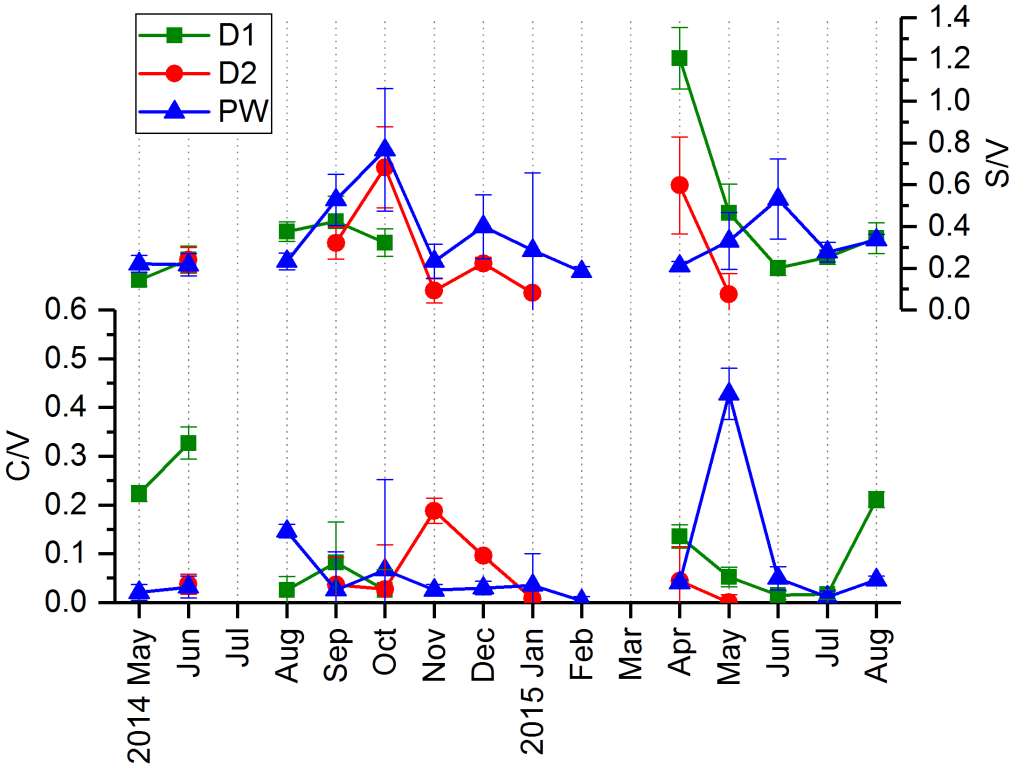

Figure 6.4: C/V and S/V ratios in the dripwater.

2017), the PCA and the correlation coefficients were calculated separately for each growth phase. As the youngest part consists of only five LOP samples, we focus the discussion on the middle and older part. (The contribution coefficients of the PCA are shown in Table B.8, the eigenvalues and percentages of variance in Table B.7, and all correlation coefficients of both Pearson's linear correlation and Spearman's rank correlation are shown in Tables B.1 to B.6 in appendix B.)

The PCA for the middle part is shown in Fig. 6.6. In the middle part, principal component 1 (PC1) explains 45.0% of the overall variance and consists mainly of P, Ba, U and Σ8 with positive contributions and C/V, S/V and δ^{13}C with negative contributions. Mischel et al. (2017) interpreted P, Ba and U in the Herbstlabyrinth as vegetation proxies, with higher concentrations of these elements indicating a more productive vegetation, coinciding with wetter climate conditions. Since lignin has its source unambiguously in the vegetation, the correlation of Σ8 with P, Ba and U supports this interpretation. δ^{13}C values were interpreted as being at least partially influenced by soil pCO_2 and soil thickness and thus indirectly affected by vegetation changes (Mischel et al., 2017). PC2 explains 23.3% of the variation and consists mainly of δ^{18}O, Mg and the growth rate on the positive side (with smaller contributions of Σ8) and, with smaller coefficients, U, C/V and S/V on the negative side. The fact that Σ8 and C/V and S/V appear in both PC1 and PC2 indicates that the Σ8 concentration and especially the C/V and S/V ratios are not only influenced by the abundance and type of vegetation, but also by hydrological and soil microbiological effects, such as the transport of organic matter through the soil and the karst system.

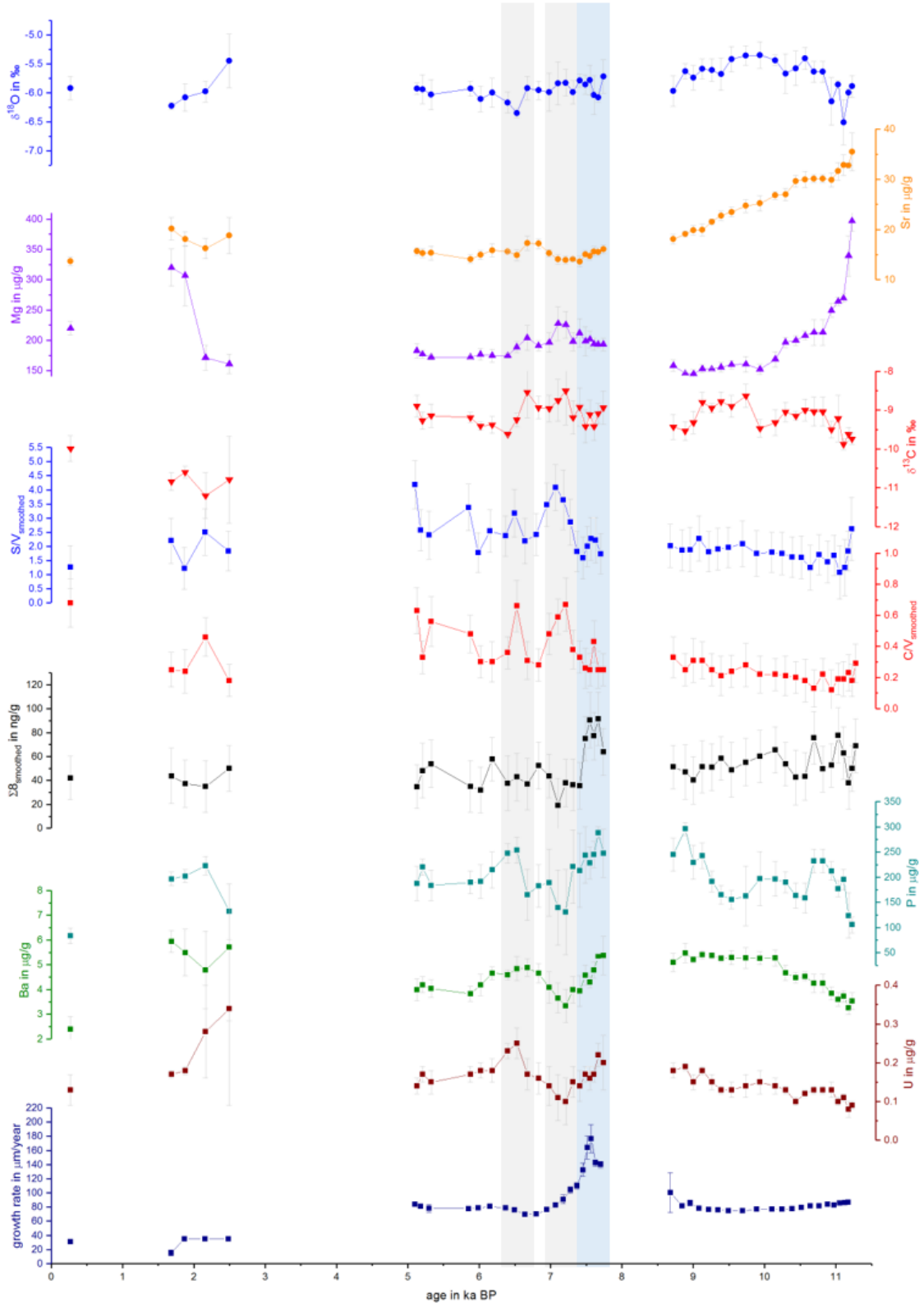

Figure 6.5: Comparison of stable isotopes, trace elements, Σ8 and C/V and S/V ratios, plotted against the age of the stalagmite. The grey bars highlight selected peaks in the C/V and S/V records and the blue bar a peak in the growth rate, which are discussed in the text.

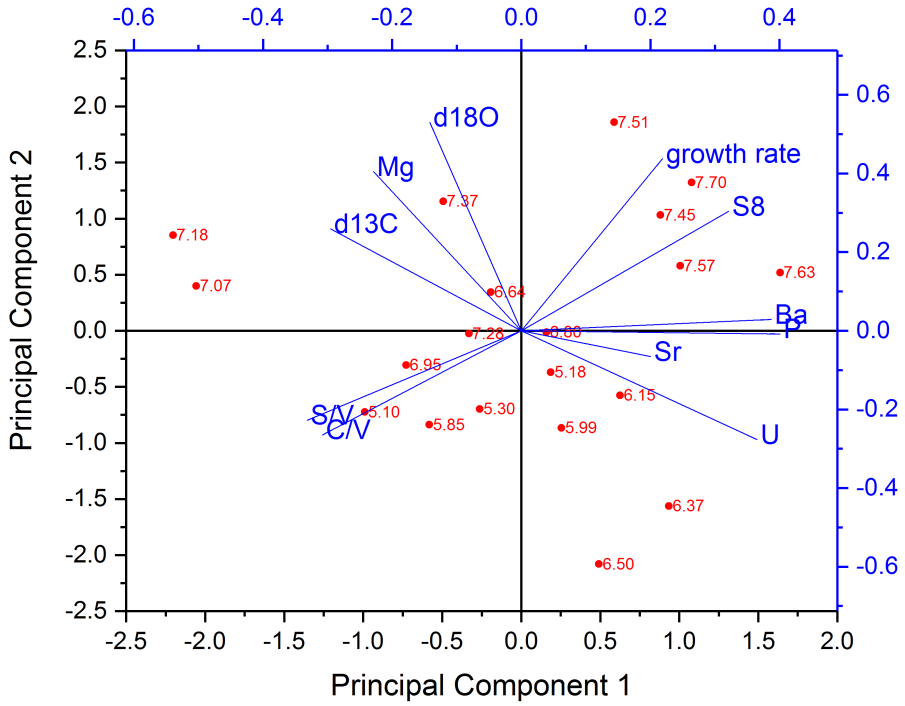

Figure 6.6: Principal component analysis for the middle part of the stalagmite.

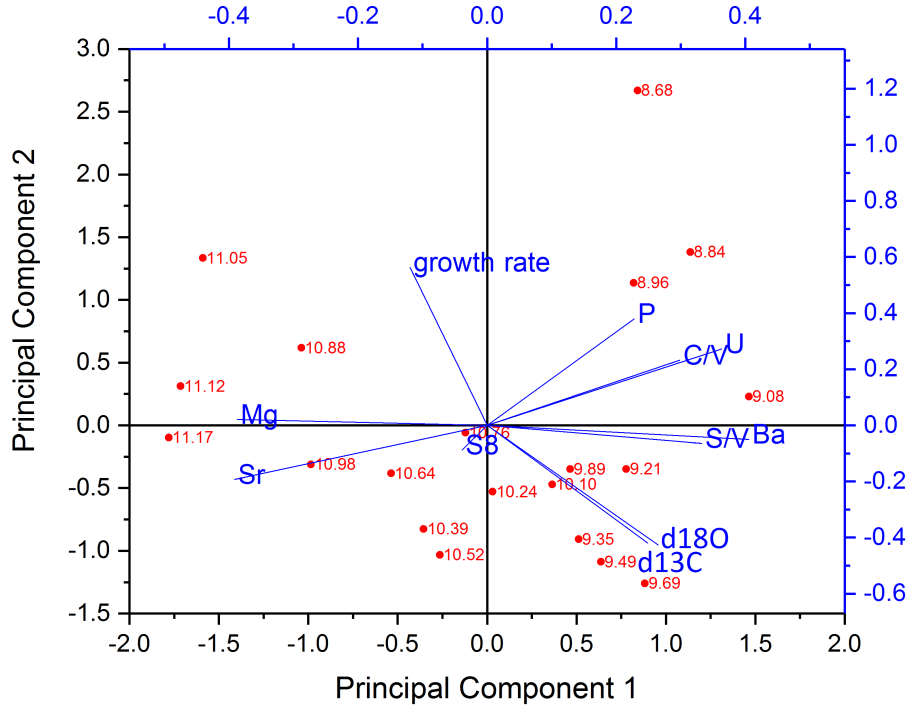

Figure 6.7: Principal component analysis for the older part of the stalagmite.

The PCA for the older part is shown in Fig. 6.7. In the older part of the stalagmite, PC1 explains 51.1% and consists mainly of C/V, S/V, U and Ba on the positive side and Sr and Mg on the negative side. It can be inferred from the scores of the individual samples that the influence of Sr and Mg is mainly dominant in the older part of the stalagmite. This long-term decrease of Sr and Mg (see Fig. 6.5) was interpreted by Mischel et al. (2017) as the result of a thin loess cover, deposited during the last Glacial, being progressively leached at the beginning of the Holocene. PC2 explains 20.4% and consists mainly of positive contributions of the growth rate and negative contributions of $\delta^{13}C$ and $\delta^{18}O$. $\Sigma 8$ only appears in the third principal component (explaining 11.4%), with a high positive contribution, together with positive contributions of P (see Table B.8 in the SI). This suggests that in the older part of the stalagmite, the influence of vegetation changes on the speleothem signals only plays a subordinate role.

Taking a closer look at the records in Fig. 6.5, there is a peak in the growth rate at the beginning of the middle part (around 8.0–7.5 ka BP, blue bar in Fig. 6.5) that is accompanied by a peak in $\Sigma 8$ and also in P, Ba, and U concentrations. A higher growth rate can be caused, inter alia, by a higher drip rate or by a higher supersaturation of the dripwater with respect to $CaCO_3$ (Dreybrodt and Scholz, 2011, Fairchild and Baker, 2012). The latter, in turn, can be caused by a higher soil pCO_2 due to a more productive vegetation and higher microbial activity in the soil, which would be in accordance with the observed higher concentrations of all vegetation proxies. On the other hand, this peak in the growth rate and the vegetation proxies occurs shortly after a hiatus. Therefore, it is also possible that a change in the flow path of the dripwater feeding the stalagmite was responsible for the faster growth of the speleothem and a higher input of organic matter. To further investigate this kind of questions, it might be useful in the future to combine LOP analysis with total organic carbon measurements and fluorescence spectroscopy to gain more information on the amount and composition of organic matter in the speleothem.

The C/V and S/V records have a distinct positive peak at around 7.2 ka BP, and a second, less distinct, positive peak at 6.5 ka BP (grey bars in Fig. 6.5). At approximately the same time, the concentrations of $\Sigma 8$ and P are lower or even show negative peaks, indicating less input of organic material. Furthermore, the records of $\delta^{13}C$ and Mg show positive peaks at approximately 7.2 and 6.6 ka BP. Higher concentrations of Mg coinciding with more positive $\delta^{13}C$ values in speleothems are often associated with prior calcite precipitation and usually indicate drier conditions (Mischel et al., 2017, Fairchild and Baker, 2012). Consequently, these peaks could be interpreted as drier periods with less input of organic material. Following the widespread interpretation of C/V and S/V as vegetation source indicators, a possible interpretation of the C/V and S/V records is therefore that during drier times with generally lower lignin input, there was less woody and more non-woody plant material available as a lignin source and the vegetation possibly consisted more of grasses and shrubs. Vice versa, at times with generally higher lignin input, the lignin consisted of more woody material and the vegetation probably consisted more of forest. However, biotic factors in the soil, such as different rates of microbial degradation for the different types of lignin, as well as transport factors in the soil or the aquifer could

also have an influence on the C/V and S/V ratios. Degradation studies of leaf litter showed that the microbial degradation of lignin high in C- and S-group monomeric units is faster than for lignin high in V-group units due to structural differences between the monomers (Bahri et al., 2006, Opsahl and Benner, 1995, Jex et al., 2014). In addition, adsorption of lignin to mineral particles can lead to an increase in the C/V and S/V ratios, indicating a preferential adsorption of lignin high in V-group monomeric units (Hernes et al., 2007, 2013). This may happen both in the soil and the aquifer. We assume that more degraded lignin is present in smaller fragments and a higher oxidation state and should therefore be better soluble in water. In addition, we hypothesize that this could lead to a more efficient transport through the soil and the aquifer to the cave. This could explain the increase of C/V and S/V ratios during drier times. In addition, the transport of lignin is also likely to involve processes such as coiling with humic substances in the soil. Currently, we cannot quantify the contribution of the individual mentioned processes to the final lignin signals in the dripwater and speleothem calcite. To further investigate all these influencing factors, comparative LOP studies of soil, dripwater and speleothem samples need to be conducted.

The pollen-based climate reconstruction by Litt et al. (2009) from the Meerfelder Maar and the Holzmaar in the Eifel region, about 120 km from the Herbstlabyrinth, shows a relatively stable vegetation development without any abrupt changes, at least not at the times observed in the C/V and S/V record (6.6 and 7.2 ka BP). This could be interpreted in different ways. One interpretation is that the assumed vegetation changes were local to the region of the the Herbstlabyrinth and did not affect the Eifel region. Another interpretation could be that our proxies are more sensitive to vegetation changes than the pollen record. And third, it is possible that the changes in the vegetation proxies and C/V and S/V were rather caused by changes in the flow paths of the dripwater or by site specific soil microbiological processes than by changes in the overlaying vegetation. However, Litt et al. (2009) state that their reconstruction method rather underestimates than overestimates climate changes. To further study the potential of LOPs as a vegetation proxy in the future, it would be beneficial to use speleothem samples from an epoch with more pronounced vegetation changes.

6.4.2 Dripwater samples

To gain a better understanding of the transport mechanisms and preservation of LOPs in the cave system, we complemented our first stalagmite LOP record with the analysis of LOPs in monthly sampled dripwater (Fig. 6.3). The study of LOP concentrations over the course of a hydrological year can yield useful information on transport processes and fluxes on a seasonal timescale, provided that the influence of a prolonged dwelling time in the epikarst zone is taken into account. By comparison of modeled and measured $\delta^{18}O$ values, Mischel et al. (2015) have calculated that the dripwater of the Herbstlabyrinth is fed by a large reservoir in the karst aquifer, where the water has a residence time of approx. 10 months and consists of rain water mixed over a period of ca. 12 months. Therefore, seasonal variations are strongly attenuated, but should not be shifted much.

In the fast drip site, *D1*, a strong seasonality with higher Σ8 concentrations in summer and lower concentrations in winter was observed (Fig. 6.3). One possible reason could be the growth season of the vegetation from spring to autumn and the activity of soil microorganisms during the warmer time of the year, which would lead to a higher abundance of – partially degraded and therefore transportable – lignin in the soil. However, the degradation of lignin in the soil takes months to years (Thevenot et al., 2010, Bahri et al., 2006). In combination with the long residence and mixing times of the dripwater, the original seasonality of the input of plant material on the surface will probably be smoothed out. It seems more likely that the observed seasonal signal is caused by hydrological effects. A possible reason could be dilution of the – otherwise relatively constant – lignin concentration from the reservoir of organic matter in winter, when the recharge of the aquifer and consequently the drip rate are higher (blue bars in Fig. 6.9 and Fig. 6.11). In summer, in contrast, the slower drip rate and lower recharge of the aquifer might cause a higher concentration of the organic matter and therefore the lignin content in the dripwater (Fig. 6.8). A combination of both factors – the activity of the vegetation and the soil microorganisms in summer and the dilution effect due to higher recharge of the aquifer in winter – is also possible to explain the observed seasonal concentration pattern of Σ8. For future experiments, it might be more useful to apply long-term sampling devices, such as in-situ preconcentration with solid-phase extraction cartridges, instead of whole-water sampling once per month. This would allow quantification of the input of lignin per month instead of the concentration per liter dripwater.

Interestingly, Bosle et al. (2014), who analyzed low-molecular weight saturated fatty acids as biomarkers for microbial activity in dripwater samples from the same cave monitoring program, found a similar seasonal trend with high concentrations during the summer months and low concentrations in winter for the longest fatty acid, arachidic acid (C_{20}), but the opposite trend for the shorter chained fatty acids C_{12} to C_{18}. Their interpretation was that C_{20} could be derived from higher plants above the cave, whereas the shorter chained fatty acids could be produced by microorganisms in the cave and the aquifer. This hypothesis seems to be supported by our LOP results.

In Fig. 6.9, the dripwater Σ8 concentrations are compared with the drip rate and phosphate concentrations (Mischel et al., 2017). Phosphate shows high concentrations in autumn and winter and lower concentrations in spring and summer. Mischel et al. (2017) interpreted this pattern as resulting from organic material being flushed into the cave in autumn and winter. However, the low Σ8 concentrations in autumn and winter do not support this hypothesis. The difference in seasonal variations of Σ8 and phosphate could be explained either by different sources, as phosphate can also be leached from the bedrock, or by different transport mechanisms, such as transport in colloids or in solution. It is important to note that we are looking at the seasonal timescale here. On seasonal timescales, the variation of the phosphate concentration in the dripwater is probably mainly influenced by direct contribution from the bedrock by different water flows, while the input of plant material from the reservoir of organic matter can be considered as relatively constant. On longer

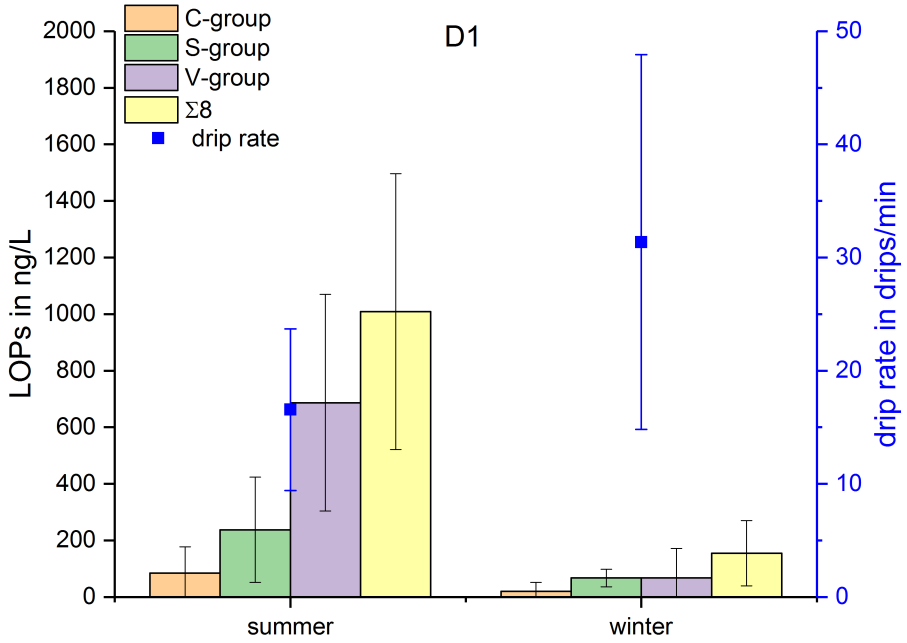

Figure 6.8: Comparison of Σ8 concentrations and drip rate in summer and winter.

timescales with a resolution of decades to centuries, as recorded in the stalagmite, the link between phosphorous concentrations and the general activity of the vegetation may be stronger. This is because the release and mobilization of phosphorous from the bedrock through weathering is related to the productivity of the vegetation above the cave since phosphorous serves as a plant nutrient. In future studies, the analysis of lignin and phosphate in dripwater should be combined with total organic carbon measurement or fluorescence spectroscopy to better quantify the general input of organic matter.

The record of the slow drip site, *D2*, shows no seasonal concentration pattern, but a high variability (Fig. 6.3). The pool water, *PW*, on the other hand, shows a smoothed out seasonality with low variance, with the exception of one month (April 2015) with exceptionally high concentrations. In Fig. 6.10, the averaged Σ8 concentrations of the fast drip site, *D1*, the slow drip site, *D2*, and the pool water, *PW*, are compared. On average, the slow drip site has a higher Σ8 concentration than the fast drip site, and the pool water has the lowest concentrations. This finding can be explained by dilution effects as discussed above, but also by different reservoirs feeding the individual drip sites.

The LOP concentrations in the dripwater samples were generally quite low, and in some samples, individual analytes were below the limit of detection. Therefore, C/V and S/V ratios could not be calculated for every sample. The missing data points make the interpretation of C/V and S/V with respect to seasonal patterns rather difficult (see Fig. 6.4). If we consider only the common interpretation of C/V and S/V as vegetation source indicators, we would not expect to see a seasonal pattern here, as the overall vegetation mixture above the cave remained unchanged throughout one year and the turnover times of lignin degradation in soil are long.

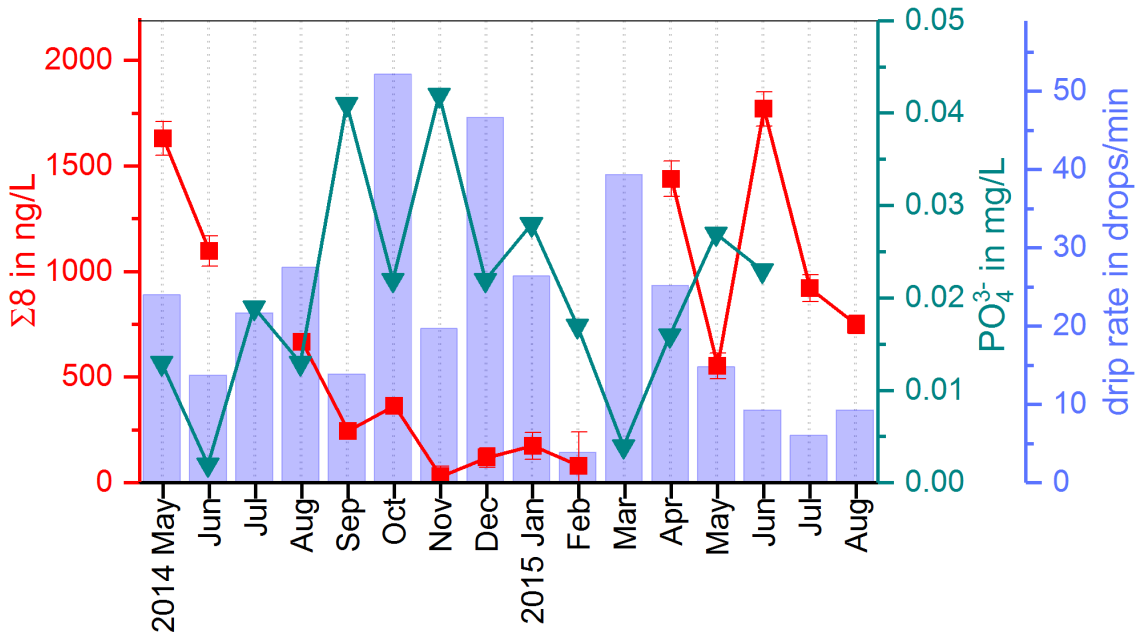

Figure 6.9: Comparison of Σ8 with PO_4^{3-} concentrations and drip rate.

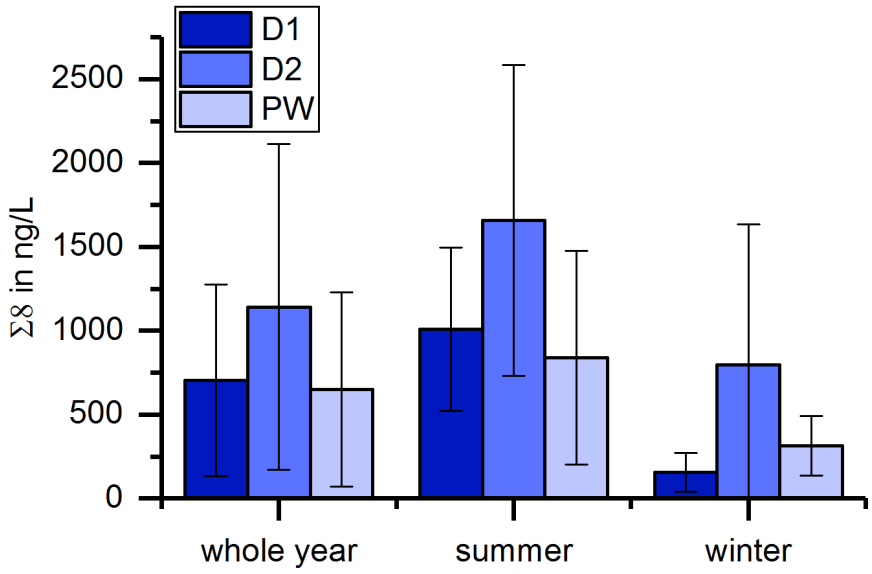

Figure 6.10: Comparison of average Σ8 concentrations of the fast drip site, D1, the slow drip site, D2 and the poolwater, PW.

In addition, radiocarbon dating studies showed that the organic matter above caves can be a mix of recent material and material that is up to several hundred years old (Trumbore, 2000, Tegen and Dörr, 1996, Fohlmeister et al., 2011). On the other hand, considering fractionation processes as described by Hernes et al. (2007), changes in dripwater C/V and S/V ratios may indicate changes in the transfer through the soil and karst system as well as changes in microbiological processes, such as degradation and interaction with soil organic matter, which are likely to change with temperature and moisture conditions.

We also compared the C/V and S/V ratios with δ^{13}C data and the drip rate (Fig. 6.11). From April to July 2015, there was a constant decrease in the drip rate and in the C/V and S/V ratios, whereas the δ^{13}C values show a constant increase in the same time interval. The increase in δ^{13}C values could be related to the decreasing drip rate and consequently a longer residence time of the drops in the cave air resulting in increased degassing (Hansen et al., 2017). An explanation for the decrease of C/V and S/V ratios could possibly be linked to the decreasing drip rate too. In times of reduced recharge of the aquifer, the transport of the lignin from the soil into the cave probably takes longer and involves more phase-changes than in times of higher recharge. According to Hernes et al. (2007) and Hernes et al. (2013), every phase-change that occurs to the lignin on its way from the plant litter to the deeper soil (and into the aquifer and the cave), for example from plant material to dissolved in water or from dissolved to adsorbed onto mineral surfaces, can lead to a fractionation and therefore to a change in the ratios of C/V, S/V as well as Acid/Aldehyde.

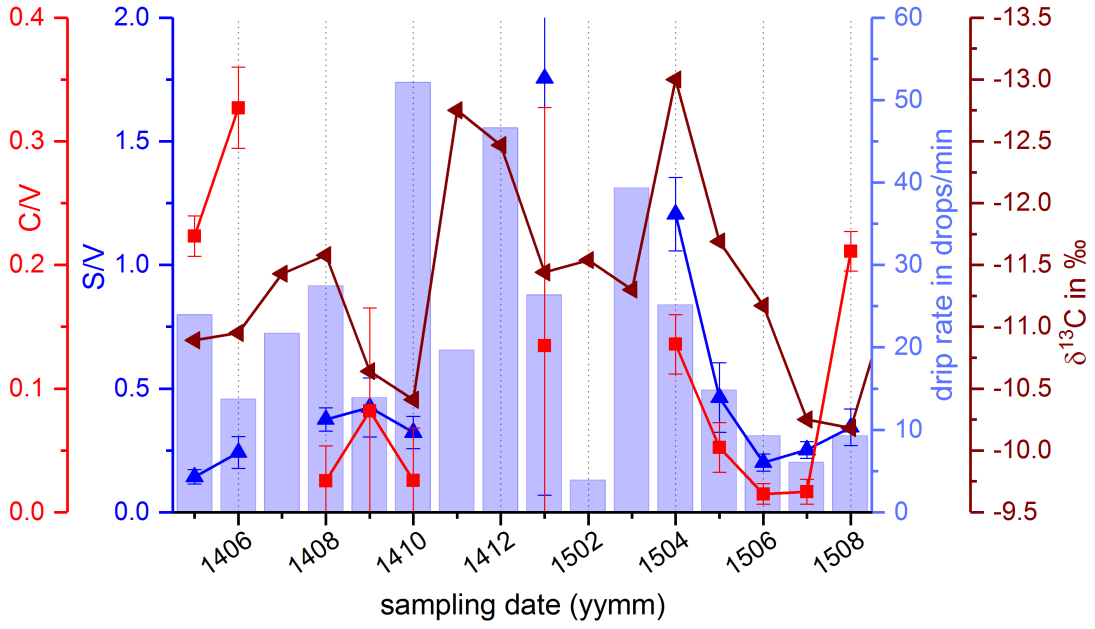

Figure 6.11: Comparison of C/V and S/V ratios with the drip rate and δ^{13}C values in the fast drip site *D1*.

The C/V and S/V ratios of the dripwater samples are lower than the ratios found in the stalagmite. This difference could also be caused by phase-change fractionation as the incorporation into the calcite of the growing speleothem represents a phase-change as well. To find out more about these effects, additional comparative studies of LOPs in speleothems and cave dripwater as well as in situ experiments in an artificial cave (Hansen et al., 2017, Wiedner et al., 2008, Polag et al., 2010) would be beneficial.

6.5 Conclusions and outlook

There are still many open questions concerning the interpretation of lignin oxidation products in speleothems and cave dripwater. However, this first quantitative record of LOPs in a stalagmite and cave dripwater shows that the quantification of LOPs is possible in both sample types, and that the signals show a significant variation over time on the centennial to millennial timescale in the stalagmite and a seasonal pattern in the dripwater. The total LOP concentration, $\Sigma 8$, in the stalagmite is correlated to P, Ba and U concentrations interpreted as vegetation proxies (Mischel et al., 2017). The clear benefit of $\Sigma 8$ compared to these trace elements is that the sources of lignin are exclusively higher plants and not, for example, microorganisms or the host rock. Therefore, $\Sigma 8$ can complement or even help to better interpret potential vegetation proxies whose sources are less clear. On the other hand, lignin can also be affected by microbial processes, such as differential degradation or incorporation into larger aggregates of organic substances, and transport processes, such as the adsorption to mineral particles. These effects seem to have a larger influence on the lignin ratios C/V and S/V, which are usually used as vegetation source indicators. Therefore, more research is needed to unravel the different influences affecting lignin oxidation products in the karst system.

In future studies, more speleothem samples from different vegetation and climate zones should be analyzed to study the relation of vegetation types above the cave and LOP ratios found in the speleothems. To get more insight into possible fractionation processes occurring on the way from the soil to the cave, comparative studies of LOPs in soil, dripwater and speleothems should be carried out and complemented with other methods, such as total organic carbon mesasurements, the calculation of C/N ratios or fluorescence spectroscopy. Annually laminated speleothems might be well suited as study objects because they often possess high organic matter content and high seasonality. In addition to stalagmites, flowstones could be valuable sample material because they are often fed by water flows with higher discharge carrying larger amounts of organic material.

Acknowledgements

We thank Simon Mischel for providing stalagmite and cave drip water samples from the Herbstlabyrinth Cave.

Author contributions

Conception and design of the work were done by IH, DS and TH. Data collection, performing of the experiments and drafting of the article were done by IH. Data analysis and interpretation, critical revision of the article, and final approval of the version to be published were done by IH, DS and TH.

7 Lignin analysis in a small stalagmite from Zoolithencave, Germany

7.1 Introduction

The purpose of this study was to test the potential of LOPs as a vegetation proxy by means of a specific paleo-vegetation question. In this case, a rapid vegetation change from grassland to deciduous forest in the landscape around the Zoolithencave in Germany was known from historical sources, but the established vegetation proxies such as $\delta^{13}C$ did not show a significant change in their signals recorded in a stalagmite. We wanted to evaluate whether LOPs can be used to detect such a vegetation change. A particular challenge of this study was the very small stalagmite resulting in a sample size of only 0.5 g per sample.

7.2 Samples and methods

The stalagmite Zoo-rez-1 analyzed here is from Zoolithencave, situated in the Franconian Jura in south-east Germany. It is only 3 cm high, has a well visible annual lamination and was sampled in 1999. The laminae consist of pairs of one brownish pigmented layer with strong fluorescence and one clear layer. The age of the stalagmite was determined by a combination of radiocarbon dating and annual laminae counting (Riechelmann et al., 2019). The methods used for sampling and analysis of LOPs were the same as described in chapter 4 and in chapter 6. Two samples with an edge length of about 0.5 cm were cut from this stalagmite. The lower sample weighed 0.49 g and had an assigned age of AD 1800–1828, and the upper sample weighed 0.55 g and had an assigned age of AD 1928–1970. During the latter period, the area above the cave was covered by a mixed deciduous forest, mainly beech forest, as it is still today (Fig. 7.1). From historical sources it is known that at the beginning of the nineteenth century, the landscape in the Franconian Jura consisted mainly of calcareous grasslands and juniper heath, which was used for grazing sheep and cattle (Lang, 2000). This can be seen on the historical postcard from 1850 in Fig. 7.2 (a). A modern example of juniper heath is shown in Fig. 7.2 (b).

Figure 7.1: Satellite image of the landscape around the Zoolithen Cave today. The green sign indicates the location of the cave.
(Image source: `http://www.caveseekers.com/caves/Zoolithenhoehle/cave.html`. Accessed 29.03.2018.)

Figure 7.2: (a) Historic view of the town Schesslitz and the surrounding landscape around 1850 (approximately 40 km distance from the Zoolithencave).
(Image source: Schesslitz. Stahlstich-Ansicht von Riegel nach Lebsche (around 1850). `https://pictures.abebooks.com/ANTIQUARIATSANZ/13995681370.jpg`. Accessed 07.02.2019.)
(b) Modern example of juniper heath landscape.
(Image source: Photo by Dr. Eugen Lehle. `https://upload.wikimedia.org/wikipedia/commons/8/82/Naturschutzgebiet_M%C3%B6nchsteig.jpg`. Accessed 11.02.2019.)

7.3 Results and discussions

Figure 7.3 shows the results of $\delta^{13}C$ analysis, LOP concentrations and C/V and S/V ratios. The $\delta^{13}C$ values, which are usually interpreted as a vegetation proxy, show almost no difference between the two samples (-8.58‰ for the older sample and -8.30‰for the younger sample). The total LOP concentration, Σ8, on the other hand, is five times higher in the younger sample (2906 ± 92 ng $\cdot$ g^{-1}) than in the older sample (512 ± 22 ng $\cdot$ g^{-1}). In addition, the S/V value in the younger sample (S/V = 0.40) is higher than in the older sample (S/V = 0.14), which indicates an increase in deciduous hardwood trees. A higher C/V value in the older sample, as expected for grasslands, was not observed (C/V = 0.12 in both samples), but this could be due to high V-group concentrations in the older sample originating from juniper. Compared to the stalagmite NG01 from the Herbstlabyrinth Cave (see chapter 6), which has a mean Σ8 concentration of 51 ± 15 ng $\cdot$ g^{-1}, the LOP concentrations in Zoo-rez-1 are 10–60 times higher.

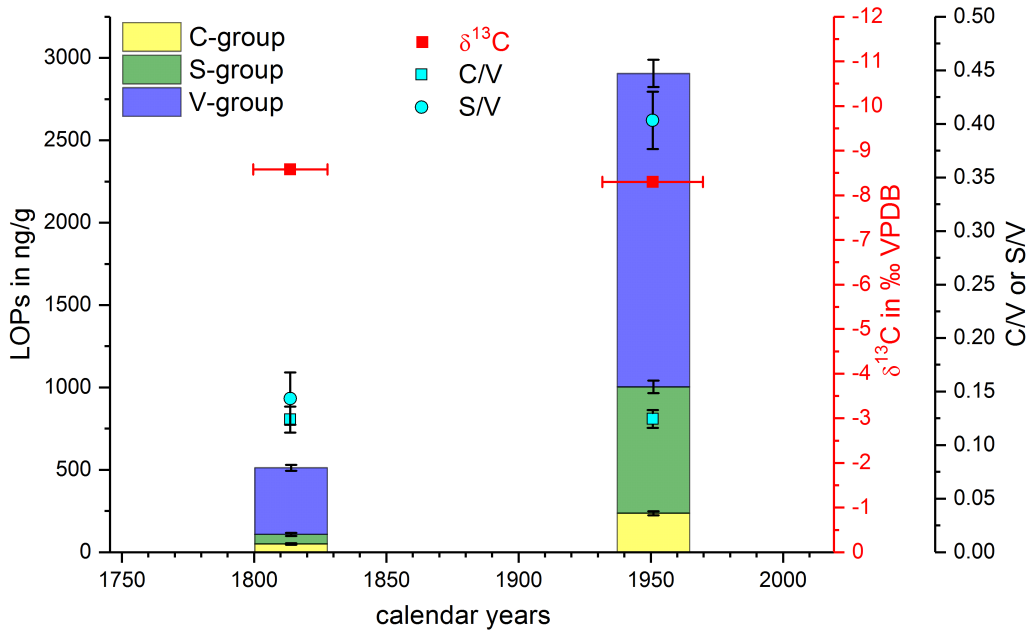

Figure 7.3: LOP concentrations, C/V and S/V ratios and $\delta^{13}C$ values of two stalagmite samples from the Zoolithencave.

7.4 Conclusion

The results of the two samples from the Zoolithencave demonstrate very well the potential of LOP analysis to reconstruct the vegetation of the past. $\delta^{13}C$ values can be influenced by many different factors, for example the host rock composition, the atmospheric $\delta^{13}C$ values, the abundance of C3- and C4-plants, soil- and root-respiration and in-cave processes such as degassing of CO_2 and prior calcite precipitation (Meyer et al., 2014). The analysis of LOPs, in comparison, enables a more direct interpre-

tation of changes in the vegetation cover. The example of stalagmite Zoo-rez-1 also shows that a stalagmite with seasonal input of high amounts of organic matter is very well suited for LOP analysis, allowing for sample sizes of only 0.5 g.

8 Lignin analysis in flowstone samples from Victoria Cave, Spain

8.1 Introduction

Cueva Victoria is a cave in the southeast of Spain, which is nowadays one of the driest regions in Europe with a strong seasonality of rainfall. In the past, however, there have been periods of more humid climate alternating with drier periods (Budsky et al., 2015, 2019a,b). In contrast to the stalagmite from the Zoolithen Cave in chapter 7, where there was a vegetation change known from historical sources but without a distinct signal in the δ^{13}C signals, the carbon isotope records of the flowstones from Cueva Victoria analyzed in this chapter show a large excursion during the Holocene and several distinct variations during the Last Glacial Period and the preceding Eemian interstadial. Budsky et al. (2019a) interpreted higher δ^{13}C values as decreased precipitation during the season of vegetation growth in spring and summer, leading over decades to a reduced vegetation cover. Since there may be many other possible causes for an increase in δ^{13}C values, this hypothesis should be supported either by pollen records from nearby sediment archives, as done by Budsky et al. (2019a) and Budsky et al. (2019b), or by vegetation proxies from the speleothem archive itself. Lignin oxidation proxies analyzed in speleothems can possibly provide such a support to isotopic records, recording not only changes in the density but also in the type of vegetation.

This study therefore serves to proof that LOPs can record relatively rapid vegetation changes in speleothem samples from different ages, in this case from the Holocene, the Last Glacial Period and the Eemian interglacial. An interesting research question during the Last Glacial Period are the so-called Dansgaard-Oeschger events. These are abrupt climate fluctuations, consisting of a rapid warming of several degrees within a couple of decades followed by a gradual cooling over several hundred years (Dansgaard et al., 1993, Bond et al., 1993). It would be interesting to see whether LOPs are able to trace vegetation changes during these climate fluctuations. However, this study does not contain a complete speleothem record, but just selected samples from flowstones from different ages as a proof-of-principal study.

8.2 Samples and methods

The flowstone analyzed here is from the cave Cueva Victoria, situated between Cartagena and Mar Menor in southeastern Spain. The region is one of the driest regions in Europe with an annual precipitation of 200–300 mm. The climate shows a strong seasonality with a moderately humid winter and spring, a hot and dry summer and a

more humid autumn (Budsky et al., 2019b). The two flowstone cores analyzed here, Vic-III-3 and Vic-III-4, had a diameter of 5 cm and a length of 41.5 cm and 31.0 cm, respectively. The upper 12 cm of Vic-III-4 correspond to the Holocene, whereas Vic-III-3 grew during the Eemian interglacial and the following last glacial period. The age of the flowstone samples was determined via ^{230}Th-U dating (Budsky et al., 2019a,b). The methods used for sampling and analysis of LOPs were the same as described in chapter 4 and in chapter 6.

8.3 Results and discussions

Figure 8.1 shows the results for LOPs, $\delta^{13}C$ and $\delta^{18}O$ (Budsky et al., 2019b) of the Holocene flowstone Vic-III-4. Additionally, xerophyte pollen (pollen from drought-tolerant plants) from a sediment record from the nearby Lake Siles are shown (Carrión, 2002). Whereas the δ^{18}O values stay relatively constant, the δ^{13}C values show a sharp excursion towards more positive values between 9.7 ± 0.3 and 7.8 ± 0.2 ka BP. At the same time, the percentage of xerophyte pollen shows a maximum. The LOP concentrations, on the other hand, are markedly lower in the samples from 8.7–8.0 and 9.1–8.7 ka BP, with 11.8 ± 0.4 and 9.5 ± 0.4 ng $\cdot$ g^{-1}, than in the sample from 12.1–10.7 ka BP with 23 ± 1 ng $\cdot$ g^{-1}. The decrease in LOPs is stronger in the V-group than in the C- and S-groups, resulting in higher C/V and S/V values in the two younger samples. This can be seen in Fig. 8.2, showing the C/V and S/V ratios plotted together with the $\delta^{13}C$ and $\delta^{18}O$ values with inverted scale. The C/V and S/V ratios of the older sample are consistent with mainly gymnosperm woody lignin sources such as a pine forest. In the two younger samples, the C/V and S/V ratios both shift towards more non-woody angiosperm lignin sources, such as grassy vegetation and shrubs.

The vegetation period in southeastern Spain only lasts from early spring to early summer because of the hot and dry summer time. If there is not enough rain during the vegetation period over several decades, this will lead to a reduced vegetation cover (Budsky et al., 2019a). In the pollen record of Lake Siles, this is reflected by an increase in xerophyte pollen, pinus pollen, herbs and shrubs and a decrease in pollen from deciduous forest in the time from approx. 10 to 7 ka BP (Carrión, 2002). The reduced vegetation cover leads to a decrease in soil pCO_2 and soil microbial activity, which in turn leads to higher δ^{13}C values (Budsky et al., 2019a). The precipitation in autumn and winter, when the main recharge of the aquifer typically occurs, was probably not reduced, as can be concluded from the constant δ^{18}O values and the constant growth rate of the speleothem (Budsky et al., 2019a). Consequently, Budsky et al. (2019a) interpreted the period between 9.7 ± 0.3 and 7.8 ± 0.2 ka BP as a climate with severe droughts in spring and summer and normal or even increased rainfall in autumn and winter. The LOP signals with a reduced total lignin concentration in the two samples from the drought period compared to the older sample and a shift from gymnosperm woody lignin sources towards more non-woody angiosperm lignin sources such as grasses and shrubs support this interpretation.

Figure 8.3 shows the LOP concentrations together with $\delta^{13}C$ and $\delta^{18}O$ values (Budsky et al., 2019b) of the older flowstone Vic-III-3. In addition, woody taxa

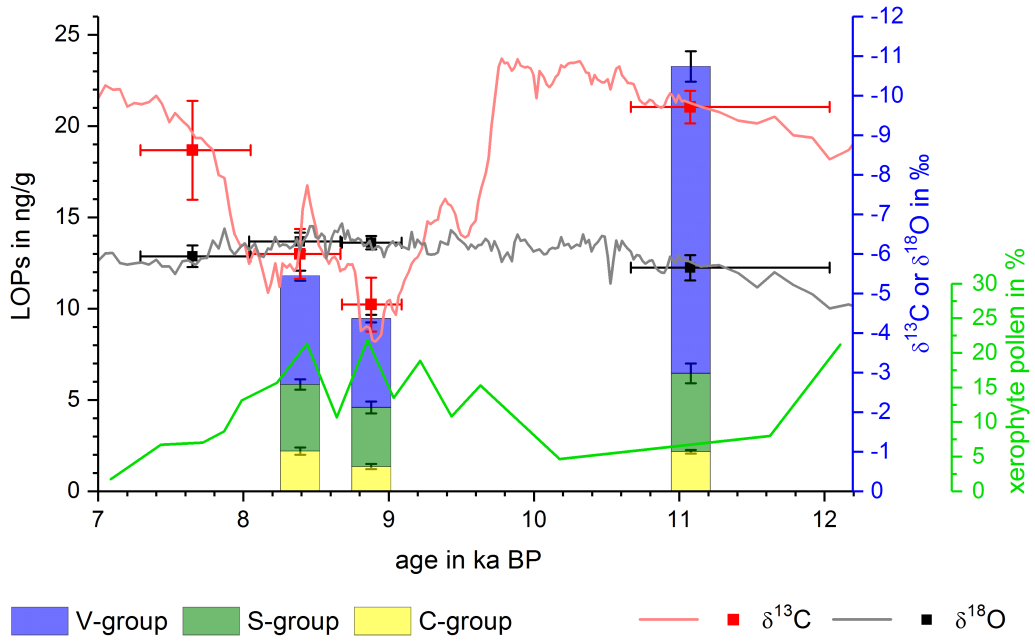

Figure 8.1: LOPs, xerophyte pollen, δ^{13}C and δ^{18}O values of flowstone Vic-III-4 from Cueva Victoria, Spain. For a clearer view of the diagram, the LOP results are depicted as columns of equal width. In fact, the temporal resolution of the LOP data is the same as of the stable isotope mean values, represented by the black and red horizontal error bars.

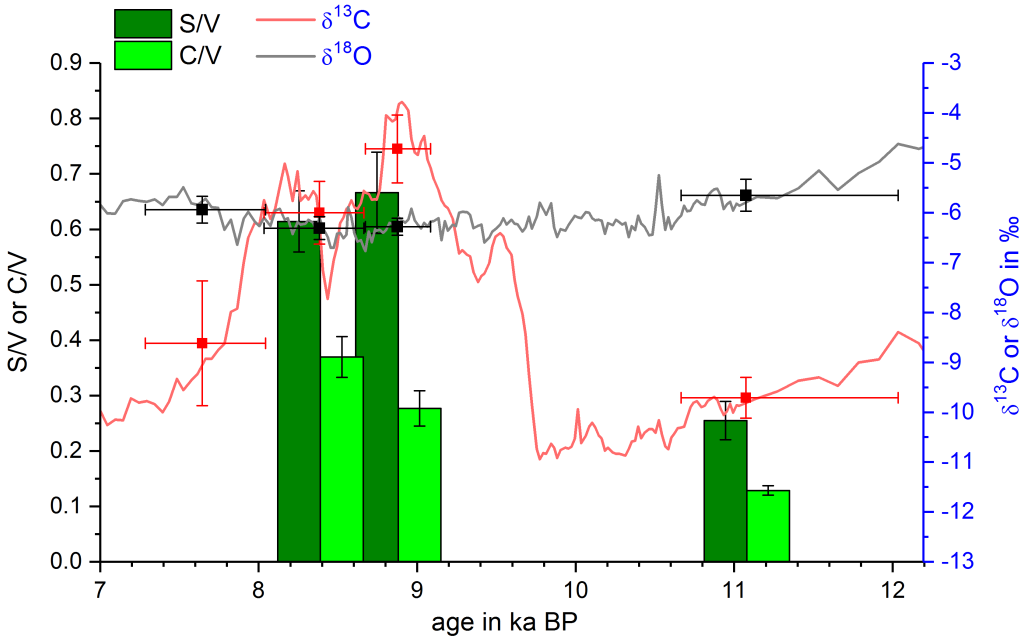

Figure 8.2: C/V, S/V, δ^{13}C and δ^{18}O values of flowstone Vic-III-4 from Cueva Victoria, Spain. For a clearer view of the diagram, the C/V and S/V results are depicted as columns of equal width. In fact, the temporal resolution of the C/V and S/V data is the same as of the stable isotope mean values, represented by the black and red horizontal error bars.

pollen from a sediment record from Lake Monticchio in southern Italy are shown for the glacial part of the flowstone (Allen et al., 1999). During the Last Glacial Period, several rapid climate fluctuations, so-called Dansgaard-Oeschger events, occured (Dansgaard et al., 1993), which also had an impact on the biosphere (Allen et al., 1999).

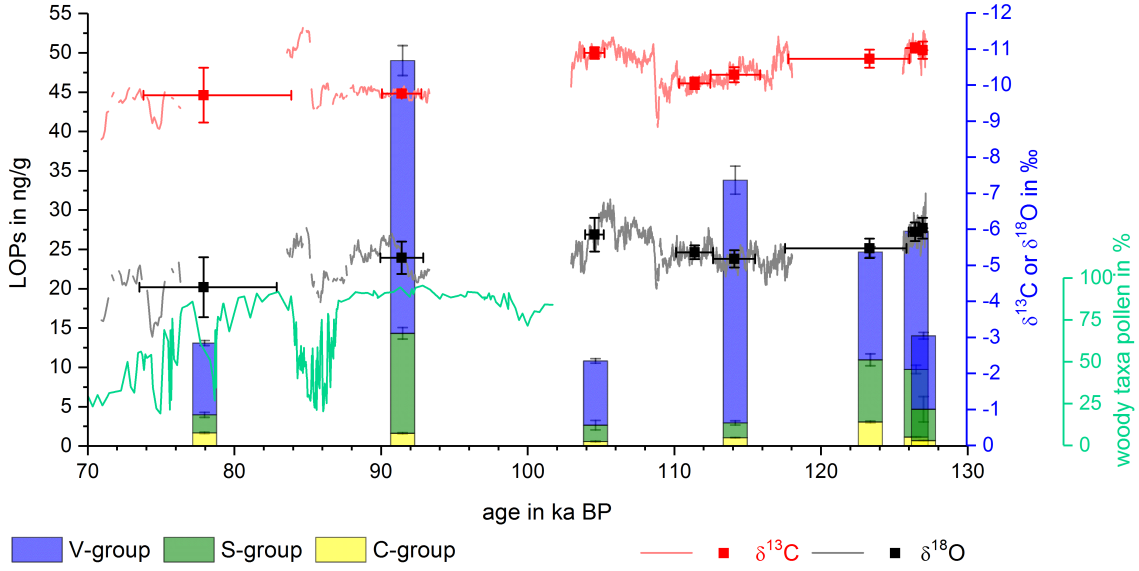

Figure 8.3: LOPs, woody taxa pollen, δ^{13}C and δ^{18}O values of flowstone Vic-III-3 from Cueva Victoria, Spain. For a clearer view of the diagram, the LOP results are depicted as columns of equal width. In fact, the temporal resolution of the LOP samples is the same as of the stable isotope mean values, represented by the black and red horizontal error bars.

Between 105 and 88 ka BP, the pollen record indicates a temperate deciduous forest with high abundance of woody taxa pollen (Allen et al., 1999). The LOP concentration in the sample from 93–90 ka BP is relatively high with 49 ± 2 ng $\cdot$ g^{-1}, and the low C/V and higher S/V ratios (Fig. 8.4) are consistent with a deciduous forest. From 83 to 70 ka BP, the abundance of woody taxa pollen decreases and shows more variability, probably caused by a Dansgaard-Oeschger driven climate that became both cooler and dryer (Allen et al., 1999). In the flowstone sample from 84–74 ka BP the LOP concentration is lower with only 13.1 ± 0.5 ng $\cdot$ g^{-1}, and the C/V value increases from 0.05 to 0.18, indicating an increase in non-woody material such as grassy vegetation. The S/V value shows a slight decrease from 0.37 to 0.25 indicating a shift towards more gymnosperm and less angiosperm trees. Both the lower LOP concentrations and the changes in the C/V and S/V ratios would be in accordance with a beginning shift towards a vegetation adapted to cooler and drier climate, such as grassland and pine forest. The δ^{13}C values are stable from 92 to 88 ka BP and then become more variable, too. However, the mean values of the two samples are almost the same with -9.8 ± 0.1 and -9.7 ± 0.8 ‰. The mean value of δ^{18}O, on the other hand, decreases slightly from -5.2 ± 0.5 to -4.4 ± 0.8 ‰, which indicates reduced precipitation and lower temperatures.

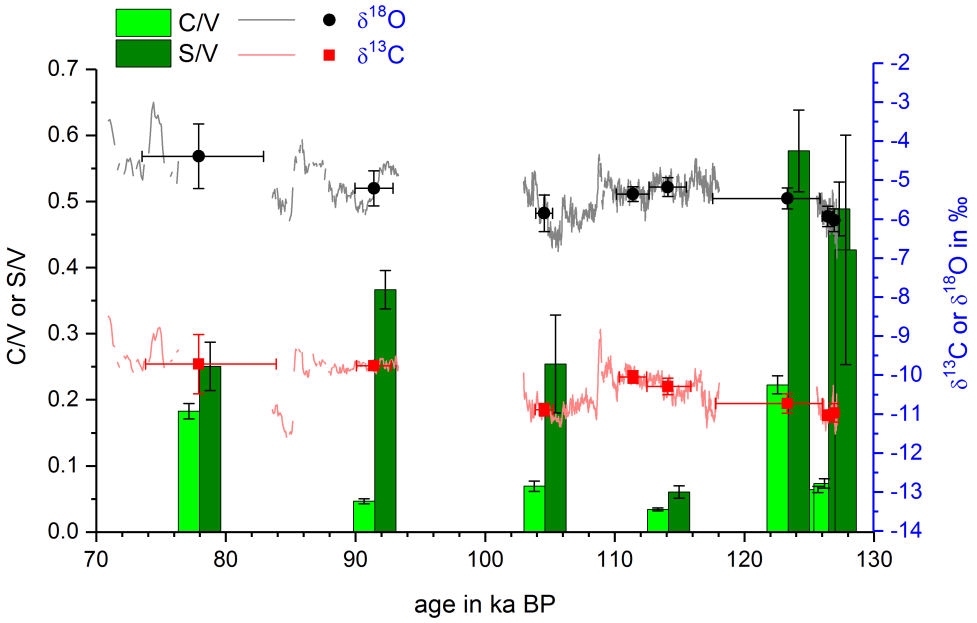

Figure 8.4: C/V, S/V, δ^{13}C and δ^{18}O values of flowstone Vic-III-3 from Cueva Victoria, Spain. For a clearer view of the diagram, the C/V and S/V results are depicted as columns of equal width. In fact, the temporal resolution of the C/V and S/V data is the same as of the stable isotope mean values, represented by the black and red horizontal error bars.

The climate of the Eemian interglacial (126–115 ka BP) was influenced by enhanced insolation and characterized by warm and humid conditions. This is generally registered in speleothems through higher growthrates and more negativ δ^{18}O values. However, the interpretation of the stable isotope signals from 128 to 102 ka BP in the Vic-III-3 flowstone has not yet been completed, and no suitable high-resolution pollen records from the Mediterranean region for the Eemian interglacial and the beginning of the Last Glacial Period were available for comparison. Therefore, the LOP results of this part of flowstone Vic-III-3 will not be discussed in detail with respect to climate or vegetation changes here.

The LOP concentrations in the samples from 127 to 104 ka BP range from 11 to 34 ng $\cdot$ g^{-1} and are in a comparable range with the glacial samples of Vic-III-3 and the Holocene samples of Vic-III-4. Also the C/V and S/V values show a comparable variability to the other samples, ranging from 0.03 to 0.22 for C/V and from 0.06 to 0.58 for S/V. This indicates that probably no significant loss or degradation of the lignin enclosed in speleothems occurred over time, allowing the use of LOPs as a vegetation proxy even in very old speleothem samples. Therefore, lignin analysis could help to interpret the stable isotope signals of flowstone VIC-III-3 and to reconstruct the vegetation cover during the Eemian interglacial and the onset of the Last Glacial Period in southeastern Spain in future analyses.

It is noteworthy that the LOP concentrations of the two flowstone cores from Cueva Victoria, Vic-III-3 with a mean value of 31 ± 20 ng $\cdot$ g^{-1} and Vic-III-4 with a mean value of 26 ± 19 ng $\cdot$ g^{-1}, are lower than in stalagmite NG01 from the Herbst-

labyrinth Cave (51 ± 15 ng $\cdot$ g^{-1}) and especially than in stalagmite Zoo-rez-1 from the Zoolithencave (512–2906 ng $\cdot$ g^{-1}). This could be due to the rather sparse vegetation cover and thinner soil thickness above the Cueva Victoria compared with the two German caves.

8.4 Conclusion

The LOP signals in the Holocene flowstone Vic-III-4 from Cueva Victoria in south-eastern Spain were able to record a strong reduction in vegetation density due to arid conditions in spring and summer in the time from 9.7 to 7.8 ka BP. This was reflected firstly in a decrease in total LOP concentration compared to pre-drought levels and secondly in a shift towards higher C/V and S/V levels, indicating a vegetation change from gymnosperm woody (e.g. pine forest) to more angiosperm non-woody vegetation (e.g. grassland and shrubs). This vegetation change was also recorded in pollen records from nearby Lake Siles.

Moreover, LOP signals in the flowstone Vic-III-3 from the Last Glacial Period were able to record a vegetation change from a temperate deciduous forest towards grassland and pine forest due to a Dansgaard-Oeschger driven climate that became both cooler and dryer in the time from 92 to 72 ka BP, which is also recorded in a pollen record from Lake Monticchio in southern Italy. This change was reflected in decreasing total LOP concentrations, increasing C/V and decreasing S/V ratios.

In the older part of flowstone Vic-III-3, dating back to the Eemian interglacial beginning about 126 ka before present, LOP concentrations in a comparable range to the younger samples have been detected, although they have not yet been interpreted with respect to climate and vegetation changes due to a lack of reliable interpretations based on stable isotopes or pollen records from Cueva Vicoria or the close proximity. All in all, the results of the Cueva-Victoria flowstones show that LOPs can serve as a valuable vegetation proxy even in very old speleothem samples and that they can be used to support the interpretation of stable isotope signals.

9 Understanding the cave system – Lignin analysis in soil, dripwater and speleothems from four different sites in New Zealand

This chapter is a reprint of the manuscript published in *Biogeosciences*:

Biogeosciences, 18, 2289–2300, 2021
https://doi.org/10.5194/bg-18-2289-2021

Lignin oxidation products in soil, dripwater and speleothems from four different sites in New Zealand

Inken Heidke[1], Adam Hartland[2], Denis Scholz[3], Andrew Pearson[2], John Hellstrom[4], Sebastian F. M. Breitenbach[5], and Thorsten Hoffmann[1]

[1]Institute of Inorganic Chemistry and Analytical Chemistry, Johannes Gutenberg University Mainz, Duesbergweg 10–14, 55128 Mainz, Germany
[2]Environmental Research Institute, School of Science, University of Waikato, Private Bag 3105, Hamilton 3240, New Zealand
[3]Institute of Geosciences, Johannes Gutenberg University Mainz, J.-J.-Becher-Weg 21, 55128 Mainz, Germany
[4]School of Earth Sciences, University of Melbourne, 253-283 Elgin St, Carlton, VIC 3053, Australia
[5]Department of Geography and Environmental Sciences, Northumbria University, Newcastle upon Tyne, NE1 8ST, United Kingdom

Correspondence: Thorsten Hoffmann (t.hoffmann@uni-mainz.de)

Received: 20 September 2020 – Discussion started: 6 November 2020
Revised: 17 February 2021 – Accepted: 2 March 2021 – Published: 8 April 2021

Abstract

Lignin oxidation products (LOPs) are widely used as vegetation proxies in climate archives, such as sediment and peat cores. The total LOP concentration, Σ8, provides information on the abundance of vegetation, while the ratios C/V and S/V of the different LOP groups also provide information on the type of vegetation. Recently, LOP analysis has been successfully applied to speleothem archives. However, there are many open questions concerning the transport and microbial degradation of LOPs on their way from the soil into the cave system. These processes could potentially

alter the original source-dependent LOP signals, in particular the C/V and S/V ratios, and thus complicate their interpretation in terms of past vegetation changes. We analyzed LOPs in leaf litter and different soil horizons as well as dripwater and flowstone samples from four different cave sites from different vegetation zones in New Zealand using ultrahigh-performance liquid chromatography coupled to high-resolution mass spectrometry. We test whether the original source-dependent LOP signal of the overlying vegetation is preserved and can be recovered from flowstone samples and investigate how the signal is altered by the transport from the soil to the cave. The LOP concentrations range from $mg \cdot g^{-1}$ in the soil to $ng \cdot g^{-1}$ in the flowstones. Our results demonstrate that, from the soil to the flowstone, the C/V and S/V ratios both increase, while the total lignin content, $\Sigma 8$, strongly decreases. This shows that the LOP signal is strongly influenced by both transport and degradation processes. Nevertheless, the relative LOP signal from the overlying soil at the different cave sites is preserved in the flowstone. We emphasize that for the interpretation of C/V and S/V ratios in terms of past vegetation changes, it is important to compare only samples of the same type (e.g., speleothem, dripwater or soil) and to evaluate only relative variations.

9.1 Introduction

Climate archives provide the means to study the climate and environment of the past, which is necessary to put ongoing climate change into a historic framework. Speleothems are valuable climate archives because they are ubiquitous across climatic and vegetational zones, preserve a range of inorganic and organic proxies (Fairchild and Baker, 2012, Blyth et al., 2016) and can be accurately dated up to ca. 600,000–700,000 years before present using U-series dating (Cheng et al., 2016, Scholz and Hoffmann, 2008). While up to the 1990s, speleothem research focused mainly on stable isotopes (e.g., $\delta^{18}O$, $\delta^{13}C$) (McDermott, 2004), today, multi-proxy studies combining, for example, stable isotopes, trace elements, fluorescent organic matter and selected molecular organic biomarkers are employed to unravel climatic and ecological signals (Blyth et al., 2016, Fairchild et al., 2006). Vegetation proxies not only complement other climate proxies, but also inform about the impact of changing temperature and precipitation on the development of vegetation. Fatty acids, originating from both plants and soil microorganisms, have been extracted from speleothems to study soil and vegetation activity (Blyth et al., 2006, Bosle et al., 2014), and long-chain *n*-alkanes from plant leaf waxes have been used to investigate vegetation changes (Xie, 2003, Blyth et al., 2007, 2011). However, the use of *n*-alkane chain length distributions to distinguish between different plant groups has been debated (Bush and McInerney, 2013, Blyth et al., 2016).

Lignin is a promising paleo-vegetation proxy because it is produced exclusively by vascular plants and represents one of the main constituents of wood and woody plants (Boerjan et al., 2003, Jex et al., 2014). In addition, the analysis of lignin has the particular advantage that it can yield information about not only the abundance, but also the type of vegetation. Lignin is a biopolymer that mainly consists of three different monomers: coniferyl alcohol, sinapyl alcohol, and p-coumaryl alcohol,

which are linked via C-C and C-O bonds in a radical coupling mechanism. The resulting structural units are guaiacyl (G), syringyl (S) and p-hydroxyphenyl (H) phenylpropanoid units, respectively, with the corresponding ratios varying with plant type. Lignin from gymnosperms (soft wood) consists mainly of G units, whereas lignin from angiosperms (hard wood) contains both G and S units. Grasses and non-woody plant parts, such as leaves and needles, are constructed from equal parts of G, S and H units. In addition, p-coumaric acid and ferulic acid can be ester-bound to the terminal hydroxyl groups of the propyl side chains, especially in grass lignin (Boerjan et al., 2003, Kögel-Knabner, 2002).

To analyze the lignin composition, the lignin polymer is oxidatively degraded into monomeric lignin oxidation products (LOPs), for example via CuO oxidation. The guaiacyl unit is oxidized to vanillic acid, vanillin and acetovanillone (V-group LOPs), and the syringyl is oxidized unit to syringic acid, syringaldehyde and acetosyringone (S-group LOPs). Ferulic acid and p-coumaric acid form the C-group LOPs. The p-hydroxyphenyl unit is oxidized to p-hydroxybenzoic acid, p-hydroxybenzaldehyde and p-hydroxyacetophenone (H-group LOPs), but because these can also originate from other sources than lignin, such as soil microorganisms or the degradation of protein-rich material, the H-group LOPs are not used as vegetation proxies. The sum of all eight individual C-, S- and V-group LOPs, $\Sigma 8$, is used to represent the total lignin concentration, whereas the ratios of the different LOP groups, C/V and S/V, are used to represent the type of lignin, with a higher C/V ratio indicating a higher contribution of non-woody vs. woody plant material and a higher S/V ratio indicating a higher contribution of angiosperm vs. gymnosperm plant material (Hedges and Mann, 1979).

The microbial degradation of lignin in the soil is comparably slow. For instance, it can take several years to break down a piece of wood (Opsahl and Benner, 1995). This is because only white-rot fungi are able to completely mineralize lignin to CO_2, mostly by co-metabolism with other energy sources. Other fungi, such as soft-rot and brown-rot fungi, are only able to induce structural changes to lignin (Kögel-Knabner, 2002). Due to this relative stability, lignin oxidation products are widely used as a paleo-vegetation proxy in climate archives, such as peat, lake sediments and marine sediment cores (see the review by Jex et al., 2014). In addition, LOPs are used as a proxy for the terrestrial input of plant biomass in natural waters (Zhang et al., 2013, Standley and Kaplan, 1998, Hernes and Benner, 2002). Blyth and Watson (2009) first detected lignin-derived compounds in speleothems, and lignin was subsequently highlighted as a promising vegetation proxy in speleothems in several review papers (Blyth et al., 2008, Jex et al., 2014, Blyth et al., 2016).

A recent study showed that trace concentrations of lignin oxidation products can be quantified in dripwater and speleothems (Heidke et al., 2018). In addition, in a Holocene stalagmite from the Herbstlabyrinth, Germany, the LOP concentrations and C/V and S/V ratios were found to co-vary with environmental changes and correlate with other proxies, such as P, U and Ba concentrations as well as $\delta^{13}C$ values (Heidke et al., 2019). This study also observed seasonal variations in LOP concentrations in monthly dripwater samples from the Herbstlabyrinth, with lower LOP concentrations in winter and higher concentrations in summer. However, there

are still many open questions concerning the transport of lignin from the soil through the karst system into the cave and speleothem. For instance, the interaction of lignin with mineral surfaces can lead to fractionation (Hernes et al., 2007, 2013), and land-use, climate, and soil characteristics may also influence the degradation of lignin (Thevenot et al., 2010, Jex et al., 2014). These effects could potentially alter the original source-dependent LOP signals, in particular the C/V and S/V ratios, and thus complicate their interpretation in terms of past vegetation changes. A schematic overview of the potential processes influencing the LOP signals is shown in Fig. 9.1.

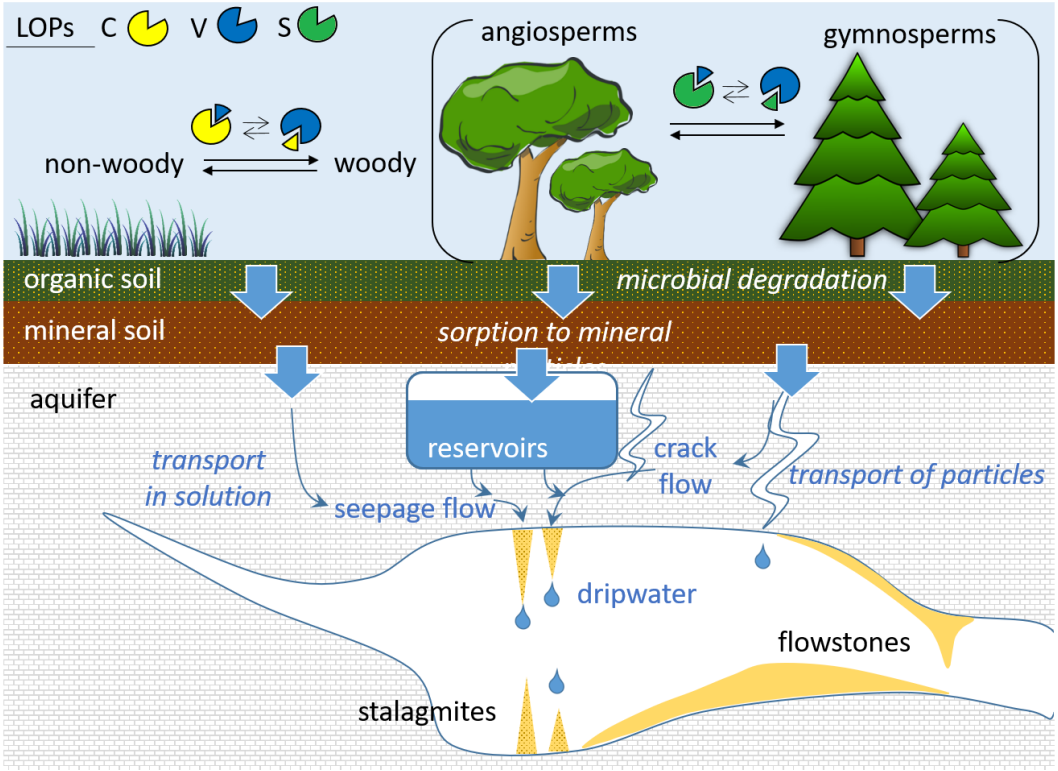

Figure 9.1: Schematic representation of the different potential processes influencing the transport and degradation of LOPs in speleothems and cave dripwater.

The vast majority of procedures for the determination of organic analytes in aqueous solutions such as dripwater rely on the collection of discrete samples of the water at a specific time. Subsequent laboratory analysis of the sample then provides a snapshot of the concentration of the target analytes at the time of sampling. In the presence of fluctuating concentrations, this method also has drawbacks, such as allowing for episodic concentration fluctuations to be missed. One solution to this problem is to increase the frequency of sampling or to install automated sampling systems that can collect numerous dripwater samples over a period of time. However, this is costly and in many cases impractical. But alternatives exist to overcome some of these difficulties. Of these, passive-sampling methods have shown to be promising tools for measuring aqueous concentrations of a wide range of organic substances. Passive samplers avoid many of the problems described above because they enrich

target analytes in situ, can be used for extended periods of time, and can be applied without continuously accessing the sampled caves. The goal is to determine the mass of target components accumulated by a sampler, thereby obtaining time-averaged concentrations. Of course, passive samplers also have their disadvantages (Vrana et al., 2005), which is why they are used here as one method in combination with other objects of investigation (leaf litter, soil and flowstone samples) and are primarily used to compare the different sampled sites with each other.

In this study, we analyzed the LOP signals in soil and dripwater samples as well as recently deposited flowstones from six different cave sites in New Zealand with different overlying vegetation. We investigated whether the original source-dependent signal of the overlaying vegetation is preserved and can be recovered from the flowstone samples. Furthermore, we investigated how the signal is altered by the transport process.

9.2 Methods and materials

9.2.1 Location and environment of the cave sites

The samples in this study were taken from six different cave sites in New Zealand (Fig. 9.2), spanning a latitudinal gradient from 38°S (Waipuna Cave) to 45°S (Luxmore Caves). Waipuna Cave (WP) is situated in the Waitomo District in the west of the North Island (S 38.3114722°, E 175.0206389°). The vegetation above the cave consists of pasture and mixed podocarp–broadleaved forest dominated by tree ferns. Soils are developed from rhyolitic tephra and are characterized by very deep *A* horizons. Hodges Creek Cave (HC: S 41.171270°, E 172.685941°) and Nettlebed Cave (NB: S 41.2104589°, E 172.7394572°) are both situated in Kahurangi National Park (40° S), in the Tasman District in the northwest of the South Island. The vegetation above both caves consists mainly of mature southern beech forest with well-developed *O* horizons. Luxmore Caves (LX), Daves Cave (DC) and Calcite Cave (CC) are all situated on Mt. Luxmore in Fiordland National Park in the Southland District in the southwest of the South Island (S 45.3894900°, E 167.6153448°). The vegetation here consists mainly of tussock grassland with alpine species present. A description of all sites including photographs of the vegetation and the soils is provided in the supplement in appendix C. From all caves, flowstones were selected for their higher organic matter content and their tendency to capture more diverse flow paths from surface environments compared to other speleothems such as stalagmites.

9.2.2 Sampling and pretreatment of samples

The overall procedure for the analysis of lignin oxidation products (LOPs) was similar to the procedure described in Heidke et al. (2018). However, since different types of samples were used, the methodology differed in some points and is thus briefly described in the following paragraphs.

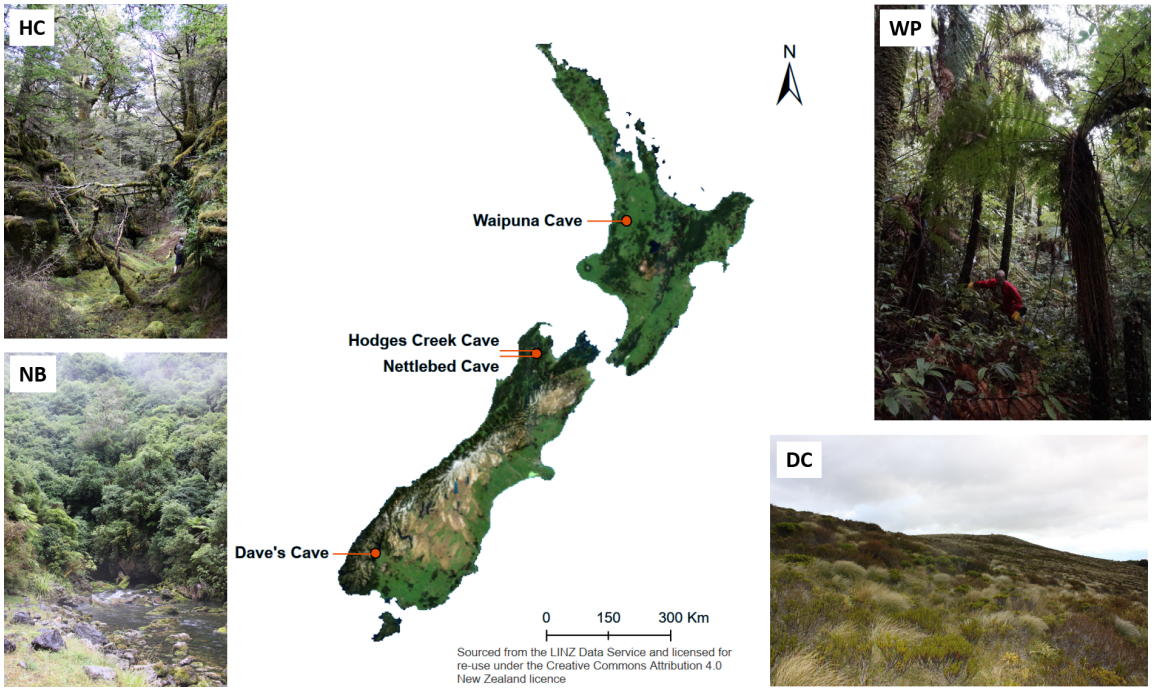

Figure 9.2: Map of New Zealand with the locations of the caves indicated. The photos give an impression of the vegetation at the sites of Hodges Creek Cave (HC), Waipuna Cave (WP), Nettlebed Cave (NB) and Dave's Cave (DC).

Sampling and pretreatment of soil and litter samples

Soil and litter samples were collected during field trips in 2014–2016 and kept refrigerated at 4°C in sealed containers prior to analysis. Soil horizons (A and O) and leaf litter (LL) were assigned on the basis of depth, color and composition of the soil with reference to the *New Zealand soil classification* manual (Hewitt, 2010) at the time of field sampling. Later, a subsample was removed, sieved over a 2.75 mm sieve and dried at room temperature beneath a fume hood. The dried samples were finely ground with a pestle and mortar and weighed into microwave reaction vessels. All soil samples were prepared and analyzed in duplicate. 0.5 g aliquots was taken from samples WP-LL, NB-LL and HC-LL (LL = leaf litter), 0.75 g was taken from NB-O (O = *O* horizon), and 1.0 g was taken from all other samples (NB-A (A = *A* horizon), LX-LL, LX-O, LX-A, WP-O, WP-A, HC-O and HC-A). 500 mg of CuO, 100 mg of $(NH_4)_2Fe(SO_4)$ and 15 mL of 2 $mol \cdot L^{-1}$ NaOH were added into the microwave reaction vessels, and microwave-assisted degradation was performed as described in section 9.2.3

Active sampling and pretreatment of dripwater samples

Dripwater from four different drip sites in Waipuna Cave was sampled in LDPE (low-density polyethylene) bottles that were precleaned with double-distilled water. The drip sites are well studied for their dynamics by Nava-Fernandez et al. (2020). Drip site WP2 is a highly seasonal drip site exhibiting high discharge following rain-

fall events; 1.0 L samples were collected from WP2 in April, July, September and November 2017 to investigate seasonal changes. From all other drip sites, 0.5 L samples were collected in November 2017. Drip site WP3 is a fast drip site with 0.5 L of water collected in about one hour; WP4 is a slow drip site with 0.5 L of water collected within four days; and WP5 was a very fast drip site with 0.5 L of water collected within a few minutes. In addition, 1.0 L of water from a stream flowing through the cave was sampled in November 2017. After collection, the samples were transferred into precleaned glass bottles and 5% (w/w) of acetonitrile was added to the water to prevent microbial growth. The samples were stored in a fridge at 4 °C awaiting further processing. Before extraction via solid-phase extraction (SPE), the samples were acidified to pH 1–2 with concentrated HCl and filtered through 0.45 µm cellulose acetate membrane filters. WP2 water samples and the stream water were divided into three subsamples equating to 0.33 L each; all other samples were divided into two subsamples equating to 0.25 L each. The SPE cartridges (Oasis HLB, 200 mg sorbent, 6 mL volume) were preconditioned with 6 mL of MeOH followed by 6 mL of water acidified with HCl. The samples were loaded by gravity flow using sample reservoirs. Afterwards, the cartridges were rinsed twice with 6 mL of acidified water and dried for 20 min by sucking ambient air through the cartridges. The dried cartridges were stored in sealed plastic bags in the fridge for several weeks to months. Eventually, the cartridges were eluted with 5 mL of MeOH in 10 portions of 0.5 mL. The eluent was evaporated in a stream of nitrogen at 30 °C. The residue was redissolved in 1.5 mL of 2 $\mathrm{mol \cdot L^{-1}}$ NaOH and transferred into the microwave reaction vessel; 250 mg of CuO, 50 mg of $(NH_4)_2Fe(SO_4)$ and a total volume of 8 mL of 2 $\mathrm{mol \cdot L^{-1}}$ NaOH were added, and the microwave-assisted degradation was performed as described in section 9.2.3.

The 0.45 µm cellulose acetate syringe filters that were used to filter the dripwater samples were stored in sealed plastic bags in the fridge for several months. The number of filters used per sample varied depending on the particulate matter load. For sample WP2-04, 3 filters per subsample were used, adding up to 9 filters in total, and for sample WP2-09, 4 filters per subsample were used (12 filters in total). For all other samples, one filter per subsample was sufficient (two filters in total for WP3, WP4 and WP5, three filters in total for WP2-07, WP2-11 and WP-stream). Three blank filters were stored, handled and analyzed in the same way as the sample filters. The filters were eluted with four portions of 1 mL of MeOH per filter. The eluent was evaporated in a stream of nitrogen at 30 °C. The residue was dissolved in 3 mL of 2 $\mathrm{mol \cdot L^{-1}}$ NaOH and then transferred into the microwave reaction vessels for further degradation and analysis.

Passive sampling and pretreatment of dripwater samples

Passive-sampling cartridges with 20 mL volume filled with XAD-7 polymeric resin were placed in the caves HC, WP, CC and DC underneath individual fast dripping drip sites for about one year in order to provide an integrated measure of dripwater organic matter fluxes. Cartridges were positioned so that the dripwater could flow through the cartridge, allowing for organic material to be adsorbed on the resin. Afterwards, the cartridges were capped and stored in the fridge before further pro-

cessing. Eventually, the cartridges were rinsed with 10 mL deionized water and dried under vacuum. To extract the organic material, the XAD-7 resin was transferred into an Erlenmeyer flask and stirred for at least 30 min with 10 mL of an elution solvent mixture consisting of 95% MeOH, 5% H_2O and 0.1 mol $\cdot$ L^{-1} NaOH. The solvent mixture with the resin was then transferred back into the cartridge, and the cartridge was eluted using positive pressure applied through a stream of nitrogen. The eluate was collected, and the resin was extracted again with fresh solvent mixture. The procedure was repeated three times in total. Finally, the cartridges were eluted with 10 mL of the solvent mixture directly in the cartridges using positive pressure applied through a stream of nitrogen. The combined eluates were filtered over 1 µm glass fiber filters (Whatman GF/F) and evaporated at 35 °C in a stream of nitrogen, until only approx. 2 mL were left. This concentrated eluate, which consisted mainly of aqueous NaOH as solvent, was transferred into the microwave reaction vessel. 250 mg of CuO and 50 mg of $(NH_4)_2Fe(SO_4)$ were added, and the volume was made up to 8 mL with 2 mol $\cdot$ L^{-1} NaOH. The microwave-assisted degradation was performed as described in section 9.2.3.

^{230}Th/U-dating of flowstone cores

Flowstone cores from the study sites were sampled in 2015. Powdered speleothem samples of 100 to 200 mg were collected from sectioned core samples and analyzed as described in Hellstrom (2003) and Drysdale et al. (2012). Briefly, samples were dissolved in concentrated HNO_3, spiked with a mixed ^{236}U-^{233}U-^{229}Th isotopic tracer solution, and capped and equilibrated on a hotplate overnight. U and Th were separated from the sample matrix using an established procedure with Eichrom TRU ion exchange resin columns, eluted together into a Teflon vial and dried down overnight. Sample U and Th were redissolved in dilute HNO_3 and HF and introduced together via a Teflon flow path to a Nu Instruments Plasma MC–ICP–MS (Multicollector–inductively coupled plasma–mass spectrometer) via a Nu DSN desolvator. ^{238}U ion beam intensities were typically 20 to 5 pA, with ^{233}U/^{234}U and ^{229}Th/^{230}Th analyzed simultaneously in twin ion counters in a peak-jumping routine. ^{230}Th/^{238}U and ^{234}U/^{238}U activity ratios for samples were normalized to those calculated for uraninite equilibrium standards run in the same analytical session. Ages were calculated using equation 1 of Hellstrom (2006) and the decay constants of Cheng et al. (2013), with initial ^{230}Th/^{232}Th and its uncertainty for each speleothem estimated using stratigraphic constraint. A table with all relevant data concerning the ^{230}Th/U-dating as well the age–depths models can be found in the supplement in appendix C.

Sampling and pretreatment of flowstone samples

Samples with 5–10 mm edge length were cut from the flowstone cores with a diamond blade saw following the direction of the growth layers. Photos of the flowstone cores are shown in the supplement in appendix C. The distance from the top of the flowstone core and the ages of the LOP samples are given in Table 9.1. The flowstone cores were embedded in a polymeric resin for stabilization, which was not resistant to

organic solvents, but could not be completely dissolved either. Therefore, the cleaning protocol described in Heidke et al. (2018) had to be slightly modified. Instead of ultrasonication with dichloromethane and methanol, the samples were merely rinsed first with EtOH, then with MeOH, and then dried in an airstream. The outer layer of calcite, where it was not covered by the resin, was etched in 0.6% HCl for 5 min. Afterwards, the samples were dried, weighed and then dissolved in 30% HCl. The sample weight was determined by weighing the resin after complete dissolution of the sample. The sample solution was diluted 1:1 with ultrapure water and then extracted via SPE as described in Heidke et al. (2018) using Oasis HLB 60 mg cartridges and eluted with 1.5 mL of methanol. The microwave-assisted degradation with 250 mg of CuO, 50 mg of $(NH_4)_2Fe(SO_4)$ and 8 mL of NaOH was performed as described in section 9.2.3.

Table 9.1: Distance from the top (DFT) of upper and lower edges of the flowstone sample cubes (DFT(upper), (DFT(lower)), ages calculated from the age model for upper and lower edges (age(upper), (age(lower)), and calculated mean sample ages for the flowstone samples (age(mean)).

Sample	DFT(upper) in mm	DFT(lower) in mm	Age(upper) in ka BP	Age(lower) in ka BP	Age(mean) in ka BP
HC1	0	5	0.00	2.19	1.1 ± 1.1
HC2	5	9	2.19	3.26	2.7 ± 0.5
NB1	0	10	0.00	0.94	0.5 ± 0.5
NB2	10	20	0.94	1.59	1.3 ± 0.3
WP1	1	10	0.22	2.08	1.1 ± 0.9
WP2	10	20	2.08	3.90	3.0 ± 0.9
DC1	0	10	0.00	0.37	0.2 ± 0.2
DC2	10	18	0.37	0.72	0.5 ± 0.2

9.2.3 CuO oxidation, extraction and analysis of lignin oxidation products

The reaction vessels filled with reagents and sample extracts were flushed with argon and capped. The oxidation, extraction and analysis procedures are described in detail in Heidke et al. (2018). In brief, the oxidation was carried out in a microwave oven at 155 °C for 90 min. After cooling, ethyl vanillin was added as an internal standard. The reaction mixture was separated from solids by centrifugation, acidified and then extracted via SPE. For the dripwater and flowstone samples, the whole sample solution was extracted, whereas for the soil samples, only 1 mL of the sample solution was extracted. Oasis HLB cartridges with 60 mg sorbent and 3 mL volume were used, which were eluted with 1 mL of acetonitrile containing 2% of NH_4OH.

The LC–MS (liquid chromatography–mass spectrometry) analysis was performed similarly as described in Heidke et al. (2018). In brief, a pentafluorophenyl column with an acetonitrile–water gradient elution was used in an ultrahigh-performance

liquid chromatography (UHPLC) system to separate the LOPs. The mass spectrometric detection was performed using a Q Exactive Orbitrap high-resolution mass spectrometer, which was operated alternately in full-scan mode and MS/MS mode. Further details as well as slight differences to the method described by Heidke et al. (2018) can be found in the supplement in appendix C.

9.3 Results and discussion

9.3.1 Comparison of soil, passively sampled dripwater and flowstone samples from different cave sites

Comparing the LOP concentrations in soil, passively sampled dripwater and flowstone samples as well as the distribution of the C-, S- and V-group LOPs (Fig. 9.3), the concentrations range from $mg \cdot g^{-1}$ in the leaf litter and soil samples to $ng \cdot g^{-1}$ in the flowstone samples. For the dripwater, the values are given in nanograms per sample, where 'sample' refers to an XAD-cartridge that was deployed in the cave for passive sampling for about one year. The total LOP concentrations, $\Sigma 8$, decrease strongly with soil depth in all caves (Fig. 9.3(a)). Large variations are observed between the different drip sites within the same cave, especially in HC (Fig. 9.3(b)). The differences between the stratigraphically younger (1) and older (2) flowstone samples are less pronounced, with slightly higher LOP concentrations in the older samples, except for LX/DC cave (Fig. 9.3(c)). In all three samples types – soil, dripwater and flowstones – the relation between the different cave sites regarding the total LOP concentration, $\Sigma 8$, is similar, with the highest LOP concentrations in samples from HC and NB and lower concentrations in samples from WP and LX (Fig. 9.3(e)).

Figure 9.3: (See page 129.) Comparison of LOP concentrations in (a) soil, (b) passively-sampled dripwater and (c) flowstone samples. The height of the columns represents the total LOP concentration, $\Sigma 8$, and the different colors refer to the C-, S- and V-group LOPs. The empty boxes show the mean values of the $\Sigma 8$ concentrations. Panel (d) shows an enlargement of panel (a) to better illustrate the concentrations of the C-group LOPs. In panel (e), the mean LOP concentrations (represented as the empty boxes in panels (a), (b) and (c)) of soil, dripwater and flowstone samples are normalized to the respective mean LOP concentration of HC. Panel (f) illustrates the different decreases between the soil and the flowstone of the C-, S- and V-group LOPs. The abbreviations in the grey boxes in panels (a) to (d) indicate the cave (see main text). Other abbreviations include LL = leaf litter, O = organic horizon, A = *A* horizon. In panel (b), different bars correspond to the individual drip sites (see main text). In panel (c), sample 1 stands for the most recently deposited flowstone sample from the cave floor (distance from the top of 0–1 cm), whereas 2 stands for the stratigraphically older flowstone sample with a distance from the top of 1–2 cm. The ages of the flowstone samples are given in Table 9.1.

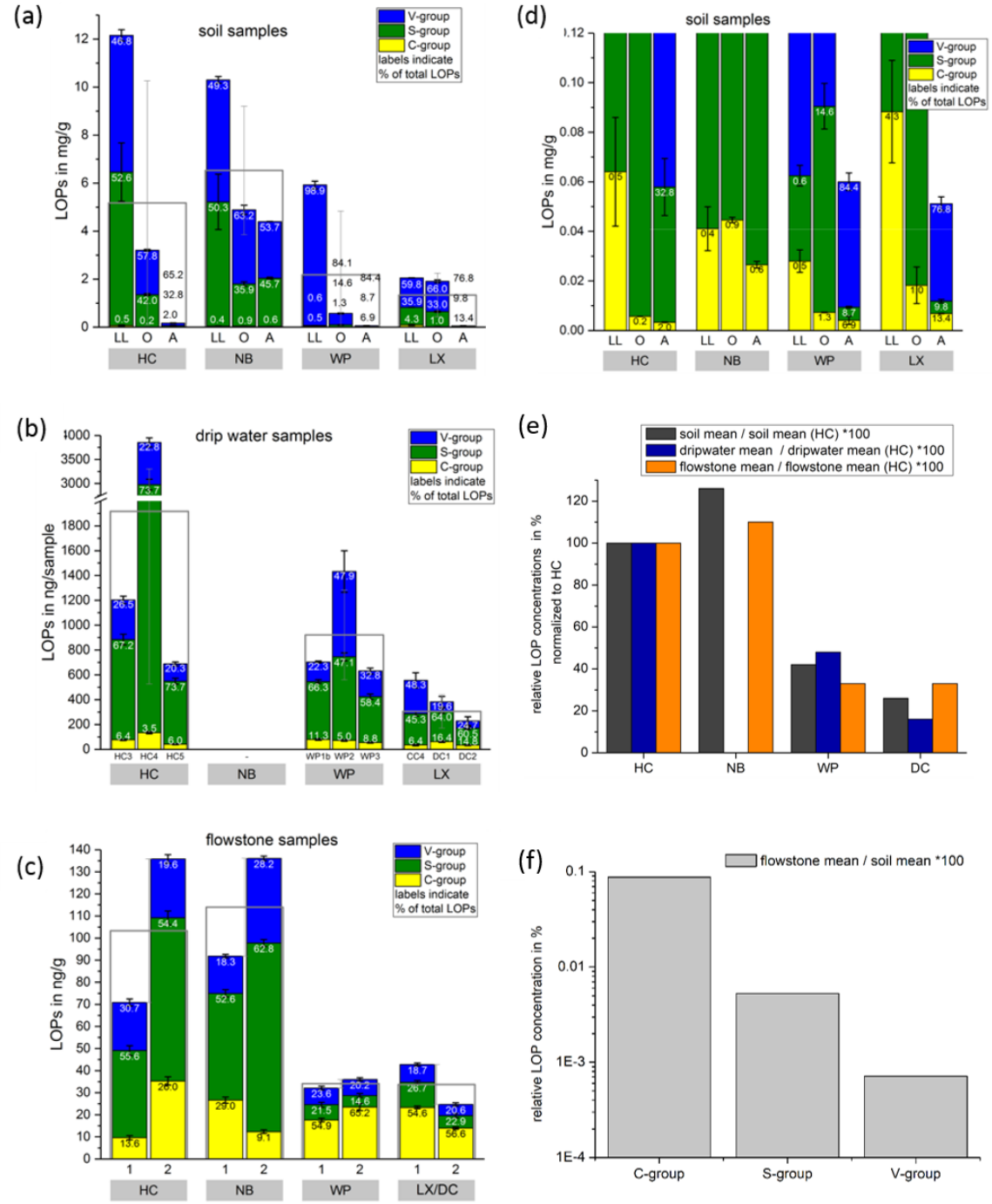
(a)
soil samples
V-group
S-group
C-group
labels indicate
% of total LOPs
LOPs in mg/g
LL O A
HC NB WP LX
(d)
soil samples
LOPs in mg/g
(b)
drip water samples
LOPs in ng/sample
HC3 HC4 HC5 - WP1b WP2 WP3 CC4 DC1 DC2
(e)
soil mean / soil mean (HC) *100
dripwater mean / dripwater mean (HC) *100
flowstone mean / flowstone mean (HC) *100
relative LOP concentrations in %
normalized to HC
HC NB WP DC
(c)
flowstone samples
LOPs in ng/g
1 2
HC NB WP LX/DC
(f)
flowstone mean / soil mean *100
relative LOP concentration in %
C-group S-group V-group

In a scatterplot of S/V versus C/V values of soil, dripwater and flowstone samples (Fig. 9.4), each sample type occupies a distinct region of the diagram, with the soil samples having the lowest C/V values and low S/V values, the dripwater samples having medium C/V and the highest S/V values, and the flowstone samples having the highest C/V and low to medium S/V values.

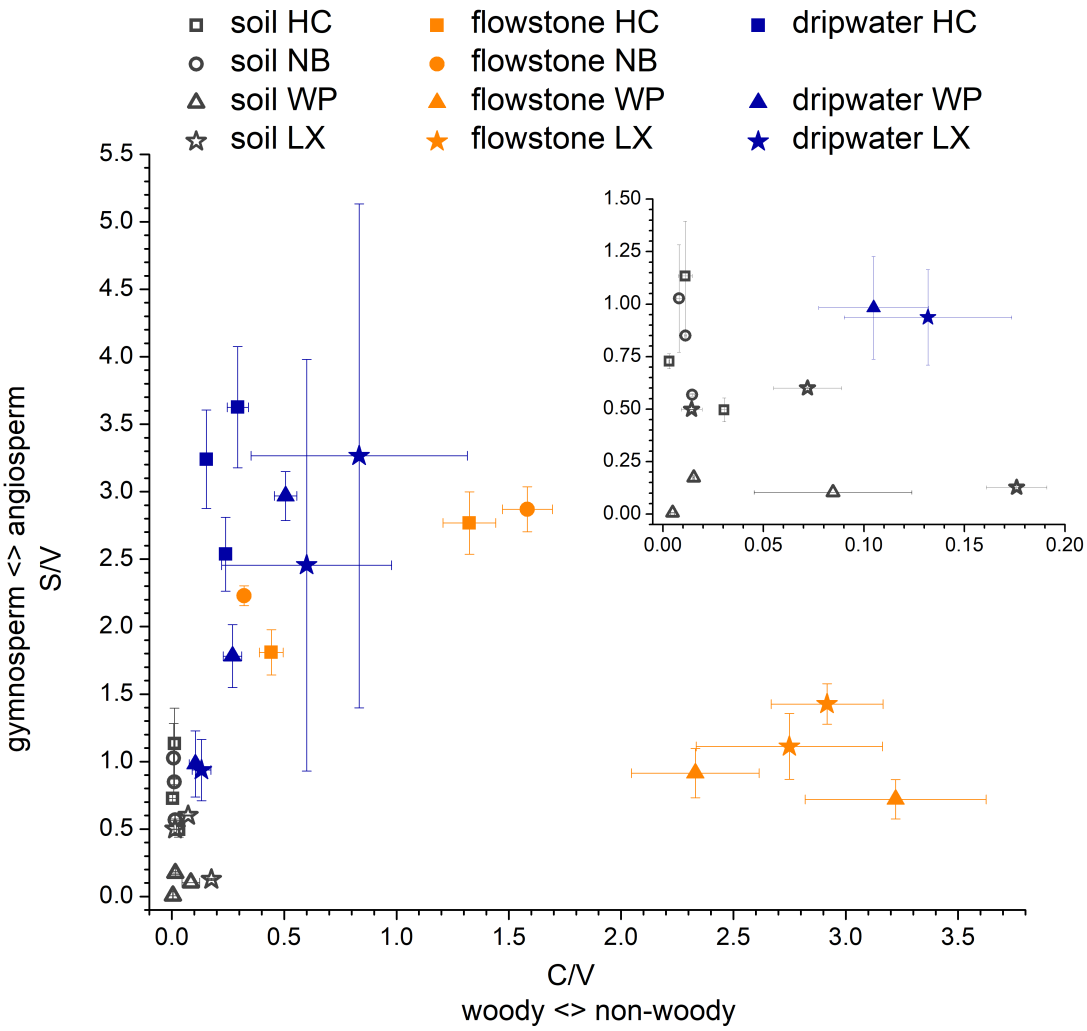

Figure 9.4: S/V versus C/V values of soil, dripwater and flowstone samples from Hodges Creek Cave (HC), Nettlebed Cave (NB), Waipuna Cave (WP) and Luxmore Caves (LX). The insert shows an enlargement of the area close to the origin.

The C/V and S/V ratios in the leaf litter samples are representative of the current vegetation cover (Fig. 9.5), with low C/V and high S/V ratios for HC and NB (angiosperm southern beech forest), low C/V and low S/V ratios for WP (gymnosperm podocarp forest, apparently dominating the lignin input over the pasture), and comparatively higher C/V and medium S/V ratios for LX (tussock grassland). This is in line with the source specific ratios established by Hedges and Mann (1979). The S/V and C/V ratios of all sample types normalized to the respective ratios of Hodges

Creek Cave (HC) are presented in Figures 9.6(a) and 9.6(b), respectively. This presentation shows that in all three sample types (soil, dripwater and flowstone), HC and NB have the highest S/V and the lowest C/V ratios, while WP has the lowest S/V ratio, and DC the highest C/V ratio. This means that although the absolute ratios increase from soil to dripwater to speleothem and the magnitude of change varies among cave sites, the relative ratios show the same trend in all sample types. This in turn suggests that the LOP signature of the overlying vegetation is at least partly preserved in dripwater and speleothem samples, which is a precondition for using LOPs as a biomarker for past vegetation changes. Possible causes for the different magnitude of change of the LOP ratios from soil to dripwater to flowstone among the different cave sites can be differences in soil thickness, types of soil and vegetation density, which can all influence transport and degradation of LOPs.

As expected, the LOP concentrations decrease from the soil to the cave. However, the C-, S-, and V-group LOPs do not diminish at the same rate. The decrease is strongest for the V group and weakest for the C group (Fig. 9.3(f)). This apparent change in the lignin composition could be caused by biotic factors, such as differential microbial degradation, or abiotic factors, such as the interaction with mineral surfaces. Degradation studies of plant litter in litter bags or in situ in the top 25 cm of the soil using CuO oxidation showed that the concentrations of C- and S-group LOPs decreased faster than the concentrations of V-group LOPs (Bahri et al., 2006, Opsahl and Benner, 1995, Jex et al., 2014). However, the faster degradation of lignin high in S- and C-group LOPs does not necessarily mean that the released lignin fragments are completely mineralized. It is also possible that they are leached to deeper soil layers since the (partial) degradation leads to a higher oxidation state, i.e., to more carboxylic acid functional groups, and thus to a better water solubility. Concerning the abiotic factors, Hernes et al. (2007) leached different plant litters in water and observed changes in the C/V ratio from -40% to up to +400% in the leachate compared to the parent litter. Subsequent sorption of the leachate to different mineral phases further increased the C/V ratio up to sevenfold compared to the leachate. For S/V, Hernes et al. (2007) observed a twofold increase by the combined effects of leaching and sorption, and the acid/aldehyde ratios increased as well by a factor of 2 or more. Both the differential microbial degradation and the effects of leaching and sorption are probably caused by structural differences between the individual lignin monomers. Lignin high in sinapyl (S-group) monomers contains mainly β-aryl ether [β-O-4] linkages, which can be chemically cleaved more easily, whereas lignin with high proportions of guaiacyl (V-group) monomers contains higher amounts of phenylcoumaran [β-5], biphenyl [5-5] and biphenyl ether [5-O-4] linkages, which are more resistant to chemical cleavage (Boerjan et al., 2003). As a result, lignin with a high contribution of S units is more easily degraded and also less branched because the [5-O-4] and [5-5] linkages represent branching points in the polymer. The C-group phenols are mainly bound by peripheral ester linkages linking lignin and cellulose and are often not part of the lignin polymer itself (Kögel-Knabner, 2002, Boerjan et al., 2003). This part of the C-group phenols can be cleaved from the lignin by mild base hydrolysis (Opsahl and Benner, 1995). Probably, hydrolysis of the ester-bound C-group LOPs also occurs in the soil and the epikarst aquifer above the cave. These

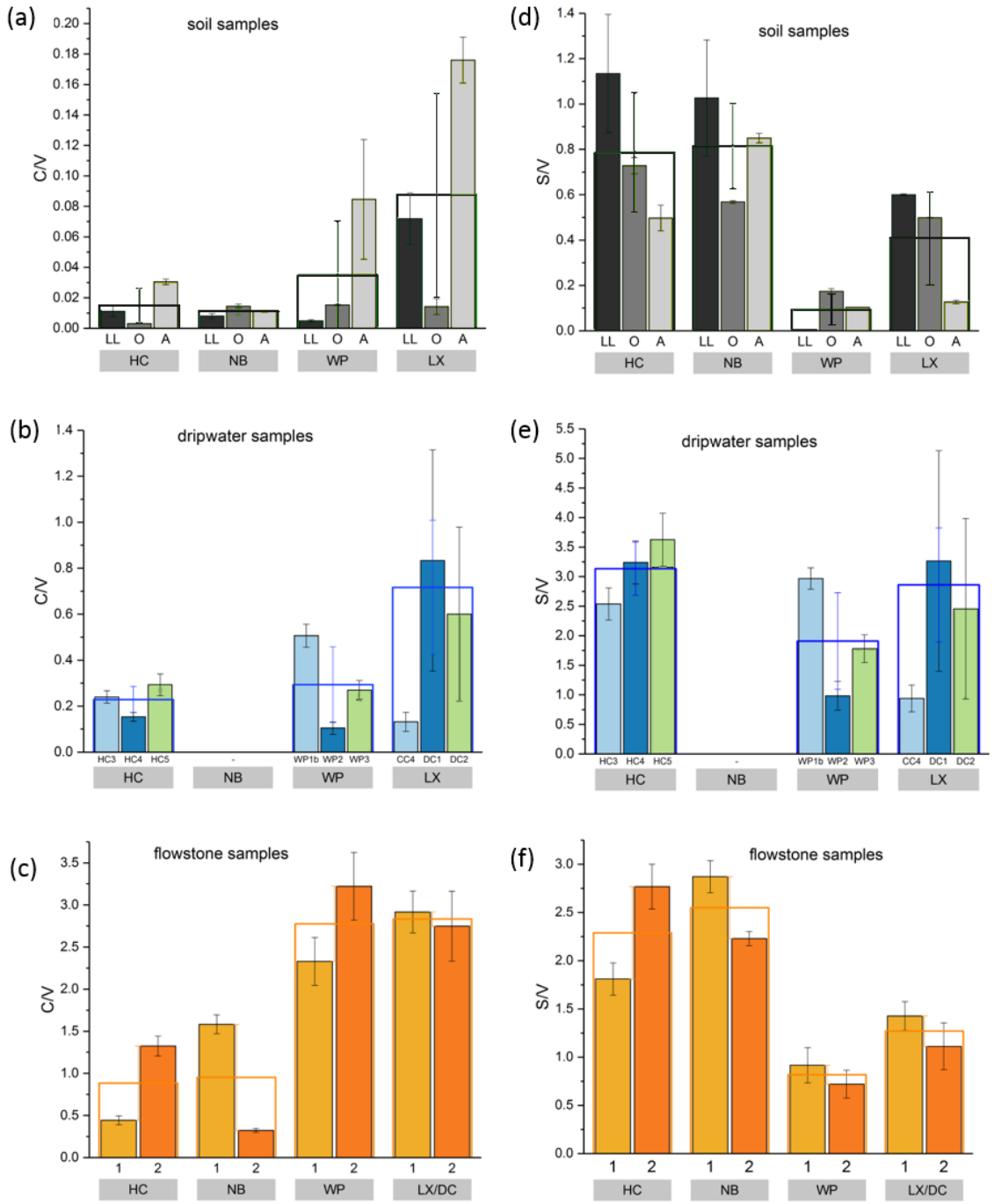

Figure 9.5: C/V and S/V values of the individual soil, dripwater and flowstone samples. The empty boxes show the mean values of the individual samples.

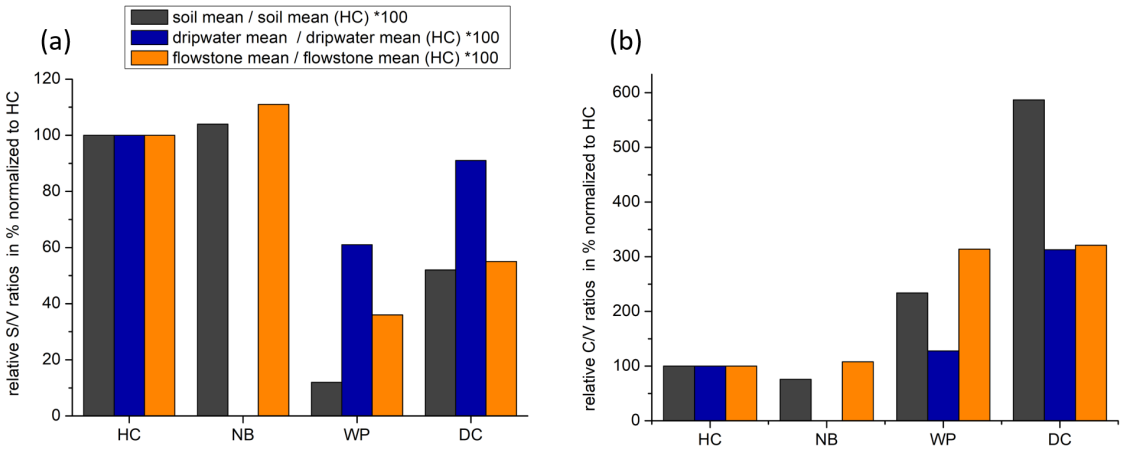

Figure 9.6: Mean S/V ratios (a) and mean C/V ratios (b) of soil, dripwater and flowstone samples normalized to the respective mean S/V or C/V ratios of HC.

hydrolyzed C-group phenols are more water soluble and may be transported to the cave more efficiently than the less soluble larger lignin particles and therefore can be enriched in cave dripwater and speleothems compared to S- and V-group phenols. This could also explain the increase of the C/V ratios from the leaf litter (LL) to the *O* and *A* horizons for all cave sites in our results (Fig. 9.5). The S/V ratios, on the other hand, decrease from the leaf litter to the *O* and *A* horizons, consistent with a higher degradation state in deeper soils, but are much higher in the dripwater and the flowstone samples than in the soil. A possible explanation lies in the fact that the adsorption of lignin from the dripwater to the XAD material and the subsequent elution as well as the incorporation of lignin into the speleothem fabric present phase change processes as well, which can be selective and cause fractionation.

Our results suggest that the lignin fragments high in C- and S-group lignins, which are more easily degraded, are preferentially transported to deeper soils, probably due to their better water solubility. Thus, they are enriched in dripwater and speleothems compared to the more stable V-group lignins, which are possibly preferentially retained by sorption to mineral surfaces. However, our results also show that the initial signals from the vegetation sources, i.e., the relative differences in Σ8, C/V and S/V between the different cave sites, are well preserved in the dripwater and flowstone samples despite these processes.

9.3.2 Dripwater study from Waipuna Cave

Figure 9.7 shows the results of the active dripwater sampling at Waipuna Cave. The total LOP concentrations, Σ8, in the filtered dripwater samples were very low, with a range of 2–290 $ng \cdot L^{-1}$. In comparison, Σ8 in the dripwater from the German Herbstlabyrinth cave system was in the range of 500–1800 $ng \cdot L^{-1}$ in summer and 30–400 $ng \cdot L^{-1}$ in winter (Heidke et al., 2019). The S-group analytes were below the detection limit in all samples, and the C-group analytes were below the detection

limit in most samples. Therefore, the C/V and S/V ratios could not be calculated. We suspect that the lignin was not dissolved homogeneously in the water samples, but instead adsorbed to particulate matter. In this case, the filtering of the samples would have affected the LOP concentrations. Therefore, we analyzed the particulate matter retained in the syringe filters. The results are shown as the hatched bars in Fig. 9.7. The two samples that had a considerable particulate matter load, WP2-04 and WP2-07, showed the highest LOP concentrations of about 2200 ng · sample^{-1}. WP2-11 and WP-stream had low LOP concentrations of about 170 and 50 ng · sample^{-1}, whereas the rest of the samples was close to or below the detection limit.

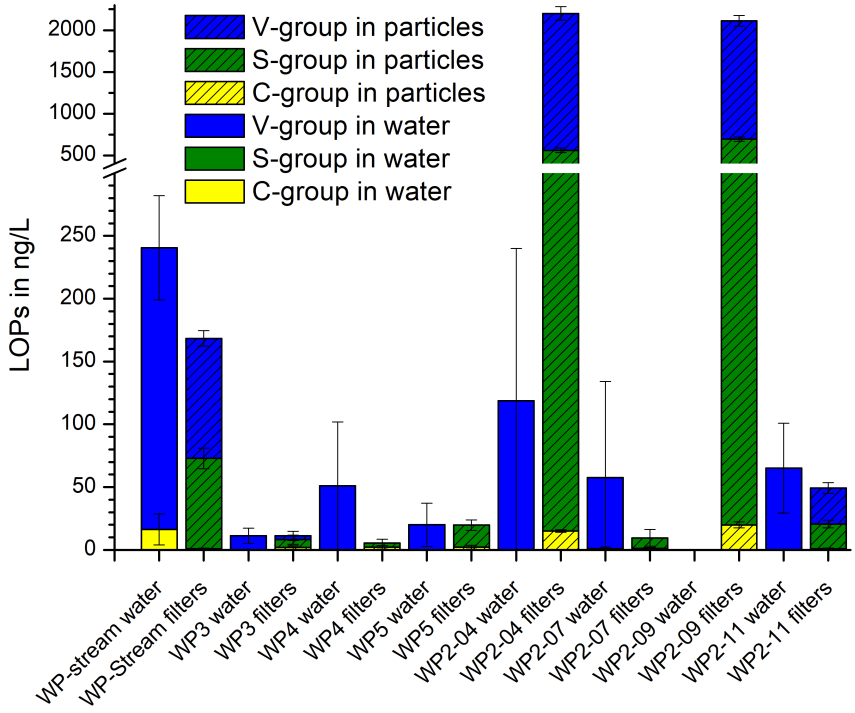

Figure 9.7: LOP concentrations of the filtered dripwater samples from Waipuna Cave and of the particulate matter retained in the filters.

The Waipuna LOP results thus suggest that lignin in dripwater is at least partly transported by particles or colloids with dimensions > 0.45 µm, which will be favored by flow along fractures rather than seepage flow (which can allow for the migration of low-molar-mass organic acids and nanoparticles; Hartland et al. (2011, 2012)). Lignin is likely to be adsorbed to mineral particles (Theng, 2012) and can also form organic colloids by coiling with other organic substances (humic matter). The adsorption and desorption of LOPs or lignin to mineral surfaces is a continuous and repetitive process that depends on many parameters, as described in the soil continuum model by Lehmann and Kleber (2015) and the regional chromatography model by Shen et al. (2015) and observed for example in the leaching and sorption experiments by Hernes et al. (2007). Our results show that the particles collected in the filters can be (at least partially) desorbed and eluted with methanol. In previous studies of lignin oxidation products in cave dripwater and speleothems, the samples were either not filtered before SPE extraction, or 1.0 µm glass fiber filters were used, which possibly

accounts for the large difference between the LOP results of filtered dripwaters from Waipuna and non-filtered dripwaters from the Herbstlabyrinth (Heidke et al., 2018, 2019). These findings should be systematically investigated in the future to better understand the transport processes of lignin into the cave system and to find a more suitable sampling method for lignin analysis in dripwater. For example, passive-sampling methods with adsorption resins or filters could be more efficient and also easier to apply than whole-water sampling. The contribution to the speleothem record of lignin transported by particles compared to lignin transported in solution and how they differ in composition are difficult to estimate on the basis of the current data. To control and reduce the number of influencing parameters, we suggest using a combination of cave-monitoring projects and artificial cave setups to study this question.

9.4 Conclusion

Our results demonstrate that, from the soil to the flowstone, the C/V and S/V ratios both increase while the total lignin content, $\Sigma 8$, strongly decreases. Nevertheless, the relative LOP signal from the overlying soil at the different cave sites is preserved in the flowstone. This shows that the LOP signal in speleothems can be used as a proxy for the lignin input in the overlying soil and therefore as a proxy for past vegetation changes. However, for the interpretation of C/V and S/V ratios, it is important that only samples of the same type (e.g., speleothem, dripwater or soil) are compared and only relative variations are examined, since the LOP signal is strongly influenced by transport and degradation processes. We suggest that a faster oxidative degradation of C- and S-group LOPs in the soil compared to the more stable V-group LOPs makes them more soluble, which in turn leads to a more efficient transport of these LOPs from the soil to the cave causing higher C/V and S/V ratios in the speleothems. On the other hand, LOPs can also adsorb to mineral particles and be transported to the cave via particle transport, which may partially override the aforementioned fractionation.

For the interpretation of paleo-vegetation records from speleothems using LOPs, it is advisable to first analyze some recently deposited speleothem samples and compare these with samples from the overlying soil to 'ground-truth' the LOP signals for the specific cave site. However, it is not clear yet whether the relationship between the LOP signals in the soil and those in the flowstones changes over time, for example with changing soil thickness and climatic conditions. The transformation of LOP signals from the soil to the cave should be further investigated by expanding the sample set to a greater number of different cave sites with different vegetation, soil type and thickness and climatic conditions to identify and quantify different influences. In addition, the incorporation of lignin into the speleothem fabric could be studied using artificial cave setups (Hansen et al., 2017, 2019, Polag et al., 2010, Wiedner et al., 2008).

Acknowledgements

We thank Steve Newcombe for his help with cutting the speleothem slabs and samples.

Author contributions

Conception and design of the work were done by IH, AH, DS and TH. Fieldwork and sample collection were done by AH, JH, AP and IH. Data collection, performing of the experiments and drafting of the article were done by IH. Data analysis and interpretation, critical revision of the article, and final approval of the version to be published were done by all authors.

Conclusions and outlook

In this work, a selective and sensitive analytical method for the quantitative analysis of lignin oxidation products (LOPs) in speleothems, cave dripwater and soil samples using UHPLC-ESI-HRMS has been developed. All steps of the sample preparation and analysis method have been optimized and adjusted to the low concentrations of organic matter in speleothems and cave dripwater. The method was successfully tested and validated and showed sufficient sensitivity to detect even trace concentrations of lignin, thus providing a new and highly specific vegetation proxy for the reconstruction of paleo-vegetation and paleo-climate from speleothem archives.

The use of the established CuO oxidation method for the degradation of polymeric lignin to monomeric LOPs allowed to compare the results to LOP records in other archives. However, the CuO oxidation step produced relatively high blank values due to the high amounts of reagents needed and was the main source of variability in the analytical method. Therefore, an approach to replace the CuO oxidation step by a cleaner and more reproducible lignin degradation step based on electrolysis was tested. Two electrolysis methods operating in galvanostatic mode at room temperature have been developed, one with an undivided electrochemical cell and one with a flowcell. Both methods showed very low blank values and allowed to study the different oxidation sensitivity of the individual LOPs. However, the LOP yields obtained from speleothem samples were not satisfactory and over-oxidation of the released LOPs was a problem. Therefore, at this stage electrolysis is not yet a suitable alternative to replace the CuO oxidation step for trace analysis of lignin.

The developed method for trace analysis of LOPs was successfully applied to different stalagmite, flowstone and dripwater samples. The analysis of LOPs in a Holocene stalagmite from the Herbstlabyrinth, Germany, showed that the signals in the stalagmite had a significant variation over time on the centennial to millennial timescale. The analysis of cave dripwater from the same cave showed a seasonal pattern with higher LOP concentrations in summer and lower concentrations in winter. The total LOP concentration, $\Sigma 8$, in the stalagmite was correlated to phosphorous, barium and uranium concentrations, which have been interpreted as vegetation proxies (Mischel et al., 2017). The clear benefit of $\Sigma 8$ compared to these trace elements is that the sources of lignin are exclusively higher plants and not, for example, microorganisms or the host rock. Therefore, $\Sigma 8$ can complement or even help to better interpret potential vegetation proxies whose sources are less clear.

The two application examples from the Zoolithenhöhle, Germany, and the Cueva Victoria, Spain, impressively demonstrated the concrete benefit of lignin analysis in addition to established proxies such as $\delta^{13}C$ for clarifying specific palaeoclimatic and paleovegetation-related questions. In the stalagmite from the Zoolithenhöhle, the LOP signals were able to record a historically known change in vegetation, while the $\delta^{13}C$ signals showed no change here. In the flowstone from the Cueva Victoria, the

LOPs were able to confirm the vegetation changes suspected on the basis of $\delta^{13}C$ signals and pollen records from a nearby lake sediment, thus making the interpretation more robust.

Besides these promising results, it became clear that the lignin composition can also be affected by various transport and degradation processes on its way from the vegetation through the soil and the karst system to the cave. These processes include for example microbial degradation, incorporation into larger aggregates of organic substances, and the adsorption to mineral particles. These effects seem to have a larger influence on the lignin ratios C/V and S/V, which are usually used as vegetation source indicators.

To gain more insight into the extent and effects of these processes, a comparative study of soil, dripwater and flowstone samples from different caves in different vegetation zones of New Zealand was carried out. The results showed that despite the various influences of transport, degradation and adsorption to minerals on their way from the soil to the cave, the "fingerprint" of the overlying vegetation is preserved in the lignin composition in the speleothem. They also demonstrated, though, that the C/V and S/V ratios of lignin in speleothems cannot be considered absolute values indicative of specific plant types, nor can they be assigned one-to-one to the areas in the diagram of Hedges and Mann (1979), since the processes during transport can significantly alter the C/V and S/V ratios. However, the relative changes caused by the temporal change of vegetation at the same cave site are likely to be preserved in the speleothem lignin as long as the transport processes and conditions above the cave do not change too much.

In the future, the transport and degradation processes of lignin should be further investigated systematically. This could be done in further field studies such as the one conducted in New Zealand in this study, but also in laboratory studies, e.g. by using mesocosms to simulate the transport of lignin through the soil or by using an artificial cave chamber to investigate the incorporation of lignin into the speleothem in more detail. In parallel, a further application of LOPs as a vegetation proxy on samples from different vegetation and climate zones would beneficial, especially in multiproxy approaches with stable isotopes, trace elements and also other organic biomarkers. This would expand the existing data base to allow a better estimation of the response of C/V and S/V ratios to different vegetation, climate and soil conditions.

Concerning the sample type, no clear recommendation for either stalagmite or flowstone samples can be given. Although flowstones are often fed by water flows with higher discharge, which could be expected to carry larger amounts of organic material than the slower flows often feeding stalagmites, the samples analyzed in this study showed a wide range of lignin concentrations for both samples types. A tentative recommendation can be given for speleothems, both stalagmites and flowstones, showing clearly visible brown laminae, because the brown colour often comes from high input of organic matter. This was observed for the stalagmite from Zoolithenhöhle and for the flowstone from Hodges Creek, which both showed relatively high lignin concentrations. However, the brown colour can also be of inorganic origin and thus might be misleading in some cases.

Concerning the analytical method development, the search for a better degradation method to reproducibly and effectively depolymerize lignin without introducing additional blank values should be continued. A promising approach could be the use of soluble $CuSO_4$ instead of the insoluble CuO as oxidizing agent (Yan and Kaiser, 2018b), as this allows a miniaturization of the digestion system, which could minimize the blank problems. Furthermore, the method could be extended to other organic biomarkers, for example by a stepwise extraction of the dissolved speleothem solution by means of solid phase extraction. Interesting analytes might be, for example, biomass burning markers, such as the sugars levoglucosan, galactosan and mannosan, or faecal sterols that indicate the presence of a mammalian fauna. Both the occurrence of forest fires and the increased presence of mammals such as grazing animals could provide information on both climatic and vegetation conditions and on the presence and influence of early humans.

Bibliography

Allen, J. R. M., Brandt, U., Brauer, A., Hubberten, H.-W., Huntley, B., Keller, J., Kraml, M., Mackensen, A., Mingram, J., Negendank, J. F. W., Nowaczyk, N. R., Oberhänsli, H., Watts, W. A., Wulf, S. and Zolitschka, B. (1999). Rapid environmental changes in southern Europe during the last glacial period, *Nature* **400**(6746): 740–743.

Armenta, S., Garrigues, S. and de La Guardia, M. (2008). Green Analytical Chemistry, *TrAC Trends in Analytical Chemistry* **27**(6): 497–511.

Bahri, H., Dignac, M.-F., Rumpel, C., Rasse, D. P., Chenu, C. and Mariotti, A. (2006). Lignin turnover kinetics in an agricultural soil is monomer specific, *Soil Biology and Biochemistry* **38**(7): 1977–1988.

Baker, A., Blyth, A. J., Jex, C. N., Mcdonald, J. A., Woltering, M. and Khan, S. J. (2019). Glycerol dialkyl glycerol tetraethers (GDGT) distributions from soil to cave: Refining the speleothem paleothermometer, *Organic Geochemistry* **136**: 103890.

Baker, A., Hellstrom, J. C., Kelly, B. F. J., Mariethoz, G. and Trouet, V. (2015). A composite annual-resolution stalagmite record of North Atlantic climate over the last three millennia, *Scientific Reports* **5**(1): 1–8.
`https://www.nature.com/articles/srep10307.pdf`

Baker, A., Jex, C. N., Rutlidge, H., Woltering, M., Blyth, A. J., Andersen, M. S., Cuthbert, M. O., Marjo, C. E., Markowska, M., Rau, G. C. and Khan, S. J. (2016). An irrigation experiment to compare soil, water and speleothem tetraether membrane lipid distributions, *Organic Geochemistry* **94**: 12–20.
`http://www.sciencedirect.com/science/article/pii/S0146638016000061`

Blyth, A. J., Asrat, A., Baker, A., Gulliver, P., Leng, M. J. and Genty, D. (2007). A new approach to detecting vegetation and land-use change using high-resolution lipid biomarker records in stalagmites, *Quaternary Research* **68**(03): 314–324.

Blyth, A. J., Baker, A., Collins, M. J., Penkman, K. E., Gilmour, M. A., Moss, J. S., Genty, D. and Drysdale, R. N. (2008). Molecular organic matter in speleothems and its potential as an environmental proxy, *Quaternary Science Reviews* **27**(9-10): 905–921.

Blyth, A. J., Baker, A., Thomas, L. E. and van Calsteren, P. (2011). A 2000-year lipid biomarker record preserved in a stalagmite from north-west Scotland, *Journal of Quaternary Science* **26**(3): 326–334.

Blyth, A. J., Farrimond, P. and Jones, M. (2006). An optimised method for the extraction and analysis of lipid biomarkers from stalagmites, *Organic Geochemistry* **37**(8): 882–890.

Blyth, A. J., Fuentes, D., George, S. C. and Volk, H. (2015). Characterisation of organic inclusions in stalagmites using laser-ablation-micropyrolysis gas chromatography–mass spectrometry, *Journal of Analytical and Applied Pyrolysis* **113**: 454–463.

Blyth, A. J., Hartland, A. and Baker, A. (2016). Organic proxies in speleothems – New developments, advantages and limitations, *Quaternary Science Reviews* **149**: 1–17.

Blyth, A. J., Jex, C. N., Baker, A., Khan, S. J. and Schouten, S. (2014). Contrasting distributions of glycerol dialkyl glycerol tetraethers (GDGTs) in speleothems and associated soils, *Organic Geochemistry* **69**: 1–10.

Blyth, A. J. and Schouten, S. (2013). Calibrating the glycerol dialkyl glycerol tetraether temperature signal in speleothems, *Geochimica et Cosmochimica Acta* **109**: 312–328.

Blyth, A. J., Shutova, Y. and Smith, C. (2013). δ^{13}C analysis of bulk organic matter in speleothems using liquid chromatography–isotope ratio mass spectrometry, *Organic Geochemistry* **55**: 22–25.

Blyth, A. J., Smith, C. I. and Drysdale, R. N. (2013). A new perspective on the δ^{13}C signal preserved in speleothems using LC–IRMS analysis of bulk organic matter and compound specific stable isotope analysis, *Quaternary Science Reviews* **75**: 143–149.
`http://www.sciencedirect.com/science/article/pii/S0277379113002370`

Blyth, A. J. and Watson, J. S. (2009). Thermochemolysis of organic matter preserved in stalagmites: A preliminary study, *Organic Geochemistry* **40**(9): 1029–1031.

Blyth, A. J., Watson, J. S., Woodhead, J. and Hellstrom, J. (2010). Organic compounds preserved in a 2.9 million year old stalagmite from the Nullarbor Plain, Australia, *Chemical Geology* **279**(3-4): 101–105.

Boerjan, W., Ralph, J. and Baucher, M. (2003). Lignin Biosynthesis, *Annual Review of Plant Biology* **54**(1): 519–546.

Bond, G., Broecker, W., Johnsen, S., McManus, J., Labeyrie, L., Jouzel, J. and Bonani, G. (1993). Correlations between climate records from North Atlantic sediments and Greenland ice, *Nature* **365**(6442): 143.
`https://www.nature.com/articles/365143a0.pdf`

Bosle, J. M., Mischel, S. A., Schulze, A.-L., Scholz, D. and Hoffmann, T. (2014). Quantification of low molecular weight fatty acids in cave drip water and speleothems using HPLC-ESI-IT/MS – development and validation of a selective method, *Analytical and Bioanalytical Chemistry* **406**(13): 3167–3177.

Brebu, M. and Vasile, C. (2010). Thermal degradation of lignin – a review, *Cellulose Chemistry & Technology* **44**(9): 353.

Budsky, A., Scholz, D., Gibert, L. and Mertz-Kraus, R. (2015). ^{230}Th/U-dating of the Cueva Victoria flowstone sequence: Preliminary results and paleoclimate implications, *in* L. Gibert and C. Ferrandez-Canadell (eds), *Geología y Paleontología de Cueva (Geology and Paleontology of Cueva Victoria)*, pp. 101–109.

Budsky, A., Scholz, D., Wassenburg, J. A., Mertz-Kraus, R., Spötl, C., Riechelmann, D. F. C., Gibert, L., Jochum, K. P. and Andreae, M. O. (2019a). Speleothem δ^{13}C record suggests enhanced spring/summer drought in south-eastern Spain between 9.7 and 7.8 ka – A circum-Western Mediterranean anomaly?, *The Holocene* **29**(7): 1113–1133.

Budsky, A., Wassenburg, J. A., Mertz-Kraus, R., Spötl, C., Jochum, K. P., Gibert, L. and Scholz, D. (2019b). Western Mediterranean Climate Response to Dansgaard/Oeschger Events: New Insights From Speleothem Records, *Geophysical Research Letters* **46**(15): 9042–9053.

Bush, R. T. and McInerney, F. A. (2013). Leaf wax n-alkane distributions in and across modern plants: Implications for paleoecology and chemotaxonomy, *Geochimica et Cosmochimica Acta* **117**: 161–179.

Carrión, J. S. (2002). Patterns and processes of Late Quaternary environmental change in a montane region of southwestern Europe, *Quaternary Science Reviews* **21**(18-19): 2047–2066.

Cheng, H., Edwards, R. L., Broecker, W. S., Denton, G. H., Kong, X., Wang, Y., Zhang, R. and Wang, X. (2009). Ice age terminations, *Science (New York, N.Y.)* **326**(5950): 248–252.

Cheng, H., Edwards, R. L., Sinha, A., Spötl, C., Yi, L., Chen, S., Kelly, M., Kathayat, G., Wang, X., Li, X., Kong, X., Wang, Y., Ning, Y. and Zhang, H. (2016). The Asian monsoon over the past 640,000 years and ice age terminations, *Nature* **534**(7609): 640–646.

Cheng, H., Lawrence Edwards, R., Shen, C.-C., Polyak, V. J., Asmerom, Y., Woodhead, J., Hellstrom, J., Wang, Y., Kong, X., Spötl, C., Wang, X. and Calvin Alexander, E. (2013). Improvements in ^{230}Th dating, ^{230}Th and ^{234}U half-life values, and U–Th isotopic measurements by multi-collector inductively coupled plasma mass spectrometry, *Earth and Planetary Science Letters* **371-372**: 82–91.

Dansgaard, W., Johnsen, S. J., Clausen, H. B., Dahl-Jensen, D., Gundestrup, N. S., Hammer, C. U., Hvidberg, C. S., Steffensen, J. P., Sveinbjörnsdottir, A. E., Jouzel, J. and Bond, G. (1993). Evidence for general instability of past climate from a 250-kyr ice-core record, *Nature* **364**(6434): 218.
`https://www.nature.com/articles/364218a0.pdf`

Delwiche, C. F., Graham, L. E. and Thomson, N. (1989). Lignin-like compounds and sporopollenin coleochaete, an algal model for land plant ancestry, *Science (New York, N.Y.)* **245**(4916): 399–401.

Dewick, P. M. (2009). The shikimate pathway: aromatic amino acids and phenylpropanoids, *Medicinal Natural Products* **137**: 86.

Dittmar, T. and Lara, R. J. (2001). Molecular evidence for lignin degradation in sulfate-reducing mangrove sediments (Amazônia, Brazil), *Geochimica et Cosmochimica Acta* **65**(9): 1417–1428.
`http://www.sciencedirect.com/science/article/pii/S0016703700006190`

Dreybrodt, W. and Scholz, D. (2011). Climatic dependence of stable carbon and oxygen isotope signals recorded in speleothems: From soil water to speleothem calcite, *Geochimica et Cosmochimica Acta* **75**(3): 734–752.

Driese, S. G., Li, Z.-H., Cheng, H., Harvill, J. L. and Sims, J. (2016). High-resolution rainfall records for middle and late Holocene based on speleothem annual UV fluorescent layers integrated with stable isotopes and U/Th dating, Raccoon Mountain Cave Tennessee, USA, *Caves and Karst Across Time. Geological Society of America Special Paper* **516**: 231.

Drysdale, R. N., Paul, B. T., Hellstrom, J. C., Couchoud, I., Greig, A., Bajo, P., Zanchetta, G., Isola, I., Spötl, C., Baneschi, I., Regattieri, E. and Woodhead, J. D. (2012). Precise microsampling of poorly laminated speleothems for U-series dating, *Quaternary Geochronology* **14**: 38–47.

Fairbanks, R. G., Mortlock, R. A., Chiu, T.-C., Cao, L., Kaplan, A., Guilderson, T. P., Fairbanks, T. W., Bloom, A. L., Grootes, P. M. and Nadeau, M.-J. (2005). Radiocarbon calibration curve spanning 0 to 50,000 years BP based on paired $^{230}Th/^{234}U/^{238}U$ and ^{14}C dates on pristine corals, *Quaternary Science Reviews* **24**(16-17): 1781–1796.

Fairchild, I. J. and Baker, A. (2012). *Speleothem Science*, John Wiley & Sons, Ltd, Chichester, UK.

Fairchild, I. J., Smith, C. L., Baker, A., Fuller, L., Spötl, C., Mattey, D., McDermott, F. and E.I.M.F. (2006). Modification and preservation of environmental signals in speleothems, *Earth-Science Reviews* **75**(1-4): 105–153.

Fairchild, I. J. and Treble, P. C. (2009). Trace elements in speleothems as recorders of environmental change, *Quaternary Science Reviews* **28**(5-6): 449–468.

Filley, T. R., Minard, R. D. and Hatcher, P. G. (1999). Tetramethylammonium hydroxide (TMAH) thermochemolysis: proposed mechanisms based upon the application of ^{13}C-labeled TMAH to a synthetic model lignin dimer, *Organic Geochemistry* **30**(7): 607–621.

Fohlmeister, J., Kromer, B. and Mangini, A. (2011). The Influence of Soil Organic Matter Age Spectrum on the Reconstruction of Atmospheric ^{14}C Levels Via Stalagmites, *Radiocarbon* **53**(01): 99–115.

Fraser, W. T., Scott, A. C., Forbes, A. E. S., Glasspool, I. J., Plotnick, R. E., Kenig, F. and Lomax, B. H. (2012). Evolutionary stasis of sporopollenin biochemistry revealed by unaltered Pennsylvanian spores, *The New Phytologist* **196**(2): 397–401.

Freudenberg, K., Lautsch, W. and Engler, K. (1940). Die Bildung von Vanillin aus Fichtenlignin, *Berichte der deutschen chemischen Gesellschaft (A and B Series)* **73**(3): 167–171.
`https://onlinelibrary.wiley.com/doi/pdf/10.1002/cber.19400730302`

Gałuszka, A., Migaszewski, Z. M. and Namieśnik, J. (2017). The role of analytical chemistry in the study of the Anthropocene, *TrAC Trends in Analytical Chemistry* **97**: 146–152.

Gałuszka, A., Migaszewski, Z. and Namieśnik, J. (2013). The 12 principles of green analytical chemistry and the SIGNIFICANCE mnemonic of green analytical practices, *TrAC Trends in Analytical Chemistry* **50**: 78–84.

Giorio, C., Kehrwald, N., Barbante, C., Kalberer, M., King, A. C., Thomas, E. R., Wolff, E. W. and Zennaro, P. (2018). Prospects for reconstructing paleoenvironmental conditions from organic compounds in polar snow and ice, *Quaternary Science Reviews* **183**: 1–22.

Goñi, M. A. and Montgomery, S. (2000). Alkaline CuO Oxidation with a Microwave Digestion System: Lignin Analyses of Geochemical Samples, *Analytical Chemistry* **72**(14): 3116–3121.

Gross, J. H. (2017). *Mass Spectrometry: A Textbook*, Springer International Publishing, Berlin Heidelberg.

Hansen, M., Scholz, D., Froeschmann, M.-L., Schöne, B. R. and Spötl, C. (2017). Carbon isotope exchange between gaseous CO_2 and thin solution films: Artificial cave experiments and a complete diffusion-reaction model, *Geochimica et Cosmochimica Acta* **211**: 28–47.

Hansen, M., Scholz, D., Schöne, B. R. and Spötl, C. (2019). Simulating speleothem growth in the laboratory: Determination of the stable isotope fractionation ($\delta^{13}C$ and $\delta^{18}O$) between H_2O, DIC and $CaCO_3$, *Chemical Geology* **509**: 20–44.

Harris, D. C. (2014). *Lehrbuch der quantitativen Analyse*, Springer-Verlag.

Harris, D. C. (2015). *Quantitative chemical analysis*, 9. edn, W.H. Freeman and Company, New York.

Hartland, A., Fairchild, I. J., Lead, J. R., Borsato, A., Baker, A., Frisia, S. and Baalousha, M. (2012). From soil to cave: Transport of trace metals by natural organic matter in karst dripwaters, *Chemical Geology* **304-305**: 68–82.

Hartland, A., Fairchild, I. J., Lead, J. R., Zhang, H. and Baalousha, M. (2011). Size, speciation and lability of NOM–metal complexes in hyperalkaline cave dripwater, *Geochimica et Cosmochimica Acta* **75**(23): 7533–7551.

Hatcher, P. G., Nanny, M. A., Minard, R. D., Dible, S. D. and Carson, D. M. (1995). Comparison of two thermochemolytic methods for the analysis of lignin in decomposing gymnosperm wood: the CuO oxidation method and the method of thermochemolysis with tetramethylammonium hydroxide (TMAH), *Organic Geochemistry* **23**(10): 881–888.
http://www.sciencedirect.com/science/article/pii/0146638095000879

Hedges, J. I., Blanchette, R. A., Weliky, K. and Devol, A. H. (1988). Effects of fungal degradation on the CuO oxidation products of lignin: a controlled laboratory study, *Geochimica et Cosmochimica Acta* **52**(11): 2717–2726.

Hedges, J. I. and Ertel, J. R. (1982). Characterization of lignin by gas capillary chromatography of cupric oxide oxidation products, *Analytical Chemistry* **54**(2): 174–178.
http://dx.doi.org/10.1021/ac00239a007

Hedges, J. I. and Mann, D. C. (1979). The lignin geochemistry of marine sediments from the southern Washington coast, *Geochimica et Cosmochimica Acta* **43**(11): 1809–1818.
http://www.sciencedirect.com/science/article/pii/0016703779900292

Hedges, J. I. and Parker, P. L. (1976). Land-derived organic matter in surface sediments from the Gulf of Mexico, *Geochimica et Cosmochimica Acta* **40**(9): 1019–1029.

Heidke, I., Scholz, D. and Hoffmann, T. (2018). Quantification of lignin oxidation products as vegetation biomarkers in speleothems and cave drip water, *Biogeosciences* **15**(19): 5831–5845.

Heidke, I., Scholz, D. and Hoffmann, T. (2019). Lignin oxidation products as a potential proxy for vegetation and environmental changes in speleothems and cave drip water – a first record from the Herbstlabyrinth, central Germany, *Climate of the Past* **15**(3): 1025–1037.
https://cp.copernicus.org/articles/15/1025/2019/

Hellstrom, J. (2003). Rapid and accurate U/Th dating using parallel ion-counting multi-collector ICP-MS, *Journal of Analytical Atomic Spectrometry* **18**(11): 1346.

Hellstrom, J. (2006). U–Th dating of speleothems with high initial ^{230}Th using stratigraphical constraint, *Quaternary Geochronology* **1**(4): 289–295.

Hennion, M.-C. (1999). Solid-phase extraction: method development, sorbents, and coupling with liquid chromatography, *Journal of Chromatography A* **856**(1-2): 3–54.

Hernes, P. J. and Benner, R. (2002). Transport and diagenesis of dissolved and particulate terrigenous organic matter in the North Pacific Ocean, *Deep Sea Research Part I: Oceanographic Research Papers* **49**(12): 2119–2132.
`http://www.sciencedirect.com/science/article/pii/S0967063702001280`

Hernes, P. J., Kaiser, K., Dyda, R. Y. and Cerli, C. (2013). Molecular trickery in soil organic matter: hidden lignin, *Environmental Science & Technology* **47**(16): 9077–9085.

Hernes, P. J., Robinson, A. C. and Aufdenkampe, A. K. (2007). Fractionation of lignin during leaching and sorption and implications for organic matter "freshness", *Geophysical Research Letters* **34**(17): 1921.

Hewitt, A. E. (2010). *New Zealand soil classification*, Vol. no. 1 of *Landcare Research science series, 1172-269X*, 3rd ed. edn, Manaaki Whenua Press, Lincoln N.Z.

Hua, Q. (2009). Radiocarbon: A chronological tool for the recent past, *Quaternary Geochronology* **4**(5): 378–390.
`http://www.sciencedirect.com/science/article/pii/S1871101409000569`

Ivanovich, M. and Harmon, R. S. (eds) (1992). *Uranium Series Disequilibrium: Applications to Earth, Marine and Environmental Sciences*, 2. rev. edn.

Jex, C. N., Pate, G. H., Blyth, A. J., Spencer, R. G., Hernes, P. J., Khan, S. J. and Baker, A. (2014). Lignin biogeochemistry: from modern processes to Quaternary archives, *Quaternary Science Reviews* **87**: 46–59.

Kaiser, K. and Benner, R. (2012). Characterization of Lignin by Gas Chromatography and Mass Spectrometry Using a Simplified CuO Oxidation Method, *Analytical Chemistry* **84**(1): 459–464.

Kirwan, J. A., Broadhurst, D. I., Davidson, R. L. and Viant, M. R. (2013). Characterising and correcting batch variation in an automated direct infusion mass spectrometry (DIMS) metabolomics workflow, *Analytical and Bioanalytical Chemistry* **405**(15): 5147–5157.

Klotzbücher, T., Kaiser, K., Guggenberger, G., Gatzek, C. and Kalbitz, K. (2011). A new conceptual model for the fate of lignin in decomposing plant litter, *Ecology* **92**(5): 1052–1062.

Kögel, I. and Bochter, R. (1985). Characterization of lignin in forest humus layers by high-performance liquid chromatography of cupric oxide oxidation products, *Soil Biology and Biochemistry* **17**(5): 637–640.

Kögel-Knabner, I. (2002). The macromolecular organic composition of plant and microbial residues as inputs to soil organic matter, *Soil Biology and Biochemistry* **34**(2): 139–162.

Konieczka, P. and Namieśnik, J. (2010). Estimation of uncertainty in analytical procedures based on chromatographic techniques, *Journal of Chromatography. A* **1217**(6): 881.

Lachniet, M. S. (2009). Climatic and environmental controls on speleothem oxygen-isotope values, *Quaternary Science Reviews* **28**(5-6): 412–432.

Lang, S. (2000). *Höhlen in Franken: Ein Wanderführer in die Unterwelt der Fränkischen Schweiz*, Verlag Hans Carl, Nürnberg.

Lechleitner, F. A., Dittmar, T., Baldini, J. U., Prufer, K. M. and Eglinton, T. I. (2017). Molecular signatures of dissolved organic matter in a tropical karst system, *Organic Geochemistry* **113**: 141–149.

Lechleitner, F. A., Lang, S. Q., Haghipour, N., McIntyre, C., Baldini, J. U. L., Prufer, K. M. and Eglinton, T. I. (2019). Towards Organic Carbon Isotope Records from Stalagmites: Coupled δ^{13}C and ^{14}C Analysis Using Wet Chemical Oxidation, *Radiocarbon* **61**(03): 749–764.

Lehmann, J. and Kleber, M. (2015). The contentious nature of soil organic matter, *Nature* **528**(7580): 60.
`https://www.nature.com/articles/nature16069.pdf`

Leppla, D. (2016). *Quantification of paleoclimatic proxies using UHPLC-HESI-MS after degradation of lignin – development of an electrochemical method*, Masterarbeit zur Erlangung des Grades Master of Science, Johannes Gutenberg-Universität, Mainz.

Li, S.-H., Liu, S., Colmenares, J. C. and Xu, Y.-J. (2016). A sustainable approach for lignin valorization by heterogeneous photocatalysis, *Green Chemistry* **18**(3): 594–607.
`https://pubs.rsc.org/en/content/articlepdf/2016/gc/c5gc02109j`

Li, X., Hu, C., Huang, J., Xie, S. and Baker, A. (2014). A 9000-year carbon isotopic record of acid-soluble organic matter in a stalagmite from Heshang Cave, central China: Paleoclimate implications, *Chemical Geology* **388**: 71–77.
`http://www.sciencedirect.com/science/article/pii/S0009254114004161`

Lima, D. L., Duarte, A. C. and Esteves, V. I. (2007). Solid-phase extraction and capillary electrophoresis determination of phenols from soil after alkaline CuO oxidation, *Chemosphere* **69**(4): 561–568.

Litt, T., Schölzel, C., Kühl, N. and Brauer, A. (2009). Vegetation and climate history in the Westeifel Volcanic Field (Germany) during the past 11 000 years based on annually laminated lacustrine maar sediments, *Boreas* **38**(4): 679–690.

Lobo, I., Mozefo, A. A. and Cass, Q. B. (2000). Determination of phenolic compounds from oxidation of lignin lake sediments by high-performance liquid chromatography, *Chromatographia* **52**(11-12): 727–731.

Loh, P. S., Miller, Axel E. J., Reeves, A. D., Harvey, S. M. and Overnell, J. (2008). Optimised recovery of lignin-derived phenols in a Scottish fjord by the CuO oxidation method, *Journal of Environmental Monitoring* **10**(10): 1187.

Louchouarn, P., Opsahl, S. and Benner, R. (2000). Isolation and Quantification of Dissolved Lignin from Natural Waters Using Solid-Phase Extraction and GC/MS, *Analytical Chemistry* **72**(13): 2780–2787.

McDermott, F. (2004). Palaeo-climate reconstruction from stable isotope variations in speleothems: a review, *Quaternary Science Reviews* **23**(7-8): 901–918.

McDowell, R. D., Pearche, J. C. and Murkitt, G. S. (1986). Liquid-solid sample preparation in drug analysis, *Journal of Pharmaceutical and Biomedical Analysis* **4**(1): 3–21.

Meyer, K. W., Feng, W., Breecker, D. O., Banner, J. L. and Guilfoyle, A. (2014). Interpretation of speleothem calcite δ^{13}C variations: Evidence from monitoring soil CO_2, drip water, and modern speleothem calcite in central Texas, *Geochimica et Cosmochimica Acta* **142**: 281–298.

Miao, Y., Ouyang, L., Zhou, S., Xu, L., Yang, Z., Xiao, M. and Ouyang, R. (2014). Electrocatalysis and electroanalysis of nickel, its oxides, hydroxides and oxyhydroxides toward small molecules, *Biosensors & Bioelectronics* **53**: 428–439.

Mischel, S. A. (2016). *Multi-proxy reconstruction of Holocene and Late Glacial climate variability using precisely dated speleothems from the Herbstlabyrinth, central Germany*, PhD Thesis, Johannes Gutenberg-Universität Mainz, Mainz. `http://unibibliografie.ub.uni-mainz.de/theses/frontdoor.php?source_opus=100000791`

Mischel, S. A., Mertz-Kraus, R., Jochum, K. P. and Scholz, D. (2017). TERMITE: An R script for fast reduction of laser ablation inductively coupled plasma mass spectrometry data and its application to trace element measurements, *Rapid Communications in Mass Spectrometry : RCM* **31**(13): 1079–1087.

Mischel, S. A., Scholz, D. and Spötl, C. (2015). δ^{18}O values of cave drip water: a promising proxy for the reconstruction of the North Atlantic Oscillation?, *Climate Dynamics* **45**(11-12): 3035–3050.

Montgomery, W., Potiszil, C., Watson, J. S. and Sephton, M. A. (2016). Sporopollenin, a Natural Copolymer, is Robust under High Hydrostatic Pressure, *Macromolecular Chemistry and Physics* **217**(22): 2494–2500.

Nava-Fernandez, C., Hartland, A., Gázquez, F., Kwiecien, O., Marwan, N., Fox, B., Hellstrom, J., Pearson, A., Ward, B., French, A., Hodell, D. A., Immenhauser,

A. and Breitenbach, S. F. M. (2020). Pacific climate reflected in Waipuna Cave dripwater hydrochemistry.

Opsahl, S. and Benner, R. (1995). Early diagenesis of vascular plant tissues: Lignin and cutin decomposition and biogeochemical implications, *Geochimica et Cosmochimica Acta* **59**(23): 4889–4904.

Opsahl, S. and Benner, R. (1997). Distribution and cycling of terrigenous dissolved organic matter in the ocean, *Nature* **386**(6624): 480–482.

Orland, I. J., Bar-Matthews, M., Ayalon, A., Matthews, A., Kozdon, R., Ushikubo, T. and Valley, J. W. (2012). Seasonal resolution of Eastern Mediterranean climate change since 34ka from a Soreq Cave speleothem, *Geochimica et Cosmochimica Acta* **89**: 240–255.
`http://www.sciencedirect.com/science/article/pii/S0016703712002402`

Pandey, M. P. and Kim, C. S. (2011). Lignin Depolymerization and Conversion: A Review of Thermochemical Methods, *Chemical Engineering & Technology* **34**(1): 29–41.
`https://onlinelibrary.wiley.com/doi/pdf/10.1002/ceat.201000270`

Pardini, V. L., Smith, C. Z., Utley, J. H. P., Vargas, R. R. and Viertler, H. (1991). Electroorganic Reactions. 38. Mechanism of Electrooxidative Cleavage of Lignin Model Dimers, *Journal of Organic Chemistry* **56**(26): 7305–7313.

Pearl, I. A. (1967). *The Chemistry of Lignin*, Edward Arnold (Publishers) Ltd, London, UK.

Perrette, Y., Poulenard, J., Protière, M., Fanget, B., Lombard, C., Miège, C., Quiers, M., Nafferchoux, E. and Pépin-Donat, B. (2015). Determining soil sources by organic matter EPR fingerprints in two modern speleothems, *Organic Geochemistry* **88**: 59–68.
`http://www.sciencedirect.com/science/article/pii/S0146638015001606`

Polag, D., Scholz, D., Mühlinghaus, C., Spötl, C., Schröder-Ritzrau, A., Segl, M. and Mangini, A. (2010). Stable isotope fractionation in speleothems: Laboratory experiments, *Chemical Geology* **279**(1-2): 31–39.

Poole, C. F. (2003a). New trends in solid-phase extraction, *TrAC Trends in Analytical Chemistry* **22**(6): 362–373.

Poole, C. F. (2003b). *The essence of chromatography*, Elsevier.

Quiers, M., Perrette, Y., Chalmin, E., Fanget, B. and Poulenard, J. (2015). Geochemical mapping of organic carbon in stalagmites using liquid-phase and solid-phase fluorescence, *Chemical Geology* **411**: 240–247.
`http://www.sciencedirect.com/science/article/pii/S0009254115003319`

Ralph, J., Lundquist, K., Brunow, G., Lu, F., Kim, H., Schatz, P. F., Marita, J. M., Hatfield, R. D., Ralph, S. A., Christensen, J. H. and Boerjan, W. (2004). Lignins: Natural polymers from oxidative coupling of 4-hydroxyphenyl-propanoids, *Phytochemistry Reviews* **3**: 29–60.

Reuter, H., Gensel, J., Elvert, M. and Zak, D. (2017). Direct Analysis of Lignin Phenols in Freshwater Dissolved Organic Matter, *Analytical Chemistry* **89**(24): 13449–13457.

Richards, D. A. and Dorale, J. A. (2003). Uranium-series Chronology and Environmental Applications of Speleothems, *Reviews in Mineralogy and Geochemistry* **52**(1): 407–460.

Riechelmann, D. F., Fohlmeister, J., Kluge, T., Jochum, K. P., Richter, D. K., Deininger, M., Friedrich, R., Frank, N. and Scholz, D. (2019). Evaluating the potential of tree-ring methodology for cross-dating of three annually laminated stalagmites from Zoolithencave (SE Germany), *Quaternary Geochronology* **52**: 37–50.

Ruiz-Dueñas, F. J. and Martínez, A. T. (2009). Microbial degradation of lignin: how a bulky recalcitrant polymer is efficiently recycled in nature and how we can take advantage of this, *Microbial Biotechnology* **2**(2): 164–177.

Rutlidge, H., Andersen, M. S., Baker, A., Chinu, K. J., Cuthbert, M. O., Jex, C. N., Marjo, C. E., Markowska, M. and Rau, G. C. (2015). Organic characterisation of cave drip water by LC-OCD and fluorescence analysis, *Geochimica et Cosmochimica Acta* **166**: 15–28.
`http://www.sciencedirect.com/science/article/pii/S0016703715003671`

Rutlidge, H., Baker, A., Marjo, C. E., Andersen, M. S., Graham, P. W., Cuthbert, M. O., Rau, G. C., Roshan, H., Markowska, M., Mariethoz, G. and Jex, C. N. (2014). Dripwater organic matter and trace element geochemistry in a semi-arid karst environment: Implications for speleothem paleoclimatology, *Geochimica et Cosmochimica Acta* **135**: 217–230.
`http://www.sciencedirect.com/science/article/pii/S0016703714002154`

Sarkanen, K. V. and Ludwig, C. H. (eds) (1971). *Lignins: Occurrence, formation, structure and reactions*, Wiley-Interscience, New York.

Schmitt, D., Regenbrecht, C., Hartmer, M., Stecker, F. and Waldvogel, S. R. (2015). Highly selective generation of vanillin by anodic degradation of lignin: a combined approach of electrochemistry and product isolation by adsorption, *Beilstein Journal of Organic Chemistry* **11**: 473–480.

Scholz, D., Frisia, S., Borsato, A., Spötl, C., Fohlmeister, J., Mudelsee, M., Miorandi, R. and Mangini, A. (2012). Holocene climate variability in north-eastern Italy: potential influence of the NAO and solar activity recorded by speleothem data, *Climate of the Past* **8**(4): 1367–1383.

Scholz, D. and Hoffmann, D. (2008). ^{230}Th/U-dating of fossil corals and speleothems, *Quaternary Science Journal* **57**: 52–76.

Scholz, D. and Hoffmann, D. L. (2011). StalAge – An algorithm designed for construction of speleothem age models, *Quaternary Geochronology* **6**(3-4): 369–382.

Schutyser, W., Kruger, J. S., Robinson, A. M., Katahira, R., Brandner, D. G., Cleveland, N. S., Mittal, A., Peterson, D. J., Meilan, R., Román-Leshkov, Y. and Beckham, G. T. (2018). Revisiting alkaline aerobic lignin oxidation, *Green Chemistry* **20**(16): 3828–3844.

Shen, Y., Chapelle, F. H., Strom, E. W. and Benner, R. (2015). Origins and bioavailability of dissolved organic matter in groundwater, *Biogeochemistry* **122**(1): 61–78. `https://link.springer.com/content/pdf/10.1007/s10533-014-0029-4.pdf`

Skoog, D. A., Holler, F. J. and Crouch, S. R. (2018). *Principles of instrumental analysis*, 7. edn, Cengage Learning, Australia.

Spencer, R. G. M., Hernes, P. J., Ruf, R., Baker, A., Dyda, R. Y., Stubbins, A. and Six, J. (2010). Temporal controls on dissolved organic matter and lignin biogeochemistry in a pristine tropical river, Democratic Republic of Congo, *Journal of Geophysical Research* **115**(G3).

Standley, L. J. and Kaplan, L. A. (1998). Isolation and analysis of lignin-derived phenols in aquatic humic substances: improvements on the procedures, *Organic Geochemistry* **28**(11): 689–697. `http://www.sciencedirect.com/science/article/pii/S0146638098000412`

Sun, L., Spencer, R. G. M., Hernes, P. J., Dyda, R. Y. and Mopper, K. (2015). A comparison of a simplified cupric oxide oxidation HPLC method with the traditional GC-MS method for characterization of lignin phenolics in environmental samples, *Limnology and Oceanography: Methods* **13**(1): 1–8.

Surowiec, I., Johansson, E., Torell, F., Idborg, H., Gunnarsson, I., Svenungsson, E., Jakobsson, P.-J. and Trygg, J. (2017). Multivariate strategy for the sample selection and integration of multi-batch data in metabolomics, *Metabolomics : Official Journal of the Metabolomic Society* **13**(10): 114.

Tarabanko, V. E., Petukhov, D. V. and Selyutin, G. E. (2004). New Mechanism for the Catalytic Oxidation of Lignin to Vanillin, *Kinetics and Catalysis* **45**(4): 569–577.

Tarabanko, V. E. and Tarabanko, N. (2017). Catalytic Oxidation of Lignins into the Aromatic Aldehydes: General Process Trends and Development Prospects, *International Journal of Molecular Sciences* **18**(11).

Tareq, S. M., Kitagawa, H. and Ohta, K. (2011). Lignin biomarker and isotopic records of paleovegetation and climate changes from Lake Erhai, southwest China, since 18.5 ka BP, *Holocene Lake Records: Patterns, Impacts, Causes And Societal*

Response Selected Papers from the 3rd LIMPACS Conference, Chandigarh, India **229**(1–2): 47–56.
http://www.sciencedirect.com/science/article/pii/S1040618210001564

Tareq, S. M., Tanaka, N. and Ohta, K. (2004). Biomarker signature in tropical wetland: lignin phenol vegetation index (LPVI) and its implications for reconstructing the paleoenvironment, *The Science of the Total Environment* **324**(1-3): 91–103.

Tegen, I. and Dörr, H. (1996). ^{14}C Measurements of Soil Organic Matter, Soil CO_2 and Dissolved Organic Carbon (1987–1992), *Radiocarbon* **38**(02): 247–251.

Theng, B. (2012). Humic Substances, *Developments in Clay Science Volume 4*, Vol. 4 of *Developments in Clay Science*, Elsevier, pp. 391–456.

Thermo Fisher Scientific (2020). QExactive Schematic.
https://planetorbitrap.com/data/fe/image/QExactive_Schematic.jpg , accessed: 17.03.2020.

Thevenot, M., Dignac, M.-F. and Rumpel, C. (2010). Fate of lignins in soils: A review, *Soil Biology and Biochemistry* **42**(8): 1200–1211.

Thurman, E. M. and Mills, M. S. (1998). Solid-phase extraction, *New York: John Wiley & Sons* **29**: 35–73.

Tooth, A. F. (2000). *Controls on the geochemistry of speleothem-forming karstic drip waters*, PhD Thesis, University of Keele, UK.

Trumbore, S. (2000). Age of soil organic matter and soil respiration: radiocarbon constraints on belowground C dynamics, *Ecological Applications* **10**(2): 399–411.

Vanholme, R., Demedts, B., Morreel, K., Ralph, J. and Boerjan, W. (2010). Lignin biosynthesis and structure, *Plant Physiology* **153**(3): 895–905.

Vrana, B., Allan, I. J., Greenwood, R., Mills, G. A., Dominiak, E., Svensson, K., Knutsson, J. and Morrison, G. (2005). Passive sampling techniques for monitoring pollutants in water, *TrAC Trends in Analytical Chemistry* **24**(10): 845–868.
https://www.sciencedirect.com/science/article/pii/S0165993605001743

Wang, C., Bendle, J. A., Greene, S. E., Griffiths, M. L., Huang, J., Moossen, H., Zhang, H., Ashley, K. and Xie, S. (2019). Speleothem biomarker evidence for a negative terrestrial feedback on climate during Holocene warm periods, *Earth and Planetary Science Letters* **525**: 115754.

Wehrens, R., Hageman, J. A., van Eeuwijk, F., Kooke, R., Flood, P. J., Wijnker, E., Keurentjes, J. J. B., Lommen, A., van Eekelen, H. D. L. M., Hall, R. D., Mumm, R. and de Vos, R. C. H. (2016). Improved batch correction in untargeted MS-based metabolomics, *Metabolomics : Official Journal of the Metabolomic Society* **12**: 88.

Wiedner, E., Scholz, D., Mangini, A., Polag, D., Mühlinghaus, C. and Segl, M. (2008). Investigation of the stable isotope fractionation in speleothems with laboratory experiments, *Quaternary International* **187**(1): 15–24.

Wynn, P. M. and Brocks, J. J. (2014). A framework for the extraction and interpretation of organic molecules in speleothem carbonate, *Rapid Communications in Mass Spectrometry* **28**(8): 845–854.

Wysocki, L. A., Filley, T. R. and Bianchi, T. S. (2008). Comparison of two methods for the analysis of lignin in marine sediments: CuO oxidation versus tetramethylammonium hydroxide (TMAH) thermochemolysis, *Organic Geochemistry* **39**(10): 1454–1461.

Xie, S. (2003). Lipid distribution in a subtropical southern China stalagmite as a record of soil ecosystem response to paleoclimate change, *Quaternary Research* pp. 340–347.

Xu, C., Arancon, Rick Arneil D, Labidi, J. and Luque, R. (2014). Lignin depolymerisation strategies: towards valuable chemicals and fuels, *Chemical Society reviews* **43**(22): 7485–7500.

Yan, G. and Kaiser, K. (2018a). A rapid and sensitive method for the analysis of lignin phenols in environmental samples using ultra-high performance liquid chromatography-electrospray ionization-tandem mass spectrometry with multiple reaction monitoring, *Analytica Chimica Acta* **1023**: 74–80.

Yan, G. and Kaiser, K. (2018b). Ultralow Sample Volume Cupric Sulfate Oxidation Method for the Analysis of Dissolved Lignin, *Analytical Chemistry* **90**(15): 9289–9295.

Younes, K. and Grasset, L. (2018). Comparison of thermochemolysis and classical chemical degradation and extraction methods for the analysis of carbohydrates, lignin and lipids in a peat bog, *Journal of Analytical and Applied Pyrolysis* **134**: 61–72.

Zakzeski, J., Bruijnincx, P. C. A., Jongerius, A. L. and Weckhuysen, B. M. (2010). The Catalytic Valorization of Lignin for the Production of Renewable Chemicals, *Chemical Reviews* **110**(6): 3552–3599.

Zhang, T., Li, X., Sun, S., Lan, H., Du, P. and Wang, M. (2013). Determination of lignin in marine sediment using alkaline cupric oxide oxidation-solid phase extraction-on-column derivatization-gas chromatography, *Journal of Ocean University of China* **12**(1): 63–69.

Zirbes, M., Schmitt, D., Beiser, N., Pitton, D., Hoffmann, T. and Waldvogel, S. R. (2019). Anodic Degradation of Lignin at Active Transition Metal-based Alloys and Performance-enhanced Anodes, *ChemElectroChem* **6**(1): 155–161.

Zirbes, M. and Waldvogel, S. R. (2018). Electro-conversion as sustainable method for the fine chemical production from the biopolymer lignin, *Current Opinion in Green and Sustainable Chemistry* **14**: 19–25.

Part IV

Appendix

A Supplement to Chapter 4 "Method development for the quantification of lignin oxidation products as vegetation biomarkers in speleothems and cave dripwater"

A.1 Evaporation effects of different elution solvents for SPE

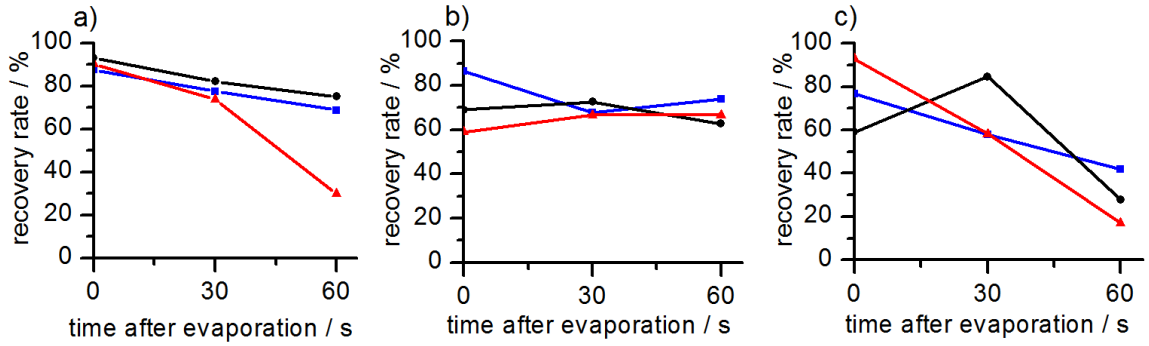

Figure A.1: Recovery rates of vanillin after evaporation in a) acetonitrile, b) methanol and c) ethyl acetate at 45 °C (red triangles), 30 °C (black circles) and 25 °C (blue squares). The residue was re-dissolved in H_2O/ACN 9:1 (v/v) and analyzed. At elevated evaporation temperatures, vanillin and other aldehydes evaporated and were lost for analysis. In ethyl acetate, this evaporative loss was more pronounced than in acetonitrile and methanol.

A.2 Linearity test of the SPE cartridges at different spiking concentrations

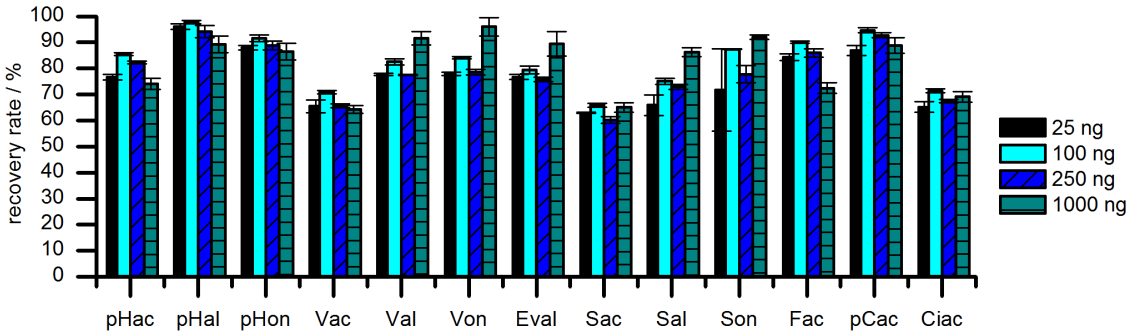

Figure A.2: Recovery rates of the solid phase extraction of LOPs at different spiking concentrations. 20 mL of a surrogate sample solution (2 mol · L^{-1} NaCl in ultrapure water, acidified with HCl to pH 2) were spiked with 25, 100, 250 and 1000 ng of LOP standards.

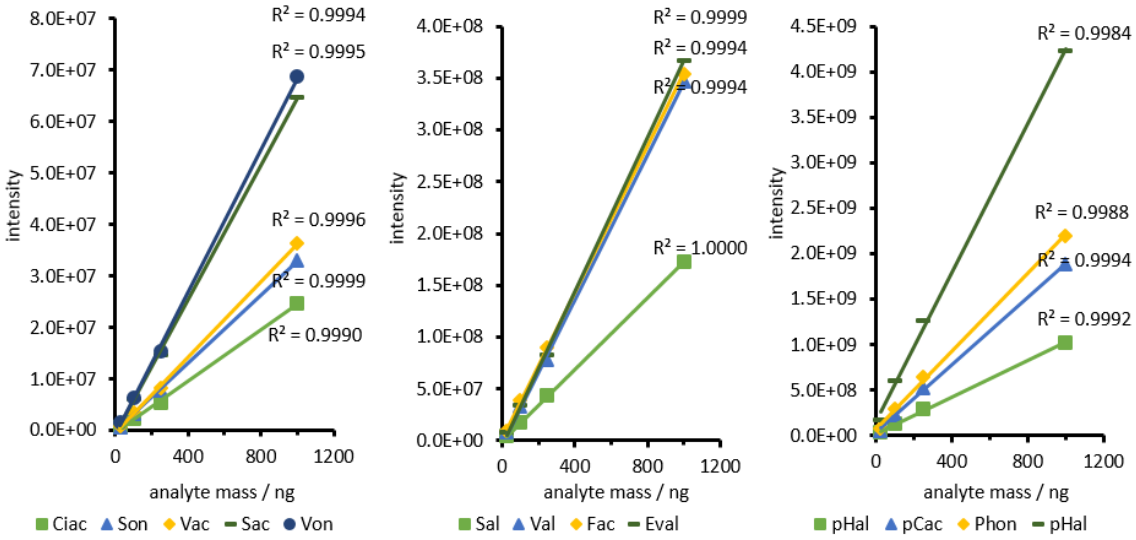

Figure A.3: Linearity test of the SPE method for the extraction of LOPs. 20 mL of a surrogate sample solution (2 mol · L^{-1} NaCl in ultrapure water, acidified with HCl to pH 2) were spiked with 25, 100, 250 and 1000 ng of LOP standards.

A.3 Test of the addition of glucose to prevent overoxidation

Many studies (e.g., Kaiser and Benner, 2012, Louchouarn et al., 2000, Spencer et al., 2010) recommended to add glucose to samples with low organic carbon content to prevent overoxidation of aldehydes. As stalagmite samples do have a low organic carbon content compared to soil or sediment samples, we tested the addition of glucose. The result was that the ratio of Vac/Val did indeed decrease from 0.48 ± 0.11 without glucose to 0.26 ± 0.12 with glucose, because the yield of vanillin increased with the addition of glucose. Nevertheless, the ratio of C/V decreased from 0.46 ± 0.12 to 0.26 ± 0.31 and the ratio of S/V decreased from 0.76 ± 0.19 to 0.41 ± 0.36 (Fig. A.4). This means that the addition of glucose did not prevent cinnamyl and syringyl phenols from overoxidation. In contrast, there were more interfering peaks in the chromatograms with glucose (Fig. A.5), which made integration difficult and lead to increased uncertainty in quantification. Consequently, no glucose was added in the CuO oxidation step.

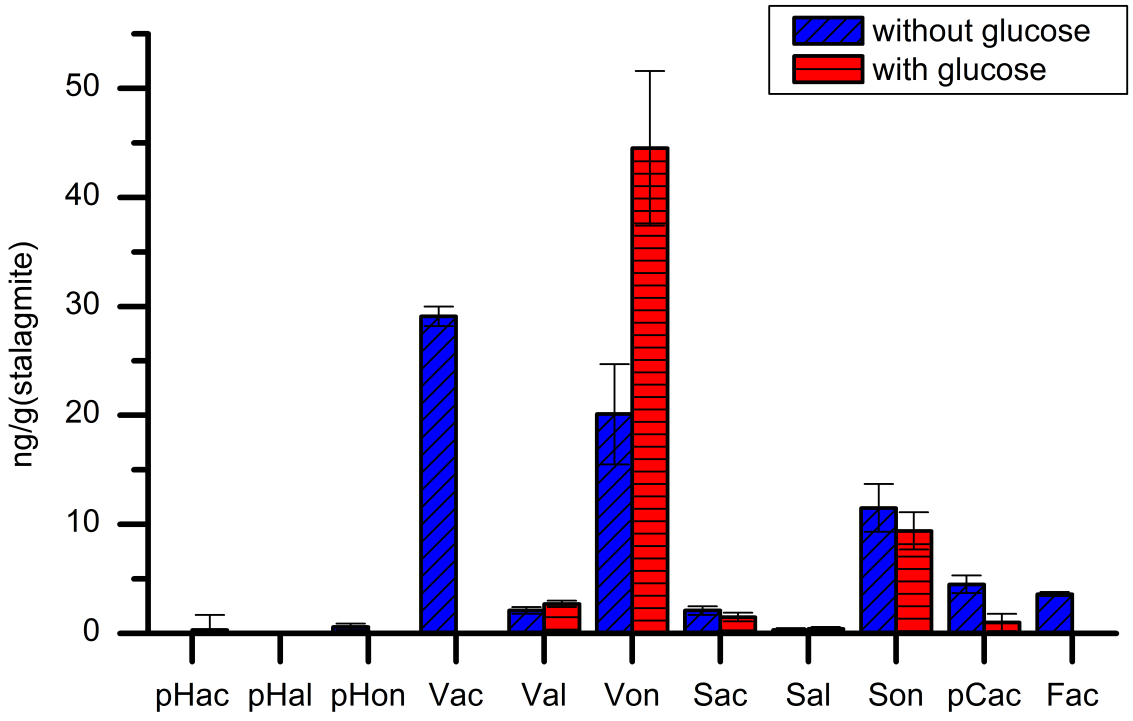

Figure A.4: Comparison of LOP concentrations with and without the addition of glucose. Only for Von, there was an increase in the concentration with the addition of glucose. For all other analytes, the method without glucose gave better results.

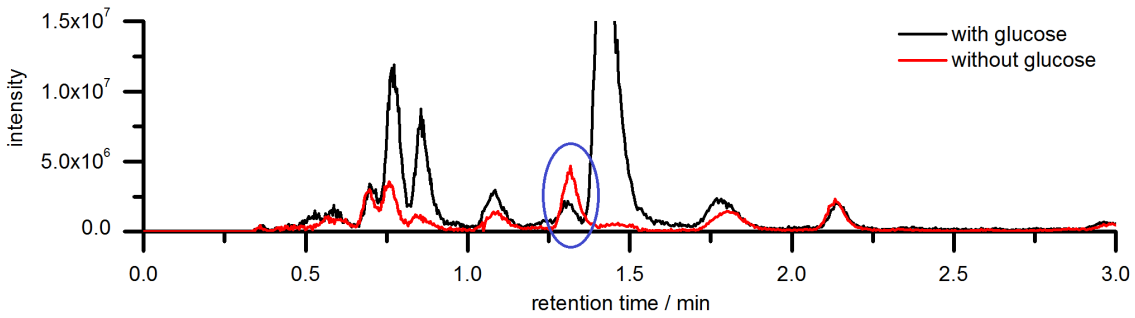

Figure A.5: Chromatogram of m/z 167.03498 (vanillic acid) with (black line) and without (red line) the addition of glucose. The peak of vanillic acid is circled. It was higher and better separated from neighbouring peaks without the addition of glucose. Similar observations were made for other analytes, too.

A.4 Linear regresssion parameters of the external calibration functions and instrumental limits of detection (LOD) and qualibration (LOQ).

Table A.1: Linear regresssion parameters of the external calibration functions and instrumental limits of detection (LOD) and qualibration (LOQ).

analyte	R^2	slope	intersept	instrumental LOD /ng · mL^{-1}	instrumental LOQ /ng · mL^{-1}
pHac	0.9998	6371269	229351	0.39	1.19
pHal	0.9949	24875695	10116687	0.05	0.15
pHon	0.9988	14313979	1679485	0.18	0.55
Vac	0.9998	206028	3287	0.48	1.46
Val	0.9997	630114	39639	0.25	0.75
Von	0.9962	129627	-6652	2.27	6.89
Sac	0.9993	270474	-23398	0.55	1.66
Sal	0.9996	170558	-17658	3.75	11.36
Son	0.9998	122729	3837	7.92	24.00
pCac	0.9978	11971947	2189589	1.08	3.26
Fac	0.9998	2028750	-169451	0.10	0.29
Eval	0.9998	1769186	929	0.24	0.73
Ciac	0.9996	100371	7569	4.44	13.45

A.5 Equations used for calculation of concentrations, lignin oxidation parameters and errors bars

The concentration c(analyte) of real samples was calculated by equation (A.1), with A = mean peak area of three LC-MS analyses of the sample, B = mean peak area of three LC-MS analyses of the blank sample, b = intersect of the Y-axis of the external calibration curve, m = slope of the external calibration curve, f_r = recovery factor of the internal standard ethylvanillin (Eval), see equation (A.2), V = volume of the final sample solution and m_{sample} = sample mass.

$$c(\text{analyte}) = \frac{A - B - b}{m} \cdot \frac{1}{f_r} \cdot \frac{V}{m_{\text{sample}}} \tag{A.1}$$

$$f_r = \frac{c(\text{Eval})_{\text{measured}}}{c(\text{Eval})_{\text{spiked}}} \tag{A.2}$$

The error Δc(analyte) of the concentration c(analyte) was calculated by equation (A.3).

$$\Delta c(\text{analyte}) = \sqrt{\begin{aligned}&\left(\frac{\partial A}{\partial c}\Delta A\right)^2 + \left(\frac{\partial B}{\partial c}\Delta B\right)^2 + \left(\frac{\partial b}{\partial c}\Delta b\right)^2 + \left(\frac{\partial m}{\partial c}\Delta m\right)^2 \\ &+ \left(\frac{\partial f_r}{\partial c}\Delta f_r\right)^2 + \left(\frac{\partial m_{\text{sample}}}{\partial c}\Delta m_{\text{sample}}\right)^2\end{aligned}} \tag{A.3}$$

The lignin oxidation parameters were calculated according to equations (A.4) to (A.9). Their errors were calculated using the law of propagation of uncertainty (equations not shown).

$$\text{C-group LOPs} = c(\text{p-Cac}) + c(\text{t-Fac}) \tag{A.4}$$

$$\text{S-group LOPs} = c(\text{Sac}) + c(\text{Sal}) + c(\text{Son}) \tag{A.5}$$

$$\text{V-group LOPs} = c(\text{Vac}) + c(\text{Val}) + c(\text{Von}) \tag{A.6}$$

$$\Sigma 8 = \text{C-group LOPs} + \text{S-group LOPs} + \text{V-group LOPs} \tag{A.7}$$

$$\text{C/V} = \frac{\text{C-group LOPs}}{\text{V-group LOPs}} \tag{A.8}$$

$$\text{S/V} = \frac{\text{S-group LOPs}}{\text{V-group LOPs}} \tag{A.9}$$

B Supplement to Chapter 6 “Lignin analysis in speleothems and cave dripwater – A first record from the Herbstlabyrinth Cave, central Germany”

B.1 Acid-to-aldehyde ratios in the stalagmite samples

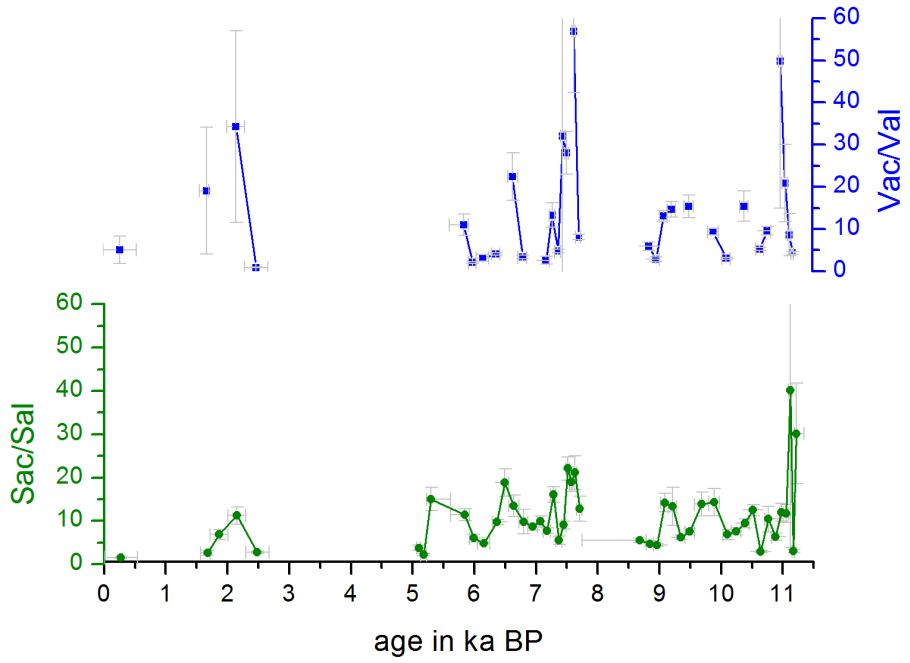

Figure B.1: Ratios of syringic acid to syringaldehyde (Sac/Sal) and vanillic acid to vanillin (Vac/Val) in plotted against the age of the stalagmite.

The ratio of Vac/Val in the stalagmite samples ranges from 0.9 to 57, and the ratio of Sac/Sal ranges from 1.6 to 40.

B.2 Acid-to-aldehyde ratios in the dripwater samples

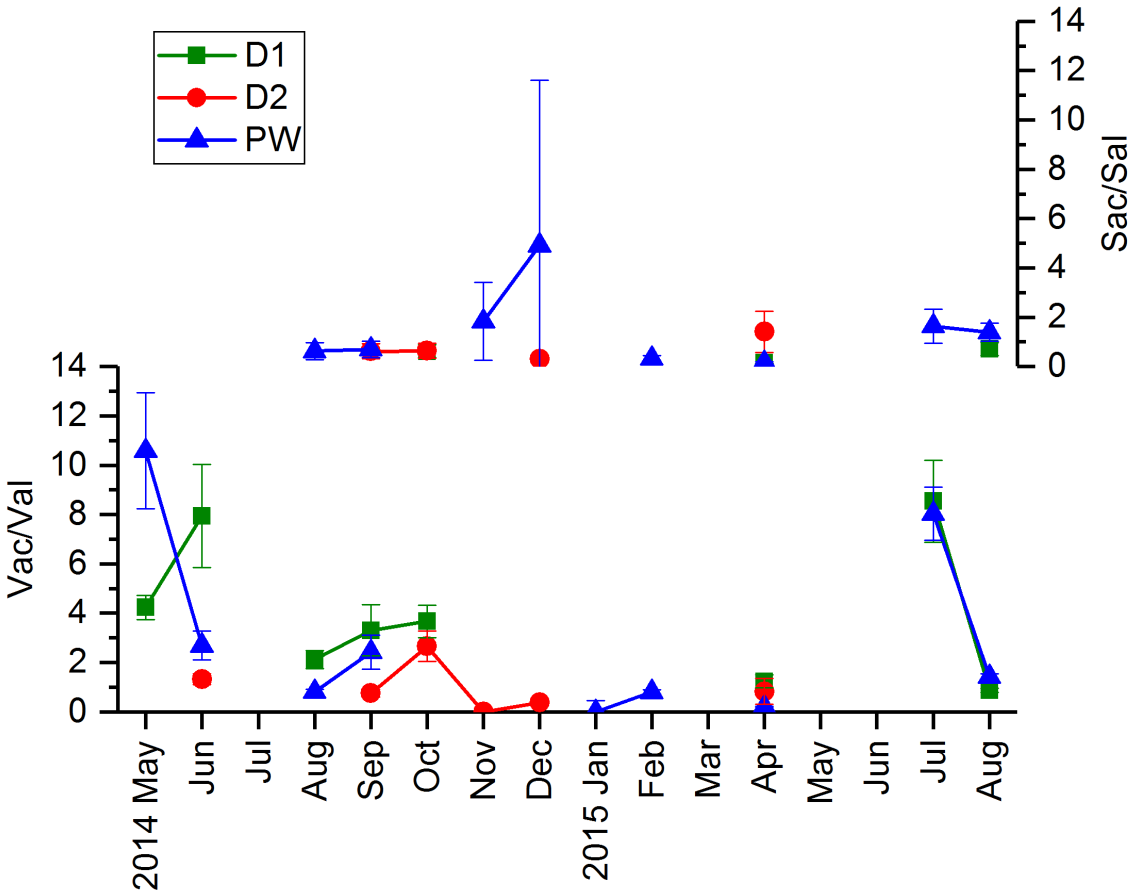

Figure B.2: Vac/Val and Sac/Sal ratios in the dripwater.

For the fast drip site *D1*, the values range from 0.9–8.5 for Vac/Val and 0.2–0.7 for Sac/Sal. For the slow drip site *D2*, the values are 0.0–2.7 for Vac/Val and 0.3–0.6 (1.4 with high uncertainty) for Sac/Sal, and for the pool water *PW*, 0.0–10.6 for Vac/Val and 0.2–1.8 (4.9 with high uncertainty) for Sac/Sal.

B.3 Correlation coefficients for the stalagmite samples

Table B.1: Pearson's correlation coefficients r (with $p < 0.05$) of the middle and older part of the stalagmite.

Pearson's r	C/V	S/V	Σ8	δ^{13}C	δ^{18}O	Mg	P	Sr	Ba	U	growth rate
C/V	-	0.88	-0.44	-	-0.34	-	-	-0.68	-	-	-
S/V	0.88	-	-0.42	0.41	-	-	-	-0.65	-	-	-
Σ8	-0.44	-0.42	-	-	-	-	0.40	-	-	-	0.58
δ^{13}C	-	0.41	-	-	0.43	-0.33	-	-	-	-	-
δ^{18}O	-0.34	-	-	0.43	-	-0.32	-	-	0.45	-	-
Mg	-	-	-	-0.33	-0.32	-	-0.49	0.53	-0.71	-0.56	-
P	-	-	0.40	-	-	-0.49	-	-0.38	0.49	0.78	0.43
Sr	-0.68	-0.65	-	-	-	0.53	-0.38	-	-	-0.63	-0.32
Ba	-	-	-	-	0.45	-0.71	0.49	-	-	0.55	-
U	-	-	-	-	-	-0.56	0.78	-0.63	0.55	-	-
growth rate	-	-	0.58	-	-	-	0.43	-0.32	-	-	-

Table B.2: Spearman's correlation coefficients ρ (with $p < 0.05$) of the middle and older part of the stalagmite.

Spearman's ρ	C/V	S/V	Σ8	δ^{13}C	δ^{18}O	Mg	P	Sr	Ba	U	growth rate
C/V	-	0.84	-0.46	-	-0.37	-	-	-0.82	-	0.45	-
S/V	0.84	-	-0.33	0.35	-	-	-	-0.70	-	0.38	-
Σ8	-0.46	-0.33	-	-	-	-	-	0.35	0.35	-	-
δ^{13}C	-	0.35	-	-	0.43	-	-0.34	-	-	-	-0.32
δ^{18}O	-0.37	-	-	0.43	-	-	-	0.34	0.43	-	-
Mg	-	-	-	-	-	-	-	-	-0.74	-0.58	0.41
P	-	-	-	-0.34	-	-	-	-	0.45	0.76	0.35
Sr	-0.82	-0.70	0.35	-	0.34	-	-	-	-	-0.51	-
Ba	-	-	0.35	-	0.43	-0.74	0.45	-	-	0.56	-0.31
U	0.45	0.38	-	-	-	-0.58	0.76	-0.51	0.56	-	-
growth rate	-	-	-	-0.32	-	0.41	0.35	-	-0.31	-	-

Table B.3: Pearson's correlation coefficients r (with $p < 0.05$) of the middle part of the stalagmite.

Pearson's r	C/V	S/V	Σ8	δ^{13}C	δ^{18}O	Mg	P	Sr	Ba	U	growth rate
C/V	-	0.82	-0.51	-	-	-	-0.48	-	-0.56	-	-
S/V	0.82	-	-0.54	-	-	-	-0.53	-	-0.57	-	-0.45
Σ8	-0.51	-0.54	-	-	-	-	0.66	-	0.60	-	0.79
δ^{13}C	-	-	-	-	0.53	0.69	-0.65	-	-	-0.59	-
δ^{18}O	-	-	-	0.53	-	0.50	-	-	-	-0.64	-
Mg	-	-	-	0.69	0.50	-	-	-	-	-0.55	-
P	-0.48	-0.53	0.66	-0.65	-	-	-	-	0.73	0.80	0.56
Sr	-	-	-	-	-	-	-	-	0.67	-	-
Ba	-0.56	-0.57	0.60	-	-	-	0.73	0.67	-	0.78	-
U	-	-	-	-0.59	-0.64	-0.55	0.80	-	0.78	-	-
growth rate	-	-0.45	0.79	-	-	-	0.56	-	-	-	-

Table B.4: Spearman's correlation coefficients ρ (with $p < 0.05$) of the middle part of the stalagmite.

Spearman's ρ	C/V	S/V	Σ8	δ^{13}C	δ^{18}O	Mg	P	Sr	Ba	U	growth rate
C/V	-	0.80	-0.53	-	-	-	-	-	-0.57	-	-
S/V	0.80	-	-	-	-	-	-0.45	-	-0.53	-	-
Σ8	-0.53	-	-	-	-	-	0.52	-	0.63	-	-
δ^{13}C	-	-	-	-	0.61	0.56	-0.64	-	-	-0.63	-
δ^{18}O	-	-	-	0.61	-	0.60	-	-	-	-0.55	-
Mg	-	-	-	0.56	0.60	-	-	-	-	-0.54	-
P	-	-0.45	0.52	-0.64	-	-	-	-	0.60	0.75	-
Sr	-	-	-	-	-	-	-	-	0.73	-	-
Ba	-0.57	-0.53	0.63	-	-	-	0.60	0.73	-	0.76	-
U	-	-	-	-0.63	-0.55	-0.54	0.75	-	0.76	-	-
growth rate	-	-	-	-	-	-	-	-	-	-	-

Table B.5: Pearson's correlation coefficients r (with $p < 0.05$) of the older part of the stalagmite.

Pearson's r	C/V	S/V	Σ8	δ^{13}C	δ^{18}O	Mg	P	Sr	Ba	U	growth rate
C/V	-	0.70	-	-	-	-0.52	-	-0.77	0.62	0.61	-
S/V	0.70	-	-	0.52	0.56	-0.54	-	-0.71	0.72	0.58	-
Σ8	-	-	-	-	-	-	-	-	-	-	-
δ^{13}C	-	0.52	-	-	0.67	-0.57	-	-	0.53	-	-0.60
δ^{18}O	-	0.56	-	0.67	-	-0.56	-	-	0.65	-	-0.65
Mg	-0.52	-0.54	-	-0.57	-0.56	-	-0.59	0.85	-0.92	-0.79	-
P	-	-	-	-	-	-0.59	-	-0.59	-	0.83	-
Sr	-0.77	-0.71	-	-	-	0.85	-0.59	-	-0.89	-0.89	-
Ba	0.62	0.72	-	0.53	0.65	-0.92	-	-0.89	-	0.81	-
U	0.61	0.58	-	-	-	-0.79	0.83	-0.89	0.81	-	-
growth rate	-	-	-	-0.60	-0.65	-	-	-	-	-	-

Table B.6: Spearman's correlation coefficients ρ (with $p < 0.05$) of the older part of the stalagmite.

Spearman's ρ	C/V	S/V	Σ8	δ^{13}C	δ^{18}O	Mg	P	Sr	Ba	U	growth rate
C/V	-	0.76	-	-	-	-0.71	-	-0.77	0.66	0.71	-
S/V	0.76	-	-	0.45	-	-0.68	-	-0.77	0.71	0.67	-
Σ8	-	-	-	-	-	-	-	-	-	-	-
δ^{13}C	-	0.45	-	-	0.58	-	-	-	0.49	-	-0.75
δ^{18}O	-	-	-	0.58	-	-0.49	-	-	0.65	-	-0.78
Mg	-0.71	-0.68	-	-	-0.49	-	-0.45	0.93	-0.88	-0.88	-
P	-	-	-	-	-	-0.45	-	-0.48	-	0.72	-
Sr	-0.77	-0.77	-	-	-	0.93	-0.48	-	-0.85	-0.88	-
Ba	0.66	0.71	-	0.49	0.65	-0.88	-	-0.85	-	0.85	-0.62
U	0.71	0.67	-	-	-	-0.88	0.72	-0.88	0.85	-	-
growth rate	-	-	-	-0.75	-0.78	-	-	-	-0.62	-	-

B.4 Principal component analysis of LOPs, trace elements and stabel isotopes in the stalagmite samples

Table B.7: Eigenvalues and explained variance of the principal component analysis of the stalagmite.

	middle and older part			middle part			older part		
	eigen-value	% of vari-ance	% cumu-lative	eigen-value	% of vari-ance	% cumu-lative	eigen-value	% of vari-ance	% cumu-lative
1	3.47	31.55	31.55	4.95	44.99	44.99	5.63	51.14	51.14
2	2.96	26.88	58.42	2.45	22.27	67.26	2.24	20.36	71.50
3	2.07	18.81	77.23	1.39	12.64	79.90	1.26	11.44	82.95
4	1.12	10.21	87.44	0.95	8.67	88.57	0.82	7.41	90.36
5	0.36	3.29	90.73	0.54	4.92	93.49	0.36	3.27	93.63
6	0.31	2.83	93.56	0.28	2.54	96.03	0.28	2.55	96.19
7	0.25	2.26	95.82	0.17	1.51	97.54	0.20	1.80	97.98
8	0.21	1.92	97.73	0.14	1.30	98.85	0.15	1.37	99.36
9	0.13	1.16	98.90	0.06	0.53	99.38	0.04	0.34	99.70
10	0.08	0.77	99.66	0.05	0.44	99.81	0.02	0.22	99.92
11	0.04	0.34	100.00	0.02	0.19	100.00	0.01	0.08	100.00

Table B.8: Coefficients of the principal component analysis of the stalagmite.

Para-meters	middle and older part PC1	PC2	PC3	PC4	middle part PC1	PC2	PC3	PC4	older part PC1	PC2	PC3	PC4
C/V	0.31	-0.42	-0.10	0.08	-0.31	-0.26	-0.21	0.46	0.30	0.23	-0.38	0.34
S/V	0.29	-0.44	-0.01	0.13	-0.33	-0.23	-0.08	0.40	0.33	-0.06	-0.19	0.54
S8	-0.01	0.44	-0.14	0.44	0.32	0.30	-0.11	0.22	-0.04	-0.09	0.72	0.61
d13C	0.15	-0.20	0.45	0.44	-0.30	0.26	0.39	0.35	0.25	-0.42	0.02	0.08
d18O	-0.08	0.14	0.59	0.22	-0.14	0.53	0.12	-0.25	0.26	-0.43	-0.07	-0.07
Mg	-0.40	-0.13	-0.35	0.15	-0.23	0.40	-0.03	0.37	-0.39	0.02	-0.18	0.21
P	0.34	0.35	-0.18	-0.15	0.40	-0.01	-0.27	0.17	0.23	0.38	0.45	-0.27
Sr	-0.48	0.15	0.09	-0.13	0.20	-0.07	0.70	0.14	-0.39	-0.19	0.08	0.03
Ba	0.25	0.36	0.36	-0.13	0.39	0.03	0.29	0.33	0.41	-0.05	-0.01	-0.09
U	0.45	0.18	-0.13	-0.26	0.36	-0.28	0.00	0.22	0.36	0.27	0.18	-0.10
growth rate	0.15	0.23	-0.33	0.62	0.22	0.44	-0.35	0.23	-0.12	0.56	-0.15	0.26

C Supplement to Chapter 9 "Understanding the cave system – Lignin analysis in soil, dripwater and speleothems from four different sites in New Zealand"

C.1 Analytical methods

For the soil samples, the LC-MS analysis of the lignin oxidation products was performed as described in Heidke et al. (2018) using a 50 mm pentafluorophenyl (PFP) column (Hypersil GOLD PFP, 50 mm × 2.1 mm with 1.9 µm particle size by Thermo Fisher Scientific). For the dripwater and flowstone samples, a 100 mm PFP column (Aquity UPLC CSH Fluoro-Phenyl, 100 mm × 2.1 mm with 1.7 µm particle size by Waters) was used for the separation of the LOPs. The gradient for this column started with 5% eluent B (98% acetonitrile, 2% H_2O) and 95% eluent A (98% H_2O, 2% acetonitrile and 0.4 $\mu L \cdot L^{-1}$ formic acid). Eluent B increased to 10% until 0.5 min, was held at this stage until 5.0 min, increased to 15% until 6.0 min and to 50% until 7.5 min. Then, a cleaning step at 99% B was run from 7.5 to 9.5 min, and finally, the initial eluent mixture with 5% B was reequilibrated from 9.5 to 11.0 min. The flow was set to 500 $\mu L \cdot min^{-1}$ and the column oven was heated to 40 °C.

The electrospray ionisation source (ESI) was operated in negative mode, so that deprotonated molecular ions $[M\text{-}H]^-$ were formed. The spray voltage was -3.5 kV, the ESI probe was heated to 150 °C to improve the evaporation of the aqueous solvent, the capillary temperature was 320 °C, the sheath gas pressure was 60 psi and the auxiliary gas pressure was 20 psi.

The mass spectrometer(Q Exactive Orbitrap high-resolution mass spectrometer by Thermo Fisher Scientific) was operated in full scan mode with a resolution of 70 000 and a scan range of *m/z* 80–500. At the respective retention time windows, the full scan mode was alternated with a targeted MS^2-mode with a resolution of 17 500 to identify the LOPs by their specific daughter ions (Heidke et al., 2018). For the MS^2-mode (i.e., *parallel reaction monitoring mode* in the software *XCalibur*, provided by Thermo Fisher Scientific), higher-energy collisional dissociation (HCD) was used with 35% normalized collision energy (NCE) for all analytes.

C.2 Description of the cave sites

Soils have been described to the most appropriate soil order following the New Zealand Soil Classification (NZSC, Hewitt (2010)). A brief description of the vegetation and soils of the four different cave sites is given in the following paragraphs.

Waipuna Cave, Waitomo (Fig. C.1, situated at S 38.3114722°, E 175.0206389°), is covered by a lush podocarp forest with a dense undergrowth of shrubs, ferns and tree-ferns. Soils in the locality are deep (> 1m) typic orthic allophanic (LO) being developed on extensive North Island rhyolitic volcanic ash deposits. These soils are exceptionally well drained and water typically reaches the cave on the timescale of days to a few weeks following rainfall events (Nava-Fernandez et al., 2020).

Figure C.1: Vegetation (a) and soils (b) of Waipuna Cave, Waitomo, North Island. Photos courtesy of Adam Hartland.

Hodges Creek Cave, Mt Arthur Tablelands, (Fig. C.2, situated at S 41.171270°, E 172.685941°) is developed within an Oligocene limestone remnant that has been heavily weathered and incised by deep grykes within which extensive litter organic (LO) soils have accumulated, which in places transition to orthic gley (GO) due to water logging leading to iron reduction, with characteristic iron mottles and concretions being found at depth (right hand picture). On the more gentle slopes, mature beech forest and well-drained orthic podzol (ZO) soils are typical with a deep brown O horizon and a weak sub-soil composed of bleached clays and weathered limestone.

The steep beech-covered slopes of Mt Arthur have only a thin orthic podzol (ZO) soil (Fig. C.3, Nettlebed Cave situated at S 41.2104589°, E 172.7394572°). Typically they are well-drained with a weak, bleached sub-soil due to the abundant, acidic leaf litter.

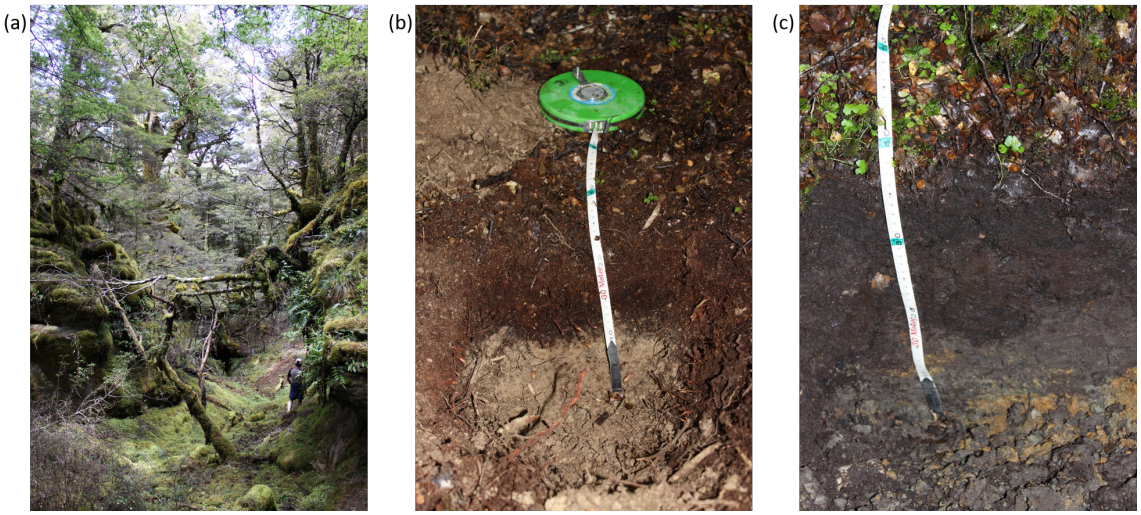

Figure C.2: Vegetation (a) and soils (b) and (c) of Hodges Creek Cave, Mt Arthur Tablelands, Kahurangi National Park, South Island. Photos courtesy of Adam Hartland.

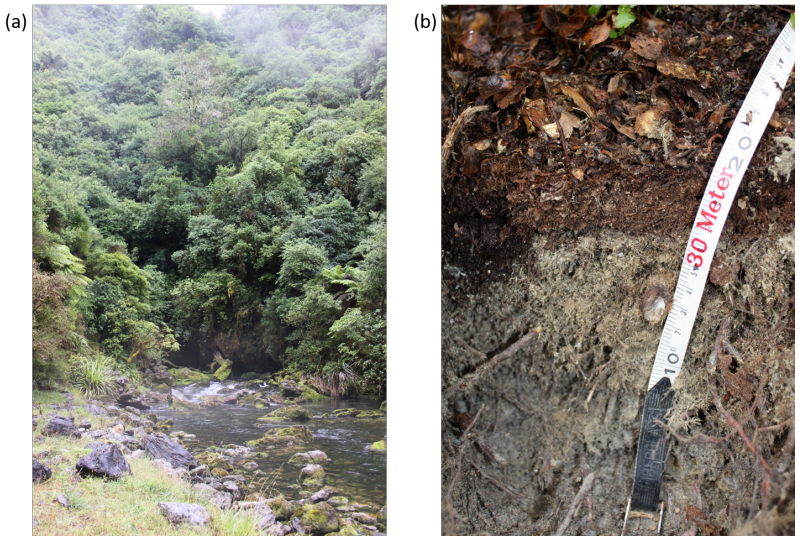

Figure C.3: Vegetation (a) and soils (b) of Nettlebed Cave, Mt Arthur, Kahurangi National Park, South Island. Photos courtesy of Adam Hartland.

The Mt Luxmore caves (Fig. C.4, Daves cave situated at S 45.3894900°, E 167.6153448°) reside above the tree line under a thick ground cover of tussock and other native alpine plants. Cold and wet conditions promote water-logging and peaty organic rich soils have developed. Soils were found to have light brown A horizons beginning at around 20 cm with characteristic iron staining indicating iron reduction and oxidation within the soil profile.

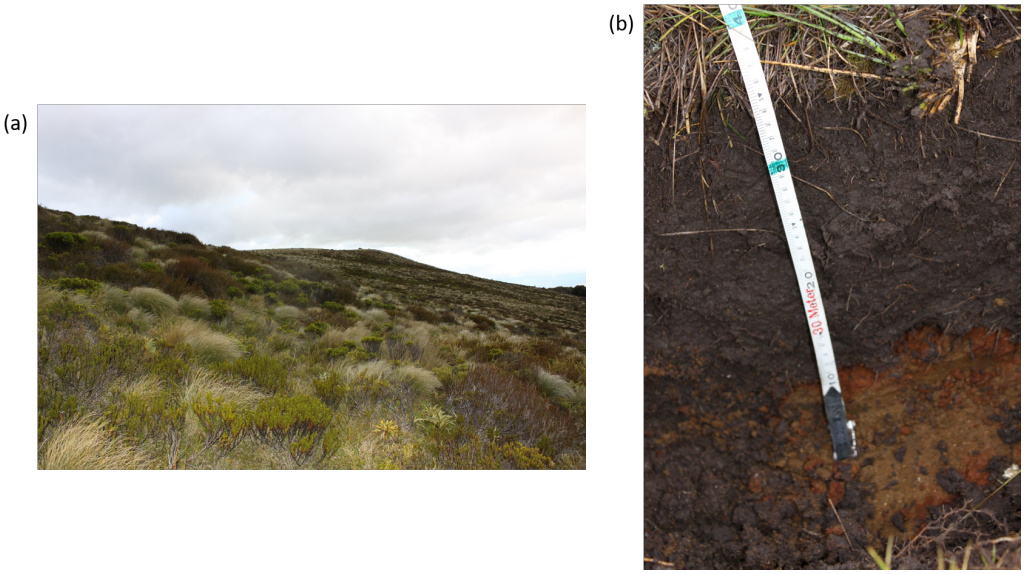

Figure C.4: Vegetation (a) and soils (b) of Dave's Cave, Mt Luxmore, Fiordland National Park, South Island. Photos courtesy of Adam Hartland.

C.3 Photographs of the flowstone samples

In Figure C.5, photographs of the flowstone cores from WP, HC, NB and DC are shown. The samples analyzed in this study are marked in red.

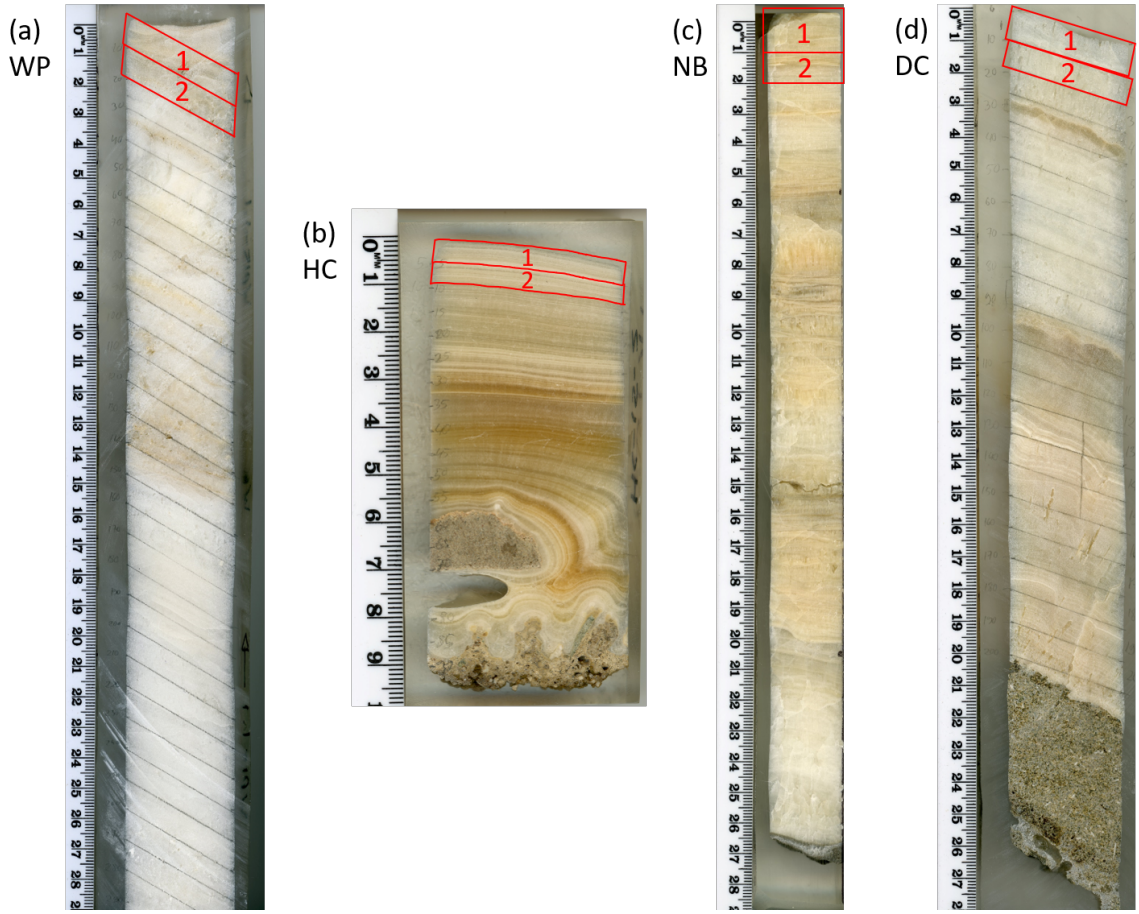

Figure C.5: Photographs of the flowstone cores from (a) Waipuna Cave (WP), (b) Hodges Creek Cave (HC), (c) Nettlebed Cave (NB), and (d) Daves Cave (DC). The samples analyzed in this study are marked in red. Photos courtesy of Adam Hartland.

C.4 ^{230}Th/U-dating of flowstone cores

Photographs of the flowstone slabs with the trenches drilled for ^{230}Th/U-dating are shown in Figure C.6. All relevant data concerning the ^{230}Th/U-dating of the flowstone cores are shown in Table C.1. Age-depth models of the four flowstone cores are shown in Figure C.7.

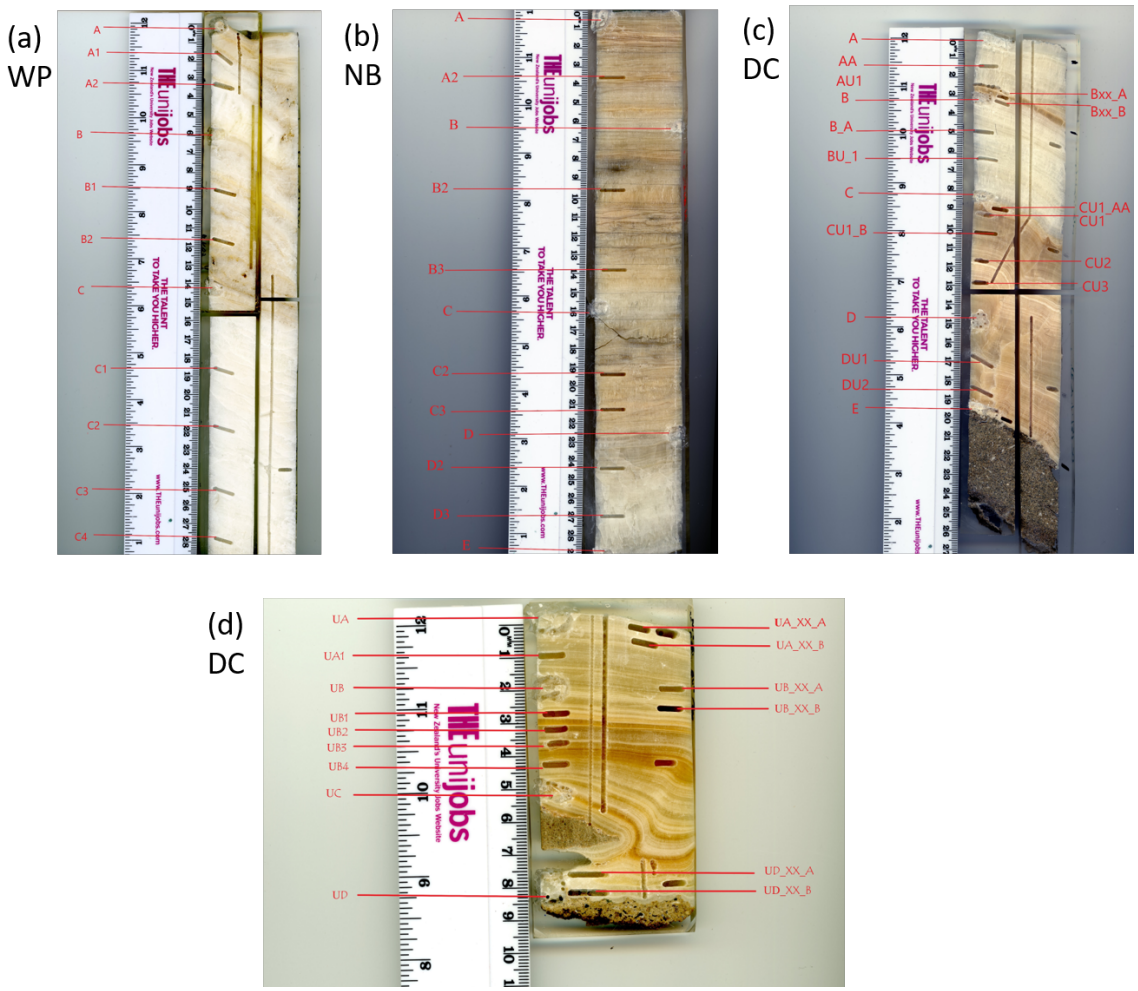

Figure C.6: Photographs of the flowstone slabs with the trenches drilled for ^{230}Th/U-dating.

Table C.1: ^{230}Th/U-dating of the flowstone cores. Data courtesy of John Hellstrom.

Sample	Lab Number	Depth in mm	U in ngg^{-1}	$[^{230}\text{Th}/^{238}\text{U}]^a$	$[^{234}\text{U}/^{238}\text{U}]^a$	$[^{232}\text{Th}/^{238}\text{U}]$	$[^{230}\text{Th}/^{232}\text{Th}]$	$[^{230}\text{Th}/^{232}\text{Th}]_i^d$	Age in ka^b	$[^{234}\text{U}/^{238}\text{U}]_i^c$
HC15 - Mt Arthur										
HC15_2_UA_XX_A	UME190501-621	2.0(1.0)	157	0.01816(32)	1.7017(27)	0.001144(23)	16	0.860(0.086)	1.109(0.021)	1.7039(27)
HC15_2_UA_XX_B	UME190501-628	6.4(1.1)	110	0.03921(53)	1.5661(26)	0.002090(42)	19	0.860(0.086)	2.635(0.039)	1.5703(26)
HC15 2 U-A-1	UMD170809-250	12.4(1.5)	120	0.05671(76)	1.5479(43)	0.001093(24)	52	0.860(0.086)	3.995(0.060)	1.5541(43)
WP15 - Waitomo										
*WP15 1.1 A	UMD170809-407	3.8(3.8)	13	0.1163(37)	1.2226(46)	0.08245(23)	1.4	0.71(0.18)	5.5(1.4)	1.2261(47)
WP15_1.1_UA_1	UME190820-307	17.0(1.0)	22	0.0758(23)	1.2027(52)	0.02191(44)	3.5	0.71(0.18)	5.67(0.43)	1.2059(52)
WP15 1.1 B	UMD170809-409	60.0(4.0)	16	0.0803(46)	1.2744(61)	0.01984(09)	4.0	0.71(0.18)	5.87(0.52)	1.2789(62)
DC15 - Mt Luxmore										
DC15 1.1A	UMD160610-423	4.0(4.0)	17	0.00200(31)	1.3917(42)	0.0007748(30)	2.6	0.75(0.50)	0.111(0.038)	1.3918(42)
DC15_1.1_AA	UME190501-657	18.0(1.0)	147	0.00976(18)	1.4468(21)	0.0002747(55)	36	0.75(0.50)	0.726(0.018)	1.4477(21)
DC15 1.1 UA1	UMD170809-343	28.5(1.0)	161	0.02195(70)	1.4894(42)	0.0010429(30)	21	0.75(0.50)	1.557(0.064)	1.4915(43)
NB15 - Mt Arthur										
NB15 2.1A	UMD170728-434	4.5(2.5)	58	0.02887(85)	1.2022(23)	0.02504(42)	1.2	0.93(0.20)	0.52(0.46)	1.2025(23)
NB15 2.1B	UMD170728-445	63.0(3.0)	68	0.0493(11)	1.1951(25)	0.003395(55)	15	0.93(0.20)	4.30(0.12)	1.1975(25)
NB15-2.1-B2	UME190624-546	95.5(0.8)	84	0.06871(81)	1.1966(26)	0.001657(33)	41	0.93(0.20)	6.297(0.085)	1.2001(26)

[a] Activity ratios determined at the University of Melbourne after Hellstrom (2003) and Drysdale et al. (2012)

[b] Age in kyr before year of measurement (2016–2019), corrected for initial ^{230}Th using eqn. 1 of Hellstrom (2006) and the decay constants of Cheng et al. (2013)

[c] Initial $[^{234}\text{U}/^{238}\text{U}]$ calculated using corrected age

[d] estimated initial $[^{230}\text{Th}/^{232}\text{Th}]$ after Hellstrom (2006)

* sample discarded as outlier

2-σ uncertainties in brackets are of the last two significant figures presented

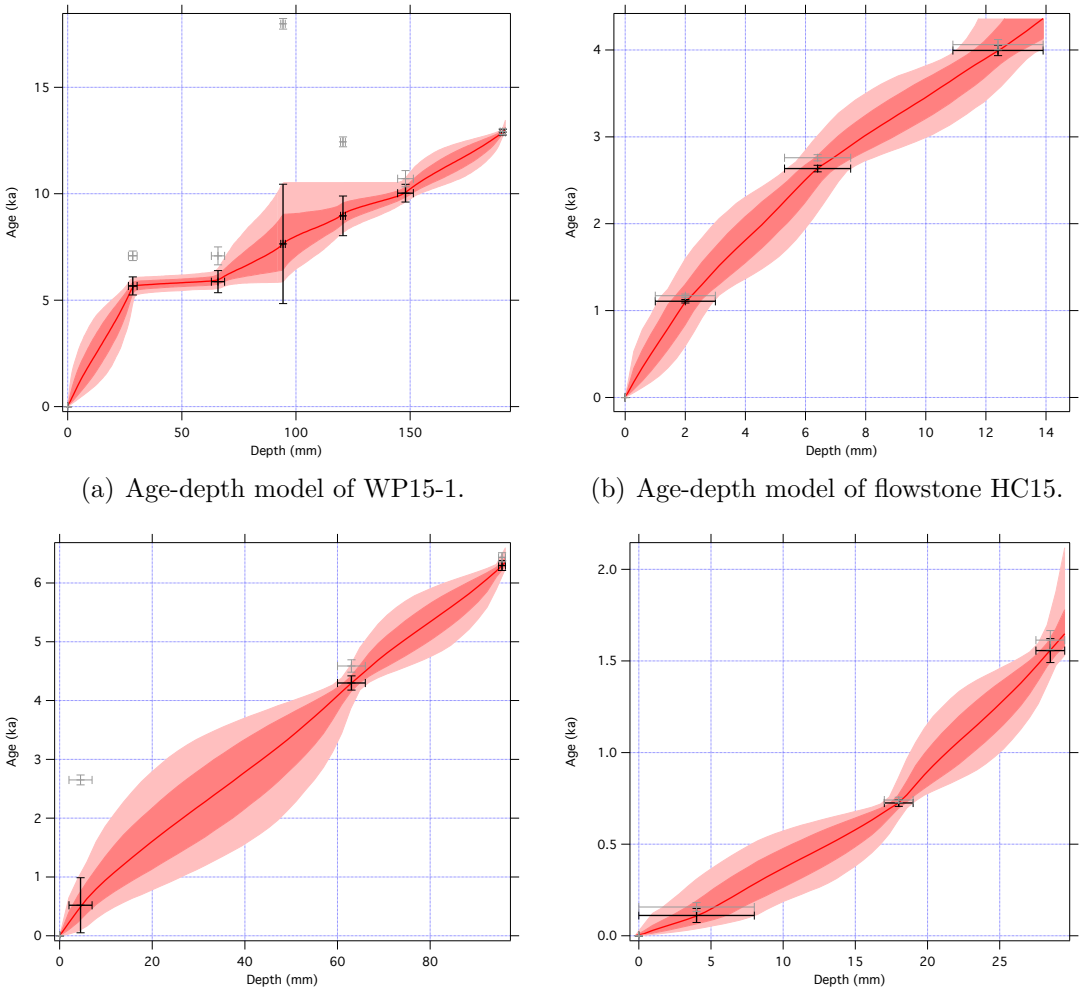

(a) Age-depth model of WP15-1.

(b) Age-depth model of flowstone HC15.

(c) Age-depth model of flowstone NB15.

(d) Age-depth model of flowstone DC15.

Figure C.7: Age-depth models of the four flowstone cores.

C.5 Data of LOP analysis

In Tables C.2, C.3, and C.5, the data of the LOP analysis are given. These data or simple calculations thereof were used to create Figures 9.3 to 9.7 in chapter 9.

Table C.2: LOP data of soil samples. The sample without number gives the mean value of the respective subsamples 1 and 2.

Sample	C in ng/g	C in % of Σ8	S in ng/g	S in % of Σ8	V in ng/g	V in % of Σ8	C/V	S/V	Σ8 in ng/g
HC-LL-1	42099 ± 3185	0.3	7612898 ± 173922	58.1	5457133 ± 140850	41.6	0.008 ± 0.001	1.395 ± 0.048	13112130
HC-LL-2	85995 ± 5751	0.8	5179573 ± 280885	46.3	5927765 ± 287069	53.0	0.015 ± 0.001	0.874 ± 0.064	11193333
HC-LL	64047 ± 21948	0.5	6396236 ± 1216663	52.6	5692449 ± 235316	46.8	0.011 ± 0.003	1.134 ± 0.261	12152731
HC-O-1	5710 ± 407	0.2	1308053 ± 79057	40.8	1889054 ± 132349	59.0	0.003 ± 0.000	0.692 ± 0.064	3202817
HC-O-2	5784 ± 387	0.2	1388208 ± 53574	43.2	1816614 ± 53042	56.6	0.003 ± 0.000	0.764 ± 0.037	3210606
HC-O	5747 ± 37	0.2	1348131 ± 40077	42.0	1852834 ± 36220	57.8	0.003 ± 0.000	0.728 ± 0.036	3206712
HC-A-1	3418 ± 409	1.8	66147 ± 6758	35.0	119431 ± 6476	63.2	0.029 ± 0.004	0.554 ± 0.064	188995
HC-A-2	3168 ± 307	2.2	43143 ± 3108	29.9	98010 ± 3657	67.9	0.032 ± 0.003	0.440 ± 0.036	144321
HC-A	3293 ± 125	2.0	54645 ± 11502	32.8	108720 ± 10711	65.2	0.030 ± 0.002	0.497 ± 0.057	166658
NB-LL-1	49962 ± 3092	0.5	4024223 ± 160874	43.3	5218472 ± 148991	56.2	0.010 ± 0.001	0.771 ± 0.038	9292658
NB-LL-2	32211 ± 2642	0.3	6334970 ± 124043	56.0	4938845 ± 134087	43.7	0.007 ± 0.001	1.283 ± 0.043	11306026
NB-LL	41087 ± 8876	0.4	5179597 ± 1155374	50.3	5078659 ± 139814	49.3	0.008 ± 0.002	1.027 ± 0.256	10299342
NB-O-1	43476 ± 2871	0.8	1843128 ± 55771	35.7	3278336 ± 75716	63.5	0.013 ± 0.001	0.562 ± 0.021	5164940
NB-O-2	45689 ± 2395	1.0	1662910 ± 69360	36.1	2896181 ± 67000	62.9	0.016 ± 0.001	0.574 ± 0.027	4604780
NB-O	44582 ± 1107	0.9	1753019 ± 90109	35.9	3087259 ± 191078	63.2	0.015 ± 0.001	0.568 ± 0.006	4884860
NB-A-1	25211 ± 1548	0.6	2053946 ± 108664	46.3	2357578 ± 55638	53.1	0.011 ± 0.001	0.871 ± 0.050	4436735
NB-A-2	27878 ± 1583	0.6	1962094 ± 43932	45.0	2366376 ± 64978	54.3	0.012 ± 0.001	0.829 ± 0.029	4356348
NB-A	26544 ± 1333	0.6	2008020 ± 45926	45.7	2361977 ± 4399	53.7	0.011 ± 0.001	0.850 ± 0.021	4396542
WP-LL-1	23470 ± 9154	0.4	38624 ± 12842	0.6	6018255 ± 204881	99.0	0.004 ± 0.002	0.006 ± 0.002	6080348
WP-LL-2	32591 ± 1516	0.6	30324 ± 10915	0.5	5703594 ± 173781	98.9	0.006 ± 0.000	0.005 ± 0.002	5766509
WP-LL	28030 ± 4561	0.5	34474 ± 4150	0.6	5860925 ± 157330	98.9	0.005 ± 0.001	0.006 ± 0.001	5923429
WP-O-1	7445 ± 377	1.2	92375 ± 5975	15.5	497093 ± 29202	83.3	0.015 ± 0.001	0.186 ± 0.016	596913
WP-O-2	7156 ± 403	1.3	73999 ± 31172	13.7	458329 ± 23842	85.0	0.016 ± 0.001	0.161 ± 0.069	539485
WP-O	7300 ± 144	1.3	83187 ± 9188	14.6	477711 ± 19382	84.1	0.015 ± 0.000	0.174 ± 0.012	568199
WP-A-1	5829 ± 337	10.1	4871 ± 1270	8.4	47055 ± 3281	81.5	0.124 ± 0.011	0.104 ± 0.028	57756
WP-A-2	2458 ± 273	3.9	5620 ± 1333	9.0	54181 ± 1496	87.0	0.045 ± 0.005	0.104 ± 0.025	62259
WP-A	4143 ± 1685	6.9	5246 ± 375	8.7	50618 ± 3563	84.4	0.085 ± 0.039	0.104 ± 0.000	60007
LX-LL-1	67625 ± 2898	3.3	742912 ± 32603	36.4	1229330 ± 30899	60.3	0.055 ± 0.003	0.604 ± 0.031	2039866
LX-LL-2	108958 ± 4367	5.3	731190 ± 29851	35.4	1226499 ± 31854	59.3	0.089 ± 0.004	0.596 ± 0.029	2066647
LX-LL	88291 ± 20667	4.3	737051 ± 5861	35.9	1227914 ± 1415	59.8	0.072 ± 0.017	0.600 ± 0.004	2053256
LX-O-1	25636 ± 1315	1.3	659252 ± 39129	32.9	1318781 ± 49196	65.8	0.019 ± 0.001	0.500 ± 0.035	2003669
LX-O-2	10881 ± 517	0.6	599536 ± 43386	33.0	1205894 ± 61752	66.4	0.009 ± 0.001	0.497 ± 0.044	1816311
LX-O	18259 ± 7377	1.0	629394 ± 29858	33.0	1262337 ± 56444	66.1	0.014 ± 0.005	0.499 ± 0.001	1909990
LX-A-1	6970 ± 338	14.6	4346 ± 1576	9.1	36486 ± 1384	76.3	0.191 ± 0.012	0.119 ± 0.043	47801
LX-A-2	6764 ± 363	12.4	5672 ± 1597	10.4	42049 ± 1437	77.2	0.161 ± 0.010	0.135 ± 0.038	54485
LX-A	6867 ± 103	13.4	5009 ± 663	9.8	39267 ± 2782	76.8	0.176 ± 0.015	0.127 ± 0.008	51143

Table C.3: LOP data of XAD samples.

Sample	C in ng/g	C in % of Σ8	S in ng/g	S in % of Σ8	V in ng/g	V in % of Σ8	C/V	S/V	Σ8 in ng/g
XAD-CC4	35.4 ± 7.7	6.4	252.0 ± 20.0	45.3	268.9 ± 61.5	48.3	0.13 ± 0.04	0.94 ± 0.23	556
XAD-DC1	62.6 ± 6.7	16.4	245.1 ± 17.8	64.0	75.1 ± 42.6	19.6	0.83 ± 0.48	3.27 ± 1.87	383
XAD-DC2	33.7 ± 4.7	14.8	138.0 ± 11.7	60.5	56.2 ± 34.6	24.7	0.60 ± 0.38	2.46 ± 1.52	228
XAD-HC3	76.4 ± 5.0	6.4	808.2 ± 42.7	67.2	318.6 ± 29.9	26.5	0.24 ± 0.03	2.54 ± 0.27	1203
XAD-HC4	134.7 ± 8.9	3.5	2844.2 ± 110.3	73.7	877.8 ± 92.8	22.8	0.15 ± 0.02	3.24 ± 0.36	3857
XAD-HC5	41.0 ± 4.6	6.0	507.3 ± 24.5	73.7	139.9 ± 16.0	20.3	0.29 ± 0.05	3.63 ± 0.45	688
XAD-WP1b	79.6 ± 6.7	11.3	466.5 ± 15.2	66.3	157.2 ± 8.1	22.3	0.51 ± 0.05	2.97 ± 0.18	703
XAD-WP2	71.9 ± 6.4	5.0	673.9 ± 32.2	47.1	686.0 ± 167.4	47.9	0.10 ± 0.03	0.98 ± 0.24	1432
XAD-WP3	55.8 ± 5.6	8.8	368.5 ± 21.9	58.4	206.8 ± 24.0	32.8	0.27 ± 0.04	1.78 ± 0.23	631

Table C.4: LOP data of flowstone samples.

Sample	C in ng/g	C in % of Σ8	S in ng/g	S in % of Σ8	V in ng/g	V in % of Σ8	C/V	S/V	Σ8 in ng/g
WP1	17.6 ± 0.8	54.9	6.9 ± 1.1	21.5	7.6 ± 0.9	23.6	2.33 ± 0.28	0.91 ± 0.18	32.1
WP2	23.5 ± 1.6	65.2	5.3 ± 0.9	14.6	7.3 ± 0.8	20.2	3.22 ± 0.40	0.72 ± 0.15	36.0
NB1	26.7 ± 1.4	29.0	48.3 ± 1.7	52.6	16.8 ± 0.8	18.3	1.58 ± 0.11	2.87 ± 0.17	91.8
NB2	12.3 ± 0.8	9.1	85.4 ± 1.6	62.8	38.3 ± 1.1	28.2	0.32 ± 0.02	2.23 ± 0.07	136.1
HC1	9.6 ± 0.9	13.6	39.4 ± 2.2	55.6	21.8 ± 1.6	30.7	0.44 ± 0.05	1.81 ± 0.17	70.9
HC2	35.3 ± 1.8	26.0	73.8 ± 3.1	54.4	26.7 ± 1.9	19.6	1.32 ± 0.12	2.77 ± 0.23	135.8
DC1	23.3 ± 0.6	54.6	11.4 ± 0.8	26.7	8.0 ± 0.7	18.7	2.92 ± 0.25	1.43 ± 0.15	42.8
DC2	14.0 ± 0.5	56.6	5.7 ± 0.9	22.9	5.1 ± 0.7	20.6	2.75 ± 0.41	1.11 ± 0.24	24.7

D General appendix

List of Abbreviations

η ..... viscosity
d_p ..... particle diameter (of the stationary phase in LC)
f ..... factor in LC depending on particle shape and packing
L ..... column length
N_{th} ..... number of separation stages in a chromatography column
p ..... pressure (in the LC column)
R ..... chromatographic resolution
r ..... column radius
T_R ..... retention time of a signal in a chromatogram
w_{base} ..... baseline width of a signal in a chromatogram
AAS ..... atomic absorption spectrometry
AC ..... alternating current
APCI ..... atmospheric pressure chemical ionization
API ..... atmospheric pressure ionization
CID ..... collision induced dissociation
CRM ..... *charged residue model* for the formation of gaseous ions from highly charged microdroplets in electrospray ionization
DC ..... direct current
DOM ..... dissolved organic matter
ESI ..... electrospray ionization
FID ..... flame ionizatio detection
FT-ICR-MS ... fourier transform ion cyclotron resonance mass spectrometry
GC ..... gas chromatography
GC-MS ..... gas chromatography coupled to mass spectrometry
HCD cell ..... higher-energy collision dissociation cell
HESI ..... heated electrospray ionization
HETP ..... height equivalent to a theoretical plate
HPLC ..... high-performance liquid chromatography
ICP-OES ..... inductively coupled plasma optical emission spectrometry
IEM ..... *ion emission model* for the formation of gaseous ions from highly charged microdroplets in electrospray ionization
LA-ICP-MS ... laser ablation inductively coupled plasma mass spectrometry
La-Py-GC-MS . laser micropyrolysis coupled to gas chromatography coupled to mass spectrometry
LC ..... liquid chromatography
LDPE ..... low-density polyethylene

LIT	linear ion trap
LLE	liquid-liquid exraction
LOPs	lignin oxidation products
LPVI	lignin phenol vegetation index
MC-ICP-MS	multicollector inductively coupled plasma mass spectrometry
MS	mass spectrometry
OM	organic matter
PCP	prior calcite precipitation
QqQ-MS	triple quadrupole mass spectrometry
RF	radio frequency
SCM	soil continuum model
SIMS	secondary ionization mass spectrometry
SPE	solid phase extraction
TIMS	thermal ionization mass spectrometry
TMAH	tetramethylammonium hydroxyde
TOC	total organic carbon
UHPLC	ultrahigh-performance liquid chromatography

List of Figures

List of Tables

List of related publications and conference contributions

Peer-reviewed publications

Heidke, I., Scholz, D., Hoffmann, T. (2018) Quantification of lignin oxidation products as vegetation biomarkers in speleothems and cave drip water. *Biogeosciences* **15**(19):5831–5845.

Heidke, I., Scholz, D., Hoffmann, T. (2019) Lignin oxidation products as a potential proxy for vegetation and environmental changes in speleothems and cave drip water - a first record from the Herbstlabyrinth, central Germany. *Climate of the Past* **15**(3):102–1037.

Heidke, I., Hartland, A., Scholz, D., Pearson, A., Hellstrom, J., Breitenbach, S. F. M., Hoffmann, T. (2020) Lignin oxidation products in soil, dripwater and speleothems from four different sites in New Zealand. *Biogeosciences* **18**(7):2289–2300.

Oral presentations

Hitzemann, I., Hoffmann, T.: Entwicklung einer LC-MS-Methode zur Quantifizierung von Ligninphenolen in Speläothemen als Klimaarchiv, *26th Ph.D. student seminar by the AK Separation Science of the GDCh*, Hohenroda, Germany, January 2016.

Heidke, I., Mischel, S. A., Scholz, D., Hoffmann, T.: Analysis of lignin oxidation products in a stalagmite from the Herbstlabyrinth-Adventshöhle in Germany and comparison with δ^{13}C and other vegetation proxies, *European Geosciences Union General Assembly*, Vienna, Austria, April 2017.

Poster presentations

Hitzemann, I., Hoffmann, T.: Organic trace analysis of lignin phenols in speleothems using UHPLC-ESI-HRMS and their use as vegetation proxy, *European Geosciences Union General Assembly*, Vienna, Austria, April 2016.

Heidke, I., Leppla, D., Hoffmann, T.: Spurenanalyse von Lignin-Oxidationsprodukten in Stalagmiten als Paläoklimaarchive, *ANAKON*, Tübingen, Germany, April 2017.

Heidke, I., Kreinbihl, S., Winkler, S., Mischel, S. A., Budsky, A., Riechelmann, D. F. C., Scholz, D., Hoffmann, T.: Application of lignin analysis to flowstone, stalagmite and drip watersamples – potentials of a new proxy, *European Geosciences Union General Assembly*, Vienna, Austria, April 2018.